Isolation and Characterisation of Novel DNA Aptamers Against *Mycobacterium Tuberculosis* Biomarkers: New Tools for Tuberculosis Diagnostics

Bianca Amos-Brown

Division of Chemical and Systems Biology

Department of Integrative Biomedical Sciences

Institute of Infectious Disease and Molecular Medicine

University of Cape Town

This dissertation is submitted for the degree of

Doctor of Philosophy in Chemical Biology

October 2018

Dedicated to my grandmother Marion Audrey Janse van Rensburg (nee Robertson), the galloping gran.

DECLARATION

I, Bianca Amos-Brown, declare that this thesis is my own work (except where acknowledgements indicate otherwise). Neither the whole work nor part thereof has been, is being, or is to be submitted for any degree or examination at any other university.

I empower the University of Cape Town to reproduce for the purposes of research either the whole or any part of the contents of this thesis, in any manner whatsoever.

Signature of candidate:

Signed by candidate

Signed on the 19th day of February 2018

ABSTRACT

Isolation and Characterisation of Novel DNA Aptamers against *Mycobacterium tuberculosis* Biomarkers: New Tools for Tuberculosis Diagnostics

B. Amos-Brown

Institute of Infectious Disease and Molecular Medicine, Division of Chemical and Systems Biology, Department of Integrative Biomedical Sciences, University of Cape Town

Tuberculosis is a curable disease with an average treatment success rate of 86 %. Despite this, there were an estimated 1.5 million deaths due to tuberculosis in 2013, most of which occurred in low and middle-income countries. In order to overcome tuberculosis in developing countries innovation in diagnostics is key to administering treatment.

While detection of whole mycobacteria has been favoured in the past to diagnose tuberculosis, culturing mycobacteria is costly, and microscopy is often not sensitive enough due to low bacterial loads. Detection of *Mycobacterium tuberculosis* biomarkers in urine, a safe and easy specimen to test, could offer a cost effective and simple solution to identify patients with tuberculosis.

Enzyme linked immunosorbent assays (ELISAs) were performed on concentrated tuberculosis patient urine to detect two *M. tuberculosis* biomarkers: lipoarabinomannan (LAM) and early secreted antigen-6 kDa (ESAT-6). Concentrating urine improved the detection of LAM in human immunodeficiency virus (HIV) negative patients and patients with a CD4 count > 200 cells/µl. ESAT-6 was not detected by ELISA due to a high background signal caused by the available antibodies cross reacting with a human protein present in urine which was identified by western blot and mass spectrometry. Targeted mass spectrometry did not detect ESAT-6 or its dimer partner, culture filtrate protein-10 kDa (CFP-10) in tuberculosis positive patient urine.

Since concentrating urine samples is impractical in a clinical setting a more sensitive diagnostic is needed to detect LAM in urine and ESAT-6 or CFP-10 in other samples. Aptamers can be packed more densely on biosensor surfaces increasing the dynamic range of detection while matching the affinity that an antibody has for a biomarker. Chemically modified DNA aptamers were isolated for LAM and the ESAT-6.CFP-10 dimer. The aptamers were characterised by enzyme linked oligonucleotide assays (ELONAs) and biolayer interferometry. One aptamer bound with high affinity to ESAT-6 while one aptamer bound with low affinity to LAM.

The use of aptamers as capture agents for detecting biomarkers in biological specimens thus appears to be a viable option for diagnosing tuberculosis, although availability and concentration of individual biomarkers seems likely to remain key to the choice of specimen in which to make diagnostic measurements.

ACKNOWLEDGEMENTS

To my supervisor Prof Jonathan Blackburn for his patience and invaluable expertise.

To my funders NRF, CSIR/UCT and Myer and Harry Brunow Scholarships.

Thanks to the following people for proofreading various bits and giving me valuable feedback.

- Dr Jessica Duarte
- Dr Lauren Arendse
- Dr Bridget Calder
- Brandon Murugan
- Dr Leshern Karamchand
- Dr Andrew Nel
- Dr Clemens Hermann

Special thanks to the following for assisting me in the lab: Dr Bridget Calder, Dr Andrew Nel and Dr Leshern Karamchand and a general thank you to all the wonderful Blackburn lab past and present.

To my Friday lunch gals Katie, Lauren and Jess you are my science inspiration. Also, to my friends who supported me through this journey Maike, Helene-Marie and all the rest.

To my family thanks for your encouragement especially my Mom and Dad.

To Alexey who championed me the most and whose Math skills came in very handy. Спасибо мой муж.

CONTENTS

LIST OF TABLES

LIST OF FIGURES

List of Abbreviations and Acronyms

AM Biotech	AM Biotechnologies, LLC
AphC	alkyl hydroperoxidase
araLAM	arabinose capped lipoarabinomannan
ATP	Adenosine triphosphate
BCG	Bacillus Calmette-Guérin
BLI	Biolayer interferometry
bp	Base pairs
BSA	Bovine serum albumin
CD4	CD4 expressing T-cells
CFP-10	Culture Filtrate Protein
CFU	Colony forming units
DNA	deoxyribose nucleic acid
DST	drug susceptibility tests
DTT	dithiothreitol
dUTP	deoxyribose uracil triphosphate (dUTP)
ELONA	Enzyme Linked OligoNucleotide Assay
EPTB	extrapulmonary tuberculosis
ESAT-6	Early Secreted Antigen 6 kDa
ESX-1	ESAT-6 secretion system 1
FIND	Foundation for Innovative New Diagnostics
GBM	glomerular basement membrane
HABA	4'-hydroxyazobenzene-2-carboxylic acid dye
HCD	Higher-energy C-trap dissociation
HIV	Human immunodeficiency virus
HRP	Horse Radish Peroxidase

IFN-γ	interferon-γ
IGRA	interferon-γ release assays
ITC	Isothermal titration calorimetry
LAM	lipoarabinomannan
LAMP	Loop mediated isothermal amplification
LED	light-emitting diode
LSPs	large sequence polymorphisms
LTBI	Latent tuberculosis infection
M. tuberculosis	*Mycobacterium tuberculosis*
MS	mass spectometry
MWCO	Molecular weight cut-off
NAAT	nucleic acid amplification test
NGS	Next generation Sequencing
NHS-biotin	N-Hydroxysulfosuccinimide biotin
NPV	negative predictive value
OD	Optical density
PAGE	Polyacrylamide Gel Electophoresis
PBMC	Peripheral mononuclear blood cells
PBS	Phosphate buffered saline
PCR	Polymerase Chain Reaction
PEP	Posterior Error Probability
PILAM	Phosphoinositol capped LAM
PNA	peptide nucleic acids
PPD	purified protein derivative
PPV	positive predictive value
PRM	parallel reaction monitoring

QCM	quartz crystal microbalance
RD-1	The region of difference 1
rESAT-6	recombinant Early secreted antigen 6 kDa
RNA	ribose nucleic acid
RP-HPLC	Reverse Phase High Performance Liquid Chromatography
RRDR	rifampin resistance-determining region
SDS	Sodium Dodecyl Sulphate
SDS-PAGE	Sodium Dodecyl Sulphate Polyacrylamide Gel Electrophoresis
SELEX	Systematic Evolution of Ligands by Exponential Enrichment
SPR	Surface plasmon resonance
SPR	Surface Plasmon Resonance
ssDNA	single stranded DNA
TB	tuberculosis
TBN	TB-Neat
TBST	Tris buffered saline with Tween-20
T-cell	Lymphocytes matured in the thymus
Th-1	T helper cell 1
TIC	total ion chromatograms
TMB	3,3',5,5'-tetramethylbenzidine
TST	tuberculin skin test (TST)
TTP	thymidine triphosphate
UTP	Uridine triphosphate
VOC	volatile organic compound
XA	X-Aptamers

LIST OF APPENDICES

1 LITERATURE REVIEW

1.1 Introduction

Mycobacterium tuberculosis is a pathogen that has evolved over an extended period in a niche environment, the human lung (Comas *et al.*, 2013). Robert Koch identified *M. tuberculosis* as the causal agent of tuberculosis (TB) over a century ago (Koch, 1890), but there was no effective treatment at the time. Drugs against TB such as isoniazid (Fox, 1961) were discovered during the mid to late 20th century and are still used today. TB is a curable disease with an average treatment success rate of 86 %. However, there were an estimated 1.5 million deaths due to TB in 2013 and the majority of these deaths occurred in low and middle income countries (WHO, 2014a). The economic cost of TB care in resource-poor countries places a large burden on strained economies (Ukwaja *et al.*, 2012). In order to overcome TB in developing countries, innovation in diagnostics is key to treating TB; without accurate diagnosis, the correct treatment cannot be administered.

1.2 Distribution and Burden of Disease/ Epidemiology

TB is most prevalent in Africa and Asia and the total number of active TB cases in 2013 was 9 million (Figure 1.1) (WHO, 2014a). Each country has its own unique challenges. Some of the risk factors associated with TB include Human Immunodeficiency Virus (HIV) infection, poverty and silicosis. An estimated 1.1 million people were co-infected with TB and HIV in 2013 (WHO, 2014a). HIV infected patients are more susceptible to TB due to their immune compromised state (Daley *et al.*, 1992; Corbett *et al.*, 2003). Malnutrition, especially a lack of protein in the diet, can also compromise cell-mediated immunity which is the primary defence against TB (Cegielski and McMurray, 2004). While poverty can lead to malnutrition, crowded

living arrangements and limited access to health care aggravate the transmission of TB. Mine workers or others with silicosis are at a higher risk of TB infection due to damaged lung tissue (Corbett *et al.*, 1999). The above factors highlight the need for interventions which are cost effective and functional in resource-poor settings.

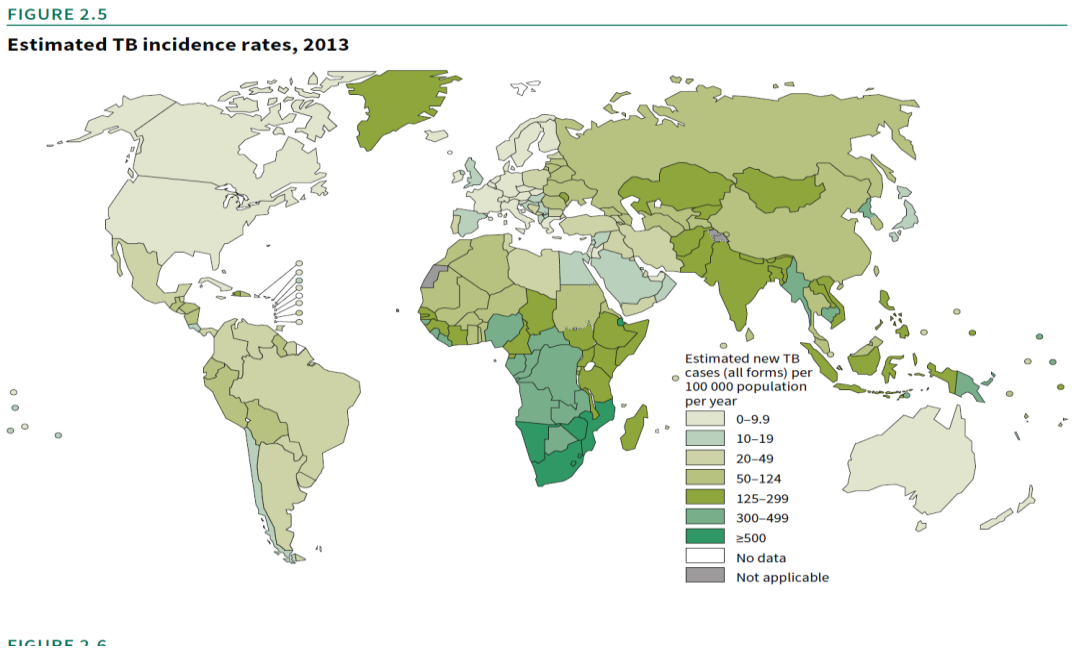

Figure 1.1 Estimated TB incidence rates

Highest incidence in Sub-Saharan Africa. Adapted from WHO 2014 Report (WHO, 2014a).

1.3 Physiology of Mycobacteria

M. tuberculosis is part of the Actinomycete family which includes environmental bacteria typically found in the soil and a subset of pathogenic bacteria, such as *M. tuberculosis, M. avium, M. bovis* and *M. kansasii*. A distinguishing feature of environmental mycobacteria is that they typically grow faster than the pathogenic species (Madigan *et al.*, 2012).

All mycobacteria are rod-shaped and Gram positive except that they have a substantially higher lipid content (40%) in their outer layer than typical Gram positive (5%) or Gram negative bacteria (10%) (Youmans, 1979). This property prevents the common red Gram stain from exiting the bacteria even after washing with 3% HCl in alcohol, hence Ziehl–Neelsen or acid-fast staining is useful for identifying mycobacteria (Madigan *et al.*, 2012). This additional layer

of lipids also helps the bacterium to survive the adverse conditions of the macrophage and deems them more resistant to drugs (Chan *et al.*, 1991; Koul *et al.*, 2011).

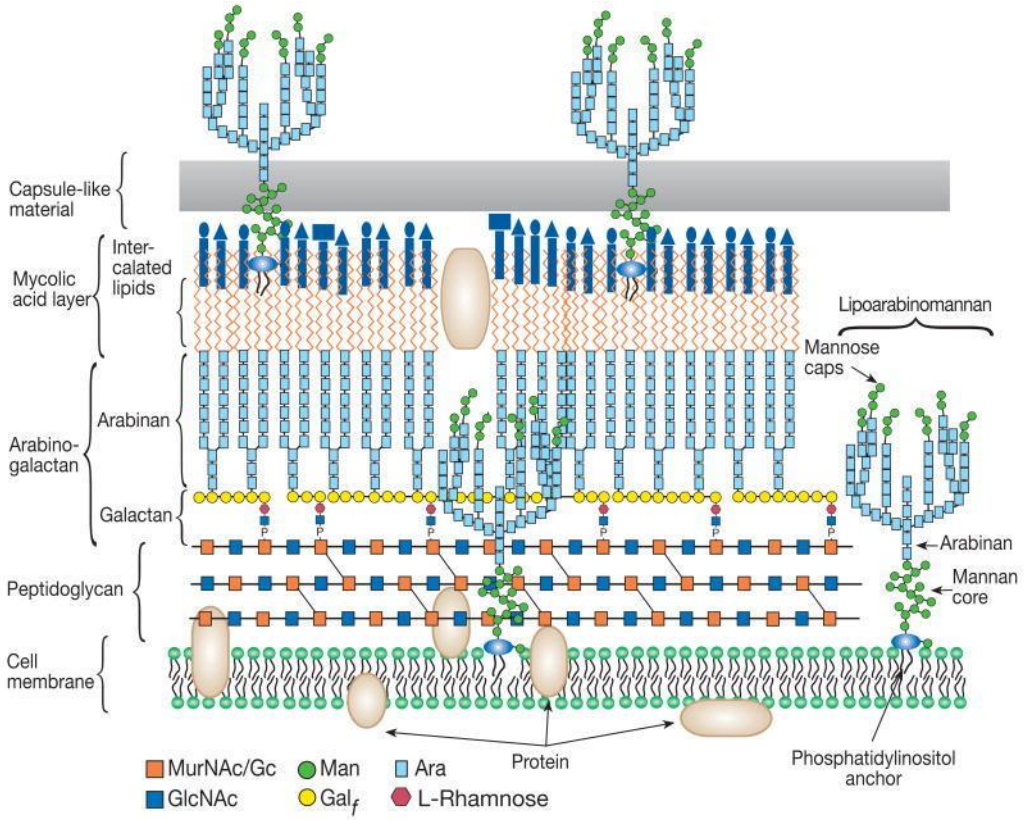

Figure 1.2 Mycobacterial cell wall

(http://2009.igem.org/wiki/index.php?title=Team:SupBiotech-Paris/Concept1&oldid=159486)

The lipid layer containing mostly mycolic acids is covalently linked to the arabinogalactan component of the wall which is in turn linked to the peptidoglycan layer (Figure 1.2). Teichoic acids which are embedded in the cell wall are responsible for the net negative charge on the cell surface. Some teichoic acids are covalently bound to lipids (Madigan *et al.*, 2012). Lipoarabinomannan (LAM) is found embedded in the cell membrane or near the surface of the cell wall (Alsteens *et al.*, 2008). LAM will be discussed in more detail in Chapter 2 and Chapter 4.

1.4 Aetiology and pathogenesis

TB is transmitted via small droplets exhaled by people with active TB (Figure 1.3). After *M. tuberculosis* is inhaled into the lungs, a complex immune response ensues and *M. tuberculosis*

orchestrates a counter attack by dysregulating several pathways of the immune system (Ellner, 1997; Baena and Porcelli, 2009; Urdahl, Shafiani and Ernst, 2011).

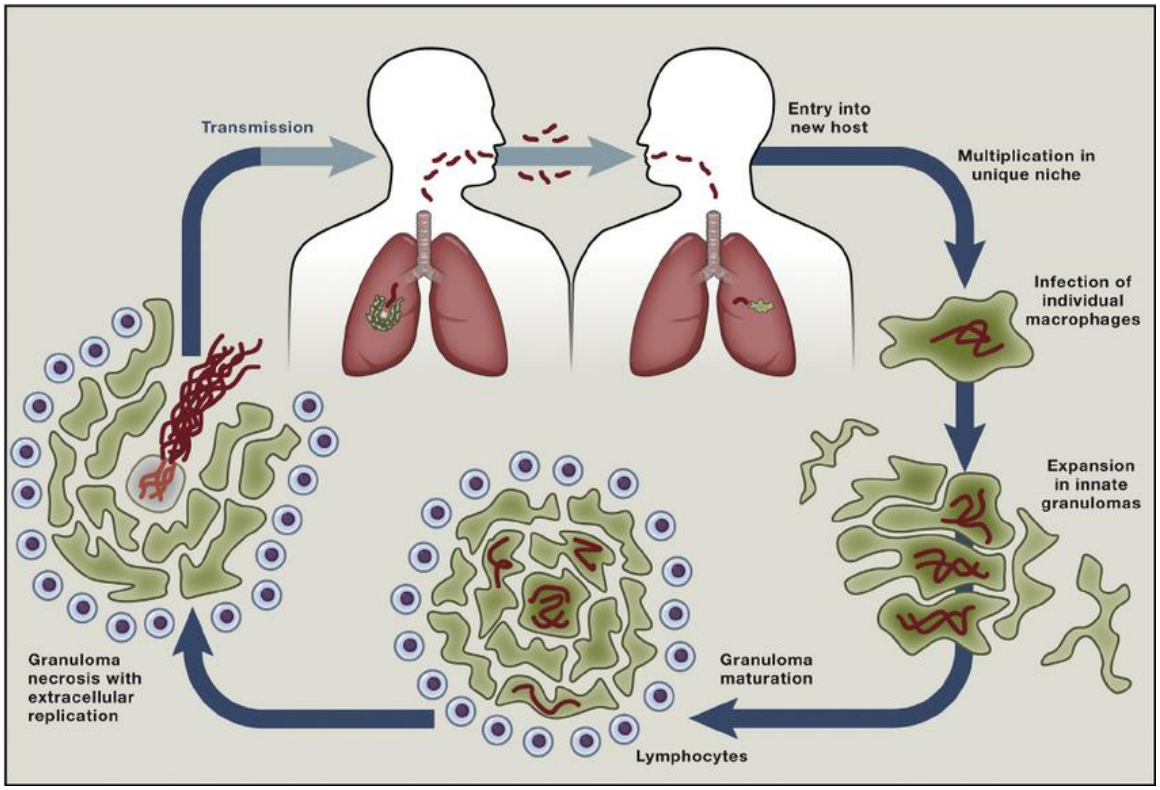

Figure 1.3 Tuberculosis pathogenesis

M. Tuberculosis is inhaled and enters the lung. Mycobacteria replicate inside macrophages and granulomas are formed. Necrotic granulomas release the mycobacteria, which are transmitted via aerosols [adapted from (Cambier, Falkow and Ramakrishnan, 2014)].

The range of virulence observed amongst clinical isolates is surprising given the limited genetic diversity of *M. tuberculosis* (Mathema *et al.*, 2006). Gagneux *et al.* suggest that six phylogenetic lineages are associated with particular geographical regions which has implications for the study of TB epidemiology (Figure 1.4)(Gagneux et al., 2006). The W. Beijing strain is of particular interest as it appears to be increasing in prevalence indicating greater fitness than other strains (Liu et al., 2014). While identifying genetic mutations may give clues to phenotypic differences (Sreevatsan et al., 1997), further proteomic studies are needed to illuminate phenotypic diversity (Parwati, van Crevel and van Soolingen, 2010; Peters et al., 2016).

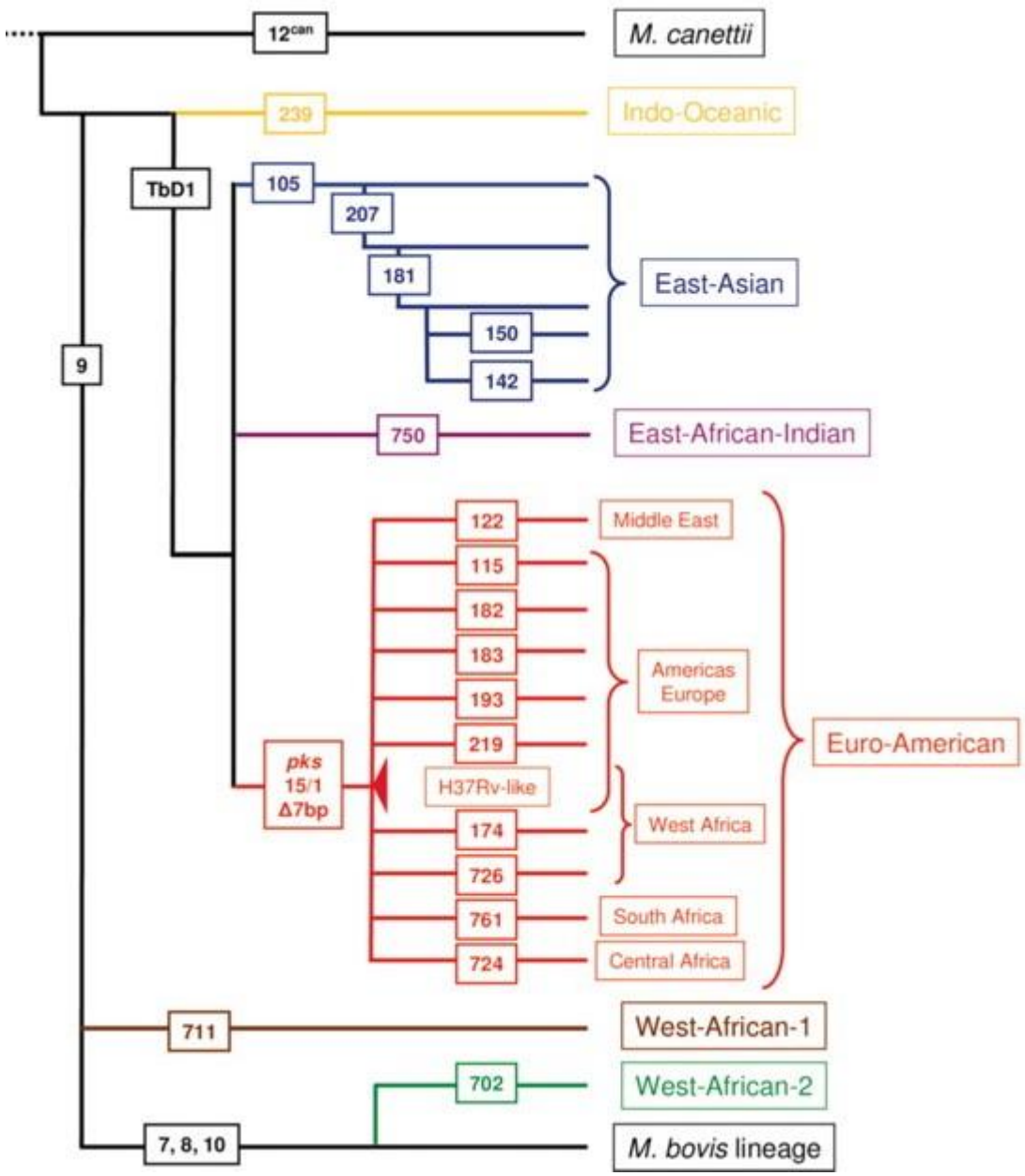

Figure 1.4 *M. tuberculosis* global phylogeny.

Large sequence polymorphisms (LSPs) define the global phylogeny for *M. tuberculosis*. Numbers indicate the names of the LSPs or regions of difference. Geographic regions are associated with specific lineages as indicated. [adapted from (Gagneux *et al.*, 2006)]

The study of the immunopathology of *M. tuberculosis* is ongoing as it is difficult to recreate the precise diseased environment found in human lungs. Many studies have been performed in mice models where *M. tuberculosis* remains inside the macrophages; as the current dogma

suggests, it is an intracellular pathogen for most of its lifespan. However, Orme argues that *M. tuberculosis* is largely an extracellular pathogen and it drives the human immune response to necrosis in order to prepare for escape (Turner, Basaraba and Orme, 2003; Orme, 2014), yet mice do not ordinarily develop necrotic lesions after *M. tuberculosis* infection. Hence, more studies are needed in the Kramnik mice model (Driver *et al.*, 2012) or guinea pigs to study *M. tuberculosis* in an extracellular necrotic environment (Turner, Basaraba and Orme, 2003).

Not all people exposed to *M. tuberculosis* progress to active disease, but may instead develop a latent infection. Latent infection is classified as having an *M. tuberculosis* infection which is not detected clinically. The state of the mycobacteria during latent infection is not well understood, but it seems they form a spectrum of dormant to replicating bacteria which are intrinsically resistant to drugs and the immune response. Orme argues that the classic idea of molecular latency is false and argues instead that *M. tuberculosis* prepares for transmission by entering a persistent state rather than a truly dormant one (Orme, 2014).

Most TB cases are restricted to lung infections. However, some cases progress to extrapulmonary disease where the bacteria spread to other organs. One of the more dangerous types of extrapulmonary TB is meningeal TB, where the mycobacteria access the membrane around the brain and can be found in the cerebrospinal fluid. It is estimated that 15-20% of TB patients develop meningeal TB and as many as 50 % of HIV positive patients (Berenguer *et al.*, 1992; Kashyap *et al.*, 2009)

The rise in TB has been partly attributed to the HIV epidemic which flared in the 1980s. HIV patients are more susceptible to TB because T-cells critical in the defence against *M. tuberculosis* are depleted in HIV patients (Kalsdorf *et al.*, 2009). The majority of co-infections are restricted to Africa rather than Asia and South America (other endemic regions) (WHO, 2011e). In an effort to reduce TB transmission, mortality and morbidity, HIV patients are screened for TB symptoms. Unfortunately, they are more difficult to diagnose due to extrapulmonary disease, paucibacillary sputum samples and lack of typical symptoms (Reid and Shah, 2009).

1.5 Vaccination

Vaccines typically dramatically lower the transmission of the target disease and can even lead to eradication of infectious diseases in some cases (e.g. polio and small pox). In the case of TB there is only one vaccine currently in use. It is derived from an attenuated strain of *Mycobacterium bovis* named *M. bovis* Bacillus Calmette-Guérin (BCG). The live BCG vaccine

confers variable protection, especially if an individual has been exposed to *M. tuberculosis* or other mycobacteria. Latitudes closer to the equator have reported reduced efficacy of the vaccine, probably due to increased exposure to environmental non-tuberculous mycobacteria. Unexposed children benefit more from vaccination than adults. BCG protects against childhood miliary or meningeal TB but has variable success in preventing pulmonary TB. This protective immunity does not last beyond childhood and booster doses of BCG do not confer any additional protection (Rodrigues *et al.*, 2005). Because of this limited benefit, BCG vaccination is currently only recommended in endemic TB regions. The question of why BCG vaccination is so ineffective in high burden settings remains the subject of much on-going research, but there is not yet a clear-cut answer.

While efforts to develop an effective vaccine continue, the complex relationship of *M. tuberculosis* with the human immune response has made it difficult to pin down an effective vaccine. Gene expression studies that map the immunopathology of TB in theory should help to design better vaccines (Bloom *et al.*, 2013). The challenge though lies in finding immune correlates of protection against TB infection. Currently the only method to verify if a vaccine is effective is to determine if the vaccinated group have higher rates of active TB than BCG vaccinated or non-vaccinated individuals (McNerney *et al.*, 2012).

1.6 Treatment

Tuberculosis is a treatable disease. The majority of bacteria are eliminated within the first two weeks of treatment for drug susceptible TB (Donald and Diacon, 2008). However, in order to eliminate persistent mycobacteria, treatment regimens are typically six to nine months. A typical regime consists of 2 months of isoniazid, rifampin, pyrazinamide, and ethambutol followed by a 4 months of isoniazid and rifampin (Nahid *et al.*, 2016). Due to this long regime, patients often default on their treatment, which increases the risk of drug resistant strains evolving and taking hold in a community (Parsons *et al.*, 2011).

Most of the first line drugs target an element of the cell wall or membrane. Isoniazid interferes with mycolic acid synthesis, while ethambutanol inhibits the polymerisation of arabinans destined for arabinogalactan and LAM (Chatterjee, 1997). Pyazinamide disrupts membrane energetics and transport, and rifampin inhibits RNA polymerase (Wehrli, 1983; Zhang, 2003).

Drug resistant strains are difficult and expensive to treat. New drugs to treat drug resistant strains have been slow to emerge. The only recent drug is bedaquiline which targets ATP synthase (Diacon *et al.*, 2009, 2012; Cox and Laessig, 2014; Pym *et al.*, 2016).

Diagnostic tests that could monitor the progress of treatment would be beneficial for identifying patients who had resistant strains and would perhaps shorten the course of treatment.

1.7 Diagnostics

Global case detection rates are estimated to be 64% of all incident tuberculosis cases, which means a projected 36% of cases remain undiagnosed and therefore untreated. In endemic countries, the estimate for case detection rates vary from 17% to 87%, leaving many infectious patients to transmit the disease (WHO, 2014b). While restricted resources and poor case reporting are factors for low case detection rates, current diagnostic tests and practices are inadequate to detect tuberculosis effectively. Hence, better diagnostics and practices are needed which can be used in diverse settings.

Diagnostic tests aimed at resource-poor settings should be cost effective and convenient (Pantoja, Kik and Denkinger, 2015). The 2012 diagnostic market in South Africa was estimated at 98 million USD while the Brazilian market was estimated at 16-17 million USD (TB Diagnostics Market Analysis Consortium, 2014, 2015). Current spending on diagnostics indicates what is affordable and if assistance is required for initial capital costs of new diagnostic tools. The successful roll-out of the Xpert MTB/RIF® assay in South Africa shows that there is a market for new and improved diagnostic tools in developing economies (TB Diagnostics Market Analysis Consortium, 2015). Disinvestment of redundant resources will also affect the market and should be considered when implementing new strategies (St John and Price, 2014).

New and current diagnostic tests are usually compared to the gold standard test to judge their effectiveness. Four metrics derived from this comparison are: sensitivity, specificity, positive predictive value (PPV) and negative predictive value (NPV).

Sensitivity and specificity are the most commonly used metrics for research and policy purposes. However, they should not be confused with analytical sensitivity and specificity, i.e. limit of detection and ability of a molecule to recognise another molecule specifically (Saah and Hoover, 1997). For the following discussion, sensitivity and specificity will refer to the diagnostic metrics. Sensitivity is the proportion of people with disease who will test positive and specificity is the proportion of people without the disease who will test negative. Note that these metrics do not give an indication of how many people may have a false positive (FP) or false negative (FN) result. PPV “represents a proportion of patients with a positive test result

in the total of subjects with positive result [true positive (TP)/TP+FP]" and NPV represents the "proportion of subjects without the disease with a negative test result in the total of subjects with negative test results [true negative (TN)/TN+FN]" (Šimundić, 2008). Hence, PPV and NPV, which indicate the probability that a positive result or negative result is true, are more useful in clinical settings. PPV and NPV values will vary depending on the prevalence of a disease in a population. Current TB diagnostics that are in routine use are described in the following sections.

1.7.1 Culture

The gold standard diagnostic for identifying *M. tuberculosis* is to culture the mycobacteria from patient specimens, typically sputum. Historically, this was time consuming due to *M. tuberculosis* only doubling every ~ 24 hours. The current automated liquid culture systems can produce results within 14 days. However, turn-around time depends on how many bacilli were in the patient specimen and logistics such as backlogs at testing centres. Automated culture systems have high sensitivity (75-100%) and specificity (>99%), and the ability to identify drug resistant strains with drug susceptibility tests (DST) (Palomino *et al.*, 2008). However, liquid cultures are prone to contamination, consequently they are subject to various tests to confirm the presence of *M. tuberculosis,* such as observing the morphology, or performing Ziehl-Neelsen staining and biochemical tests (Asmar and Drancourt, 2015) . While this method serves well as a gold standard, it requires disproportionate time, infrastructure and highly trained personnel to be an effective diagnostic.

1.7.2 Smear Microscopy

Ziehl–Neelsen or acid-fast smear microscopy is the most common first line diagnostic because it is affordable and rapid. However, the sensitivity varies from 32 to 94 % depending on the bacterial burden, quality of the sputum sample and the skill of the technician (Steingart, Henry, *et al.*, 2006). The proportion of smear negative patients increases in regions with high rates of HIV-associated TB (Elliott *et al.*, 1993; Colebunders and Bastian, 2000; Getahun *et al.*, 2007). Historically, smear negative tuberculosis had reasonable outcomes; however, smear negative HIV positive patients are at greater risk of mortality (Mukadi, Maher and Harries, 2001). Children also tend to be smear negative since they have difficulty producing sputum without swallowing (Zar *et al.*, 2005).

Sputum induction improves the diagnosis of HIV and paediatric patients by smear microscopy, a less invasive method than gastric or bronchial lavages (Zar *et al.*, 2005; Peter *et al.*, 2014).

Other techniques to improve sensitivity include concentrating sputum samples, light emitting diode (LED) microscopes and fluorescent auramine staining. FM-LED microscopy improves sensitivity by an average of 10% due to the larger area of the slide that is examined. Only a 25x objective lens is needed for FM-LED microscopy, which reduces the risk of technicians missing bacilli in low density samples (Steingart, Henry, *et al.*, 2006; Steingart, Ng, *et al.*, 2006). The WHO recommended FM-LED microscopy to replace Ziehl-Neelsen staining in 2011, but by 2013 only 6 % of labs worldwide had adopted this system (WHO, 2011b, 2016a). South Africa is one of the exceptions with 97% penetration of FM-LED microscopy (WHO, 2013b).

Despite improvements to this method, sensitivity remains variable: it cannot be used for determining drug resistance, and it requires infrastructure and highly trained technicians (Steingart, Henry, *et al.*, 2006). Hence smear microscopy is being phased out in many countries in favour of the rapid Xpert® MTB/RIF assay for diagnostics (WHO, 2016a).

1.7.3 Nucleic Acid Amplification Tests (NAAT)

The Xpert® MTB/RIF assay uses real-time PCR for the detection of *M. tuberculosis* and mutations in the 81-bp rifampin resistance-determining region (RRDR) of the *rpoB* gene.

The assay sensitivity is better than smear microscopy, thus detecting patients that are typically smear negative (Blakemore *et al.*, 2010; Helb *et al.*, 2010; Armand *et al.*, 2011; Boehme *et al.*, 2011; Marlowe *et al.*, 2011; Detjen *et al.*, 2015). The new Xpert® MTB/RIF Ultra assay has been designed to overcome some of the shortfalls of the first-generation assay with improvements in sensitivity in the hope of targeting paucibacillary samples from paediatric, HIV-associated and extrapulmonary TB. It promises to be of equal sensitivity as culture, needing only 61 CFUs, but specificity may be sacrificed in patients who have non-viable bacilli present after a recently treated TB infection (Alland *et al.*, 2015; Foundation for Innovative New Diagnostics (FIND), 2017; Zar, Workman and Nicol, 2017).

Additionally, it was found to be a cost effective first line diagnostic in sub-Saharan Africa but more studies are needed to assess other endemic regions (WHO, 2013a; Langley *et al.*, 2014).

The disadvantages of this technique are the continued need for skilled personnel and laboratories, the dependence on intact mycobacteria (Scott *et al.*, 2011) and an inability to distinguish between live and dead bacteria (WHO, 2011c).

Loop mediated isothermal amplification (LAMP) is another method of detecting *M. tuberculosis* DNA. It does not require a constant supply of electricity which is a benefit in developing

countries where electricity may be intermittent, and it can be performed in under an hour. This method allows for large amounts of amplicon to be generated which can be visually detected by using "double-stranded DNA-binding dyes, such as SYBR green, by detecting the turbidity caused by precipitating magnesium pyrophosphate or by using a non-inhibitory fluorescing reagent that is quenched in the presence of divalent cations" (WHO, 2016b) .

LAMP has been used to target several genes as tabulated by Aryan *et al* (2013). The *IS6110* gene is commonly used since there are multiple copies of this gene in *M. tuberculosis* (Aryan *et al.*, 2013). Current genes targeted by LAMP assays do not detect drug resistance though, hence the Xpert® MTB/RIF assay is recommended ahead of LAMP unless there is an electricity supply issue (WHO, 2016b).

LAMP is more sensitive than smear microscopy and is recommended for smear negative cases. Compared to the Xpert® MTB/RIF assay, LAMP is less sensitive (78%), but has the same specificity (98%) as the first-generation assays. However, LAMP is more cost effective than the Xpert® MTB/RIF assay given that it is cheaper to implement and requires less infrastructure as per cost-effectiveness calculations performed for Malawi and Vietnam. TB-LAMP had a weighted average cost of between USD 13.78 and USD 16.22 and the Xpert MTB/RIF assay was USD 19,17 to USD 28,34 (Sohn, 2016). The WHO has recommended it for pulmonary TB, i.e. sputum samples, but not extrapulmonary specimens in labs where microscopy can be performed (WHO, 2016b).

While most efforts to improve tuberculosis diagnostics have focussed on NAATs there is an inherit limitation to this approach. DNA is quickly hydrolysed in serum restricting NAATs to samples where DNA is preserved within the whole bacterium such as sputum. Sputum poses a risk to health care workers and the most vulnerable patients (HIV patients and children) have difficulty producing sputum or have paucibacillary specimens (Zar *et al.*, 2005; J. G. Peter *et al.*, 2012). Additionally, the need for electricity and skilled personnel are not trivial drawbacks, especially in the case of the Xpert® MTB/RIF assay.

1.7.4 Immune Response Diagnostics

Diagnostic assays such as interferon-γ (IFN-γ) release assays (IGRAs), the tuberculin skin test (TST) or antibody response assays measure the adaptive immune response against *M. tuberculosis*. Briefly, interaction with foreign antigens activates the differentiation of T helper (Th) cells into Th-1 and Th-2 cells. Activated Th-1 cells secrete cytokines such as IFN-γ to activate the bactericidal pathways of macrophages and dendritic cells. Th-2 cells stimulate

a B-cell response to produce antibodies, which is less well understood in the context of TB (Achkar, Chan and Casadevall, 2015). Adaptive immunity retains memory T-cells after an infection is cleared, thus repeat infections can be dealt with swiftly.

Immuno-diagnostics are primarily used to diagnose latent TB or determine exposure to *M. tuberculosis*. The WHO (2015a) state that "latent tuberculosis infection (LTBI) is defined as a state of persistent immune response to stimulation by *Mycobacterium tuberculosis* antigens without evidence of clinically manifested active TB". However, TB is a spectrum between latent and active dependent on several variables rather than two binary states (Barry *et al.*, 2009).

For the TST or "Mantoux" test, *M. tuberculosis* antigens are injected under the skin and a delayed hypersensitivity reaction is measured the following day. The TST has been improved over time by using more specific antigens, hence the modern TST is able to discriminate between BCG vaccinated individuals and those exposed to *M. tuberculosis* (Elhay, Oettinger and Andersen, 1998; Colangeli *et al.*, 2000; Arend *et al.*, 2008; Wu *et al.*, 2008).

For IGRAs, whole blood or PBMC's are stimulated with TB antigens to elicit the release of IFN-γ from T-cells that have been previously sensitized by *M. tuberculosis*. IGRAs were designed to replace the TSTs for diagnosis of latent TB, but they are more expensive and do not outperform the TST in low- and middle-income countries (WHO, 2011d). Lower sensitivity in the QuantiFERON-TB assay can be attributed to the peptide used, which is not the most immuno-reactive for all populations (Horvati *et al.*, 2016). A high incidence of HIV-associated TB also results in lower sensitivity, since the general immune response is lower (WHO, 2011d).

The goal of latent TB diagnosis is to determine if isoniazid preventative therapy should be administered. In endemic settings, it is not feasible to treat everyone with latent TB as it would be too costly. It would be valuable if IGRAs could predict conversion to active disease. The potential for IGRAs to predict the risk of developing active TB has been investigated but there is a poor correlation between IGRA result and those that develop TB, including immunocompromised patients (Mandalakas *et al.*, 2008; Rangaka *et al.*, 2012; Sester *et al.*, 2014).

Hence, IGRAs are only recommended for use in upper middle to high income countries where prevalence of TB is low enough to manage latent TB infections (WHO, 2011d, 2015a).

Another strategy to diagnose certain infectious diseases is to detect the antibody response to the pathogen, such as the HIV serodiagnostic test which is simple and takes only a few minutes to perform and read. Previously Steingard *et al.* explored the range of commercial serological

TB diagnostics and concluded that no current serodiagnostic is robust enough for routine use (Steingart *et al.*, 2011). Hence the WHO recommended against the use of rapid serological tests for the diagnosis of TB (WHO, 2011a). However, more recently, a study using highly immunogenic peptides from cell wall proteins has revived the possibility of a lateral flow point-of-care test (Gonzalez *et al.*, 2014).

1.8 New Diagnostics

Improvements to current diagnostics should in principle reduce incidence, decrease the duration of disease and increase case detection (Keeler *et al.*, 2006; Abu-Raddad *et al.*, 2009). As discussed above, current diagnostics have shortcomings and new tools at different levels of the health care system are needed. There is no silver bullet to solve tuberculosis diagnosis. Hence several avenues need to be explored.

A key discussion in 2014 prioritised the following point-of-care tests for diagnosis of active tuberculosis (WHO, 2014b; Denkinger *et al.*, 2015):

- The triage test: "a point-of-care triage test, which should be a simple, low-cost test that can be used by first-contact health-care providers to identify those who need further testing"
- The biomarker test: "a point-of-care non-sputum-based test capable of detecting all forms of TB by identifying characteristic biomarkers or bio-signatures"
- The smear replacement test: "a point-of-care sputum-based test to replace smear microscopy for detecting pulmonary TB "

Several studies have used the 2014 WHO meeting report above to model the effect of the hypothetical point-of-care tests on various markets with positive results (Denkinger *et al.*, 2014; Kik *et al.*, 2015; Pantoja, Kik and Denkinger, 2015).

A triage test with high sensitivity can be used as a rule out test which would be followed up by a more sensitive test. Paired with a more time- and cost-efficient system at the peripheral lab level, this approach would increase the detection rate of TB, allow for earlier treatment and reduce transmission of tuberculosis. This is predicted to ultimately reduce the burden in a region and contributes to the WHO's goal of ending TB by 2030 (WHO, 2016a). A study by Van't Hoog *et al.* explored if it would be cost effective to have a triage test before Xpert® MTB/RIF assay. Testing in Uganda, South Africa and India determined that the test should have the same sensitivity as the Xpert® MTB/RIF assay, 75% specificity and cost of 5 USD to be accepted (Van't Hoog *et al.*, 2013).

A non-sputum biomarker or smear replacement test with moderate sensitivity and high specificity would rule-in patients at the point-of care, as patients could be treated immediately. A non-sputum test would be beneficial for EPTB since conventional tests start off with sputum. Although it is important to be able to detect TB in difficult cases such as EPTB, children or HIV patients, a model by Denkinger *et al.* suggests that detecting active pulmonary cases is more efficient at reducing mortality than targeting difficult cases (Denkinger *et al.*, 2014). Hence, most patients would be diagnosed at the point-of-care and more difficult to diagnose patients would be referred for more sensitive laboratory based tests.

Which diagnostics will be commercially viable depends on how effective they are and whether a particular market is ready to spend money on new diagnostics. For example, an excellent biomarker test could replace the need for a sputum smear replacement test (Kik *et al.*, 2015)

Currently there are several new diagnostics in the pipeline at different levels of the health care system: point-of-care, peripheral lab, and reference lab (Figure 1.5). New diagnostics typically go through several stages before they are released onto the market or endorsed by WHO. Currently, there are few point-of-care diagnostics on the market due to the challenges of delivering this type of diagnostic (McNerney and Daley, 2011). Some point-of-care tests in various stages of development include antigen detection in urine, volatile organic compound (VOC) detection, ß-lactamase detection and 2nd generation NAATS (Cheon *et al.*, 2016).

VOC detection was initially restricted to laboratories, but mobile electronic noses are being developed for use as point-of-care diagnostics (Kolk *et al.*, 2010; Phillips *et al.*, 2010; Bruins *et al.*, 2013). This technique has poor performance during validation as VOCs are produced for several clinical conditions and are not easily linked to a particular disease (Bruins *et al.*, 2013).

Global BioDiagnostics Corp, Texas, USA is developing a point-of-care diagnostic based on the hydrolysis of a β-lactamase fluorogenic modified substrate by the BlaC enzyme expressed by *M. tuberculosis*. A LED based portable imaging set-up makes it suitable for low resource settings, but it needs further evaluation in the field (Xie *et al.*, 2012).

Loop-mediated isothermal amplification is well suited for point-of-care as a steady electricity supply is not essential. LAMP products in development target various genes including *IS6110*, *rpoB* and REP13E12 (McNerney *et al.*, 2015). Evaluation of these products is ongoing.

Antigen or biomarker detection is a promising option for a non-sputum point-of-care test. Determine TB-LAM (Alere Inc., USA) is the only commercial test. Currently, it is only recommended for severely immunocompromised HIV patients due to low sensitivity in other

tuberculosis patients(Peter, Theron and Dheda, 2013)

New approaches to tuberculosis diagnostics rarely move past the initial stages of development and many have not been tested in clinical settings. Those that have made it into clinical settings have not performed well. Hence further innovation is needed in this space.

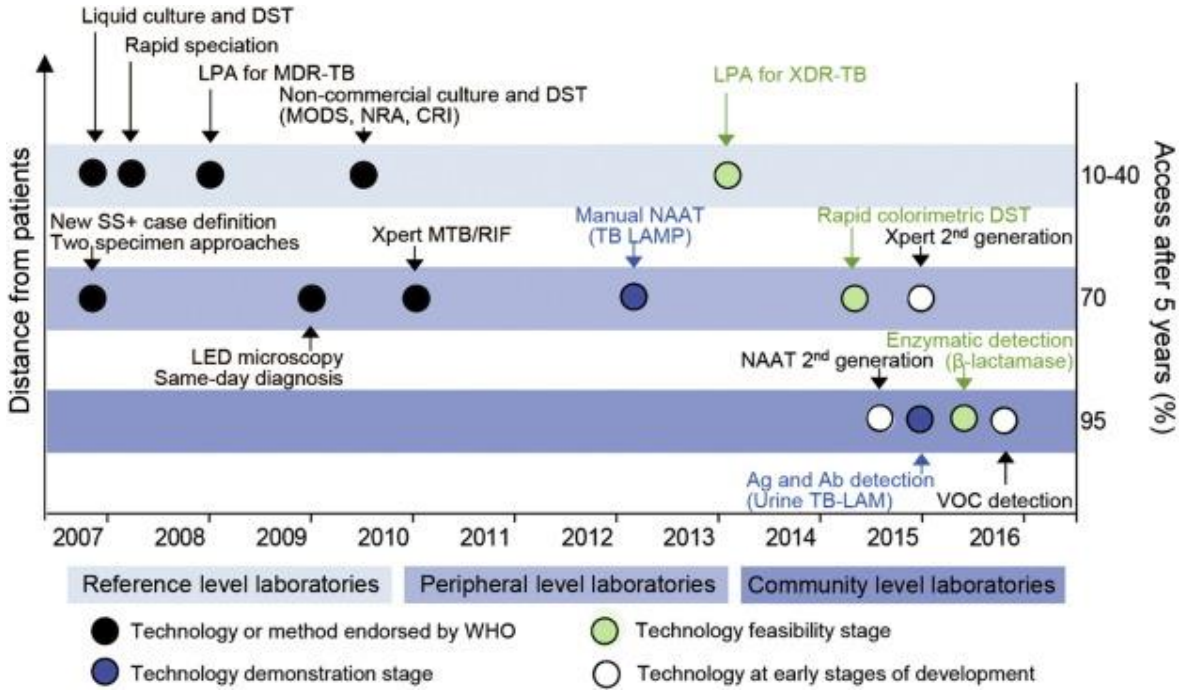

Figure 1.5 Novel tuberculosis diagnostic pipeline

There are innovations at different levels of the health care system. Image adapted from Cheon *et al.* (Cheon *et al.*, 2016).

1.9 Biomarkers of disease

The Biomarkers Definitions Working Group defined a biomarker as "a characteristic that is objectively measured and evaluated as an indicator of normal biological processes, pathogenic processes, or pharmacologic responses to a therapeutic intervention."(Atkinson *et al.*, 2001). Typical biological molecules that are used in diagnosis include: metabolites, lipids, proteins and nucleic acids.

A key criterion for biomarkers intended for diagnostic purposes is that they should be detectable in patient specimens. Several promising biomarkers have been identified for tuberculosis diagnostics (Walzl *et al.*, 2008; Tucci, González-Sapienza and Marin, 2014; Young *et al.*, 2014). The concentration of biomarkers in TB patient specimens is often correlated with bacterial load (Yanez *et al.*, 1986; Boehme *et al.*, 2005; Wallis *et al.*, 2009), although Chanteau *et al.* speculated that secreted antigens cannot accumulate in sputum as they might in serum.

Sputum is continuously expectorated, but antigens in serum circulate for some time (Chanteau *et al.*, 2000). Diagnostics with several biomarkers or a bio-signature tend to have increased specificity and sensitivity.

1.9.1 Patient Specimens

Previous studies detecting biomarkers in sputum had poor specificity (33.3-95.6%) and sensitivity (9-60%) despite sputum originating at the site of disease and containing live mycobacteria (Yanez *et al.*, 1986; Chanteau *et al.*, 2000; Dheda *et al.*, 2010; Reither *et al.*, 2010). Culturing patient sputum specimens improves biomarker detection and allows for speedy verification of *M. tuberculosis* presence. However this approach does not contribute towards a point-of-care diagnostic (Park *et al.*, 2009; Feng *et al.*, 2011; Namba, 2013). Additional drawbacks are that collecting sputum poses a risk to health care workers and that some patients have difficulty producing sputum or have paucibacillary specimens, including HIV patients and children (Zar *et al.*, 2005; J. G. Peter *et al.*, 2012). Sputum could be a useful specimen for biomarker detection if sensitivity and specificity are improved. However, other patient specimens should be considered to avoid putting health care workers at risk and so as to diagnose patients who cannot readily produce sputum or who have extrapulmonary TB.

Several extrapulmonary specimens have been studied for biomarker based diagnostics including biopsies, cerebrospinal fluid and lymph node aspirate. Diagnostic sensitivity and specificity range from 8-100% and 76-100% respectively across several types of extrapulmonary specimens and biomarkers, as laid out by a meta-analysis (Flores *et al.*, 2011). Some of the most promising studies were in meningeal TB, which often has poor outcomes due to late diagnosis. However, obtaining cerebrospinal fluid or other extrapulmonary specimens is invasive; hence, an alternative procedure would be preferable (Wang *et al.*, 2002; Kashyap *et al.*, 2009; Flores *et al.*, 2011).

Serum is a commonly used specimen for diagnosis of other diseases due to its extensive contact with the rest of the body. While serum collection is less invasive and dangerous than sputum collection, the needle prick is a risk factor when patients are HIV positive. Host protein bio-signatures in serum have been identified for TB; however, they have not been validated or are too expensive to implement as a diagnostic tool (Achkar *et al.*, 2015; Xu *et al.*, 2015). *M. tuberculosis* antigens have also been identified but not validated and may be sequestered into immuno-complexes (Chan *et al.*, 2000; Kruh-Garcia *et al.*, 2014). Looking for novel biomarkers in serum by mass spectrometry is complicated by albumin and immunoglobulins that mask less

abundant proteins. Moreover, depleting samples of albumin can result in loss of low abundance proteins.

Urine is a particularly attractive specimen because it is easy to collect from everyone, is non-invasive and poses little risk to health care workers. However, pathogen-derived biomarkers may be excluded by the glomerular basement membrane or, if antigenic they may be cleared by antibodies before reaching the urinary compartment. Hence the concentration of biomarkers in urine is usually low, resulting in poor sensitivity (Reither *et al.*, 2009; Minion *et al.*, 2011; Pollock *et al.*, 2013), unless the urine samples are concentrated (Tessema *et al.*, 2001; Choudhry *et al.*, 2002; Savolainen *et al.*, 2013). Despite low concentrations, several biomarkers including proteins, lipids and DNA have been identified in urine (Choudhry *et al.*, 2002; Boehme *et al.*, 2005; Kashino *et al.*, 2008; Napolitano *et al.*, 2008; Alves da Cruz *et al.*, 2011; Young *et al.*, 2014). However, few have yet been validated or used in commercial test kits (WHO, 2015b; Cheon *et al.*, 2016; Haas *et al.*, 2016).

In the context of TB, either host or pathogen-derived biomarkers may serve as indicators of active or latent disease. Host-derived biomarkers arise from changes in the host in response to the pathogen. Pathogen-derived biomarkers are cell components or products of the pathogen.

1.9.2 Host-derived biomarkers

Host-derived biomarkers include dysregulated human proteins or lipids, changes in gene expression, or immunological biomarkers (Walzl *et al.*, 2011). Host-derived biomarkers are typically grouped to form a bio-signature or barcode. While serum is the typical clinical sample, differences in urine have been observed (Young *et al.*, 2014). The two main drawbacks with host-derived biomarkers are: the changes are usually small and often it is difficult to find a bio-signature that is specific to one disease state.

Gene expression studies aim to analyse the change in transcripts of microRNA or RNA between healthy and diseased states (Maertzdorf *et al.*, 2012; Zhang *et al.*, 2014). Most differentially expressed human genes for TB are related to inflammatory responses to disease, for example, IFN-γ inducible genes (Berry *et al.*, 2010; Bloom *et al.*, 2013; Lee *et al.*, 2016). The caveat with this approach then is that the signature is not specific to TB. To minimise this caveat, gene expression profiles from TB patients have been compared to other diseases that are clinically similar to TB or are common co-infections (Bloom *et al.*, 2013; Kaforou *et al.*, 2013). However, these comparisons have only been performed with small cohorts. Gene expression signatures could be helpful in identifying individuals at risk of converting from latent to active TB or for

treatment monitoring. However, it is currently an expensive and unreliable method for a point-of-care diagnostic (Berry *et al.*, 2010; Zak *et al.*, 2016).

Differentially expressed host proteins have also been identified which could be used as a bio-signature (Liu *et al.*, 2010; Young *et al.*, 2014; Xu *et al.*, 2015).

1.9.3 Pathogen-derived biomarkers

Lipid, and nucleic acid based biomarkers are the most studied biomarkers for TB diagnosis, although small molecule and protein biomarkers are also being explored (Tucci, González-Sapienza and Marin, 2014; McNerney *et al.*, 2015; Pan *et al.*, 2015). Nucleic acid based biomarkers typically have to be extracted from whole bacterium. Whole bacteria are usually acquired from sputum which is problematic as discussed above. Small molecule biomarkers are currently only detectable by mass spectrometry (Pan *et al.*, 2015) hence this discussion will focus on protein and lipid biomarkers.

Pathogen-derived biomarker diagnostics have typically been aimed at cerebrospinal fluid for meningeal TB and severely immunocompromised HIV patients. Nevertheless, there is scope for diagnosis of pulmonary and other types of extrapulmonary TB with biomarkers (Flores *et al.*, 2011; Tucci, González-Sapienza and Marin, 2014; Shah *et al.*, 2016).

Currently, most assays detect secreted protein biomarkers such as MPT64 after culturing the mycobacteria from patient samples rather than directly from the samples (Parsons *et al.*, 2011; Namba, 2013; Tu *et al.*, 2015). The secreted protein biomarkers are in low concentrations in patient samples and current techniques cannot detect them. Culturing the mycobacteria in large volumes increases the amount of secreted protein to levels that can be detected.

As technology has developed, the ability to identify a broader set of potential protein biomarkers has improved. Instead of relying on mycobacterial components that are recognised by antibodies, proteins can be detected directly. For example, mycobacterial proteins have been identified in serum and urine using mass spectrometry (Kashino *et al.*, 2008; Napolitano *et al.*, 2008; Kruh-Garcia *et al.*, 2014; Young *et al.*, 2014). A disadvantage of protein biomarkers is that, unlike nucleic acids, they cannot be amplified by a process such as PCR albeit, they are less prone to degradation than nucleic acids.

Lipids, such as the mycolic acids and LAM can also serve as biomarkers. Mycolic acids can be used to distinguish between mycobacterial species and to diagnose tuberculosis. However, current methods require expensive equipment and highly trained personnel (Butler and

Guthertz, 2001; Shui *et al.*, 2012; Szewczyk *et al.*, 2013).

LAM is the most well-known biomarker of TB and has been extensively studied (Flores *et al.*, 2011). An advantage of LAM as a biomarker is that it can be detected while still part of an intact mycobacterium or as a free molecule (Hunter, Gaylord and Brennan, 1986). Detection of LAM in sputum is problematic however due to current antibodies not being able to distinguish between LAM and glycolipids from related organisms (Dheda *et al.*, 2010). While LAM is a promising biomarker in urine, it is present in picomolar concentrations for pulmonary tuberculosis (Savolainen, 2014). Hence, new analytically sensitive assays are needed to take advantage of this biomarker. This biomarker will be discussed in further detail in Chapter 2.

New biomarkers as well as new means to measure biomarkers are still needed to underpin the next generation TB diagnostics.

1.10 Biosensor Assays

In order to use non- nucleic acid biomarkers as a diagnostic indicator, they typically need to be captured onto a surface or bead. Once the biomarker is "fixed" on the surface, a detection strategy can be employed with a complementary labelled recognition element or a label-free method. Detection (or signal transduction) techniques for biosensors include electrochemical detection, fluorescence and colorimetric outputs, as well as label-free methods such as SPR and SERS (Zhou, Battig and Wang, 2010; Citartan *et al.*, 2012; Ping *et al.*, 2015).

Point-of-care biosensors are typically either part of a handheld device or a compact benchtop system. Current handheld devices are mostly restricted to lateral flow systems. Although there have been incremental developments in lateral flow technology, features inherent to this technology limit sensitivity and multiplexing (Posthuma-Trumpie, Korf and Van Amerongen, 2009; St John and Price, 2014). Emerging lab-on-chip technology or microchips are set to overcome the short comings of lateral flow systems (Stedtfeld *et al.*, 2012; Sanghavi *et al.*, 2015).

Molecules can adsorb non-specifically to surfaces. However in most diagnostic assays, the biomarker is captured onto the surface by a molecular recognition element (Lopez and Schnaar, 2006). Specific immobilisation onto the surface with a molecular recognition element is preferable for heterogeneous solutions such as patient samples. Target molecules can be purified from other components of a mixture that may contribute to the background signal. Binding affinity is a measure of how well a molecular recognition element binds to its target and it is usually expressed as a molar concentration such as nanomolar affinity. It is defined at

equilibrium by the dissociation equilibrium constant (K_D) which is the quotient of the reactant concentrations and product concentration or the ratio of the dissociation and association rate constants, k_{off} and k_{on} respectively, at equilibrium. For fluorescent and colorimetric detection systems, a secondary binding agent attached to an a fluorescent molecule or enzyme is required (Khatkhatay and Desai, 1999). The two recognition elements must bind in two discrete locations on the target molecule. Hence a label free method of detection is desirable. Antibodies are the most common molecular recognition elements, but aptamers are now also becoming prominent.

Further discussion will focus on aptamers as molecular recognition elements.

Aptamers are short nucleic acid or peptide molecules that have binding capabilities against several types of molecules including proteins, lipids and carbohydrates with affinities from the micromolar to nanomolar range (Betat *et al.*, 2003; Masud *et al.*, 2004; Boese and Breaker, 2007; Bruno *et al.*, 2009; Low, Hill and Peccia, 2009). Nucleic acid aptamers are typically selected by an *in vitro* selection called **S**ystematic **E**volution of **L**igands by **Ex**ponential Enrichment (SELEX)(Tuerk and Gold, 1990), which will be discussed in more detail in Chapter 4. Peptide aptamers can be selected by phage or ribosome display, where peptides are displayed on the exterior of a phage or ribosome and exposed to the target of interest (Kase *et al.*, 2004; Zahnd, Amstutz and Plückthun, 2007).

Peptide aptamers have greater chemical diversity, but the number of molecules that can be tested or selected with phage display methods is more limited than for DNA or RNA aptamers with SELEX. During phage display, the diversity of the library is limited by the transformation efficiency of bacterial cells, but ribosome display overcomes this. Ribosome display does not rely on any transformation into bacterial cells. Random mutations can also be introduced after each round with ribosome display (Zahnd, Amstutz and Plückthun, 2007). Peptide aptamers function in much the same way as binding pockets of enzymes or antibodies where the most favourable amino acids are selected for the ligand. Peptide interactions typically rely on hydrogen bonds, acid base interactions and hydrophobic pockets (Hermann and Patel, 2000).

Nucleic acid aptamer interactions depend on deep pockets to make up for imperfect fitting, pi interactions with nitrogenous bases, ionic interactions with the phosphate backbone, grooves created by Hoogsteen pairing and other interactions depending on the target. Hydrogen bonds are important because they offer short-range directionally specific interactions which often confers specificity.

DNA aptamers tend to have lower affinity for their targets compared to RNA or peptide aptamers (Rowe, Miller and Plaxco, 2010) due to the lack of the reactive 2' hydroxyl group present on RNA and the several amino acid side chains on peptide aptamers. Nucleic acid aptamers have more flexibility because each monomer has seven rotatable bonds whereas proteins only have two(Davies *et al.*, 2012).

Aptamers are well suited for biosensors for several reasons. Aptamers can be raised against non-immunogenic biomarkers identified by for example mass spectrometry. Synthesizing oligonucleotides, especially ssDNA, is more cost effective and reproducible than polyclonal antibody production. Since aptamers are smaller than antibodies, they can be immobilised with higher density on surfaces which provide a larger dynamic range for detection (Tijssen, 1985; Liss *et al.*, 2002; Esteban *et al.*, 2013). Biosensor surfaces with aptamers can be more easily reused by regenerating the surfaces (Kirby *et al.*, 2004). While antibodies need refrigeration, DNA aptamers are more resilient at ambient temperatures which would be beneficial for resource-poor settings without electricity.

Aptamers have been used in several biosensor formats. An adaption of the antibody-based ELISA using aptamers is called an Enzyme Linked OligoNucleotide Assay (ELONA) or enzyme linked aptamer assay (ELAA) (Drolet, Moon-McDermott and Romig, 1996).

Aptamers have also been used in more modern technology such as label-free electrochemical sensors and lab-on-chip or microfluidic devices (Huh and Erickson, 2010; Rowe, Miller and Plaxco, 2010; Janssen *et al.*, 2012; Larguinho *et al.*, 2015; Liu *et al.*, 2015; Ueno *et al.*, 2015; Zheng *et al.*, 2015)

However, DNA aptamers have the disadvantage of being chemically limited, having a tendency for high off-rates. Chemical limitations are somewhat offset by the large shape repertoire in a oligonucleotide library (Davies *et al.*, 2012).

In order to expand the scope of interactions between nucleic acid aptamers and targets, the nucleotides may be modified. Modified aptamers have been shown to have increased affinity and are better at targeting challenging targets such as glycoproteins (Li *et al.*, 2008). Drawbacks of modified aptamers include the variable success with modified aptamers and the time consuming processes needed. However, these pitfalls are being addressed with improved technology and certain modifications have had continued success (Diafa and Hollenstein, 2015).

Aptamers may be modified at the sugar base, nitrogenous base or phosphate backbone (Diafa

and Hollenstein, 2015). A combination of modifications can be used. For example, the aptamer against the hyaluronic acid binding domain of CD44 had a modified backbone and a small drug like molecule attached to the nitrogenous base (He *et al.*, 2012).

Base modifications are made at the C5 of pyrimidines (e.g. UTP, TTP) or the N7 of 7-deaza-purines (ATP) (Figure 1.6). Modifications can be tailored to most likely improve binding to a particular molecule, for example a positive amino group, and was attached at the C5 position when selecting against the negatively charged sialyllactose (Masud *et al.*, 2004). Other examples include a boron modified aptamer against a glycolipid molecule (Li *et al.*, 2008) and attaching hydrophobic groups to facilitate hydrophobic interactions (Vaught *et al.*, 2010). Aptamers modified with amino acid side chains to mimic proteins have been dubbed SOMAmers. Simplistically SOMAmers aim to mimic the hydrophobic pockets of immunoglobulins with amino acid side chains attached to the base (Figure 1.7).

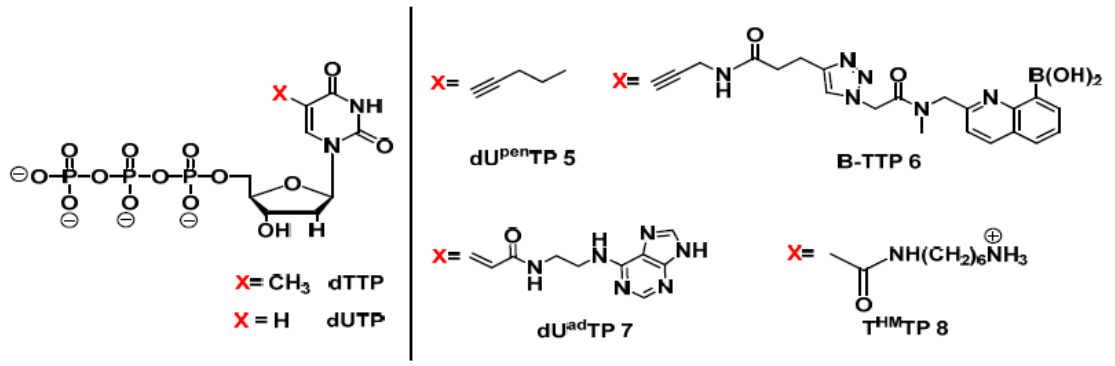

Figure 1.6 Examples of base modifications

Several different molecules can be attached to the nucleotide base. Image adapted from Diafa and Hollenstein (Diafa and Hollenstein, 2015).

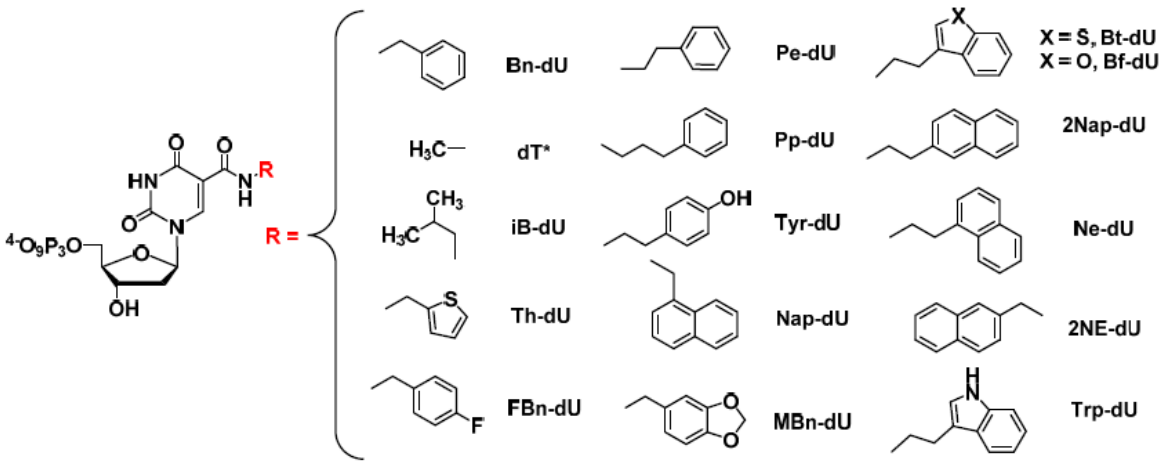

Figure 1.7 SOMAmers

Examples of amino acid side chains attached to nucleotides to generate SOMAmers. Image adapted from Diafa and Hollenstein (Diafa and Hollenstein, 2015).

The *in vitro* selection should be done with the modifications in place, as post selection modification has been shown to diminish binding rather than to improve it as the whole structure changes (Lato *et al.*, 2002). Modification made post-selection is sometimes tolerated (Mendelboum Raviv *et al.*, 2008)

In order to select modified aptamers against a target the modification should not disrupt the ability of RNA or DNA polymerase to replicate the aptamer sequence during the PCR step of the selection process. However, some selection processes do not require replication (Boiziau and Toulmé, 2001). Methodologies for aptamer selection will be discussed in a later chapter. Hence, modified aptamers are viable and promising molecular recognition elements for the detection of TB biomarkers.

1.11 Aims and Objectives

The aim of this thesis is to explore an innovative approach towards developing a point-of-care diagnostic tool for tuberculosis in resource-poor settings. While the focus of this thesis is tuberculosis, this methodology can be in principle applied to new biomarkers identified in any disease.

The main objectives of the thesis are as follows:

- To determine if LAM can be detected in TB patient urine by concentrating the urine.
- To use an in-house ELISA to determine if a secreted *M. tuberculosis* protein can be detected in urine.
- To select modified aptamers against *M. tuberculosis* derived biomarkers.
- To characterise aptamers selected against tuberculosis derived biomarkers.

Secondary objectives arose during the course of this thesis which will be discussed in individual chapters.

2 LAM IN URINE

2.1 Introduction

2.1.1 LAM

LAM is a glycolipid embedded in the cell envelope of *M. tuberculosis*. It is found both in the membrane and as a free lipid in the outer lipid layer. LAM consists of a branched arabinose structure with a mannan core attached to a phosphatidyl-myo-inositol mannoside (Hunter, Gaylord and Brennan, 1986; Hunter *et al.*, 1990; Chatterjee *et al.*, 1992) with two carbon chains, usually tuberculosteric acid (C19) and palmitic acid (C16) (Gilleron *et al.*, 2000). The most abundant size of LAM is 17.4 kDa, however it can vary $\pm$ 4 kDa due to different numbers of glycan units or other appendages (Venisse *et al.*, 1993; Nigou, Vercellone and Puzo, 2000).

LAM also has various capping motifs on the tip of the arabinose branches depending on the species of mycobacteria (Figure 2.1). Pathogenic species such as *M. tuberculosis*, *Mycobacterium bovis* (including the BCG vaccine strain) (Venisse *et al.*, 1993), *Mycobacterium avium (Khoo, Tang and Chatterjee, 2001)*, *Mycobacterium kansasii* and *Mycobacterium leprae* have mannose caps; this type of LAM is designated manLAM. Non-pathogenic mycobacteria may have inositol phosphate caps (piLAM) such as *Mycobacterium smegmatis (Khoo et al., 1995)* or no capping motifs (araLAM) such as *Mycobacterium chelonae (Guerardel et al., 2002)* and an avirulent strain of *M. tuberculosis* (H37Ra) (Chatterjee *et al.*, 1991).

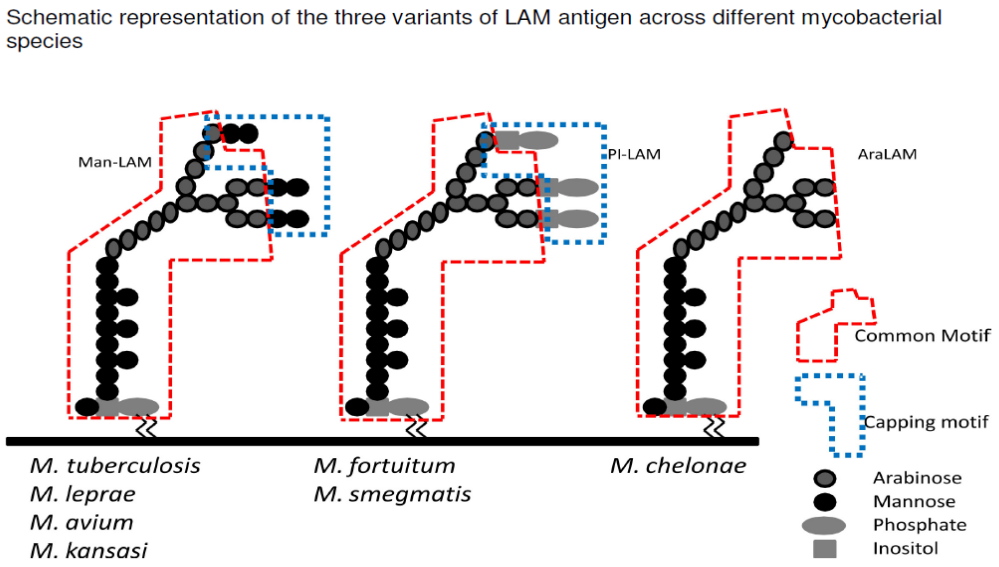

Figure 2.1 Structure of LAM across various species

The common structure of LAM consisting of the mannan backbone and phosphoinositol group is delineated by a red dotted line. Three different capping motifs are delineated by a blue dotted line. From left to right; ManLAM; piLAM and AraLAM. Image from Sarkar *et al.* (Sarkar *et al.*, 2014).

LAM is an immunomodulator, which means it helps the bacterium to avoid destruction within the macrophage (Knutson *et al.*, 1998; Nigou *et al.*, 2001). The differing caps affect how the host immune response reacts; AraLAM is proinflammatory (Gilleron *et al.*, 1997) and manLAM is anti-inflammatory, hence manLAM stalls the inflammatory response. LAM vesicles are intentionally released by *M. tuberculosis* at the primary site of infection to regulate the host response. Therefore, LAM may serve as a good diagnostic biomarker as it is able to escape the macrophage phagosome and be released into the blood stream, making it more likely to be present in urine which is a convenient and safe specimen (Xu *et al.*, 1994; Beatty *et al.*, 2000).

Antibodies against *M. tuberculosis* antigens have been previously detected in patient blood, which led to the investigation of serologic-based diagnostics by many researchers (Sada *et al.*, 1992; Steingart *et al.*, 2011). Later, LAM was identified as a specific antigen, amongst others (Sada *et al.*, 1990). Although several studies have successfully detected antibodies against *M. tuberculosis* antigens, a feasible serum-based diagnostic test has yet to be developed and commercialized (Steingart *et al.*, 2007). A diagnostic test that does not require growing or

visualizing the mycobacterium may lead to faster and more affordable diagnosis of patients suspected of having tuberculosis.

Sada *et al.* suggested that if there was an antibody response to LAM, it was likely that LAM would be present in tuberculosis patient blood and thus an antigen could be detected, rather than antibodies (Sada *et al.*, 1992). Unfortunately the detection of LAM in patient blood samples is hampered because LAM forms complexes with anti-LAM antibodies and high density lipoproteins, concealing LAM amongst the immunoglobulins and micelles (Chan *et al.*, 2000, 2015; Sakamuri *et al.*, 2013). Given this limitation, other matrices were explored, which included urine.

M. tuberculosis antigens in urine were recognised by Wildbolz in the early 20th century (Young, 1924), and LAM is currently the most frequently studied tuberculosis antigen in urine (Flores *et al.*, 2011). However the sensitivity of detection varies from 8-80% when clinical and culture-confirmed cases are combined (Minion *et al.*, 2011). Patients with a high bacterial load in their sputum are more likely to have a positive urinary LAM ELISA (Boehme *et al.*, 2005). The sensitivity of ELISAs also increases for HIV patients, as they become more immunosuppressed. Increased levels of LAM detected in urine samples may be due to genitourinary TB, renal failure and mycobacteriuria (Dheda *et al.*, 2010; Shah *et al.*, 2010; Jonathan G Peter *et al.*, 2012).

Up to 20% of pulmonary patients develop the urogenital form of extrapulmonary TB (Abbara and Davidson, 2011), which would account for some of the LAM detected in urine (Figure 2.2). A report that compares Xpert MTB/RIF® to the Clearview® LAM ELISA supports the idea that LAM in urine originates from viable *M. tuberculosis* being present in the renal tract compartment (Wood *et al.*, 2012). While not all LAM positive patients were Xpert MTB/RIF® positive, the limit of detection of the LAM ELISA is approximately 10-fold lower than that of the Xpert MTB/RIF® assay. A recent study showed that 10 CFUs (culture forming units) of *M. tuberculosis* is sufficient to give a signal of ~1.5 OD, which is well above the cut-off value for the LAM ELISA (Savolainen *et al.*, 2013), while the limit of detection for Xpert MTB/RIF® is nominally about 130 CFUs although in practice the limit of detection is closer to 1000 CFUs. Few cells are necessary for a positive test because LAM makes up a large proportion of the cell wall (15mg/g of the dry weight of mycobacteria) (Hunter, Gaylord and Brennan, 1986).

Viable *M. tuberculosis* and LAM from degraded bacteria in the blood may also contribute to the levels of LAM in urine (Shah *et al.*, 2010). The glomerular basement membrane (GBM) would have to be damaged for viable *M. tuberculosis* or immuno-complexed LAM to enter the urinary tract, however free LAM can fit through the intact glomerular membrane (Figure 2.2) (Cox *et*

al., 2015). BCG-vaccinated individuals tend to have more circulating anti-LAM antibodies, and therefore less free LAM is likely to be present in those individuals (Chan *et al.*, 2015). Since most TB patients do not have either extrapulmonary disease or renal dysfunction, only small amounts of free LAM are likely to enter the urinary tract. Consequently, some studies have concentrated urine samples as a means to increase the likelihood of LAM detection.

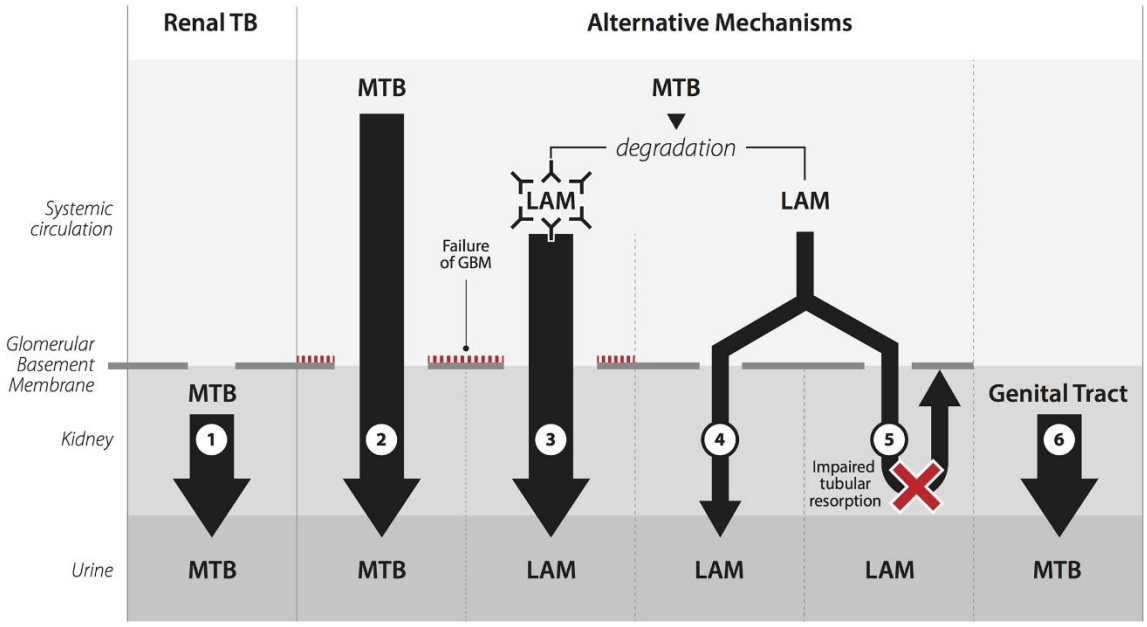

Figure 2.2 Mechanisms of LAM entry into urine

1 and 6) *M. tuberculosis* is present in the urogenital organs so whole bacteria can be detected in urine. **2 and 3)** A damaged GBM allows whole *M. tuberculosis* cells or immuno-complexed LAM to enter the urine. **4 and 5)** Free LAM filters through the GBM into the urine and is not reabsorbed into the blood stream.

Image from Cox *et al.* (Cox *et al.*, 2015).

Tessema concentrated urine samples and achieved good sensitivity and specificity in his assays (Tessema *et al.*, 2001). However this approach is impractical in a clinical setting, and others attempted to create assays using unprocessed urine samples instead (Boehme *et al.*, 2005; Daley *et al.*, 2009). After poor sensitivity results were obtained with unprocessed urine, a study concentrated urine with a 10 kDa molecular weight cut off (MWCO) filter before applying it to the Clearview LAM ELISA in a cohort of advanced immunosuppressed HIV patients. Concentrating the urine only marginally increased the mean sensitivity from 33% to 38%

(Lawn *et al.*, 2009). The increase in sensitivity may have been greater if a smaller filter pore size had been used, as some LAM (17 kDa) could have been lost through the 10 kDa filter. Salvolain *et al.* used a cohort of HIV negative patients and concentrated urine 100-fold with a 7.5 kDa MWCO filter, and were able to improve the assay sensitivity from 7 % to 57% (Savolainen *et al.*, 2013). These findings suggest that LAM is present in urine, however it cannot be detected by current tools without prior sample concentration.

The detection of LAM in urine is very specific unless the patient has certain urinary tract or bladder infections, such as *Candida albicans,* that can cross react with the anti-LAM antibodies. Hence urine is preferable to sputum, as the latter has too many oral commensals that may cross react with the anti-LAM antibodies (Dheda *et al.*, 2010).

2.1.2 Aims and Objectives

We set out to confirm the findings of Tessema *et al.* and others across a small sample of patients using the Clearview LAM ELISA and a concentration method which should reduce the likelihood of LAM loss. Concentrating the urine samples increases the amount of LAM bound to antibodies at equilibrium, and therefore should increase the resulting absorbance reading.

The first objective of the following experiments was to determine whether concentrating urine by lyophilisation or evaporation would negatively affect the ELISA assay. The second objective was to demonstrate that by concentrating these TB patient urine samples, and consequently the biomarker LAM, more patients would have a positive diagnostic test, particularly if they were not severely immunocompromised due to HIV.

2.1.3 Methodology

Enzyme linked immunosorbent assays have been used since the 1970's as a method of capturing and detecting various molecules (Engvall and Perlmann, 1971). The basic principle of ELISAs is to measure the amount of antigen adsorbed on the surface *via* colorimetric feedback dependant on the amount of enzyme indirectly attached to the antigen *via* one or two antibodies. The antigen can be adsorbed directly to the surface or captured onto the surface by an antibody adsorbed onto the surface (sandwich assay). A blocking agent such as BSA or casein prevents molecules binding non-specifically to the surface once the antibody or antigen has been adsorbed to the surface (Crowther, 2009). Sandwich assays tend to be more sensitive probably due to better retention and presentation of the antigen (Kemeny *et al.*, 1985). Direct ELISAs detect the antigen with an antibody directly conjugated with an enzyme whereas

indirect ELISAs have two antibodies for detection, one binds the antigen (primary antibody) and another enzyme conjugated antibody binds the constant region of the first antibody (secondary antibody) (Crowther, 2009). While several enzymes can be used, antibodies are typically conjugated with Horse Radish Peroxidase (HRP). HRP is a monomeric glycoprotein which forms stable conjugates with antibodies and has a high substrate turnover rate (Khatkhatay and Desai, 1999). While several substrates are available for use in conjunction with HRP, 3,3',5,5'-tetramethylbenzidine (TMB) is the most sensitive and rapid.

2.2 Methods

2.2.1 Patient Population

Ethical approval was obtained from the Human Research Ethics committee at the Faculty of Health Sciences, UCT. HREC/REF: 787/2014 to collect and use patient urine for research pertaining to diagnostic research. Healthy volunteers do not require ethical approval.

UA cohort patient samples used in these experiments were HIV positive with a CD4 count < 200 cells/µl (Appendix A: Table A1), whereas LAMP cohort patients were either HIV negative or had a CD4 > 200 cells/µl (Table 2.1).

TB disease was confirmed with culture and IGRA tests were performed to classify latent tuberculosis disease.

Table 2.1 LAMP Cohort

LAMP Study No	**HIV**	**CD4**	**TB status**
28	Positive	486	TB-Pos
33	Negative	n/a	TB-Pos
44	Negative	n/a	TB-Pos
151	Positive	214	TB-Pos
227	Negative	n/a	TB-Pos
254	Positive	n/a	TB-Pos
271	Negative	n/a	TB-Pos
275	Positive	240	TB-Pos
298	Negative	n/a	TB-Pos

2.2.2 Urine preparation

Urine samples collected from healthy volunteers and patients were thawed (if needed) and centrifuged for 15 min at 3000 rcf to remove debris. The supernatant was concentrated either by lyophilisation or evaporation, and reconstituted in a smaller volume. Urine samples were frozen at -80 °C in volumes of 10 ml, and were then lyophilised for ~8 h to remove most liquid. Samples were also concentrated by evaporation while being centrifuged to retain dried material. Lyophilised and evaporated samples were reconstituted in 1-1.5 ml of PBS (Sigma # P4417; pH 7.4). Any particulate matter was pelleted by centrifugation for 5 min at 3000 rcf and the supernatant was used for the subsequent assays. Whilst the UA cohort urine samples were fresh, the LAMP cohort of urine samples were frozen. Additionally, neat healthy volunteer urine was adjusted to pH 7 with sodium hydroxide (NaOH) to approximately match the pH of PBS. After processing all urine samples were frozen at -80 °C.

2.2.3 LAM ELISA

The Clearview® ELISA was performed as per manufacturer's instructions. Briefly, 100 µl of urine was incubated in a well of a 96 well plate for ~1 h. After ~1 h the urine was discarded, and the plate was washed three times with wash buffer (PBS, pH 7.4; 0.05% Tween 20). Anti-LAM HRP conjugated antibody (100 µl) supplied in the kit was added to the wells and incubated for ~ 1 h. Another set of three washes was performed and then 100 µl of the substrate TMB was added. TMB was incubated for 15 min before the reaction was stopped with 100 µl of 1 M sulphuric acid (H_2SO_4), and the absorbance of each well was read at 450 nm with an iMark microplate reader (BioRad). A negative and positive control were included (supplied in kit) and samples were performed in duplicate or triplicate. The cut-off value was calculated as per the manufacturer's recommendation by adding 0.1 to the negative control. Incubations with urine and antibody were performed at 37 ºC.

Binding curves where created using purified LAM kindly donated by the Lung and Infection Immunity Unit, University of Cape Town or BEI Resources, NIAID, NIH (*Mycobacterium tuberculosis*, Strain H37Rv, Purified Lipoarabinomannan (LAM), NR-14848). A 2-fold dilution was performed in order to plot a binding curve.

2.3 Results

2.3.1 Binding curves

In order to assess if concentrating urine or adjusting the pH of the urine would change the performance of the ELISA, five different media based on healthy volunteer urine were spiked with LAM at various concentrations. The binding curves are presented in Figure 2.3. The different media did not change the linear nature of the curve, although the lyophilized and evaporated samples had slightly reduced signals overall. The concentrated samples had a signal ~0.1 OD units lower than the PBS based sample at the highest concentration of LAM. Urine with a neutral pH did not change considerably compared to neat urine.

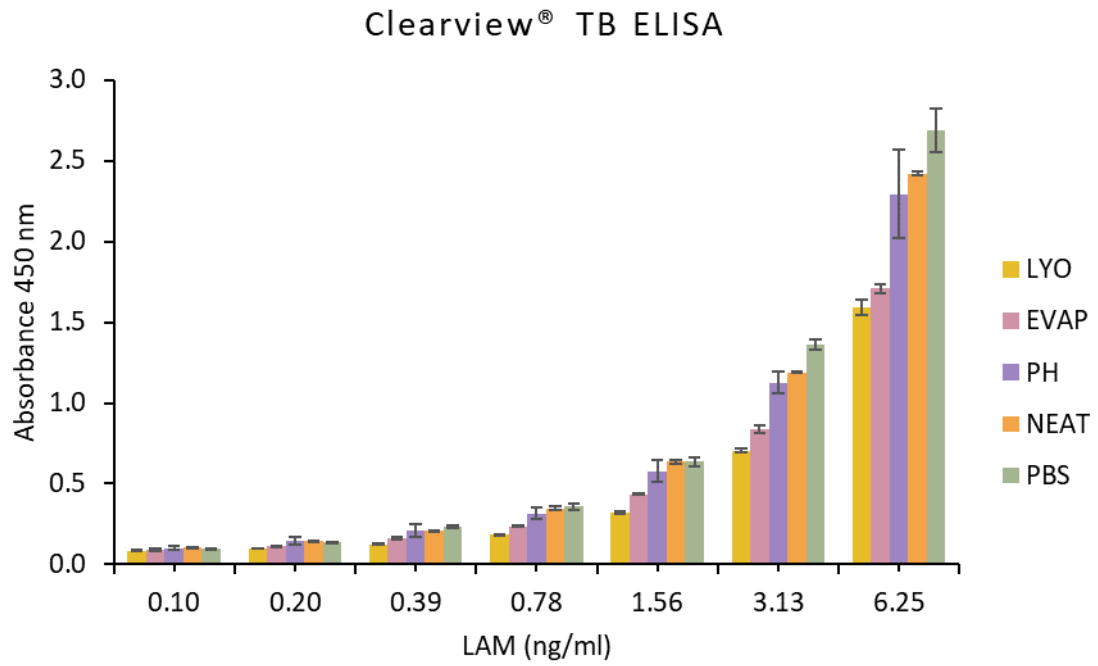

Figure 2.3 Binding curves for concentrated, neat and pH adjusted healthy volunteer urine spiked with LAM.

PBS-Phosphate Buffered Saline (control); NEAT-unconcentrated urine; LYO-urine concentrated by lyophilisation; EVAP-urine concentrated by evaporation; PH-urine adjusted to ~pH 7. Columns indicate the mean reading of duplicate wells. Error bars indicate the minimum and maximum readings taken.

2.3.2 Concentrated Urine Samples

Given that concentrating the urine did not severely impact the performance of the spike-in assay, we concentrated patient urine samples to compare the differences in LAM detection using concentrated and unconcentrated samples.

LAM ELISA - UA Cohort

Ten random culture-confirmed TB patient's urine from the UA cohort were concentrated via lyophilisation from 10 ml to 1-1.5 ml and compared to unconcentrated urine or to previous results of the unconcentrated sample (Figure 2.4). The results are presented in Table 2.2, and results from previous experiments are denoted "neat (database)". Some neat samples were not tested again. It appeared that all samples that were positive in the concentrated batch were also positive when neat urine was tested, with the exception of UA 133 which was negative in the repeat experiment but had previously tested positive. The ratio of concentrated versus neat urine was calculated to estimate the fold change in signal (Table 2.2). The UA310 and UA215 concentrated sample gave a marginally greater signal than the neat urine.

LAM ELISA - LAMP Cohort

Nine culture confirmed TB patients with a CD4 count >200 cells/µl or who were HIV negative were selected from the LAMP cohort. Urine samples were concentrated via lyophilisation from 10 ml to 1-1.5 ml and compared to unconcentrated urine. The results are presented in Figure 2.5. Two out of the nine patients had a positive result with neat urine. Two additional patients had a positive result after concentrating the urine. All patients who had a positive result had a higher signal after concentrating the urine. The ratio of concentrated versus neat urine was calculated to estimate the fold change in signal (see Table 2.3 LAMP cohort results). Concentrating the urine improved the signal for four of the nine TB patients. Two changed from negative to positive after concentrating.

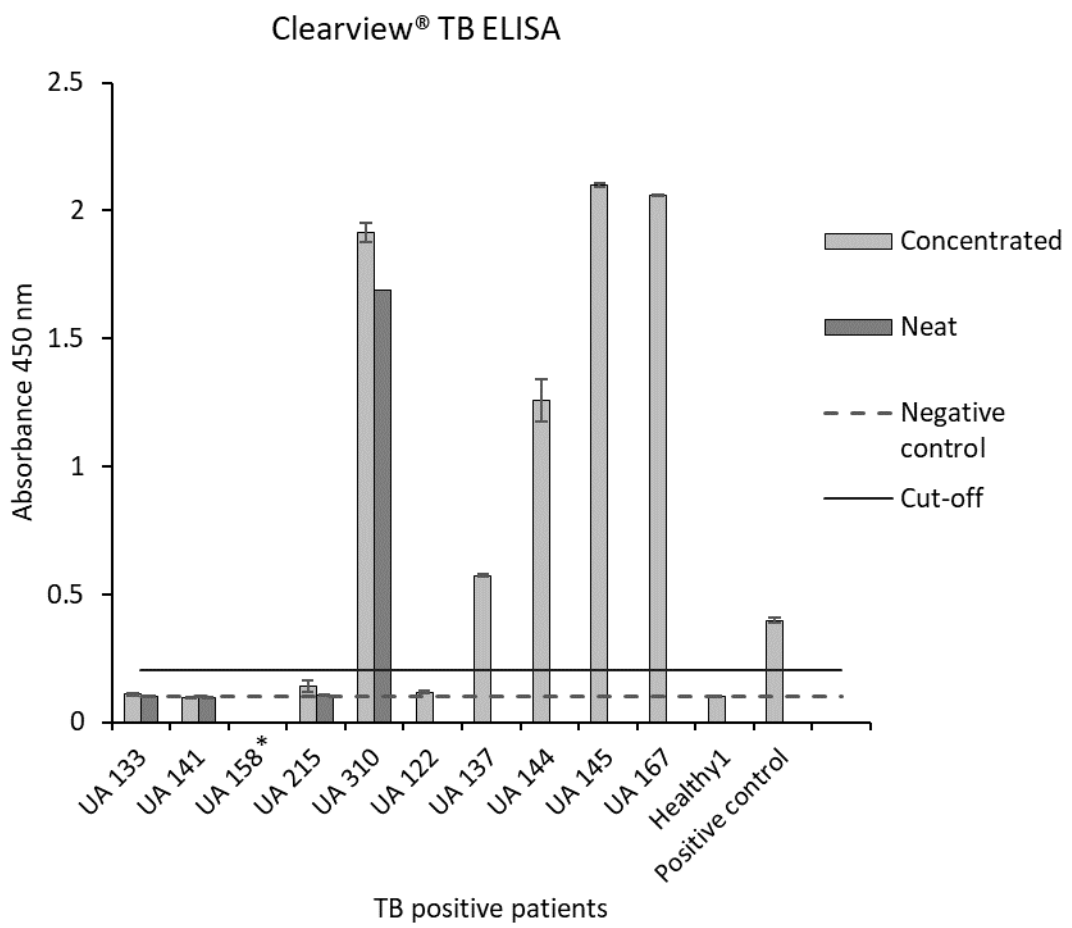

Figure 2.4 Concentrated and Neat urine for UA cohort

*UA158 had absorbance >3.5 OD for concentrated and neat samples and the indication range of the iMark (BioRad) is 0.0-3.5 OD. Neat samples for UA122, UA137, UA144, UA145 and UA167 were not tested in this experiment. Cut-off was determined by adding 0.1 to the negative control. Columns indicate the mean reading of duplicate or triplicate wells. Error bars indicate the minimum and maximum readings taken.

Table 2.2 UA Cohort results

	UA 133	**UA 141**	**UA 158**	**UA 215**	**UA 310**	**UA 122**	**UA 137**	**UA 144**	**UA 145**	**UA 167**
Concentrated	-	-	*	-	+	-	+	+	+	+
Neat	-	-	*	-	+	np	np	np	np	np
Neat (database)	+	-	+	-	+	-	+	+	+	+
Conc: Neat ratio	1.06	1.03	*	1.34	1.13	np	np	np	np	np

* Signal >3.5 Note: Indication range of iMark (BioRad) is 0.0-3.5 OD, np: not performed.

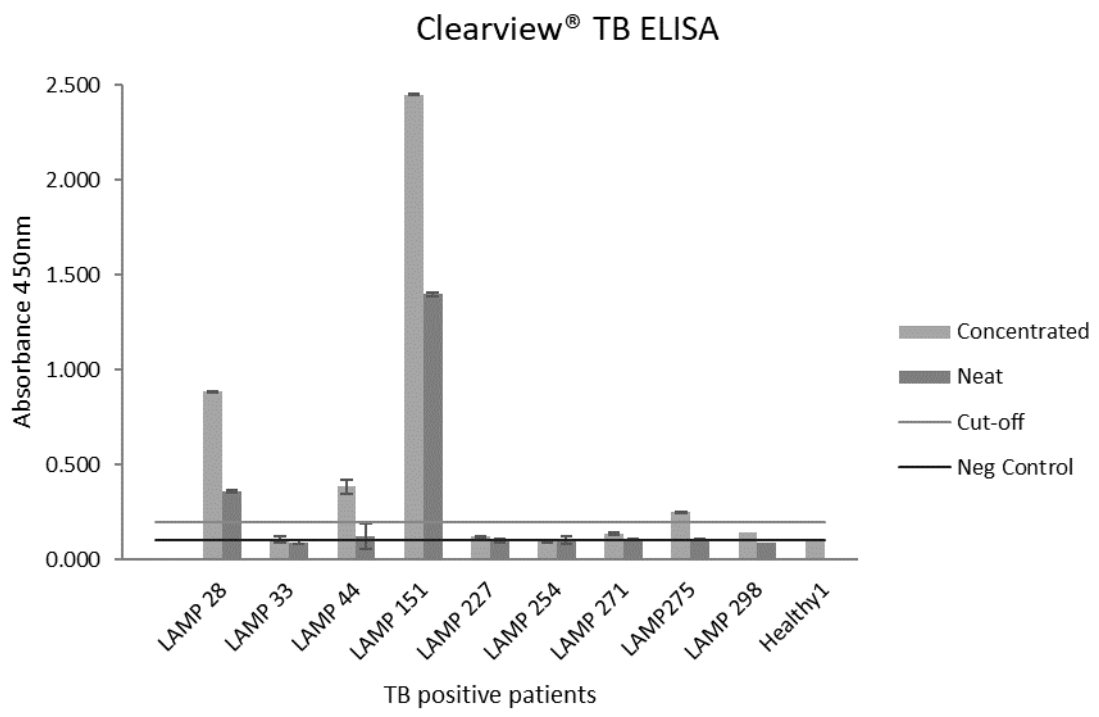

Figure 2.5 Concentrated and Neat urine for LAMP cohort

Conc urine: Urine concentrated by lyophilisation; Neat urine; unprocessed urine from the same patient sample. Cut-off was determined by adding 0.1 to the negative control. Columns indicate the mean reading of duplicate or triplicate wells. Error bars indicate the minimum and maximum readings taken.

Table 2.3 LAMP cohort results

	LAMP 28	LAMP 33	LAMP 44	LAMP 151	LAMP 227	LAMP 254	LAMP 271	LAMP 275	LAMP 298
Conc urine	+	-	+	+	-	-	-	+	-
Neat urine	+	-	-	+	-	-	-	-	-
Conc: Neat ratio	2.5	1.1	3.1	1.8	1.2	0.9	1.3	2.3	1.6

2.4 Discussion

2.4.1 Binding curves

Samples concentrated by lyophilisation or evaporation were compared to PBS and neat urine.

The concentrated urine matrix gave a slightly lower signals compared to the PBS or the neat samples. This could be due to the method of concentration which increased the salt concentrations of the samples. Solutions with a higher ionic strength are known to increase the disassociation between antibodies and their targets (Reverberi and Reverberi, 2007) which would result in a lower OD reading. In future experiments it would be beneficial to use methods of concentration that do not result in high salt concentrations, such as MWCO columns. Purification columns and MWCO filters have been used in the past, however some LAM could be lost during this kind of process if the filter pore sizes are too large (Tessema *et al.*, 2001; Lawn *et al.*, 2009).

Urine adjusted to pH 7 was also compared to PBS and neat urine. Urine with a neutral pH did not change considerably compared to neat urine which suggests the slightly acidic pH of urine is not detrimental to the assay.

Since the matrix effects due to concentration of urine did not appear to be significant, lyophilization of a test cohort of patient urine samples was used to explore the effect of concentrating urine on LAM ELISA results.

2.4.2 UA cohort

In the first ELISA with concentrated patient urine, patients had culture confirmed TB and were HIV positive. Patients with culture confirmed TB were selected to assess if concentrating the urine would allow for increased detection of LAM. Eight of these patients had a CD4 count of < 200 cells/µl, except for patients UA144 and UA167 whose CD4 count was unknown. In agreement with several publications most of these patients who were HIV positive with a CD4 count of less than 200 cells/µl were LAM positive (Jonathan G Peter *et al.*, 2012; Lawn *et al.*, 2012). In addition, patient UA310 had renal disease which could have likely led to antigenuria. However, patient UA215 also had renal disease and did not have a positive LAM result with concentrated or unconcentrated urine although the concentrated urine sample did have a higher OD reading than the neat sample. Hence, renal disease is not necessarily a predictor of whether a TB patient will be LAM positive or not. UA133 was LAM negative in this set of experiments however in an ELISA performed by collaborators this patient was LAM positive. This could be due to LAM being lost in the precipitation that sometimes forms when freezing urine (Mataija-Botelho et al., 2009).

UA310's signal did not increase dramatically after concentrating the urine, which could be due to the fact that the antibodies were saturated, and thus the signal could not be further increase. According to the binding curve performed by Savolainen *et al*. the maximum concentration of LAM is ~20 ng/ml that yields a reading of 3 OD (Savolainen et al., 2013). A limitation of this study is that a saturation curve of LAM spiked in urine was not performed to quantify the amount of LAM in each patient.

2.4.3 LAMP cohort

In the second set of LAM ELISA experiments patients had culture confirmed TB and were either HIV negative or HIV positive with a CD4 count of >200 cells /µl. Patients LAMP 28 and LAMP 151 were positive before and after concentration, while LAMP 44 and LAMP 275 became positive after concentration. LAMP 44 was HIV negative and LAMP 151 was HIV positive with a CD4 count of 214 cells /µl. The fold increase of the signal was not proportional to the 10-fold concentration of the urine, which may be partially due to the slightly dampened signal observed in the concentrated urine matrix in the calibration curves (Figure 2.5).

In this second experiment we have shown that the sensitivity of the conventional LAM ELISA is suboptimal, as patients may have LAM present in their urine even if they are HIV negative, but it is not detected by the LAM ELISA without concentrating the urine. This warrants the

exploration of methods which are more sensitive, while retaining specificity for detection of LAM in urine.

2.5 Conclusion

Although concentrating urine samples caused the signal to be slightly dampened concentrating TB patient urine still increased the number of patients that were LAM positive. This exploratory work formed the foundation for the search of a more sensitive and specific capture agent in order to improve the detection of LAM in unprocessed urine. In future work the BCG status of patients should be taken into consideration.

3 PROBING FOR ESAT-6 AND CFP-10 IN URINE AND SPUTUM

3.1 Introduction

3.1.1 ESAT-6 and CFP-10

Early secreted antigen target 6 kDa (ESAT-6) was first discovered as part of a cohort of T-cell antigens secreted by *Mycobacterium tuberculosis* (*M. tuberculosis*) (Andersen *et al.*, 1991, 1995; Sørensen *et al.*, 1995). Although initially estimated to have a molecular weight of 6 kDa, ESAT-6 is in fact a ~9 kDa protein (The UniProt Consortium, 2014). It was subsequently revealed that culture filtrate protein 10 kDa (CFP-10) is co-expressed with ESAT-6 because they are encoded together in an operon (Berthet *et al.*, 1998). Although both proteins are found in culture filtrate they lack classic secretion signal sequences (Vizcaíno *et al.*, 2010). Guinn *et al.* identified key genes for the ESAT-6 secretion system 1 (ESX-1) by mutating genes flanking ESAT-6 (*Rv3875*) and CFP-10 (*Rv3874*) (Guinn *et al.*, 2004). Many of the genes do not have readily predictable functional domains, however ATPases and transmembrane proteins have been identified among the key components (Digiuseppe Champion and Cox, 2007).

ESAT-6 forms a tight 1:1 heterodimer with CFP-10 which provides thermodynamic and biochemical stability to both proteins (Figure 3.1) (Renshaw *et al.*, 2002; Meher *et al.*, 2006). However, they also form homodimers, and CFP-10 can interact with another protein encoded by gene *Rv3873* (Teutschbein *et al.*, 2009). In an acidic environment, such as inside the macrophage (Vandal, Nathan and Ehrt, 2009), ESAT-6 and CFP-10 dissociate and the monomeric ESAT-6 binds to lipid bilayers *via* hydrophobic helices; this may be important for *M. tuberculosis* escape from phagosomes (de Jonge *et al.*, 2007).

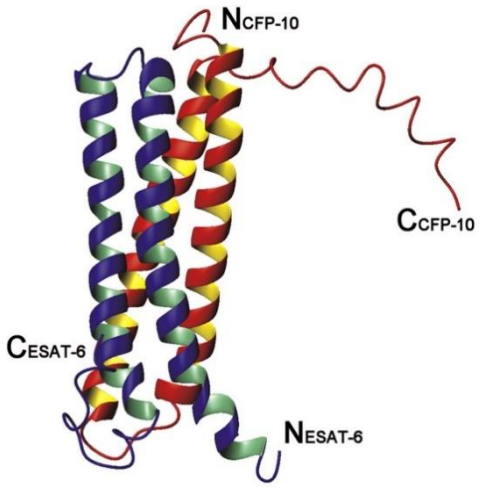

Figure 3.1 ESAT-6 and CFP-10 heterodimer

Image adapted from Renshaw *et al.* (Renshaw *et al.*, 2005)

3.1.2 Pathogenesis

The region of difference 1 (RD-1) that encodes ESAT-6 and CFP-10 is absent in the attenuated BCG vaccine strain (Figure 3.2) (Harboe *et al.*, 1996; Cole *et al.*, 1998). *M. tuberculosis* with a RD-1 deletion imitates the attenuated BCG vaccine strain implicating this region directly in pathogenesis (Lewis *et al.*, 2003). Similarly, insertion of the RD-1 region into an attenuated strain increases virulence (Pym *et al.*, 2002) and decreased virulence is observed when ESAT-6 and CFP-10 expression or secretion is halted (Wards, de Lisle and Collins, 2000; Stanley *et al.*, 2003; Guinn *et al.*, 2004). Other mycobacteria and Gram positive microbes have orthologs of ESAT-6, as well as the other genes found in the RD-1, but mycobacteria have multiple copies of the gene cluster containing ESAT-6 and CFP-10 in contrast to other Gram positive bacteria (Gey Van Pittius *et al.*, 2001).

The means by which ESAT6, CFP-10 and other components of the RD-1 contribute to pathogenesis are unclear however several mechanisms have been proposed: modulating macrophages (Basu *et al.*, 2006; Tan *et al.*, 2006; Pathak *et al.*, 2007; Kumar *et al.*, 2012); participating in macrophage cytolysis (Hsu *et al.*, 2003; Derrick and Morris, 2007; Guo *et al.*, 2012); facilitating escape from vacuoles (van der Wel *et al.*, 2007; Smith *et al.*, 2008); and driving granuloma formation (Volkman *et al.*, 2010).

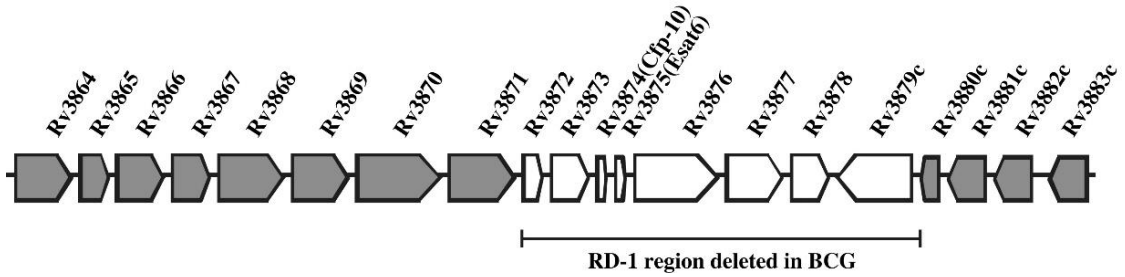

Figure 3.2 Region of deletion 1 (RD-1)

The RD-1 is absent in BCG (Ganguly, Siddiqui and Sharma, 2008).

3.1.3 Immunodiagnostics

TB diagnostic assays such as IGRAs, the TST and antibody response assays measure the adaptive immune response against *M. tuberculosis*. ESAT-6 and CFP-10 induce a strong Th-1 cell response (Ravn *et al.*, 1999; Colangeli *et al.*, 2000; van Pinxteren *et al.*, 2000), accordingly they are used in commercially available IGRAs such as the T-SPOT®.TB (Oxford Immunotec, Abingdon, UK) and QuantiFERON®-TB Gold (Cellestis, VIC, Australia), and the improved TST (Elhay, Oettinger and Andersen, 1998). The use of RD-1 antigens in these tests differentiates BCG vaccinated individuals from those exposed to a mycobacterial infection (Whelan *et al.*, 2010). However, these tests cannot distinguish between patients exposed to *M. tuberculosis*, clinically latent TB patients and active TB patients (Janssens *et al.*, 2007) since memory T-cells from previous exposures are activated when they are exposed to mycobacterial antigens. Nevertheless, a positive IGRA, negative culture result and no clinical signs of TB is often used as the definition of latent TB disease in studies (Lalvani *et al.*, 2001; Demissie *et al.*, 2006) since at present it is the best workable definition researchers can offer. The state of *M. tuberculosis* during clinical latent disease is unclear although *in vitro* and animal models suggest that the bacteria enter a persistent, non-replicating state (Wayne and Sohaskey, 2001). More recently TB disease has been viewed as a continuum between latent and active TB disease where *M. tuberculosis* is at varying stages of persistence, making the definition of active and latent disease less clear cut (Young, Gideon and Wilkinson, 2009). Hence, when patients are classified as "latent TB infection" the assumption should not be that the mycobacteria are in a latent or non-replicating state.

Other studies have assayed the humoral immune response against ESAT-6, CFP-10 (Dillon *et al.*, 2000; Silva *et al.*, 2003; Legesse *et al.*, 2013) and a combination of fused *M. tuberculosis*

proteins (Feng *et al.*, 2014). However, antibody based TB diagnostic assays typically suffer from low sensitivity hence they are not employed in diagnosis and there are no commercial assays available (Steingart *et al.*, 2011).

3.1.4 ESAT-6 and CFP-10 as diagnostic biomarkers

Given the caveats of measuring immune responses to *M. tuberculosis* proteins an alternative strategy is to detect proteins directly in patient samples to diagnose TB. Sputum contains whole mycobacteria hence secreted proteins such as ESAT-6 and CFP-10 ought to be present in the mucus matrix. Urine from TB patients contains mycobacterial proteins, some of which may be degraded (Choudhry *et al.*, 2002; Kashino *et al.*, 2008; Young *et al.*, 2014). Proteins from the same PE/PGRS family as ESAT-6 and CFP-10 are among the proteins detected, hence it is plausible that they are also present in urine (Young *et al.*, 2014).

ESAT-6 and CFP-10 are good candidates for diagnostic biomarkers since *M. tuberculosis* maintains a high level of ESAT-6 transcripts in a mouse model during the replicating and non-replicating state although expression was reduced during the non-replicating state (Shi, North and Gennaro, 2004; Davidow *et al.*, 2005; Rogerson *et al.*, 2006). Immune response studies in humans provide indirect evidence that ESAT-6 and CFP-10 are expressed during various disease states including clinically latent, mild and extensive TB (Ulrichs *et al.*, 2000; Pathan *et al.*, 2001; Doherty *et al.*, 2002; Silva *et al.*, 2003; Ravn *et al.*, 2005).

One caveat to keep in mind is that ESAT-6 and CFP-10 orthologs are present in other mycobacteria (Gey Van Pittius *et al.*, 2001), hence using these biomarkers may be prone to cross reactivity in certain settings. For example, non-tuberculous mycobacteria such as *Mycobacterium avium* can be pathogenic especially in immune suppressed individuals (Hawkins et al., 1986), so any cross-reactivity of tests for *M. tuberculosis* ESAT-6 or CFP-10 with *M. avium* orthologs could be confounders to diagnosis.

Basic tools for detecting ESAT-6, CFP-10 and other secreted proteins are available. For example, ESAT-6, CFP-10 and MPT-64 have been used to differentiate *M. tuberculosis* complex isolates from contaminating species in cultures in place of traditional biochemical tests or expensive molecular methods (Park *et al.*, 2009; Shen *et al.*, 2011). Additionally, CFP-10 was detected in the urine of extrapulmonary TB patients (Hong *et al.*, 2011; Kim *et al.*, 2013, 2015), ESAT-6 in cerebrospinal fluid (Kashyap *et al.*, 2009) and both proteins in pleural fluid (Feng *et al.*, 2011).

The detection of ESAT-6 and/or CFP-10 in patient samples could provide a simple approach to diagnosing TB. However, current tools for detecting these proteins require a concentration of

~5 µM for a ESAT-6/CFP-10 fusion protein (Feng *et al.*, 2011) or 10^5 CFU/ml for culture supernatants (Park *et al.*, 2009) while detection of biomarkers in urine and unprocessed sputum would require more sensitive assays. Hence, improved tools are needed for the detection of biomarkers in urine and sputum.

3.1.5 Aims and Objectives

The aim of the experiments described in this chapter was to determine if ESAT-6 and CFP-10 could be detected in TB patient urine and sputum samples.

First an in-house ELISA was used for the detection of ESAT-6, however following the observation of a high background signal in human derived samples western blot and mass spectrometry analysis was performed to identify a cross reactive element.

Secondly, targeted mass spectrometry techniques were used to probe for ESAT-6 and CFP-10 in TB patient urine samples.

3.1.6 Methodology

ELISA

This method was described in the previous chapter. An in-house ELISA was developed in our lab to detect ESAT-6 using an indirect sandwich format (Figure 3.3).

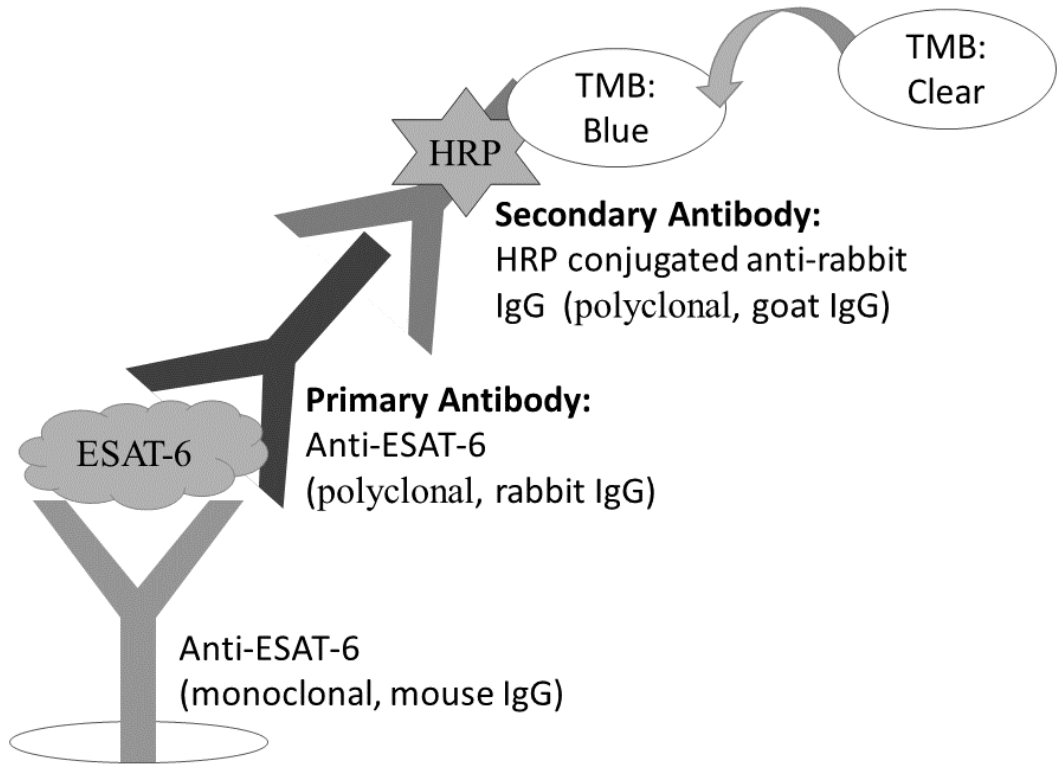

Figure 3.3 In house ESAT-6 indirect sandwich ELISA diagram

Summary:

- Immobilised anti-ESAT-6 monoclonal antibodies capture ESAT-6.
- A polyclonal anti-ESAT-6 antibody (primary antibody) binds to immobilised ESAT-6.
- HRP conjugated anti-rabbit IgG (secondary antibody) binds to the primary antibody.
- TMB substrate is converted to a blue solution if HRP is present.
- Sulphuric acid is used to stop the reaction which results in change of colour from blue to yellow.
- The absorbance of the wells is then measured at 450 nm.

There are washes between each incubation to remove excess reagents.

Western Blot

Western blots are a common molecular biology tool. Briefly, proteins separated by electrophoresis are transferred to a 0.45 μM nitrocellulose membrane before being incubated with a primary antibody and an HRP conjugated secondary antibody. An HRP substrate is converted into a chemiluminescent product which is used to detect proteins that bound to the primary antibodies (Gallagher, 2004). Diagrams of the western blots used in this study can be viewed in Figure 3.4 and Figure 3.5.

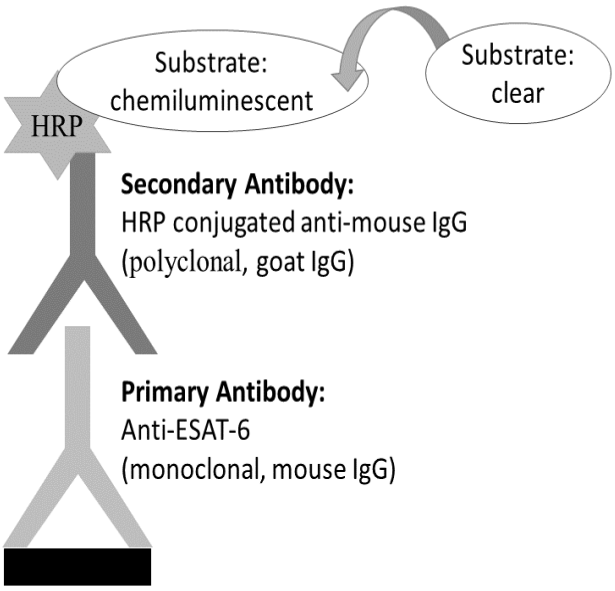

Figure 3.4 Diagram of the western blot to detect ESAT-6

Summary:

- A monoclonal anti-ESAT-6 antibody (primary antibody) binds to protein band.
- HRP conjugated anti-mouse IgG (secondary antibody) binds to the primary antibody
- An HRP substrate is converted to a chemiluminescent product.
- Protein bands bound by antibodies are visualised.

There are washes between each incubation to remove excess reagents.

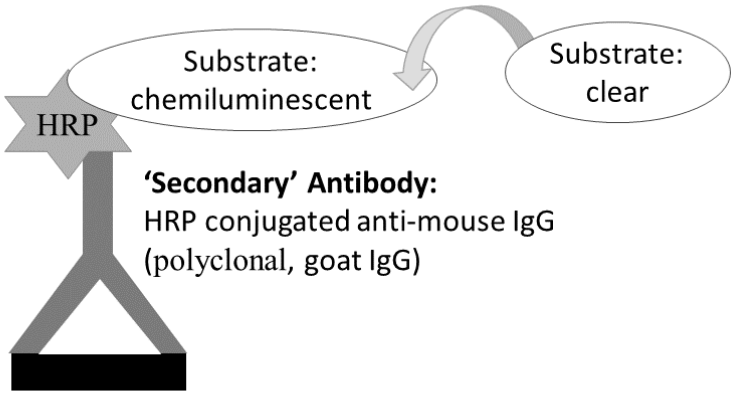

Figure 3.5 Diagram of the western blot to test cross reactivity

The HRP conjugated anti-mouse IgG antibody is denoted as the 'secondary' antibody to show the relationship to the previous western blot (Figure 3.4) although it is the primary antibody in this assay.

Summary:

- HRP conjugated anti-mouse IgG binds to a protein band.
- An HRP substrate is converted to a chemiluminescent product.
- Protein bands bound by antibodies are visualised.

There are washes between each incubation to remove excess reagents.

RP-HPLC MS/MS

Proteins are commonly digested with trypsin, and the resulting peptides are separated by hydrophobicity with **R**everse **P**hase **H**igh **P**erformance **L**iquid **C**hromatography (RP-HPLC) before analysing the peptides with tandem mass spectrometry (McLafferty, 1981; Murray *et al.*, 2013). Peptides are ionised by electrospray ionization (ESI) to form precursor ions as they are eluted off the RP-HPLC column. The Q-Exactive mass spectrometer is commonly used for targeted mass spectrometry since molecules with a known mass to charge ratio can be selectively filtered and quantified (Figure 3.6) (Miller and Denton, 1986). The Orbitrap mass analyser has high mass resolution, and allows for parallel reaction monitoring (PRM), where many product ions can be detected after fragmentation of the precursor ion in parallel (Makarov, 2000; Peterson *et al.*, 2012). Product ions are generated by predictably fragmenting precursor ions by Higher-energy C-trap dissociation (HCD) and can be computationally deconvoluted for analysis (Tang, Thibault and Boyd, 1993; Olsen *et al.*, 2007).

The intensity measurements of the fragment ions can be used to generate an MS2 spectrum for the product ions. A chromatogram can also be generated with intensity plotted against time to indicate when the peptides were eluted off the column. In the total ion chromatograms (TIC), the intensity signal contains the summed intensities for all ions of several m/z values at a certain time point (Figure 3.7) (Hoffmann *et al.*, 2007). Using a database of proteins digested *in silico,* peptides can be inferred by matching MS1 and MS2 mass spectra to a database (Eng, McCormack and Yates, 1994). Proteins can be inferred from these peptides although unique peptides are necessary to distinguish proteins that contain the same peptides. A decoy database, usually a reverse of the real database, is used to reduce false positive identifications (Elias and Gygi, 2007).

All product ions associated with a particular precursor ion are visualised together on the chromatogram at the retention time of the peptide (Figure 3.8). This information can be used to specifically detect and quantify peptides in a sample. For targeted mass spectrometry peptides should be consistently observed *i.e.* have good ionisation and at least one peptide should be unique for specific detection (Gallien, Duriez and Domon, 2011).

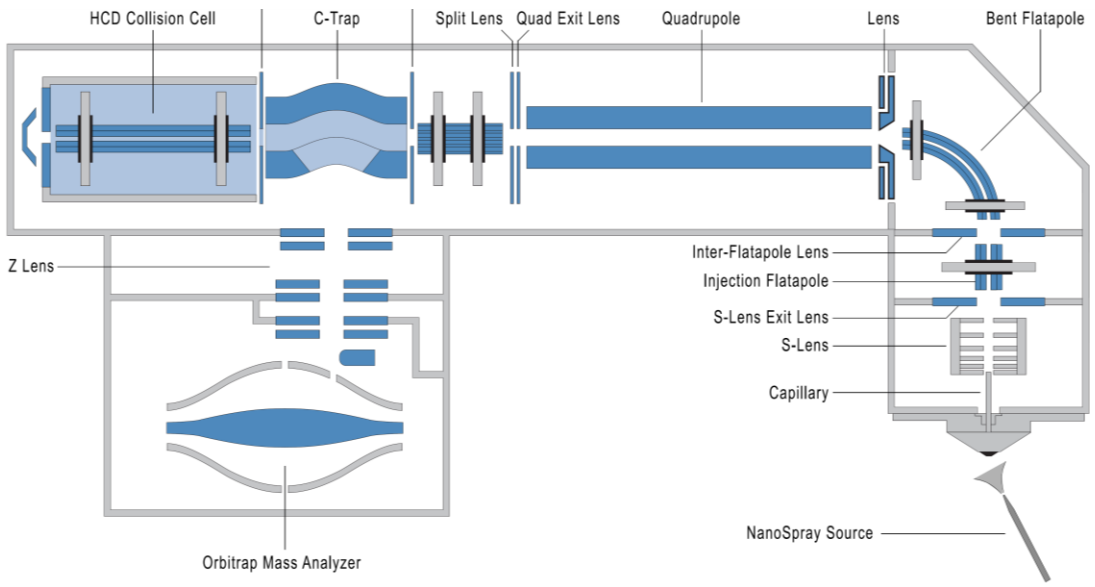

Figure 3.6 The Q-Exactive quadrupole-orbitrap mass spectrometer

Note the high-energy collision dissociation (HCD) cell and the quadrupole and orbitrap mass analysers. Adapted from (Michalski *et al.*, 2011)

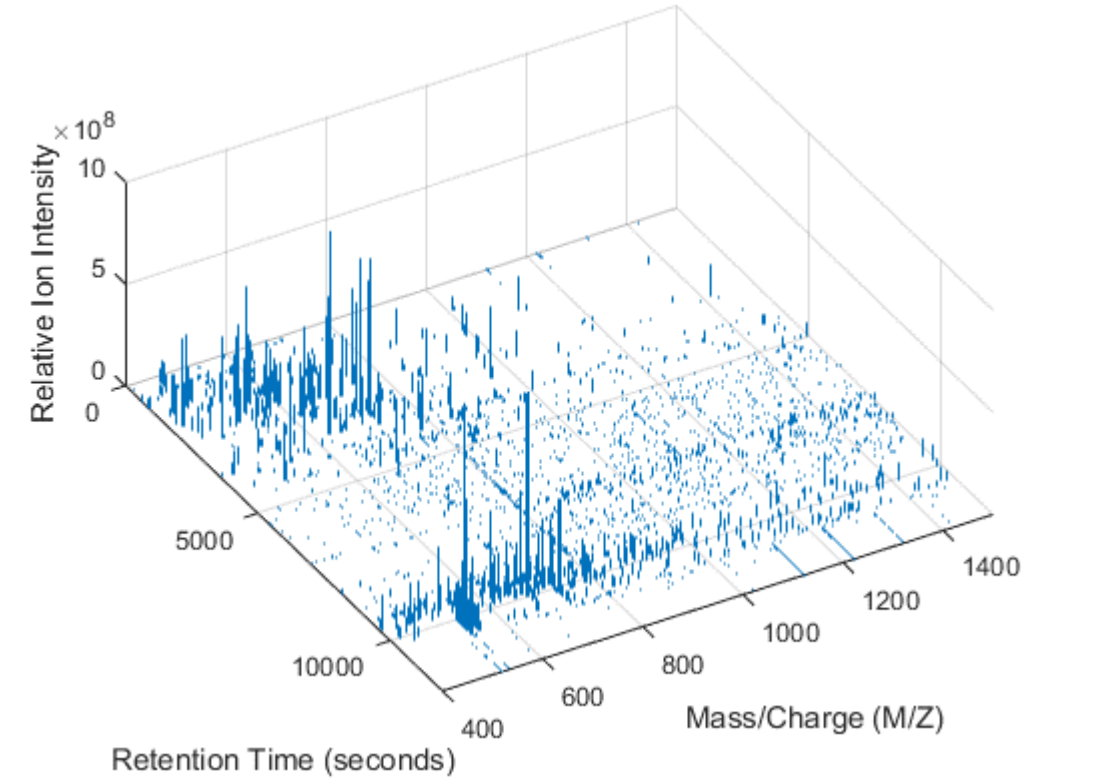

Figure 3.7 Mass spectra depicted on a graph

Image from Math Works (Math Works, 2017).

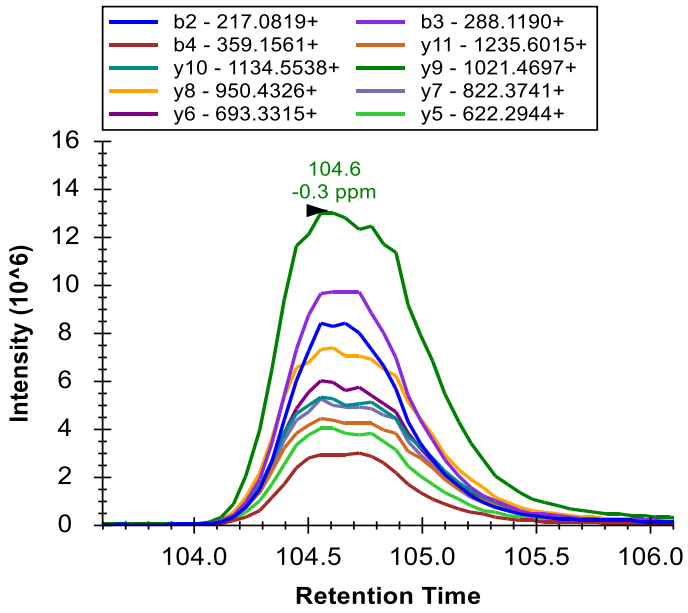

Figure 3.8 A set of product ions on a chromatogram

Each colour represents a different product ion. The y-axis indicates intensity of the ion and the x-axis indicates the retention time. Retention time is in minutes.

3.2 Methods

3.2.1 Patient Population

Ethical approval was obtained from the Human Research Ethics committee at the Faculty of Health Sciences, UCT. HREC/REF: 787/2014 to collect and use patient urine and sputum for diagnostic research purposes.

Active TB patients are defined as having a positive sputum culture result for *M. tuberculosis* while LTBI patients had a negative culture but two positive T-SPOT®.TB results. Patients were classified TB negative if the culture and T-SPOT®.TB result were negative. Where indicated patients were tested for HIV infection.

UA cohort urine samples from TB positive patients were used. Healthy volunteers donated urine samples to be used as controls. Patient details can be viewed in Appendix A: Table A3.

TB-Neat (TBN) cohort patient sputum samples with active TB (TB positive), latent TB infection (LTBI) and no TB (TB negative) were used. Additional details about sputum samples can be viewed in Appendix A: Table A5.

OI/E cohort urine samples were grouped into 1) TB positive; HIV negative 2) TB positive; HIV positive 3) TB negative; HIV positive and 4) TB negative; HIV negative (Appendix A:Table A 8)

3.2.2 Urine Sample Preparation

Urine samples collected from healthy volunteers and patients were thawed. Debris and precipitant formed during freezing was removed by centrifugation at 3000 rcf for 15 min prior for ELISA experiments.

For the ELISA and in-gel digestion experiments the supernatant was concentrated either by lyophilisation or a molecular weight cut off (MWCO) filter. For lyophilisation urine samples were frozen at -80 ºC in 10 ml aliquots and lyophilised for ~8 h to remove most liquid. Lyophilised samples were reconstituted in 1-1.5 ml of PBS (Sigma # P4417; pH 7.4). Another 10 ml aliquot was filtered through a 5 kDa MWCO (Vivaspin) until the sample had been concentrated approximately 10-fold. Concentrated samples were stored at -20 °C. Any particulate matter was pelleted by centrifugation for 5 min at 3000 rcf before use in any subsequent assays.

3.2.3 Sputum Sample Preparation

Sputum was processed by the Lung Infection and Immunity Unit at the University of Cape Town. The sputum samples were liquefied by incubating the sputum with two volumes of 0.01% dithiothreitol (DTT) in PBS. Once the DTT was added the sputum was vortexed briefly and then placed on a roller for 30 min. After 30 min, the sputum was deemed liquefied. The liquefied sputum was then heat inactivated at 100 °C for 30 min.

3.2.4 ESAT-6 ELISA

A 96- well microplate (Corning® 96 well EIA/RIA plates; CLS3590-100EA) was coated with mouse anti-ESAT-6 monoclonal antibody (BioPorto) in bicarbonate/carbonate coating buffer (100 mM) at pH 9 overnight at 4 °C. The plate was washed once with wash buffer before incubating the plate with 200 µl of blocking buffer (PBS containing 1% Bovine Serum Albumin (BSA) and 0.02% azide) for 1-2 h. The plate was washed before adding 100 µl of samples (urine or sputum) and controls in duplicate or triplicate. Plates were incubated for 1-2 h. After washing, rabbit anti-ESAT-6 polyclonal antibody (ABR-Affinity Bioreagents), diluted 1:500 in PBS was added and incubated for 1-2 h. After washing, the secondary antibody, horse radish

HRP-conjugated anti-rabbit IgG (R&D Systems, #HAF008), was diluted 1:500 in PBS and added to each well and incubated for 1-2 h. The plate was washed before adding 100 µl of chromogenic substrate TMB and incubated at room temperature for 20 min in the dark. Stop solution (1 M sulphuric acid) was added to terminate the reaction. The absorbance of each well was read at 450 nm with an iMark microplate reader (BioRad).

PBS was used as the negative control except for the binding curve assay where each curve had the corresponding medium as a control. All incubations were at 37 °C with a plate sealer and the plate was washed four times with wash buffer (PBS containing 0.05% Tween-20) unless otherwise stated.

Binding curves were generated by performing a 1:2 serial dilution of recombinant ESAT-6 (rESAT-6) homodimer (Statens Serum Institute) starting with 10 ng/ml in the various media. Healthy volunteer urine was used for binding curve assays. The cut-off value was determined by calculating the standard deviation of the negative control and adding three times the standard deviation to the negative control.

3.2.5 Sodium Dodecyl Sulphate Polyacrylamide Gel Electrophoresis

For Sodium Dodecyl Sulphate Polyacrylamide Gel Electrophoresis (SDS-PAGE) sample was denatured by boiling in sample loading buffer (12 mM Tris-HCl pH 6.8, 1% (v/v) β-mercaptoethanol, 0.4% (w/v) Sodium Dodecyl Sulphate (SDS), 5% glycerol, 0.02% (w/v) bromophenol blue) for 10 min. Samples were loaded onto a 16% tricine polyacrylamide gel and proteins were separated by electrophoresis for 30 min at 50 V (constant voltage) then at 120 V (constant voltage) until the dye front had reached the end of the gel (Schägger, 2006). Alternatively, urine samples were loaded on a pre-cast 4-20% gradient gel (BioRad, #456-1093) and separated at 100 V (constant voltage) until the dye front reached the end of the gel (~1.5 h). A protein ladder (10 µl) (#26619, Thermo Scientific) was used to estimate the molecular weight of proteins.

3.2.6 Western Blot

After the proteins had been separated by electrophoresis the polyacrylamide gel was transferred to a western blot apparatus where the proteins were transferred to a 0.45 µm nitrocellulose membrane for 50 min at 300 mA or 30 min at 500 mA (constant current). The nitrocellulose membrane was blocked overnight with 5% (w/v) fat free milk (Elite, Clover) in Tris buffered saline (20 mM Tris and 150 mM NaCl) with 0.1% (v/v) Tween-20 (TBST), and

then probed with anti-ESAT-6 monoclonal antibody (BioPorto), diluted 1:500 or 1:1000 in blocking solution. Excess antibody was removed by washing with TBST three times for 5 min. After washing the membrane was incubated with the secondary antibody, anti-mouse IgG-HRP (R&D Systems, #HAF007) diluted 1:500 or 1:1000 in blocking buffer for 1.5 h. After washing the membrane, it was incubated with the recommended volume of SuperSignal West Pico Chemiluminescent Substrate (Thermo Scientific) for 5 min or Western Bright enhanced chemiluminescence substrate (Advansta #K-12045-D20) for 2 min. The membrane was then exposed to film for varying time periods (1-30 min) and developed with manual developer and fixer (AGFA Healthcare # E43HP G150 and # E43JR G354) or bands were visualised with a Syngene G-Box and analysed with GeneTools and GeneSnap.

3.2.7 Proteomics

Bicinchoninic Acid (BCA) Assay

The concentration of the total protein in the urine samples was determined using the Pierce™ BCA protein assay kit (#23225; ThermoScientific). A two-fold dilution series of BSA (0.03-2 mg/ml) was used to generate a standard curve. 25 µl of each standard and the protein samples was added to microtitre wells in duplicate. The BCA working reagent was prepared by combining 50 parts reagent A with 1 part Reagent B. 200 µl of the working reagent was added to each well and incubated for at 30 min at 37 °C. The absorbance was read at 595 nm. The standard curve was used to interpolate the total protein concentration for each urine sample.

In Gel Digestion

Four TB culture positive patients from the UA cohort were used for this experiment. Urine samples were concentrated using a 5 kDa MWCO filter (Vivaspin) (Appendix A: Table A3).

Proteins in the urine sample were resolved on a 4-20 % pre-cast gradient gel (BioRad, #456-1093) (see 3.2.5) and stained using AcquaStain (Bulldog-Bio; #AS001000). The gel was placed over the western blot image and the corresponding bands were cut from the gel. Gel slices were sliced into 1 mm^3 cubes and transferred to glass vials (#702_283; Machery-Nagel). Two bands were cut out per patient namely a 25-35 kDa and 130-250 kDa band.

The excised gel pieces were processed as previously described by (Shevchenko *et al.*, 2007). Gel pieces were destained with 100 mM ammonium bicarbonate/ acetonitrile (1:1 v/v) for ~30 min. The destaining solution was removed before 80 µl of 10 mM of DTT in 100 mM ammonium bicarbonate was added. The gel pieces were incubated with DTT at 60 °C for 30 min

and cooled to room temperature before incubating for 10 min adding with 500 µl of acetonitrile. The acetonitrile was removed and 80 µl of 55 mM iodoacetamide (IAA) in 100 mM ammonium bicarbonate was added. The gel pieces were incubated for 20 min in the dark and acetonitrile was added to shrink the gel pieces.

Once gel pieces were shrunk they were saturated with 13 ng/µl trypsin (Promega; #V5111) in ammonium bicarbonate containing 10 % (v/v) acetonitrile for 120 min on ice. Additional ammonium bicarbonate was added to keep the gel pieces moist. The tubes were placed in a wet chamber at 37 ºC overnight (~16 h) to digest the proteins.

To extract the resulting peptides, 100 µl of extraction buffer (1:2 (v/v) formic acid/ acetonitrile) was added to each tube. The supernatant containing the peptides was transferred to glass inserts (#0609035; Aluglas) and dried in a vacuum centrifuge in preparation for C18 stage tips clean up.

In solution Digestion

Recombinant CFP-10 (rCFP-10) and rESAT-6 (100 ng), and urinary protein from the E/OI cohort samples were precipitated with methanol and chloroform, and digested with trypsin in-solution by Dr B. Calder.

One volume of protein in solution was added to one volume of methanol and a three-quarter volume of chloroform in a glass bottle (e.g. 400 µl protein + 400 µl methanol + 300 µl chloroform). After mixing, the sample was centrifuged for 5 min at 13 000 rpm (~17 800 rcf). The upper phase was removed and discarded; proteins are present in the white interphase disc and in the bottom phase. An additional three-quarter volume of methanol was added to the bottom phase and the protein was pelleted by centrifugation for 1 min at 13 000 rpm (~17 800 rcf). The supernatant was discarded, and the pellet was air dried. The pellet was resuspended in as little denaturation buffer (6 M urea, 2 M thiourea in 10 mM Tris pH 8.0) as possible (ideal concentration: 1- 2 µg/ml).

The resuspended protein was quantified *via* a modified Bradford assay: 1 µl sample, 90 µl 0.1 M HCl and 150 µl Bradford reagent (BioRad). Samples were incubated for 5 min before measuring the absorbance at 595 nm. 100 µg of protein was tryptically digested, except for rESAT-6 and rCFP-10 where ~100 ng was used.

For the in-solution digestion reduction buffer (1 M DTT in 50 mM ammonium bicarbonate (ABC)) was added to the sample to a final concentration of 1 mM DTT and incubated for 1 h at room temperature. Next, alkylation buffer (550 mM iodoacetamide in 50 mM ABC) was added

to a final concentration of 5.5 mM IAA and incubated for 1 h at room temperature in the dark. Samples were then diluted with four volumes of 20 mM ABC buffer. If pH was not ~ pH 8 it was adjusted with 20 mM ABC. Trypsin was added to the sample at a 100:1 ratio (Promega; #V5111) overnight at room temperature (at least 16 h).

The reaction was stopped by acidification with 1 % formic acid until pH 2 to 3 was achieved. Samples (10 µg) were cleaned up with in-house C18 stage, prepared by packing C18 filters (Empore) into pipette tips (Rappsilber, Ishihama and Mann, 2003). All stage-tip centrifugation was performed at 4000 rpm (~1440 rcf). C18 stage tips were activated with solvent B (80 % acetonitrile with 0.1 % formic acid) and then equilibrated with solvent A (2 % acetonitrile with 0.1 % formic acid). Samples were resuspended in 100 µl of solution A and loaded onto the HPLC columns. The bound samples were then washed three times with solvent A. The peptides were eluted with solvent C (60 % acetonitrile with 0.1 % formic acid) into a glass vial and dried in a vacuum centrifuge. Samples were resuspended in 15 µl of solvent A for mass spectrometry analysis.

LC/MS Instrumentation and Parameters

Mass spectrometry analysis was performed with the assistance of Dr B. Calder, Mr B. Murugan and Dr A. Nel.

Discovery and targeted proteomic analysis was performed on a Q-Exactive Quadrupole-Orbitrap mass spectrometer (Thermo Scientific), coupled to a Dionex UltiMate 3500 RSLC nano-LC system (Thermo Scientific). Sample (400 ng) was introduced onto a 100 µm x 4 cm trap column packed in-house with C18 coated silica beads (5 µm Luna C18 resin, Phenomenex). Separation was performed by reversed phase chromatography on a nanoscale analytical column, also packed in-house (Aeris peptide solid bead C18 #04A-4507, 75 µm x 40 cm). Ionisation was attained by application of charge over a stainless-steel emitter (Thermo Scientific, Cat#: TFES542) affixed to the end of the analytical column.

Discovery MS

Mass spectrometric analysis was controlled by Xcalibur software (Thermo Scientific; v2.2). and acquisition parameters were developed in-house based on the work by Pirmoradian et al. (Pirmoradian et al., 2013). Default settings were as follows: 'Top 10', data-dependent and positive ion mode. MS1 settings included a resolution of 70000**,** scan range of 300-1750 m/z automatic gain control (AGC) target of 3E6, and an ion injection time of 250 ms. At the MS2 level the setting were as follows: isolation window of 4.0 m/z, a normalised collision energy (NCE) of

25, resolution of 17500, AGC target of 5E4 and ion injection time of 80 ms. Data dependent settings included an underfill ratio of 1% (which equates to an intensity threshold of $1.7x10^4$), peptide match set to "preferred, isotopic exclusion, and a dynamic exclusion of 30 s. Charge exclusion was set to all unassigned charges, as well as all charges other than 2 or 3.

Samples were eluted using a linear 145 min gradient at a constant flow rate of 300 nl/min. The sample was loaded onto the column with 2% acetonitrile (ACN, LC-MS Ultra, Sigma in UPHPLC grade water) for 10 min. The sample was then eluted with 8% ACN at 12 min, 40% ACN at 130 min and finally with 80% ACN at 135 min. Washes were performed between each sample with 80% ACN for 10 min. An additional wash was performed after four samples.

Targeted MS

Targeted assays were generated in Skyline for CFP-10 and ESAT-6 tryptic peptides based on a spectral library generated from discovery MS data. A spiked sample was included, which contained 100 ng of purified CFP-10 and ESAT-6 proteins as a positive control. 2-plex PRM data was acquired at a resolution of 35000, with the AGC target set to maximum and a 50 ms injection time. The normalized collision energy was set to 27 and a 2.0 m/z mass error tolerance was allowed. The chromatography conditions used for targeted MS were identical to those used for discovery MS.

3.2.8 Bioinformatics

Protein/Peptide Identification

Data from the discovery experiments were processed by MaxQuant version 1.5.3.12 which uses the Andromeda search engine (Cox and Mann, 2008; Cox *et al.*, 2011). A human and *M. tuberculosis* proteome database from UniProt were used (Human_UP000005640 and *M. tuberculosis* (strain ATCC 25618 / H37Rv)_ UP000001584 downloaded Feb 2016) (The UniProt Consortium, 2014). Raw files from the in-gel digestion were run separately using the human proteome (one 25-35 kDa and 130-250 kDa gel slice per patient). Data from urine samples spiked with rESAT-6 or rCFP-10 were run using with the human and *M. tuberculosis* proteomes.

The Andromeda search engine identified peptides by matching experimental MS1 and MS2 spectra with theoretical spectra generated from an *in silico* tryptically digested human proteome. False identifications were predicted by the target-decoy approach using a reversed

decoy database (Elias and Gygi, 2007). PSM, peptide, and protein FDRs were set at 1% and a minimum of one unique peptide were required to make an identification. Unique peptides belong to only one protein or protein group and do not share complete sequence homology with any other protein or protein group. MaxQuant parameters are tabulated in Appendix A:Table A6.

Analysis of protein groups from in-gel digestion

The MaxQuant data output was assessed using the *protein.groups.txt* file. Contaminants, reverse sequence hits and trypsin (A6XMV8) were excluded from the protein groups.

To narrow the search for the cross-reactive elements the following filters were applied to the *proteingroups.txt* file. Experiments were divided into the 25 kDa-35 kDa and 130-250 kDa fractions. Within each fraction, proteins or protein groups that were not present in all four patients and without a least one unique peptide in each patient were excluded. Protein group refers to a group of proteins which share peptides and unique peptides therefore they cannot be differentiated from each other. Unique peptides were used as a measure of confidence in the protein identity. The lists were sorted from largest to smallest intensity. Proteins or protein groups with a high intensity also having a high protein score indicating a more significant hit were included. The protein score in the *proteingroups.txt* document is derived from the Posterior Error Probability (PEP) which gives a significance score.

To simplify further analysis the majority protein in a protein group was used; this protein has the most peptide hits in the protein group. The majority protein of each protein group was searched in the UniProt database for further information including names and domain properties. The reduced lists for each fraction were compared using BioVenn (Hulsen, de Vlieg and Alkema, 2008).

Generation of targeted proteomics isolation list

The MaxQuant data output was assessed using the *protein.groups.txt* and *peptide.groups.txt* files. All detected peptides for ESAT-6 and CFP-10 were included in the isolation list for targeted proteomic analysis (Appendix A: Table A 9). A spectral library was generated in Skyline based on the MaxQuant *msms.txt* output, and used to select the best fragment spectra for each peptide in the isolation list.

Skyline Analysis

All spectral data was manually inspected in Skyline (64-bit version 3.6.0.10493) to confirm

auto-selected peak boundaries. Where the auto-selected peak boundaries did not match the control spike retention time the boundaries were manually corrected to within a 1-2 min window of the control spectra. Five to ten ions for each precursor where chosen based on intensity, symmetry of the peak and assigned rank. Product ions not present in both the control spike and the spectral library were deleted. Three peptides for each protein were chosen for displaying the data based on control spike dot-p values and proteotypic peptides that had previously been observed (Schubert *et al.*, 2013).

3.3 Results

3.3.1 ESAT-6 ELISA

An in-house ESAT-6 ELISA protocol developed by Dr Teri Roberts was used to explore the detection of ESAT-6 in patient samples (Figure 3.3). Previously no ESAT-6 was detected in neat urine samples from TB patients. To determine if ESAT-6 could be detected in urine, TB positive patient urine was concentrated to increase the likelihood of detection of any ESAT-6 that may be present.

Binding Curves

In order to assess the effect of concentrated urine on the performance of the ELISA and to determine the limit of detection of the assay, three different media were spiked with ESAT-6 at various concentrations (Figure 3.9 and Figure 3.10): neat urine, urine concentrated ~10 fold *via* lyophilisation and PBS, which served as the control. The cut-off for a positive result was defined as an absorbance signal greater than the negative control mean plus three standard deviations. Hence the limit of detection for each medium was the lowest absorbance reading above the cut-off. The approximate limit of detection for PBS, lyophilised urine and neat urine were 1.25 ng /ml; 0.63 ng/ml and 0.31 ng/ml of recombinant ESAT-6 (rESAT-6) respectively.

The neat urine and lyophilised urine resulted in favourable shaped curves with good linearity in the lower concentration range. However, the lyophilised urine did not reach saturation at a similar concentration to the PBS or neat urine and the overall absorbance readings were greater than the PBS and neat urine readings.

ESAT-6 ELISA with urine samples

Patient urine samples were concentrated to compare the differences in ESAT-6 detection using concentrated (concentrated ~10 fold using lyophilisation or 5 kDa MWCO filter) and

unconcentrated samples (Figure 3.11). No neat urine samples gave a reading above the negative control. Concentrating with the MWCO filter resulted in greater absorbance signals than concentration by lyophilisation for most samples with a reading above the cut-off. Concentrating the urine increased the signal above the cut-off for two TB positive patients, however, two healthy volunteers also had a reading above the cut-off (Appendix A: Table A4). Of the two TB patients with a signal above the control, one had renal disease and proteinuria (UA215), but the other patient did not have renal disease or proteinuria (UA141). Additionally, patient UA310 had renal disease but did not have a signal above the negative control (Appendix A: Table A3). Concentrating urine with a MWCO filter generally increased the ESAT-6 ELISA signal more than concentration by lyophilisation.

ESAT-6 ELISA with sputum samples

Sputum samples were also tested in duplicate using the in-house ESAT-6 ELISA. Three groups of patients were tested: TB positive, latent TB infection and TB negative. Three TB positive, four latent TB and four TB negative patients had a signal above the cut-off (Figure 3.12 and Appendix A: Table A5). Most of the patients were HIV negative except for patients TBN 58 and TBN 59 who were HIV positive and TBN 274 who was not tested for HIV.

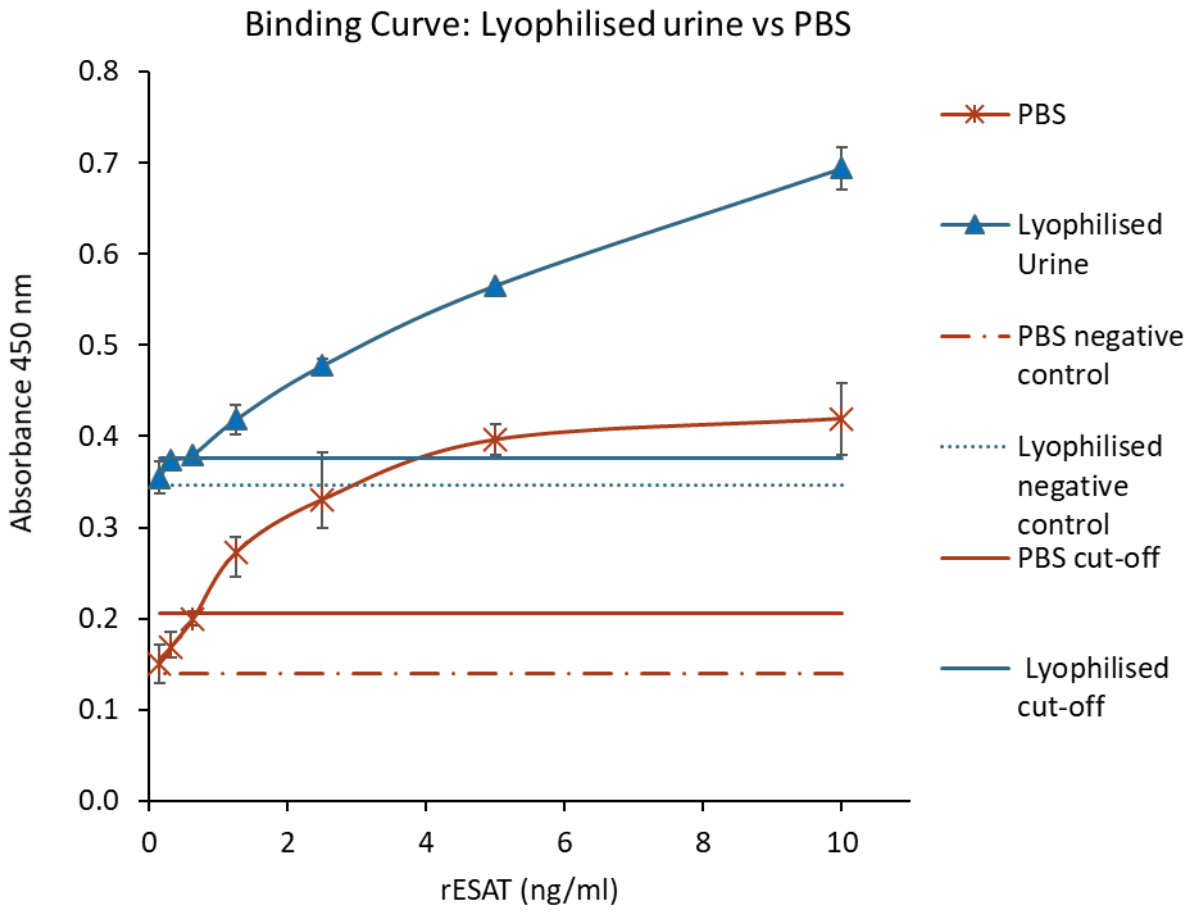

Figure 3.9 Binding Curve for ESAT-6 ELISA

A rESAT-6 homodimer was spiked into different media namely PBS, lyophilised urine, and neat urine. All conditions were in triplicate except for the two highest concentrations of the PBS curve which were in duplicate. Points indicate the mean reading of duplicate or triplicate wells. Error bars indicate the minimum and maximum readings taken.

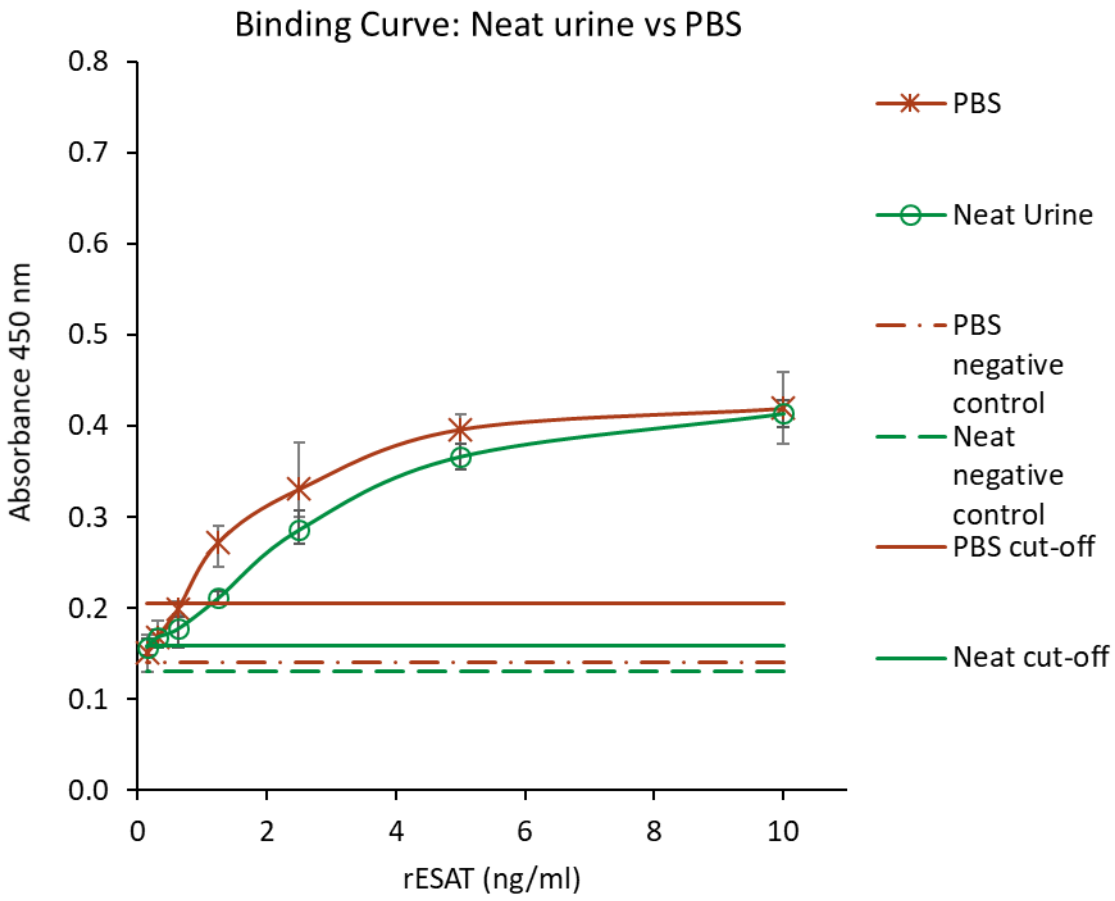

Figure 3.10 Binding Curve for ESAT-6 ELISA

A rESAT-6 homodimer was spiked into different media namely PBS, lyophilised urine, and neat urine. All conditions were in triplicate except for the two highest concentrations of the PBS curve which were in duplicate. Points indicate the mean reading of duplicate or triplicate wells. Error bars indicate the minimum and maximum readings taken.

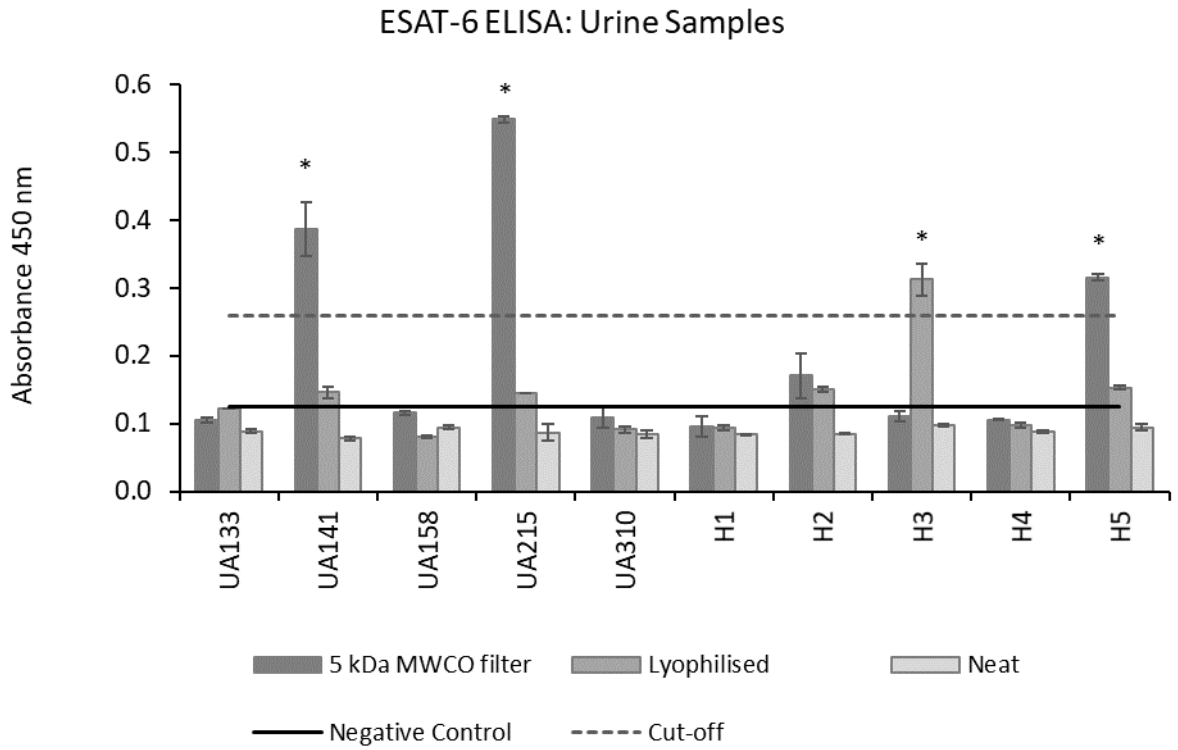

Figure 3.11 ESAT-6 ELISA with urine samples

UA denotes TB positive patients and H denotes healthy volunteers. Samples were concentrated with a 5kDa MWCO filter or by lyophilisation and compared to neat urine. PBS was used as a negative control. Each sample was tested in duplicate. The cut-off was calculated by adding 3 standard deviations of the negative control to the mean negative control value. Samples with a mean reading above the cut-off are marked with "*". Columns indicate the mean reading of duplicate wells. Error bars indicate the minimum and maximum readings taken.

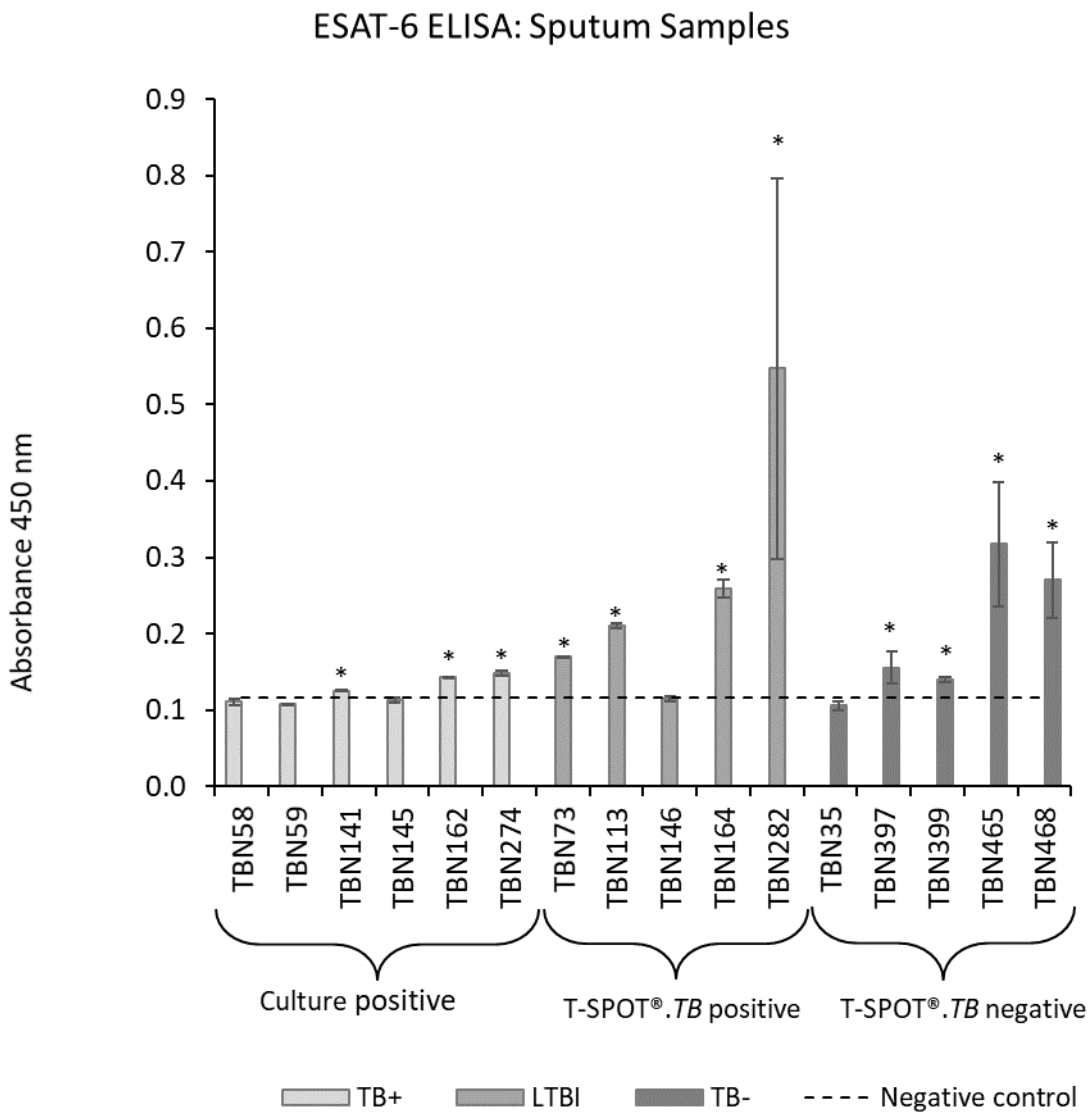

Figure 3.12 ESAT-6 ELISA with Sputum

TB+: TB positive; LTBI: clinically latent or previous TB infection; TB-: TB negative. Each sample was tested in duplicate. Samples with a mean reading above the negative control are marked with "*". Columns indicate the mean reading of duplicate wells. Error bars indicate the minimum and maximum readings taken.

3.3.2 Western Blots

To investigate the source of the positive signal in the ESAT-6 ELISA in the healthy volunteer urine and TB negative sputum, samples were separated by electrophoresis on a SDS-PAGE and probed with the monoclonal anti-ESAT-6 antibody (primary antibody) followed by the anti-

mouse IgG-HRP antibody (secondary antibody) (Figure 3.4). A ~26 kDa band was seen in healthy volunteer and TB positive patient urine (

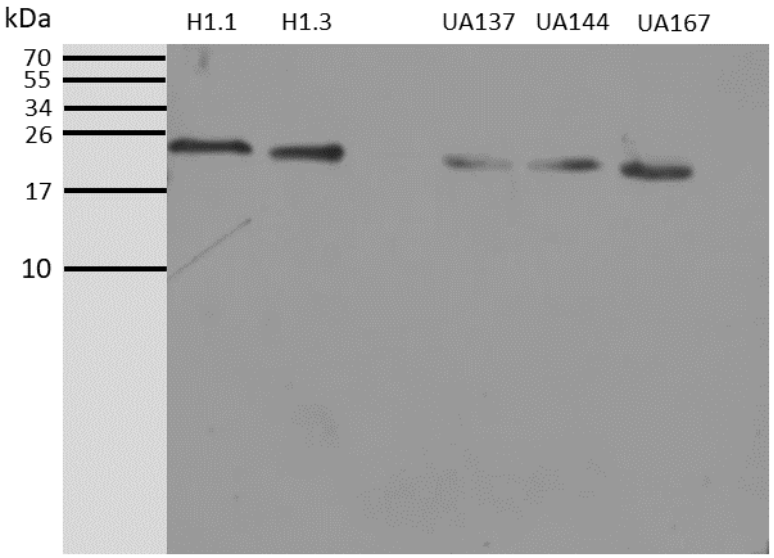

Figure 3.13). In some samples higher molecular weight bands were also recognised at ~26, ~42, ~52 and >135 kDa such as in this healthy sample (Figure 3.14). The ~26 kDa band was also observed in sputum samples from TB positive and TB negative patients which were tested alongside additional urine samples from TB positive patients and healthy volunteers. The TB positive samples with additional higher molecular weight bands also had 1-3 mg/ml of protein in their urine according to clinical data (Figure 3.15; Appendix A: Table A3). ESAT-6 which is ~9 kDa was not detected in any of the TB positive samples.

To determine which antibody was responsible for the cross-reactive bands healthy patient urine was also probed with only the anti-mouse IgG-HRP antibody (Figure 3.5). When urine samples were probed with only the secondary antibody the ~26 kDa band was present, but the higher molecular weight bands were not observed (Figure 3.16).

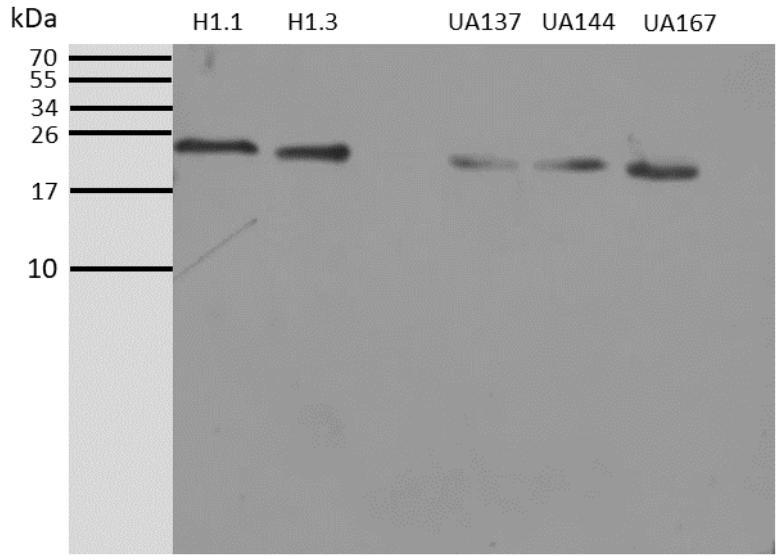

Figure 3.13 Western Blot with anti-ESAT-6 antibody using urine. Healthy volunteer urine (H.1.1, H1.3) and TB positive patient urine (UA137, UA144, UA167)

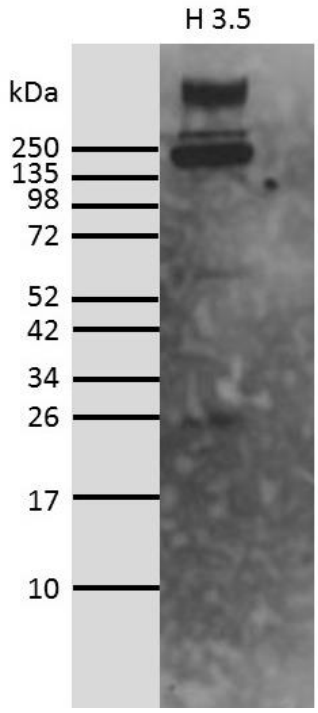

Figure 3.14 Western Blot with anti-ESAT-6 antibody showing high molecular weight bands.

Faint bands at ~26 and ~52 kDa were also noted. H3.5: Urine from healthy volunteer

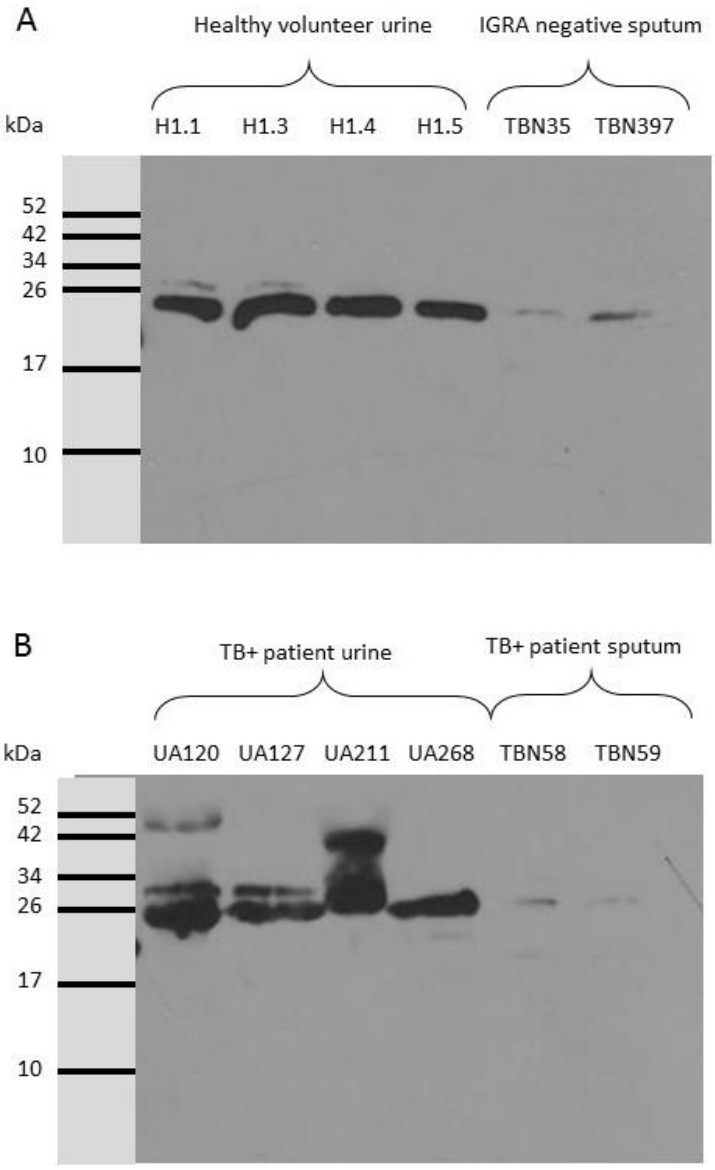

Figure 3.15 Western Blot with anti-ESAT-6 Antibody using urine and sputum samples.

A) A ~26 kDa band is visible for healthy volunteer urine samples (H1.1-1.5) and a faint band of the same molecular weight is present for TB negative patients (negative culture and negative T-SPOT®.TB).

B) A ~26 kDa band and some other larger bands are visible for TB positive patients (culture or smear positive). The ~26 kDa bands for the sputum are faint.

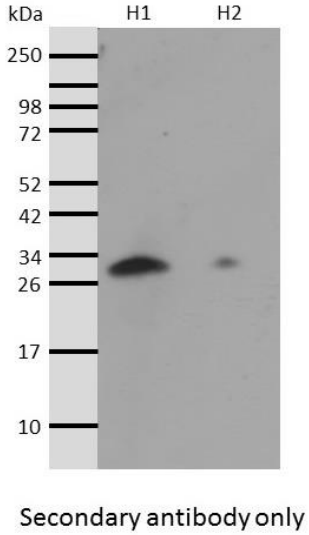

Figure 3.16 Western blot with only anti-mouse IgG-HRP antibody.

Two samples of concentrated urine from a healthy volunteer were probed with anti-mouse IgG-HRP antibody (secondary antibody).

3.3.3 Discovery Proteomics

SDS-PAGE and Western Blot

To identify the proteins cross reacting with either the anti-ESAT-6 primary antibody and/or the anti-mouse IgG secondary antibody the appropriate molecular weight protein bands were cut from a SDS-PAGE gel and subjected to mass spectrometry analysis (Figure 3.17). Protein bands were identified by a western blot that was run in parallel and overlaid onto the gel (Figure 3.17). We focussed on the ~26 kDa and the >130 kDa bands which were the most commonly observed bands.

BCA Assay

The total protein concentration for each urine sample was interpolated from the BSA standard curve (Table 3.1). By rough approximation there are seven prominent bands on the SDS-PAGE (Figure 3.17) therefore each of the bands removed from the gel for mass spectrometry analysis is about one seventh of the total protein. All samples were processed in duplicate except for UA120.

Table 3.1 Total protein concentration of each urine sample

Urine Samples	Absorbance 595 nm	Protein concentration (mg/ml)	Dilution factor x10 (mg/ml)	~ Protein/gel slice (mg/ml)
UA120	0.767	1.269	12.69	1.813
UA127	1.040	1.732	17.32	2.474
UA211	1.790	2.971	29.71	4.244
UA268	2.745	4.512	45.12	6.445

LC-MS/MS

The raw files show the MS1 and MS2 total ion chromatograms (TICs); 1st and 2nd panel respectively (Figure 3.18). Product ions are derived from precursor ions selected by the top 10 method for sequencing. Spectra had several single peaks across the gradient with no visible contaminants. Large single peaks may indicate abundant peptides. Peptides are well distributed and separated across the gradient. Raw data was further processed using bioinformatic tools.

Bioinformatics analysis of MS data using Max Quant

Protein identification by MaxQuant and Andromeda identified 546 protein groups excluding contaminants, reverse hits, and trypsin. A wide range of protein sizes were identified in both gel slices (2.2 to 856.8 kDa). The majority proteins with the highest intensities for each gel slice can be seen in Figure 3.19 and Figure 3.20. The overall intensity is the summed up Extracted-ion Chromatogram (XIC) of all isotopic clusters associated with the identified amino acid sequence. The intensity for each protein group varies between patients.

After protein groups were excluded as described, the list was reduced from 546 to 77 protein groups for the 25-35 kDa gel slice and 68 protein groups for the 130-250 kDa gel slice (Appendix A: Table A7). About a third of all the proteins identified had Ig-like domains; the number of total proteins with an immunoglobulin related domain can be seen in Table 3.2 (MaxQuant Results).

Several of the protein groups were identified in both fractions after sorting for at least one

unique peptide (**Error! Reference source not found.**Figure 3.21 and Appendix A: Table A7).

The majority protein, Ig kappa chain C region (A0A087WZW8) had the highest overall intensity in both gel slices and would be close to 26 kDa in a dimer form and shared several Ig-like domains (Table 3.2)

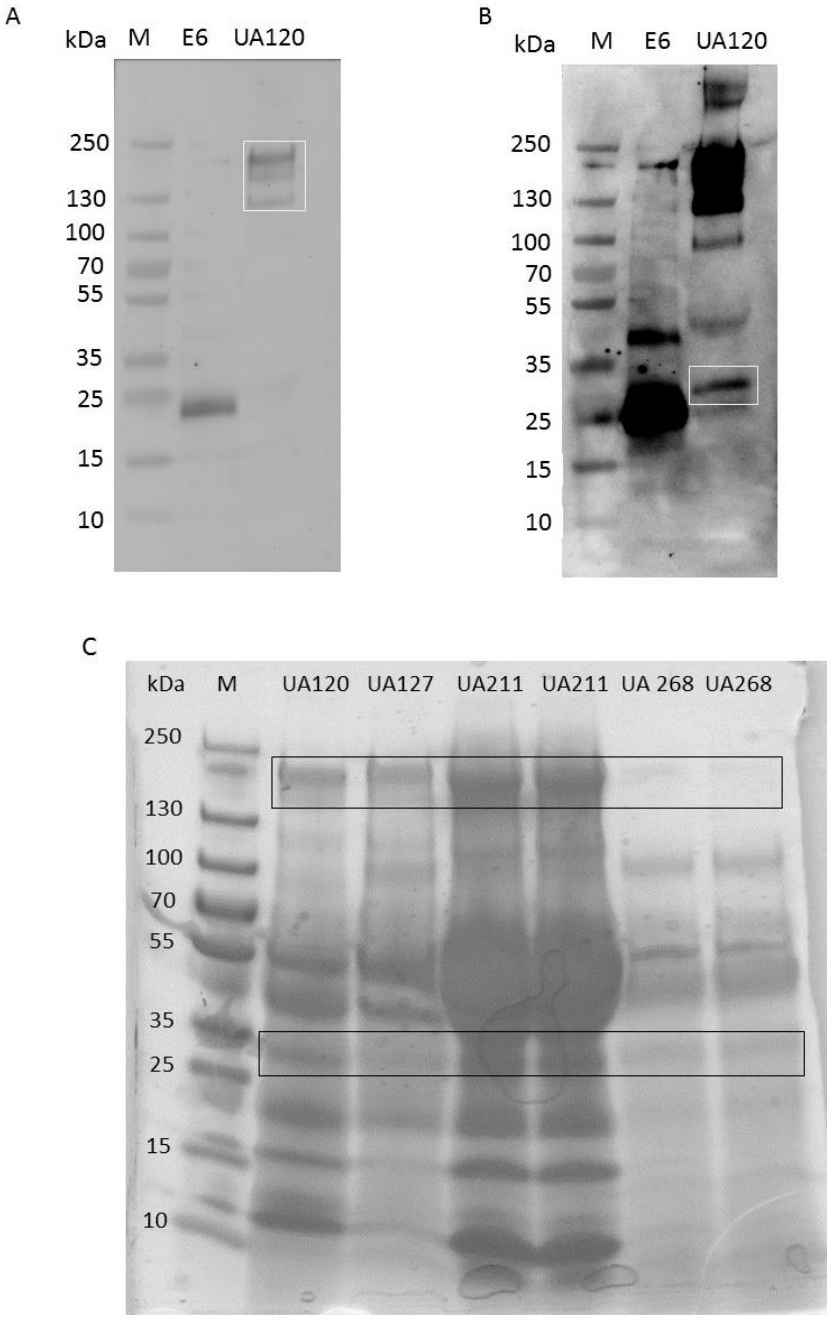

Figure 3.17 Western Blot and SDS PAGE to identify bands to be excised for mass spectrometry analysis.

A) 130-250 kDa bands to be excised B) 25-35 kDa band to be excised. C) Bands excised from SDS PAGE. E6: Positive control rESAT-6 dimer (~18 kDa); UA: TB positive patients. Bands to be cut out are indicated by the rectangle boxes. M: Protein ladder)

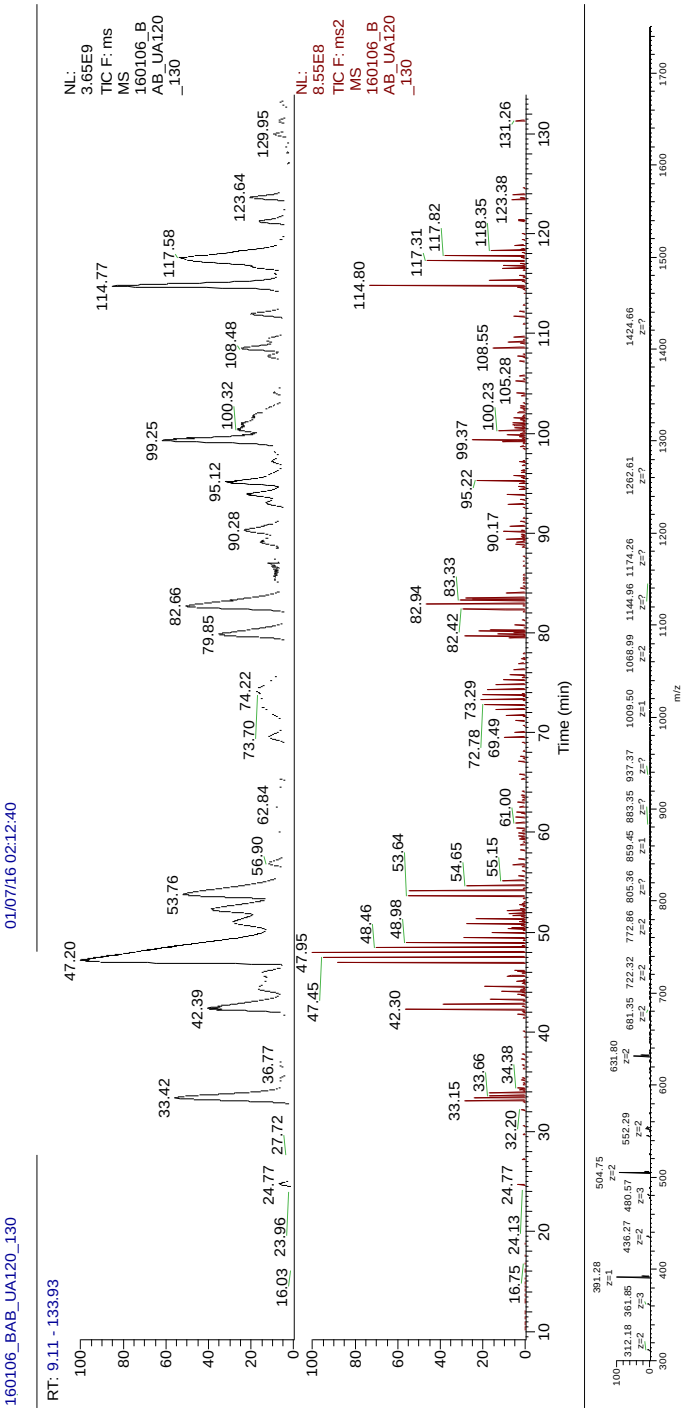

Figure 3.18 Representative Ion Chromatogram.

MS1 and MS2 Spectrum for urine samples from patient UA120.

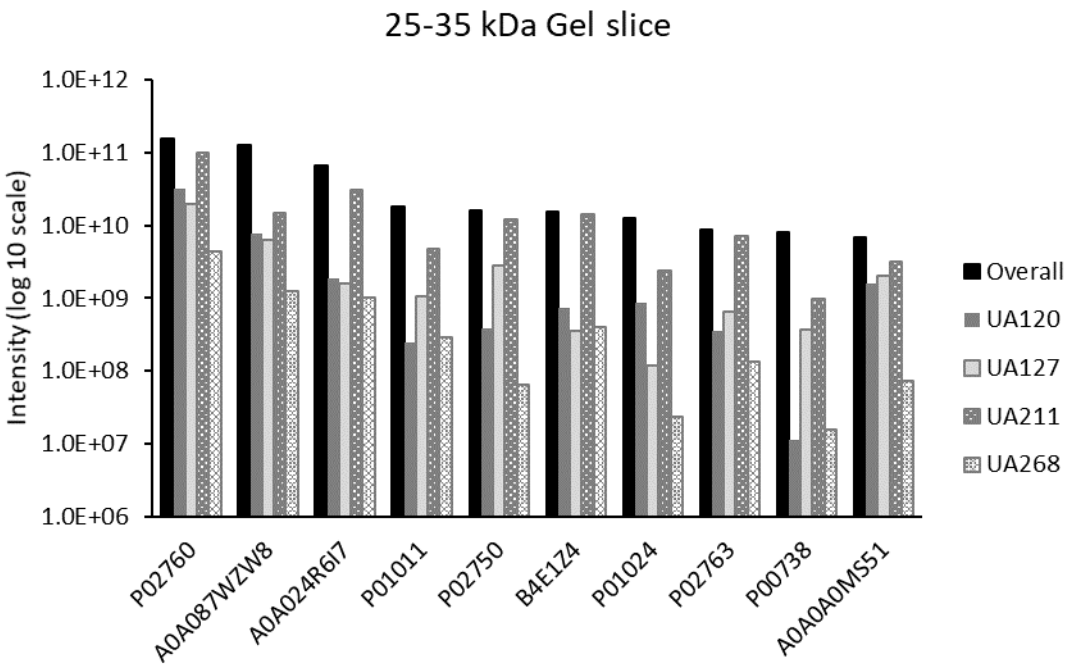

Figure 3.19 Protein groups identified in the 25-35 kDa gel slice.

Protein Groups with the highest overall intensity values (top ten) and the corresponding intensity values for each patient. Patient identifiers: UA120, UA127, UA211 and UA268

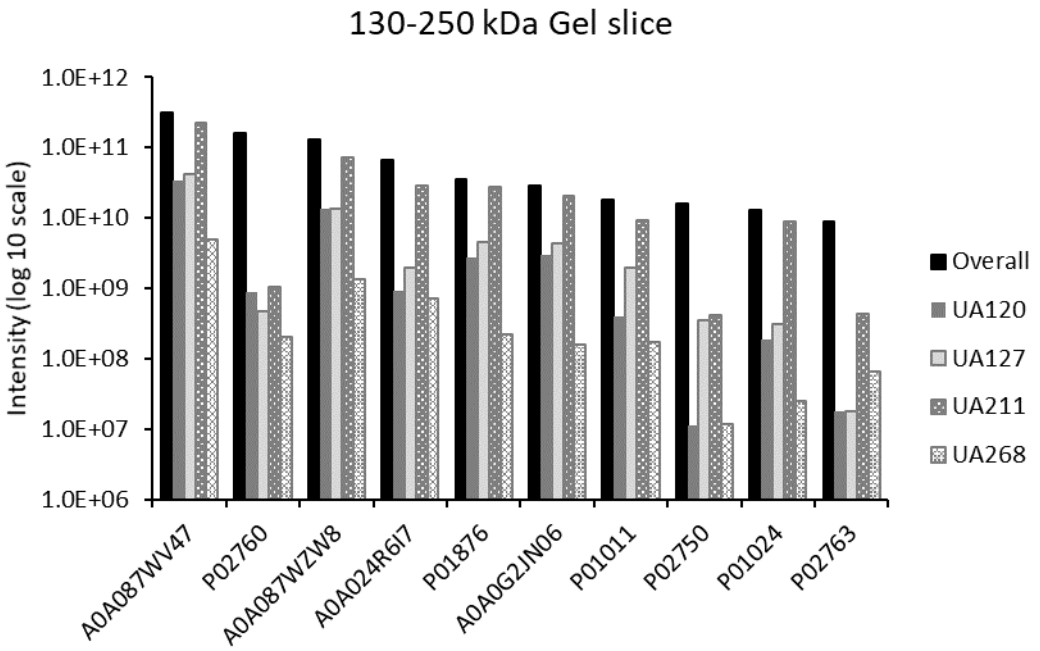

Figure 3.20 Protein Groups with the highest overall intensity values (top ten) and the corresponding intensity values for each patient in the 130-250 kDa gel slice.

Figure 3.21 Venn diagram of protein groups identified in different size gel slices.

Generated using BioVenn © 2007-2016 Tim Hulsen.

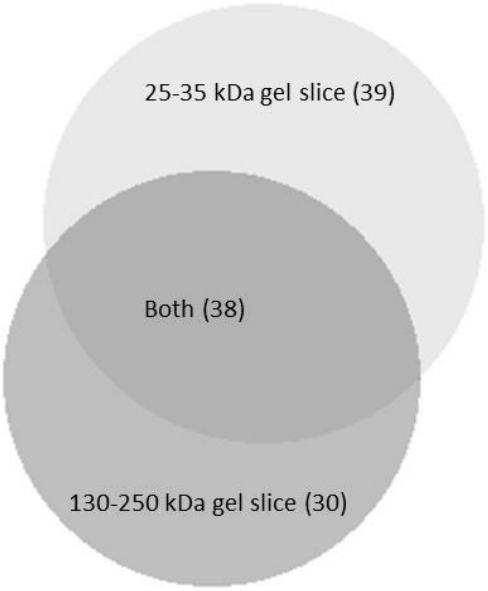

Several protein groups with at least one unique peptide were present in both gel slices fractions (see Appendix A: Table A7 for protein IDs).

Table 3.2 Immunoglobulin related domains identified in Ig kappa chain C region (A0A087WZW8)

ID	**Name**
IPR007110	Immunoglobulin-like domain
IPR013783	Immunoglobulin-like fold
IPR013106	Immunoglobulin V-set domain
IPR003597	Immunoglobulin C1-set
IPR003006	Immunoglobulin/major histocompatibility complex, conserved site

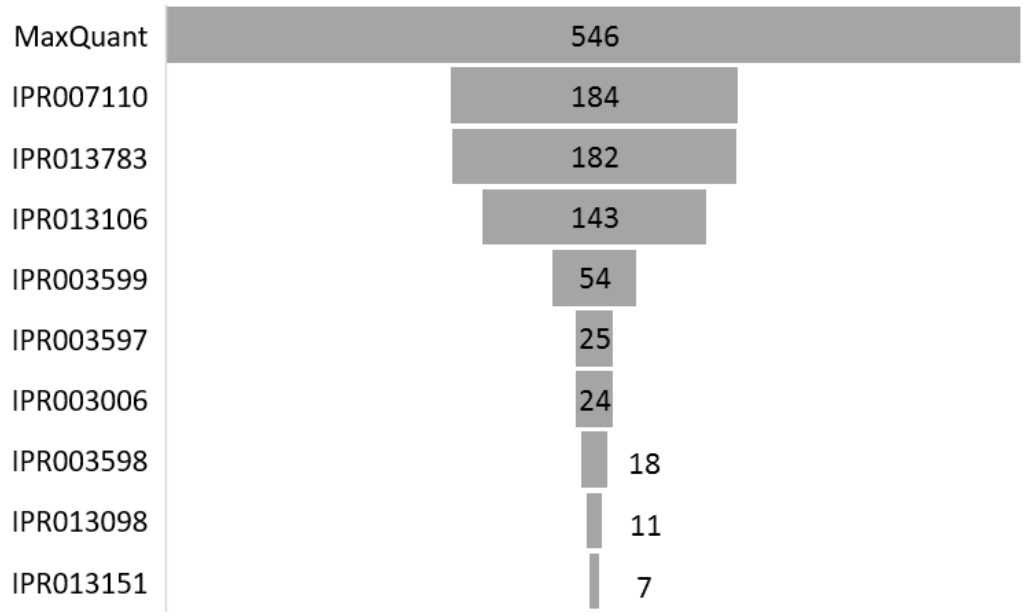

Figure 3.22 Immunoglobulin domains associated with majority proteins identified by MaxQuant.

Domain names for IDs are presented in the key below (Table 3.3).

Table 3.3 Key for immunoglobulin domain names of identified proteins

KEY	
MaxQuant	All MaxQuant IDs
IPR007110	Immunoglobulin-like domain
IPR013783	Immunoglobulin-like fold
IPR013106	Immunoglobulin V-set domain
IPR003599	Immunoglobulin subtype
IPR003597	Immunoglobulin C1-set
IPR003006	Immunoglobulin/major histocompatibility complex, conserved site
IPR003598	Immunoglobulin subtype 2
IPR013098	Immunoglobulin I-set
IPR013151	Immunoglobulin

3.3.4 PRM

Discovery proteomics was performed on rCFP-10 and rESAT-6 spiked into a healthy urine sample. From the discovery proteomic data peptides were selected for targeted proteomics on patient urine samples. The four groups of patient urine samples were 1) TB positive; HIV negative 2) TB positive; HIV positive 3) TB negative; HIV positive 4) TB negative; HIV negative (Appendix A: Table A 8).

The total ion chromatogram spectra had several single peaks across the gradient with no visible contaminants. Large single peaks may indicate abundant peptides. Peptides are well distributed and separated across the gradient. Raw data was further processed using bioinformatic tools. (Appendix A: Figure A 3). Six peptides for ESAT-6 and eight peptides for CFP-10 were identified by MaxQuant and included in the isolation list (Appendix A: Table A 9).

The library dot-product (dot-p) value shows how similar the unknown samples are to the spectral library, which is the reference: a value of one represents a complete match. The control spikes of rESAT-6 and rCFP-10 had good dot-p values in the range of 0.90 to 0.98 while most of the patient samples had poor dot-p values ranging from 0 to 0.69 (Figure 3.24 and Figure 3.23). The poor dot-p values are corroborated by the chromatographs which show no appreciable peaks in the expected retention window (Figure 3.25 and Figure 3.26). Additional chromatograms for each protein are available in Appendix A (Figure A 10 to Figure A 13).

Sample 1275 from a TB and HIV positive patient had a dot-p of 0.90 for peptide TQIDQVESTAGSLQGQWR from CFP-10 (Figure 3.23- B) and although the detected peaks had a low intensity, their shape matched that of the control spike sample and the reference spectrum in the spectral library (Figure 3.27). For this reason, this should be considered a positive match.

The peak area graphs also show that transition peaks from the spectral library and the control spikes of rESAT-6 and rCFP-10 were comparable in terms of the type of ions detected and the proportion of each ion, while most patients samples were not similar to either the spectral library or the control spike sample (Appendix A: Figure A 4 to Figure A 9). Patient sample 1275 was comparable to the spectral library for peptide TQIDQVESTAGSLQGQWR (Appendix A: Figure A 7).

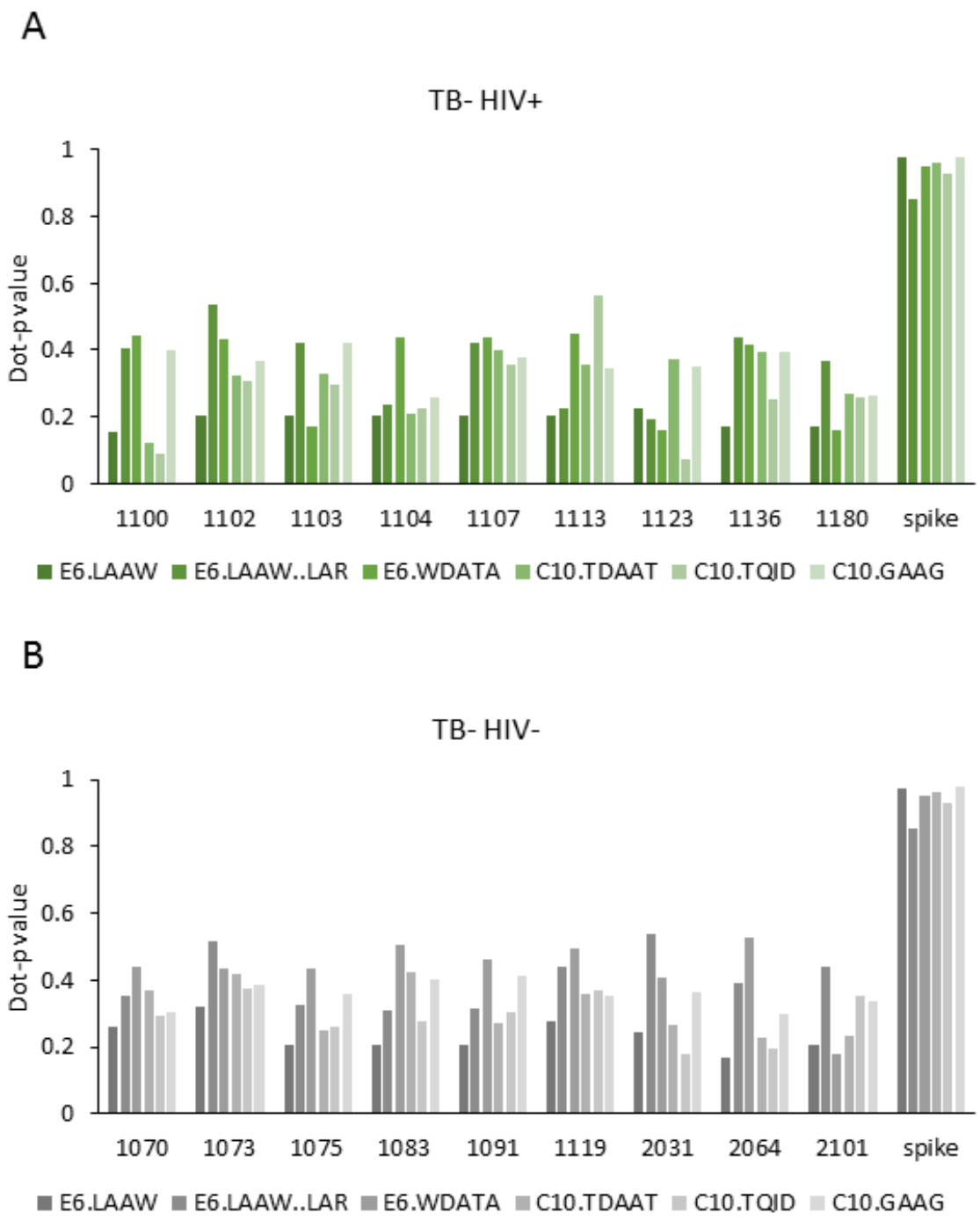

Figure 3.23 Dot-p value comparison between TB negative patients and the control spike.

A) TB negative and HIV positive patients B) TB negative and HIV negative patients. Three peptides where chosen from ESAT-6 and CFP-10. E6.xxxx denotes a ESAT-6 derived peptide. C10.xxxx denotes a CFP-10 derived peptide

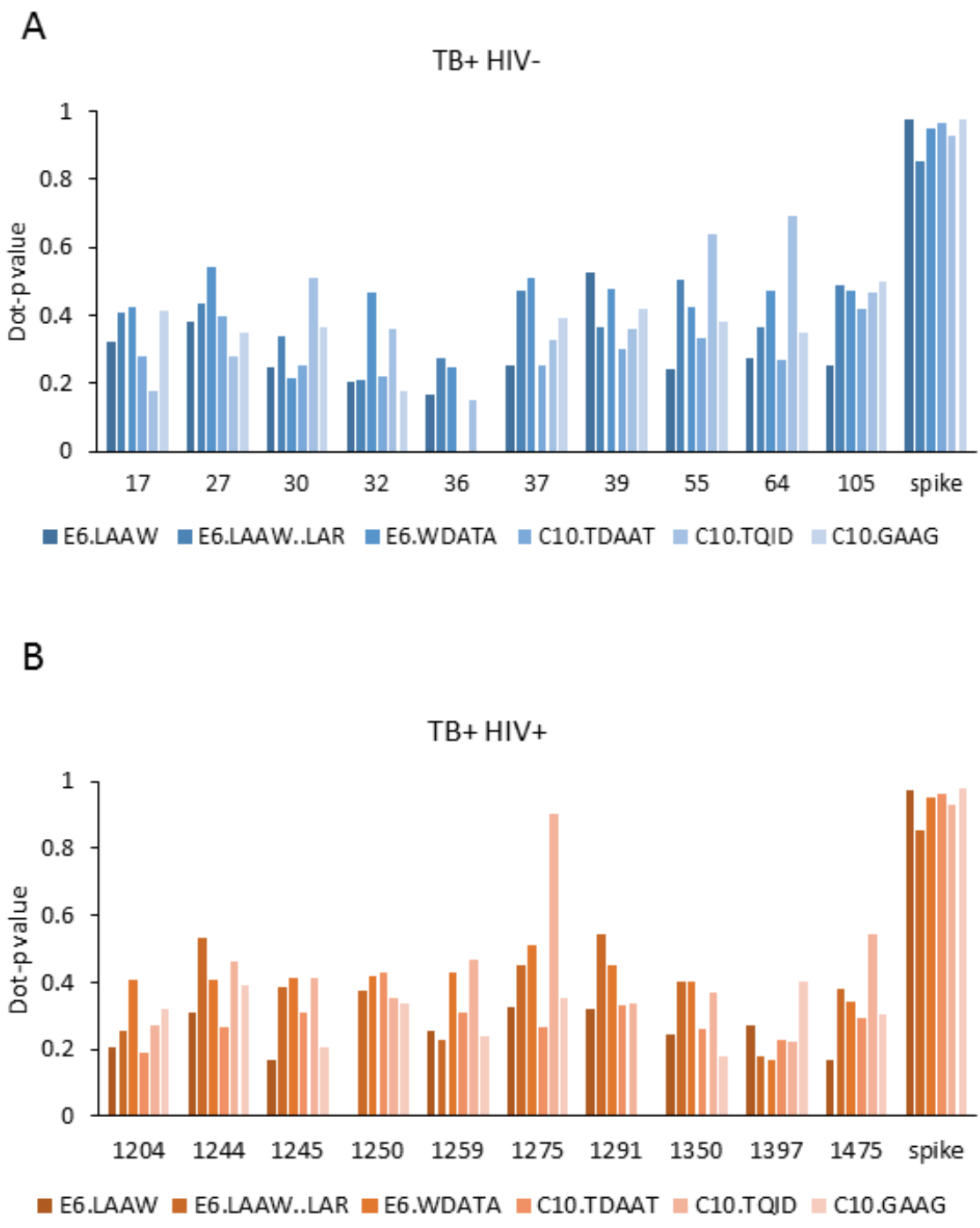

Figure 3.24 Dot-p value comparison between TB positive patients and the control spike with the spectral library.

A) TB positive and HIV positive patients B) TB positive and HIV negative patients. Three peptides where chosen from ESAT-6 and CFP-10. E6.xxxx denotes a ESAT-6 derived peptide. C10.xxxx denotes a CFP-10 derived peptide

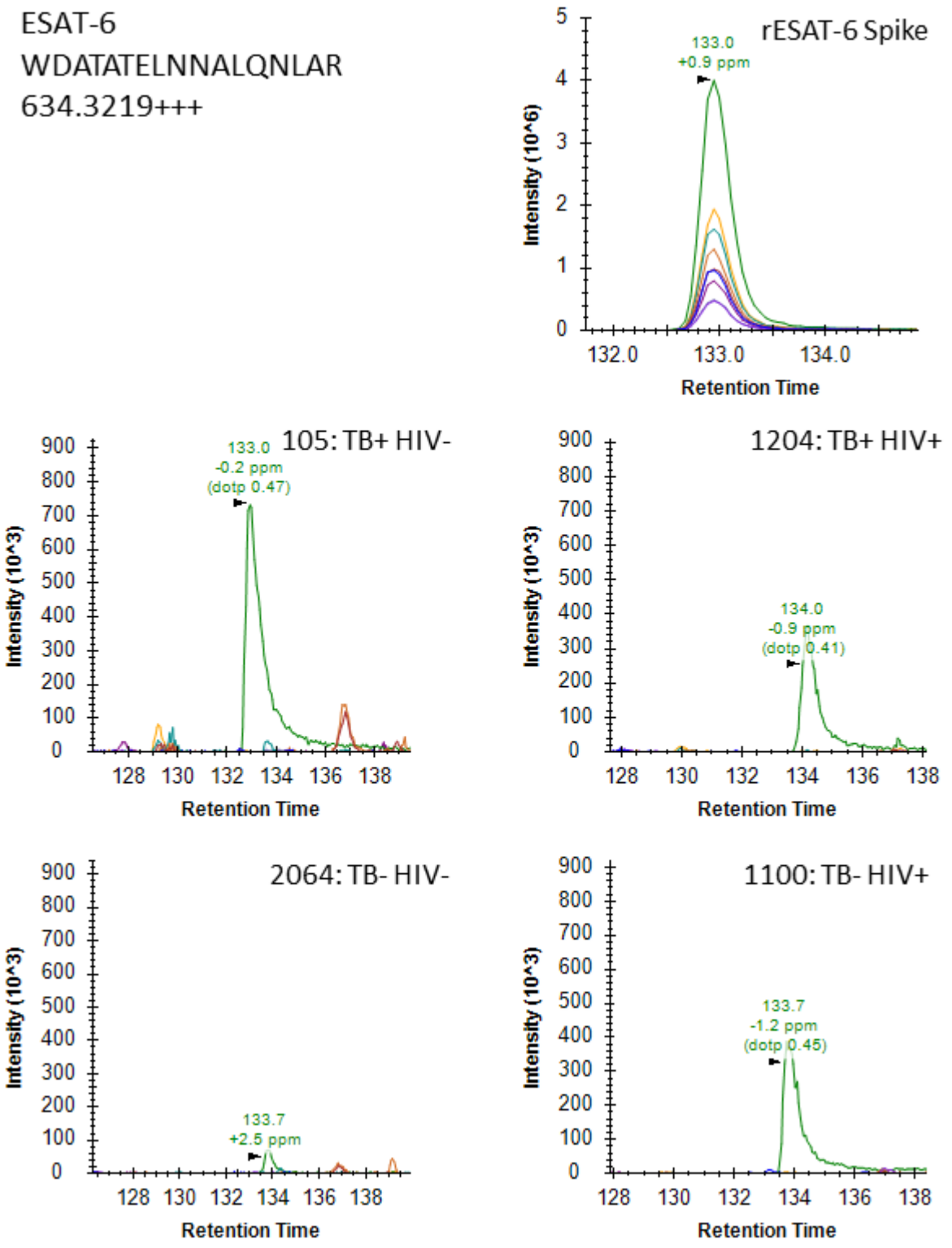

Figure 3.25 Transition chromatogram of peptide WDATATELNNALQNLAR

Transition chromatogram of the rESAT-6 control spike for peptide WDATATELNNALQNLAR and four representative patient chromatograms from each patient group at the same retention time.

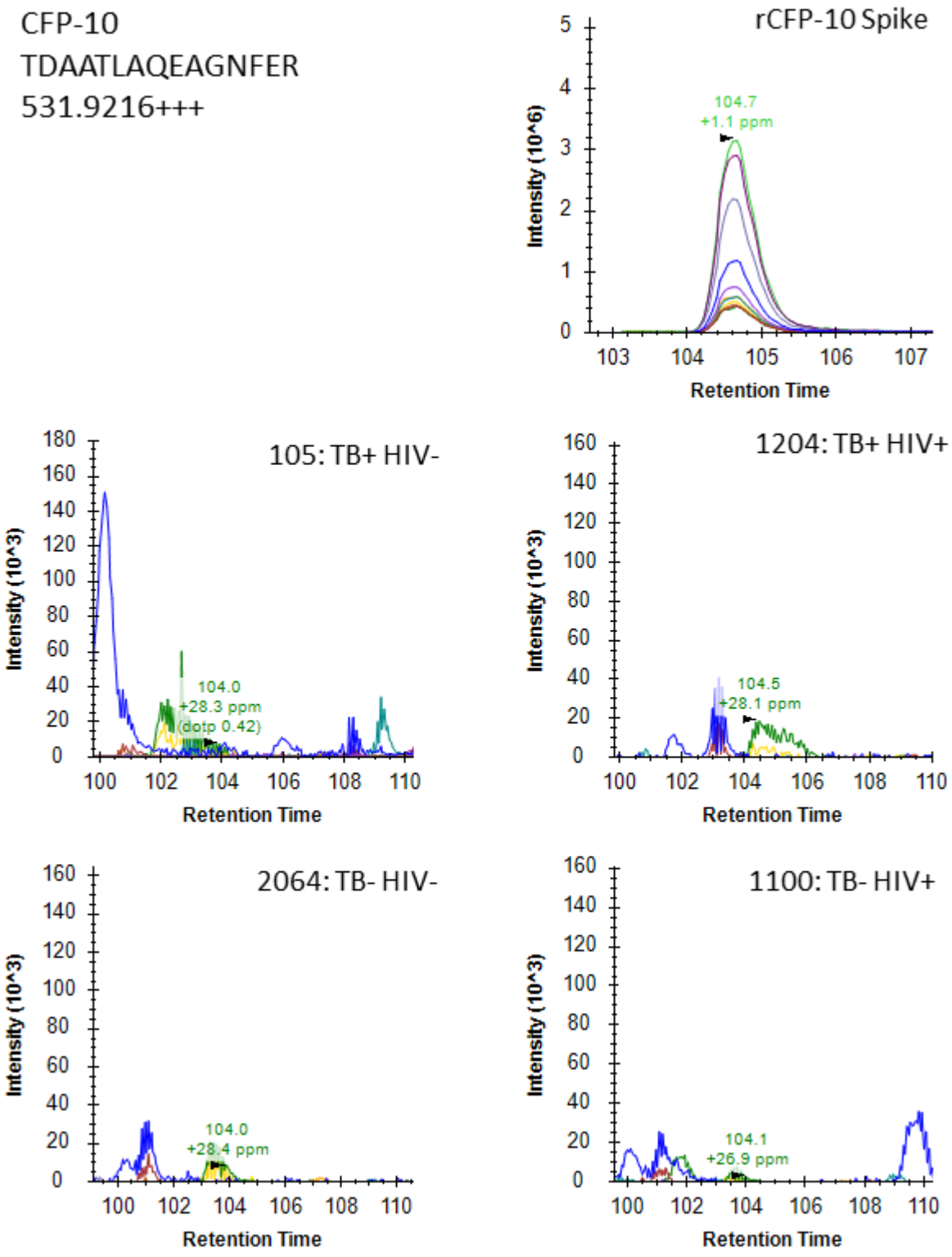

Figure 3.26 Transition chromatogram for peptide TDAATLAQEAGNFER

Transition chromatogram of the rCFP-10 control spike for peptide TDAATLAQEAGNFER and four representative patient chromatograms from each patient group at the same retention time.

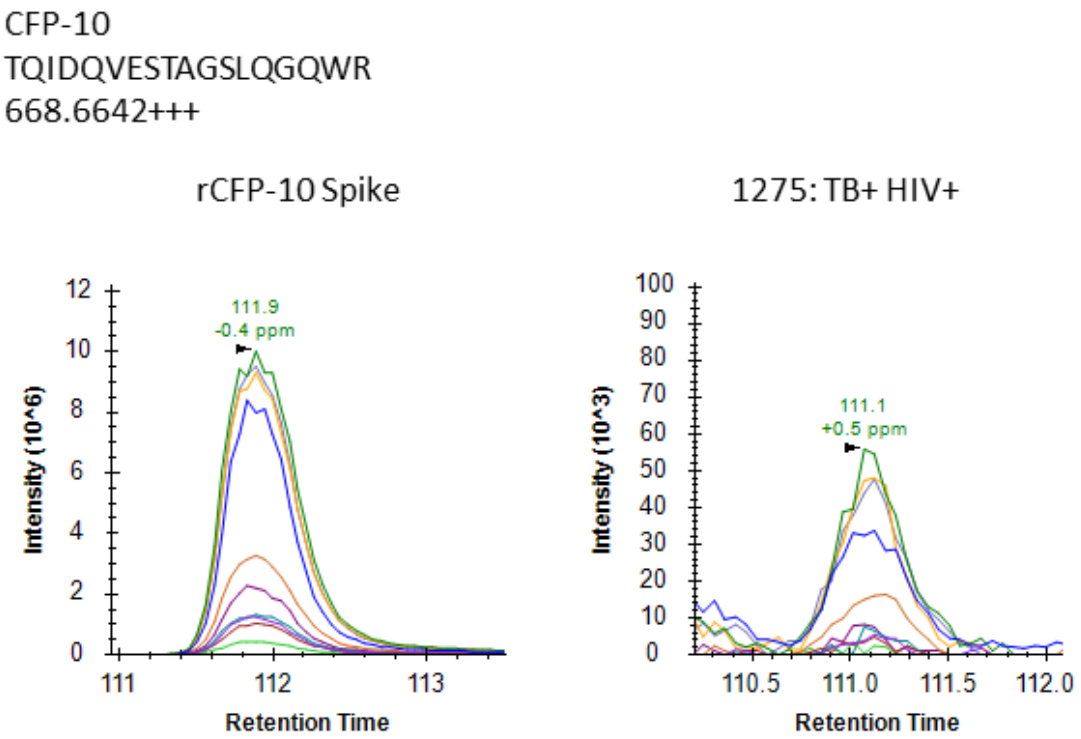

Figure 3.27 Comparison between spike and TB positive patient

Comparison of rCFP-10 spike chromatogram and patient 1275 (TB+; HIV+) for peptide TQIDQVESTAGSLQGQWR from CFP-10.

3.4 Discussion

3.4.1 ESAT-6 ELISA

Binding Curve

When rESAT-6 was serially diluted and spiked into neat urine, the absorbance readings from the ELISA produced a concentration dependant curve similar to the PBS control (Figure 3.9). The curve produced by rESAT-6 spiked into lyophilised urine produced a concentration dependant curve but did not become saturated at a similar concentration of rESAT-6 as the PBS and neat urine curves (Figure 3.10). An increased saturation point and greater background signal is an indication that the antibodies are binding non-specifically or cross reacting to other proteins.

The limit of detection of rESAT-6 in neat urine was ~0.21 ng/ml. This suggests that if ESAT-6 is present in urine it is at a concentration less than ~0.21 ng/ml since ESAT-6 was previously not detected in neat urine. Alternatively, ESAT-6 is degraded and the epitopes detected by the antibodies are no longer intact. In lyophilised urine the limit of detection was ~0.49 ng/ml due to the higher background signal. Despite the increased background, we speculated that ESAT-6 would be detectable if urine was concentrated. The limit of detection of the PBS control was the highest at ~0.72 ng/ml due to the greater variance in the negative control absorbance readings although this was still an improvement on a limit of detection of 1 mg/ml (125 nM) reported for another ESAT-6 ELISA (Mukundan *et al.*, 2012).

Urine and Sputum Samples

In order to increase the likelihood of detecting ESAT-6 in patient urine samples, samples were concentrated. Although samples were concentrated approximately ten-fold with the MWCO filter and lyophilisation techniques the samples concentrated with the MWCO filters were found to be more likely to have a reading above the cut-off value (Figure 3.11). This perhaps suggests that some proteins in lyophilised samples do not solubilise when resuspended. Previous observations were confirmed, in this experiment with no neat urine samples giving a positive signal. By concentrating the urine some TB patients had a positive signal above the PBS control, however some healthy volunteer urine samples also gave a positive signal after concentration (Figure 3.11). This suggests that the cross reactivity between a human protein and the antibodies used in the ELISA created a background signal that masked the signal of any ESAT-6 that may be binding. The cross reactivity could be exacerbated when patients have

proteinuria as with patient UA215 who had the highest absorbance reading.

Sputum samples from TB positive, latent TB and TB negative patients were also tested with the ESAT-6 ELISA assay (Figure 3.12). While some TB positive and latent TB patients had a positive signal, patients diagnosed as TB negative also had a signal above the cut-off. Hence, a pattern similar to that of the urine samples was noted in the sputum samples suggesting that sputum also contains a cross reactive element.

3.4.2 ESAT-6 Western Blots

To investigate the cause of the cross reactivity in the ELISA, sputum and concentrated urine samples were probed *via* western blot using the same anti-ESAT-6 antibody used in the ELISA. Several cross-reactive bands were noted in TB patients and healthy individuals however the most commonly observed band was approximately 26 kDa (Figure 3.13, Figure 3.14, and Figure 3.15). Patients with several cross reactive bands tended to be positive for proteinuria for example UA120 and UA211 (Figure 3.15; Appendix A: Table A3). Previously, anti-ESAT-6 antibodies have been reported to show cross reactivity against another secreted *M. tuberculosis* protein called MTP-64 which is 24 kDa (Harboe *et al.*, 1996), however since the cross-reactive band is also present in healthy urine and TB negative sputum samples, it seemed most likely that the cross-reactive protein is of human origin rather than from *M. tuberculosis*.

Since it is unlikely that the cross-reactivity stems from a monoclonal antibody, the secondary antibody (anti-mouse IgG-HRP) was tested alone (Figure 3.16). The same ~26 kDa band was visible in the blot that was only probed with the secondary antibody but no higher molecular weight bands were observed suggesting that both the primary and secondary antibodies are binding non-specifically to proteins in the urine.

Although cross reactive bands were seen in TB positive patients no band correlating to ESAT-6 which is ~9 kDa was observed (Figure 3.13 and Figure 3.15). Western blot assays are typically less sensitive than ELISAs hence this result does not inform about the presence of ESAT-6 in urine. Also, ESAT-6 may be degraded since non-tryptic *M. tuberculosis* peptides have previously been detected in urine by mass spectrometry (Young *et al.*, 2014).

3.4.3 Discovery Proteomics

To investigate the cross reacting antibodies used in the ELISA and western blot, the bands corresponding to the proteins bound by the primary and secondary antibodies were excised from a SDS-PAGE gel and analysed by mass spectrometry. Initially, an immunoprecipitation

based approach was attempted, but the yield of recovered protein was poor (data not shown) therefore an alternative method was needed to identify the cross reacting protein.

Spectra obtained had several single peaks across the gradient with no visible contaminants (Figure 3.18), consistent with urine typically containing less protein than other samples such as lysed.

MaxQuant identified 546 protein groups of various sizes (2.2 to 856.8 kDa) across all the samples (Appendix A: Table A7). The protein list was narrowed down as described above in order to identify probable candidates for the cross-reactive protein. A cut-off of one unique peptide was used to increase the confidence in the identifications. The overall intensity was used to gauge the most abundant proteins in the gel slices. The protein groups with the highest intensity varied across all the samples, but the top ten for each gel slice was similar across the four patients (Figure 3.19 and Figure 3.20). After reducing the protein lists for each gel slice several proteins were identified which were present in both the 25-35 kDa fraction and the 130-250 kDa gel fractions (Figure 3.21**Error! Reference source not found.**). Dimers or oligomers due to disulphide bonds are usually separated by β-mercaptoethanol during reducing SDS-PAGE protocols, however it is possible for incomplete reduction to occur especially with proteins rich in cysteine residues.

Since the secondary antibody was raised against mouse IgG (western blot) or rabbit IgG (ELISA) it is suspected that the antibodies were cross reacting with similar motifs in human proteins that are homologous to mouse IgG or rabbit IgG. Indeed, several majority proteins in both gel slices had Immunoglobulin (Ig) or Ig–like related polypeptides (Figure 3.22).

Ig gamma-1 chain C region (A0A087WV47) had a high intensity and score across all samples (Figure 3.19 and Figure 3.20), several Ig-like domains (Table 3.2) and is ~26 kDa when it forms a dimer (Appendix A: Table A7). Given these factors it is plausible that is the source of the ~26 kDa cross reactive band observed in the western blot assay and ELISAs. However, it is possible that several proteins cross reacted with the secondary antibodies as there were many proteins identified with Ig-like domains and a broad range of bands were observed in the western blot assays (Figure 3.22).

3.4.4 PRM

Since antibody based techniques were deemed not suitable for detecting ESAT-6 in patient samples a targeted proteomic approach was used to probe urine samples for ESAT-6 and CFP-10.

ESAT-6 and CFP-10 were not observed in the majority of TB positive urine samples (Figure 3.23). Similarly, CFP-10 and ESAT-6 were not detected in exosomes from serum (Kruh-Garcia *et al.*, 2014), however free *M. tuberculosis* proteins were detected in urine including secreted proteins from the PE-PGRS family (Young *et al.*, 2014).

In the one patient where a CFP-10 peptide was detected the clinical data revealed that the patient had pyuria which indicates that the patient likely had disseminated tuberculosis in the genitourinary organs (Figure 3.27)(Altintepe *et al.*, 2005).

Factors that influence the detection of biomarkers in urine include; endogenous proteolysis, sample preparation and low abundance of proteins in urine. First morning urinary samples are more prone to have degraded proteins due to endogenous proteolysis during the night, which reduces detection of biomarkers (Klein *et al.*, 2013). Non-tryptic peptides were not examined but proteins that are inconsistently lysed are impractical for a diagnostic test. Pre-processing of the sample such as freezing or removing cell debris also decreases biomarker yield in the sample since almost half of the total protein excreted in urine is in the sediment fraction (Barratt and Topham, 2007). The yield of low abundance proteins in urine and other samples can be increased with methods such as combinatorial peptide ligand libraries or nanoparticle hydrogels as discussed by Harpole *et al.* (Harpole, Davis and Espina, 2016).

These biomarkers could still be useful for accelerated characterisation of cultures and detecting *M. tuberculosis* in other patient samples such as sputum and pleural fluid (Park *et al.*, 2009; Feng *et al.*, 2011; Shen *et al.*, 2011).

3.5 Conclusion

In conclusion, the ESAT-6 ELISA provided no compelling evidence for ESAT-6 in urine or sputum and was compromised by too low selectivity. While ESAT-6 and CFP-10 are undetectable in urine, molecular recognition elements which do not cross react with human proteins would be useful for detecting these biomarkers in other bodily fluids and cultures.

4 SELECTING X-APTAMERS AGAINST MYCOBACTERIAL DERIVED BIOMARKERS

4.1 Introduction

Detection of *M. tuberculosis* proteins or glycolipids in clinical samples is often plagued by poor specificity and/or sensitivity (Kashyap *et al.*, 2009; Dheda *et al.*, 2010; Rotherham *et al.*, 2012). Improvements in sensitivity and specificity may be achieved by enhancing the molecular recognition and signal transduction phases of the binding event.

Here we selected modified aptamers, as molecular recognition elements, against CFP-10, CFP-10·ESAT-6, LAM and KatG as a possible means to improve the detection of *M. tuberculosis* biomarkers in patient samples.

4.1.1 Aptamers

Aptamers are short, single-stranded 15 mg/ml, RNA or peptide molecules that bind specifically to other molecules. These versatile molecules have been employed for a wide range of purposes including analytical applications, therapeutics and diagnostic biosensors (Keefe, Pai and Ellington, 2010; Radom *et al.*, 2013; Gülbakan, 2015; Hong and Sooter, 2015).

This discussion focuses on ssDNA aptamers, because they are more robust and affordable to synthesize than RNA or peptide aptamers (Keefe, Pai and Ellington, 2010). ssDNA aptamers have been selected against a wide range of targets including small molecules (Ellington and Szostak, 1992), proteins (Choi *et al.*, 2011), and whole bacteria (Duan *et al.*, 2013; Lamont *et al.*, 2014).

DNA aptamers have also been developed against whole mycobacteria and several mycobacterial target molecules for diagnostic and therapeutic purposes (Bannantine *et al.*, 2007; Chen *et al.*, 2007; Qin *et al.*, 2009; Shum *et al.*, 2011). Indeed, aptamers have been selected against our biomarkers of interest; LAM and the CFP-10·ESAT-6 heterodimer (Rotherham *et al.*, 2012; Pan *et al.*, 2014; Tang *et al.*, 2014).

While ssDNA aptamers are less likely to degrade, they have limited binding configurations, which impacts the affinity with which DNA aptamers can bind to their targets. High affinity aptamers against proteins are more common since the diversity of amino acid side chain moieties provide a variety of binding interactions, whereas lipids and carbohydrates are limited in this respect.

It is, however, possible to take advantage of the positive attributes of ssDNA aptamers, and simultaneously increase the scope of binding interactions, and achieve slower off-rates by modifying DNA with additional chemical groups (Gold *et al.*, 2010; Diafa and Hollenstein, 2015). This discussion focuses on the specific chemical modifications that could enhance the binding affinity and specificity of ssDNA aptamers selected against LAM, CFP-10·ESAT-6 and KatG.

4.1.2 LAM

LAM is a promising biomarker for diagnosing tuberculosis disease. It is an abundant component of the cell wall, which is released as vesicles and shed from mycobacteria into the blood stream (Sada *et al.*, 1992; Beatty *et al.*, 2000). Also, Hamasur *et al.* commented that LAM is less likely to be degraded *in vivo* as no known human glycosidases target the specific linkages present in LAM (Hamasur *et al.*, 2001). However, LAM is typically present in low concentrations in urine (Savolainen *et al.*, 2013), cannot be detected specifically in sputum with current assays (Dheda *et al.*, 2010), and is mostly immunocomplexed or clumped in lipid rafts in blood (Chan *et al.*, 2000, 2015; Sakamuri *et al.*, 2013). Hence, innovative and sensitive biosensors are needed to detect LAM in patient samples.

The only commercial assay for detecting LAM involves anti-LAM antibodies either in an ELISA or lateral flow assay format produced by Alere™. Inherent limitations of these assays include, batch to batch variation of polyclonal antibodies and the expensive production of antibodies. Using these assays, LAM in urine is typically detected in patients with a high bacillary load (Boehme *et al.*, 2005), a low CD4 count due to HIV (Shah *et al.*, 2010; Peter, Theron and Dheda, 2013), or disseminated tuberculosis (Cox *et al.*, 2015). LAM may be detected with suitable sensitivity for other TB patients when the urine is concentrated, however this is impractical in low-resource clinical settings (Tessema *et al.*, 2001; Savolainen *et al.*, 2013). In sputum, the anti-LAM antibodies cross-react with Actinobacteria and other commensal oral microorganisms resulting in poor specificity (Dheda *et al.*, 2010). Other bodily fluids, such as cerebrospinal fluid, also contain LAM which is useful for diagnosing extrapulmonary tuberculosis (Patel *et al.*, 2009). So, while LAM is present in many bodily fluid compartments, its detection remains

suboptimal.

Several studies have attempted to improve the detection of LAM *via* various techniques. One study developed a chimeric antibody that targets the distinctive mannose capping motifs present on *M. tuberculosis* LAM (Chan *et al.*, 2015). Targeting the mannose caps could overcome the specificity problem in patient sputum, however the chimeric antibody was tested only on urine and serum samples. In their HIV negative cohort, the authors observed improved detection of smear negative and smear positive TB patients, however their intrinsic limit of detection (0.5 to 2 ng/ml) is within the same range of current assays (Savolainen *et al.*, 2013). The authors could discriminate between *M. tuberculosis* and the previously cross-reactive *Nocardia cyriacigeorgica,* but not between *M. tuberculosis* and *Tsukamurella paurometabolum* (Venisse *et al.*, 1993; Petzold, Stanton and Leary, 2005; Chan *et al.*, 2015). *T. paurometabolum* and *Corynebacterium matruchotii* also express terminal mannose motifs. Hence, the level of background signal from these organisms have to be determined before this chimeric antibody can be heralded as a solution to the poor specificity of the current LAM antibodies observed in patient sputum (Sutcliffe, 1995; Gibson *et al.*, 2004; Dheda *et al.*, 2010).

Another study used a combination of monoclonal antibodies and gold coated magnetic nanoparticles to achieve a detection limit of 0.05 ng/ml LAM; a 20-fold improvement on the detection limit of 1 ng/ml observed when the same antibodies were used in an ELISA format. The authors used a small cohort of pulmonary and extrapulmonary TB patient urine samples to test their Uri-TB direct assay with promising results. However, their finding that a patient with urogenital extrapulmonary TB tested negative for LAM is counterintuitive, which warrants further investigation in a larger cohort (Hamasur *et al.*, 2015).

Other studies have focussed on detection platforms to improve the current ELISA limit of detection (~64 pM) (Savolainen *et al.*, 2013). The use of fluorescent antibodies and single molecule scanners or waveguide sensors permit detection limits of 10^{-12} to 10^{-15} M for LAM spiked into urine or plasma. The limitations of these strategies include the poor stability of the fluorescent antibodies, and the cost of both the antibodies and equipment. Innovation in portable versions of these devices is ongoing and may present an affordable solution in the future (Schmidt *et al.*, 2011; Mukundan *et al.*, 2012).

A label free detection platform using a quartz crystal microbalance (QCM), functionalised with anti-LAM antibodies, failed to improve on current methods having achieved a limit of detection of ~60.6 nM, however the method could be improved with better molecular recognition elements (Hiatt and Cliffel, 2012). Specifically, Hiatt and Cliffel mentioned that a limitation of

their study was the amount of anti-LAM antibody that could be immobilised to the QCM cantilevers due to steric hindrance (Hiatt and Cliffel, 2012). Instead, DNA aptamers (2-3 nm in diameter), which are substantially smaller than antibodies (12-15 nm in diameter), can permit higher surface density functionalisation of the QCM cantilevers with concomitantly higher LAM binding capacities, thereby achieving lower detection limits for LAM. Additionally, a more specific molecular recognition element could overcome the challenge of poor specificity associated with sputum samples.

Two previous studies claim to have selected ssDNA aptamers against LAM with a K_D of 400-670 nM (Tang *et al.*, 2016) (Pan *et al.*, 2014). Tang *et al*. reported sensitivity and specificity values in the 80-90% range for sputum and serum. However, the lowest LAM concentration noted on their standard curve is 180 ng/ml (~9 nM), which is an order of magnitude higher than other reported concentrations of LAM in patient serum (0.8-3.1 pM) (Sakamuri *et al.*, 2013; Tang *et al.*, 2016).

Aptamers selected against other carbohydrate and lipid molecules have modest affinities with K_D values ranging from 10^{-5} to 10^{-7} M (Fukusaki *et al.*, 2000; Betat *et al.*, 2003; Masud *et al.*, 2004; Boese and Breaker, 2007; Low, Hill and Peccia, 2009; Wang *et al.*, 2014). Carbohydrates and lipids have limited ability to bind to ssDNA aptamers since they lack positively charged moieties and aromatic structures, hence it is not surprising that high affinity aptamers have not been previously selected against these classes of biomarkers. Additionally, the negatively charged phosphate group on LAM may hinder selection of an aptamer due to repulsion from the DNA sugar-phosphate backbone. However, aptamers can bind to unsaturated carbon chains by either π-interactions or shape complementarity (Betat *et al.*, 2003; Grimme, 2008).

Modified aptamers provide an opportunity to increase the chemical diversity of ssDNA and to overcome the challenges of selecting aptamers against a glycolipid. Boronic acid modified aptamers have been used previously to improve the binding capability of aptamers to carbohydrate moieties (Lato *et al.*, 2002; Li *et al.*, 2008). Boronic acid reacts with the diols of carbohydrate molecules to form stable cyclic boronate esters, which should provide an anchor to mediate further interactions between other parts of LAM and the ssDNA aptamer. Other advantageous ssDNA modifications include, hydrophobic moieties such as indole, napthyl or indole that facilitate binding to lipid core of LAM (Vaught *et al.*, 2010), and positively charged moieties such as 5-N- (6-aminohexyl)carbamoylmethy or 5-(3′′-Aminopropynyl) that interact with the negatively charged phosphate group of LAM (Battersby *et al.*, 1999; Masud *et al.*, 2004).

4.1.3 ESAT-6 and CFP-10

ESAT-6 and CFP-10 are secreted proteins that form a tight heterodimer, although CFP-10 is more stable than ESAT-6 as a monomer (Renshaw *et al.*, 2002; Meher *et al.*, 2006). Concentrations of these biomarkers may be high in sputum samples depending on the number of bacteria present. As discussed previously, ESAT-6 could not be detected with an in-house ELISA assay, which had a nanomolar limit of detection, so it is plausible that CFP-10 is similarly scarce. Hence, innovative and sensitive biosensors are needed to detect ESAT-6 and/or CFP-10.

There are no commercial assays to detect ESAT-6 or CFP-10, however there have been several immunoassays using a variety of detection methods. Assays that have achieved the lowest limit of detection (10-60 pg/ml) used a colourimetric detection method (Feng *et al.*, 2011; Kim *et al.*, 2013), while other methods, such as, waveguide optical sensors coupled with fluorescent antibodies or surface plasmon resonance (SPR), achieved detection limits of 100-900 ng/ml (Hong *et al.*, 2011; Mukundan *et al.*, 2012). None of these assays have been tested in urine or sputum from patients with pulmonary tuberculosis, however the best performing ELISA could detect ESAT-6 in pleural fluid with a sensitivity of 100% and specificity of 95.4%, and CFP-10 with a sensitivity of 81.6% and specificity of 92.2% (Feng *et al.*, 2011). Each of these methods used antibodies, which as previously mentioned, are expensive especially when coupled to fluorescent reporters.

Two studies have explored raising ssDNA aptamers against ESAT-6 and CFP-10. The first study selected aptamers against the CFP-10·ESAT-6 heterodimer, however the aptamers bound primarily to CFP-10. They reported 100% sensitivity and 68.75% specificity when detecting CFP-10 in sputum with aptamer CSIR 2.11 (K_D = 8 nM) (Rotherham *et al.*, 2012). CSIR 2.11 cross-reacts with *M. smegmatis, M. bovis* BCG and *Pseudomonas aeruginosa,* of which, two have RD1 homologues, whereas BCG does not. The cross-reactivity of aptamer CSIR 2.11 underscores the poor specificity associated with assays performed on sputum samples (Rotherham, 2012).

Another research group reported aptamers with nanomolar affinity (K_D = 10^{-7} M) against a recombinant CFP-10·ESAT-6 linked heterodimer. The aptamers were used in an ELONA assay to detect ESAT-6 and/or CFP-10 in pulmonary TB patient sera (Tang *et al.*, 2014). While they claimed 100% sensitivity and 94.1% specificity, the lowest concentration in their binding curve was 50 ng/ml (5 nM) which seems high given that a previous study estimated that LAM, a more abundant biomarker, was detectable within the picomolar range (Mukundan *et al.*, 2012).

While some progress has been made in detecting ESAT-6 and CFP-10 with aptamer assays, improvements are needed to be useful under real world conditions, especially in low resource

settings. Modified aptamers could provide the additional sensitivity and specificity needed for an affordable and effective assay to detect ESAT-6 and/or CFP-10. Modified aptamers, particularly thioaptamers, have been selected against several proteins (Min *et al.*, 2008; Mann *et al.*, 2010; Gandham *et al.*, 2014), but other modifications can provide specific advantages, for example; ESAT-6 and CFP-10 have hydrophobic regions that could be targeted with hydrophobic modifications, such as the aptamers developed by Kimoto *et al*. (Kimoto *et al.*, 2013). Additionally, boronic acid can form bonds with nucleophilic amino acid side chains (Whyte, Vilar and Woscholski, 2013), and positively charged moieties can interact with negatively-charged amino acid side chains.

4.1.4 KatG

The *M. tuberculosis* catalase peroxidase has a molecular weight of ~80 kDa, and is referred to by its gene name, *katG*. Catalase converts peroxide to water and oxygen, whereas peroxidase generates water and an activated donor molecule. Reactive oxygen species, such as peroxide, are by-products of aerobic respiration, which are also used by phagocytes as a bactericide to defend against infections. Most bacteria have an adaptive stress response triggered by the OxyR transcription factor to respond to reactive oxygen species (Nathan and Shiloh, 2000). OxyR in *M. tuberculosis* appears to be non-functional due to mutations in the gene, but Sherman *et al* suggest that KatG, alkyl hydroperoxidase (AhpC), and the thick cell wall composed of oxidation resistant lipids, provide a constitutive oxidative stress response (Sherman et al. 1996). Later research showed that KatG is important for resisting the oxidative surge produced by phagocytes, but does not appear to have additional functions (Ng *et al.*, 2004).

A tuberculosis prodrug, isoniazid, is activated by KatG, however some strains have developed resistance to isoniazid due to mutations in the *KatG* gene. While KatG is important for counteracting reactive oxidative species in phagocytes, reciprocal mutations resulting in increased activity of AhpC appear to compensate for the loss of KatG functionality in isoniazid resistant strains (Sherman *et al.*, 1996).

A molecular diagnostic test called a line probe assay is available to detect the mutations that lead to isoniazid resistance, however it is expensive and not widely used. Line probe assays initially amplify the *KatG* gene *via* PCR after which, the gene products are incubated with mutant or wild type *KatG* probes. DNA that either hybridises with mutant probes, or alternatively does not hybridise with the wild type probe indicates a mutation in the *KatG* gene. While a particular mutant may not be present in the mutant probe library, failure of the

amplified *KatG* gene to hybridise to the wild type probe alerts to the need for further testing (Barnard *et al.*, 2008). While this test is useful for detecting drug resistance, it is ill suited for point of care diagnostics.

The KatG catalase-peroxidase has not been used as a biomarker in any commercial assays, however it was detected in exosomes retrieved from serum by mass spectrometry analysis (Kruh-Garcia *et al.*, 2014). KatG is thought to be secreted as it is found in culture filtrate, however some cytosolic proteins were also present in the filtrate due to harvesting at the late log phase (Sonnenberg and Belisle, 1997). Later work argued that KatG is associated with the cell surface rather than actively secreted (Raynaud *et al.*, 1998). Since it is present on the surface of the bacterium, and may be actively secreted in exosomes this protein could act as a biomarker of disease.

While no assays have been developed to detect KatG using monoclonal antibodies, ssDNA aptamers have previously been generated against KatG (Sonnenberg and Belisle, 1997; Harroun, 2014). KatG is part of the class I peroxide catalases, which share homology across many bacterial species (Zámocký *et al.*, 2014). Any diagnostic test using KatG as a biomarker should therefore take into consideration possible cross reaction of the molecular recognition element with commensal bacteria present in the mouth or associated with urinary tract infections. In this regard, other studies have used actinomycetes, streptococcal species, and other oral isolates to test the cross reactivity of their TB biomarker assays (Dheda *et al.*, 2010; Rotherham *et al.*, 2012).

Current platforms to detect these biomarkers are costly and/or ineffective. Any assay using current antibodies is limited by the affinity of the antibody, and steric hindrance when antibodies are immobilised onto surfaces. It is therefore apparent that improvements in molecular recognition and signal transduction are needed to improve the specificity and sensitivity of TB biomarker detection assays.

4.1.5 Methodology

Systematic **E**volution of **L**igands by **Ex**ponential Enrichment (SELEX), a term coined by Tuerk *et al*. (Tuerk and Gold, 1990), is the classic method for selecting aptamers against various targets. The SELEX method evolved from studying protein-DNA interactions (Oliphant and Struhl, 1987), and *in vitro* evolution of ribozymes (Green *et al.*, 1991) with random oligonucleotide sequences. The next development involved selecting oligonucleotides against molecules that do not conventionally bind to RNA or DNA (Ellington and Szostak, 1990). The

SELEX methodology has been adjusted to improve the process and to customise it for a range of targets from whole cells to small molecules (Stoltenburg, Reinemann and Strehlitz, 2007; Darmostuk *et al.*, 2015).

Conventional SELEX has four key steps, in which the oligonucleotide sequences (from a random oligonucleotide pool) that bind to the target are isolated and selectively enriched with each successive cycle (Figure 4.1). When the aptamer pool enrichment plateaus, the oligonucleotide pool is cloned for sequencing, or sequenced with next generation methods (Ellington and Szostak, 1990).

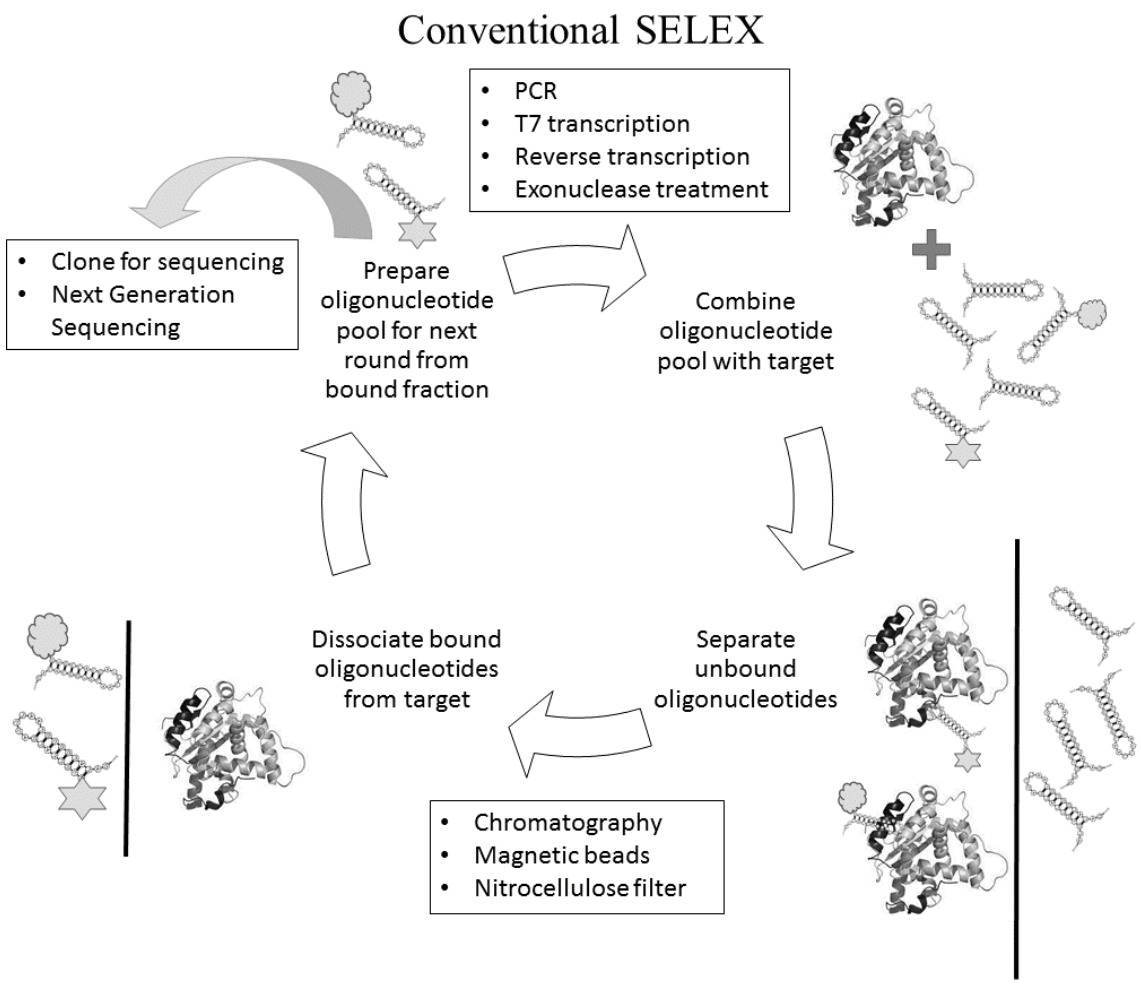

Figure 4.1 Diagram of conventional SELEX workflow

While conventional SELEX requires repeated cycles, some studies have reduced the need for multiple cycles by adapting the SELEX process (Nitsche *et al.*, 2007; Fan *et al.*, 2008; Arnold *et*

al., 2012). Reduced cycles or a single cycle accelerates the selection process and reduces the number of PCR cycles, which would otherwise lead to the amplification of unwanted DNA products (Musheev and Krylov, 2006).

Another advancement is the use of high throughput sequencing which allows monitoring of the selection process, and elimination of random cloning techniques where high affinity binders may be lost (Cho *et al.*, 2010).

We selected modified aptamers against our targets in collaboration with AM Biotechnologies, LLC (AM Biotech) who have developed a bead based method for the selection process, and use next generation sequencing to identify putative aptamers in the final pool (Figure 4.2) (view an animation of process online here) (Lokesh *et al.*, 2017).

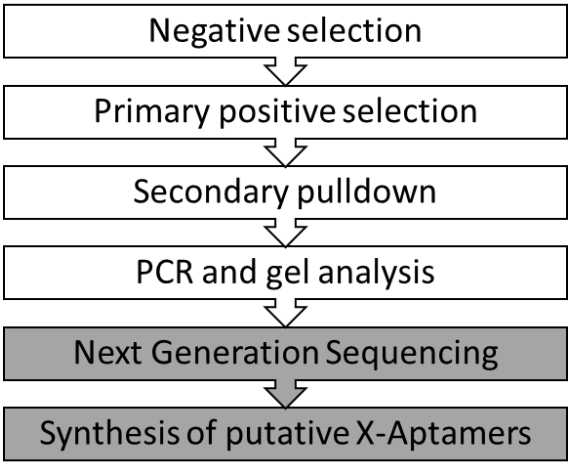

Figure 4.2 Bead based X-Aptamer Selection Process.

Negative selection: The random library, attached to polystyrene beads, is incubated with naked streptavidin coated magnetic beads to remove the bulk of non-specific binders. **Primary selection:** Library beads not bound during the negative selection are incubated with target attached to magnetic beads. **Secondary Pulldown:** Unbound oligonucleotides are removed and the bound sequences are cleaved from their polystyrene beads. Cleaved sequences are incubated with a fresh aliquot of target attached to magnetic beads. **PCR:** Unbound sequences are removed and putative aptamers are amplified by PCR. **Next Generation Sequencing:** PCR products are subjected to next generation sequencing and enriched sequences are identified. **Synthesis of putative X-Aptamers:** Enriched sequences are synthesized with original modifications for validation.

The pseudorandom library is generated by a split and pool scheme which has an estimated 10^8 sequences. A library with modified nucleotides synthesized by the split-pool method allows for the positions of the various modifications to be known so that the putative aptamers can be re-synthesized accordingly after the selection process (Gorenstein *et al.*, 2014).

The chemical modifications introduced to our oligonucleotide library were incorporated at position five of deoxyribose uracil triphosphate (dUTP) with either boronic acid, phenol, indole or hydroxymethyl (Figure 4.3). Indole and phenol mimic hydrophobic amino acid side chains, whereas hydroxymethyl mimics a polar uncharged side chain. Boronic acid interacts with diols and nucleophilic amino acid side chains such as serine (Whyte 2013). Boronic acid was specifically included to aid binding to the mannan backbone of LAM while the other modifications were chosen to increase the general variety of binding interactions possible.

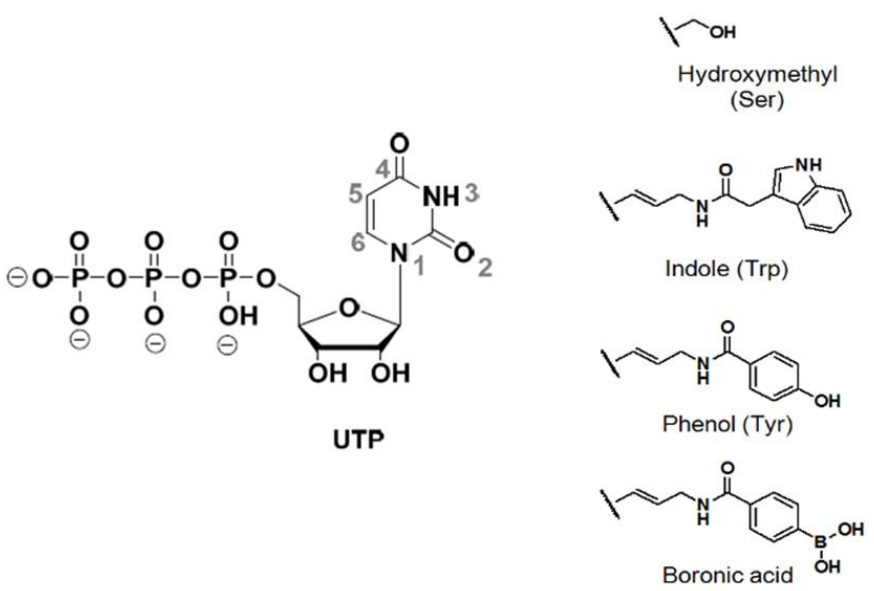

Figure 4.3 Base modifications to UTP by AM Biotech

Base modifications made at position 5 of UTP with one of the four moieties on the right. Image adapted from Diafa and Hollenstein (Diafa and Hollenstein, 2015).

After the selection process and secondary pull-down, the enriched library sequences are amplified by PCR in preparation for next generation sequencing (Figure 4.2). The data from the next generation sequencing is analysed using the Aptaligner© software. The software typically reduces the number of sequences from ~5 million to ~3.5 million unique sequences by

reducing noise and removing sequences of the incorrect length. Enriched sequences are identified by comparing the primary selection and secondary pulldown sequences. It uses the library design file to match unmodified sequences to the original modified sequences since modifications are lost during the PCR process. Aptaligner© also performs clustering analysis using a Markov model. Sequences with similar sequences that may bind to a lesser extend are good aptamer candidates (Lu *et al.*, 2014). Final sequences are moderated to limit hydrophobic groups before they are synthesized for validation experiments with the targets.

4.1.6 Aim and Objective

The aim was to select X-Aptamers against CFP-10, CFP-10·ESAT-6, LAM and KatG *via* a bead based selection method to create selective molecular recognition elements for use in a biosensor diagnostic platform.

4.2 Methods

4.2.1 Biotinylation of targets

KatG and CFP-10

KatG was expressed in house by Dr Andrew Nel and CFP-10 was obtained from BEI Resources (NR-14869) (see Appendix B for protein sequence information). Each protein was incubated with biotin-N-hydroxysuccinimide ester (NHS-biotin) at a 20:1 molar ratio (biotin: protein) for 4 h with gentle agitation in the dark at room temperature. Excess biotin was removed with the use of SigmaSpin™ post reaction clean-up columns (#S5059, Sigma Aldrich). The columns were prepared and used as per the manufacturer's instructions. Briefly, the storage buffer was removed by centrifugation before the sample was applied to the column and centrifuged for 4 min at 750 rcf. The eluate containing the protein was collected. The column was washed with an equal volume of PBS (137 mM NaCl; 2.7 mM KCl; 10 mM Na_2HPO_4; 2 mM KH_2PO_4; 1 mM $MgCl_2$), and the eluate was collected to determine if protein was retained on the matrix.

Bradford Assay

The biotinylated protein concentration was determined using a Bradford assay in a 96-well microplate format. A two-fold dilution series of BSA (0.06-1 mg/ml) was used to generate a standard curve. 10 µl of each standard and the biotinylated proteins was added to microtitre wells in duplicate. 200 µl of diluted Bradford dye reagent (#500-0006, BioRad) was added to each microtitre well containing either BSA standard or biotinylated protein, and incubated for at least 5 min but not more than 1 h. The absorbance was read at 595 nm. The mean absorbance values of the BSA dilutions were plotted against their corresponding absorbance values to generate a standard curve. The concentrations of biotinylated KatG and CFP-10 were interpolated from the BSA standard curve using their corresponding mean absorbance values. The mean absorbance value for the negative control (PBS only) was subtracted from all other absorbance values before interpolation. The two aliquots of each biotinylated protein were pooled for the selection process.

LAM

100 µg of LAM from *M. tuberculosis* (H37Rv) (BEI Resources; NR-14848) or *M. smegmatis* (BEI Resources; NR-14849) was oxidized in a solution of 1 mM sodium periodate dissolved in a 100 mM sodium acetate buffer (pH 5.5) for 10 min in an ice bath (0-4 °C) in the dark. Excess periodate was neutralised with a solution of sodium sulphite (final concentration of 80 mM) for

5 min at room temperature. EZ link Hydrazide-LC-Biotin (Thermo Scientific #21340) in DMSO was added to the oxidised LAM to a final concentration of 3.75 mM, and the reaction was incubated for 1 h at room temperature. The reaction was stopped by dialysing (Slide-A lyzer 3.5 K; Thermo Scientific #88403) against a dialysis buffer (50 mM sodium phosphate, 150 mM NaCl, pH 7.4) for 2 h at room temperature. The initial dialysis buffer was replaced with fresh buffer and placed at 4 °C overnight. Adapted from (Venisse *et al.*, 1995). The concentration of biotinylated LAM was estimated based on initial concentration and final volume after dialysis.

HABA Assay Biotinylation quantitation

The extent of biotinylation was estimated with the HABA (4'-hydroxyazobenzene-2-carboxylic acid dye) displacement method (ImmunoPure HABA kit; Pierce). HABA is displaced from streptavidin by biotin due to the significantly higher binding affinity of biotin for streptavidin. 180 µl aliquots of a solution of HABA and streptavidin (prepared as per the manufacturer's recommendations) were pipetted into microtitre wells and the absorbance was read at 490 nm (500 nm filter was not available). Then 1 µg of biotinylated protein or 4 µg of LAM from *M. smegmatis* was added to each well, and the absorbance was read again. The average number of biotin moieties per LAM molecule was calculated from the difference in absorbance between the two readings using the ThermoScientific online HABA calculator. A paired two-tailed T-test was used to assess if the absorbance reading before and after addition of the biotinylated molecule was significantly different using Microsoft Excel 2013.

Western Blot

Biotinylation of the targets was confirmed *via* western blot performed with a Streptavidin-HRP conjugate. Amounts of each sample loaded onto the gel can be viewed in Appendix B: Table A 13. Samples were denatured by boiling in sample loading buffer (12 mM Tris-HCl, pH 6.8, 1% (v/v) β-mercaptoethanol, 0.4% (w/v) SDS, 5% (v/v) glycerol, 0.02% (w/v) bromophenol blue). A protein ladder (#26619, Thermo Scientific) was used to estimate the molecular weights of proteins. Proteins were separated by electrophoresis on a 12% SDS-PAGE gel for 1-2 h at 120 V (constant voltage), and then transferred to a 0.45 µm nitrocellulose membrane at 300 mA (constant current) for 50 min. The nitrocellulose membrane was blocked overnight with 5% (w/v) fat free milk (Elite, Clover) in Tris buffered saline (20 mM Tris and 150 mM NaCl) with 0.1% (v/v) Tween-20 (TBST), and then probed with 0.1 µg/ml streptavidin conjugated HRP (KPL #14-30-00). The membrane was washed three times for 5 min with TBST with gentle agitation. After washing the membrane, it was incubated in the recommended volume of

Western Bright Chemiluminescence reagent (Advansta) for 2 min at room temperature. The membrane was then exposed to film for varying time periods and developed with the manual AGFA developer (#E43HP G150) and fixer (#E43JR G354).

Formation of ESAT-6·CFP-10 heterodimer

Biotinylated CFP-10 and ESAT-6 (BEI Resources; NR-14868) were incubated together in Buffer B (PBS and 0.05% (v/v) Tween-20) in equimolar amounts (5 μM) for 1 h at room temperature (Rotherham *et al.*, 2012).

4.2.2 X-Aptamer Selection

A custom library (~10^8 members) of modified of DNA (16% Phenol and Indole, 68% Indole and Boronic acid, 16% Phenol and Hydroxymethyl) attached to polystyrene beads was synthesised by AM Biotech and provided together with forward primers and barcoded reverse primers (He *et al.*, 2012; Gorenstein *et al.*, 2014).

- **Buffer A (with BSA)** [PBS (137 mM NaCl; 2.7 mM KCl; 10 mM Na_2HPO_4; 2 mM KH_2PO_4; 1 mM $MgCl_2$); 0.05% (v/v) Tween20 and 0.2% (w/v) BSA]
- **Buffer B (without BSA)** [PBS (137 mM NaCl; 2.7 mM KCl; 10 mM Na_2HPO_4; 2 mM KH_2PO_4; 1 mM $MgCl_2$) and 0.05% (v/v) Tween20]

Target Coupling to Magnetic beads

Streptavidin coated magnetic beads (Invitrogen Dynabeads M270; #11205D) were resuspended, and a 100 μl aliquot was transferred into a 1.5 ml microfuge tube for each target. The magnetic particles were pelleted with the use of a magnet and the supernatant was discarded. The magnetic beads were washed by initially resuspending in 250 μl Buffer B, followed by pelleting with a magnet to remove the supernatant. The beads were washed three times. The biotinylated targets were resuspended in Buffer B (Appendix B: Table A 14) and incubated with the magnetic beads in 100 μl of Buffer B at room temperature for 30 min with rotation. The magnetic bead pellets were recovered using a magnet and washed three times with 250 μl of Buffer B. The magnetic beads with biotinylated targets attached were resuspended in 100 μl of Buffer A.

Bead library preparation

The DNA library was resuspended in 10 ml of Buffer B, transferred to a conical tube and pelleted by centrifugation at 3000 rcf for 10 min at room temperature. The supernatant was discarded except for ~100 μl. The beads were resuspended in 3 ml of Buffer B, heated to 95 ºC for 5 min and allowed to cool slowly over ~30 min. Buffer A (7 ml) was added and the beads

were pelleted again for 10 min at 3000 rcf at room temperature. The supernatant was discarded leaving 100 µl of buffer. Buffer A was added to a total volume of 1.8 ml and transferred to a 2 ml tube.

Negative Selection

Streptavidin coated magnetic particles were resuspended and 300 µl was transferred to a 1.5 ml tube. The magnetic beads were pelleted with a magnet and the supernatants were discarded. 500 µl of Buffer A (with BSA) was added to wash the beads. The beads were washed 3 times as described above. After the last wash, the pellet was resuspended in 50 µl of Buffer A and the prepared aptamer bead library was added. The aptamer and magnetic beads were incubated for 1 h with rotation. Magnetic particles and any associated aptamer beads were pelleted with a magnet, and unbound aptamer beads were transferred into a 15 ml conical tube. The magnetic beads were washed repeatedly with 500 µl of Buffer A until all unbound aptamer beads were recovered. The magnetic beads with non-specifically bound aptamer beads were discarded. The remaining aptamer library beads were washed 3 times with 10 ml of Buffer A, and resuspended in a final volume of ~1.8 ml of Buffer A before the aptamer beads were transferred to a 2 ml tube.

Positive Primary Selection

KatG, CFP-10 and LAM were coupled to streptavidin-coated magnetic beads, and the aptamer beads recovered from the negative selection step were combined into one tube and incubated with rotation for 90 min at room temperature. About half of the mixture was transferred into a 1.5 ml tube where the magnetic beads were pelleted and the supernatant containing the unbound beads removed. The remaining magnetic bead and aptamer mixture was added to the tube, and the supernatant was removed. The pelleted magnetic particles were washed repeatedly with 500 µl to1 ml of Buffer A until the supernatant became clear *i.e.* no remaining unbound aptamer beads. For the final two washes, Buffer B was used. Typically, a total wash volume of approx. 10 ml was used. Finally, the pellet was resuspended in 50 µl of Buffer B.

Cleavage of Putative aptamers

50 µl of 1 N NaOH was added to the 50 µl magnetic particle resuspension containing the positively selected bound library beads and incubated at 65 ºC for 30 min. The reaction was neutralised by adding 40 µl of 2 M Tris-HCl (pH 7.5). The magnetic particles were pelleted using a magnet, and the supernatant containing the cleaved oligonucleotide pool of primary selection,

was transferred to a 1.5 ml tube.

Secondary Pull Down Selection: B) Multiple protein target selection

7 µl of the cleaved oligonucleotide pool was aliquoted into each of 5 tubes (labelled 1-5). Biotinylated targets were added to the following tubes: KatG into tube #2, CFP-10 into tube #3 or CFP-10·ESAT-6 heterodimer into tube #3b and LAM into tube #4 to yield final concentrations of ~100 nM in a total reaction volume of 140 µl with Buffer A (with BSA) (Table 4.1). Tube #1 and #5 were controls, therefore 133 µl of Buffer A (with BSA) was added to give a total reaction volume of 140 µl. The cleaved oligonucleotides and targets were incubated together at room temp with rotation for 1 h.

50 µl of magnetic particles were washed 3 times with 500 µl Buffer B (without BSA) and resuspended with 25 µl of Buffer B (without BSA). 5 µl of washed magnetic particles were added to tube #2, #3, #4 and #5. Note that magnetic particles were not added to tube #1, as it was the starting pool reference point control. All tubes were incubated with rotation at room temperature for 30 min to 1 h. The magnetic particles were pelleted using a magnet and the supernatant was removed. The magnetic particles were then washed 3 times with 150 µl of Buffer B (without BSA). The pellets were resuspended in 100 µl Buffer B. This putative aptamer pool was used as templates for PCR in the following step (10-40 µl from each tube).

Table 4.1 Secondary Selection

		Incubation #1				**Incubation #2**
Tube	**Condition final**	**Cleaved pool (µl)**	**C initial (µM)**	**Biotinylated target (µl)**	**Buffer B (µl)**	**Magnetic particles**
#1 & #1b	Start control	7	0	0	133	0
#2	100 nM Target 1: KatG	7	0.85	19.8	114	+
#3	100 nM Target 2: CFP-10	7	19.91	0.74	132	+
#3b	100 nM Target 2: CFP-10·ESAT-6	7	2.75	5	128	+
#4	100 nM Target 3: LAM H37Rv)	7	5.88	2.38	131	+
#5 & #5b	Negative control	7	0	0	133	+

4.2.3 Polymerase Chain Reaction (PCR)

PCR was performed in a G-storm thermal cycler (Gene technologies). Each tube was matched with the corresponding reverse primer for PCR (e.g. tube #1 with reverse primer #1). Each reverse primer had a unique sequence to tag the products of each tube with a 'barcode' for

differentiation during sequencing. The PCR reaction for each tube contained dNTPs (Thermo Scientific; R0192), reverse and forward primer (AM Biotechnologies), DreamTaq, DreamTaq buffer, additional $MgCl_2$ (Thermo Scientific; EP0702) and the bead suspension containing the aptamer pool as a template (Table 4.2). PCR tubes were only placed in the heating block once it had reached 95 °C to minimise the formation of primer dimers (hot start PCR). The cycling conditions are presented in Table 4.3.

Table 4.2 Polymerase Chain Reaction (PCR) Reaction

Component	Final concentration
DreamTaq Buffer	1X (includes 2 mM $MgCl_2$)
$MgCl_2$	2.5 mM
dNTP Mix	0.2 mM
Forward Primer	0.1-0.4 µM
Reverse Primer	0.1-0.4 µM
Template DNA	10-40 µl of aptamer pool per 50 µl reaction
DreamTaq DNA Polymerase	2.5 U per 50 µl reaction
PCR-grade water	make up to total volume (50µl)

Table 4.3 PCR Cycling conditions

Step	Temperature	Duration	Cycles
Initial denaturation	94 °C	1 min	1
Denaturation	94 °C	30 s	
Annealing (T_A)	50 °C	30 s	4-25
Extension	72 °C	1 min	
Final extension	72°C	1 min	1

In order to optimise the number of cycles, 4 µl of the reaction mixture was removed for analysis every 4 cycles for analysis. The various fractions were analysed by separating the PCR product on a ~12% native polyacrylamide gel (PAGE) at 200 V for 30 min. After the optimal number of cycles were determined, the bulk of the PCR reaction was performed. PCR products were purified using the Nucleospin II kit (Machery-Nagel) as per the manufacturer's instructions and eluted into water or elution buffer (3#-CFP-10 was gel purified). Putative aptamers for the same target were pooled and the concentration of the DNA was measured with a Nanodrop

spectrophotometer (Thermo Scientific; Nanodrop 2000).

4.2.4 Next Generation Sequencing and Synthesis of X-Aptamers

The purified PCR products were combined in one tube and shipped to AM Biotechnologies to be sequenced *via* next generation sequencing using Ion Torrent (ThermoFisher) with either an Ion 316™ or 318™ chip. The intensity of some bands did not correspond to the nanodrop readings. To ensure that enough material was shipped for sequencing, additional aliquots of #3, #1b #3b and #5b were sent, which equated to 200 or 300 ng as per the nanodrop reading (Appendix B:Table A 16). Although the first and second selection PCR products were sent separately, the positive controls (#1 and #1b), CFP-10 and CFP-10·ESAT6 heterodimer (#3 and #3b), and the negative controls (#5 and #5b) were combined for sequencing, and the subsequent selection of sequences.

Aptamers were selected for re-synthesis with the aid of the Aptaligner© software (Lu *et al.*, 2014). Aptamers were selected based on their enrichment in the secondary pull down relative to the start pool, negative control, and to other targets in the selection. Other considerations for selecting sequences where: whether there were other closely related sequences that were also enriched and the number of hydrophobic moieties (Lokesh *et al.*, 2017). AM Biotechnologies synthesized six to nine biotinylated putative aptamers with the appropriate phenol, indole, boronic acid or hydroxymethyl modifications for each target using a split-pool scheme (Gorenstein *et al.*, 2014).

4.3 Results

4.3.1 Biotinylation of targets

In preparation for the selection of aptamers against the targets, the latter were biotinylated in order to couple them to the streptavidin coated magnetic beads. Biotinylation was confirmed by western blot, and the degree of biotinylation was estimated with the HABA assay.

CFP-10 and KatG

Protein targets were successfully tagged using NHS-biotin and visualised by western Blot using Streptavidin-HRP and a chemiluminescent substrate. CFP-10 was clearly visualised slightly above 10 kDa after a 5 min exposure (Figure 4.4). The expected molecular weight of Hexa-HIS tagged CFP-10 is ~11.8 kDa. KatG (80 kDa) was visualised by western Blot slightly above 70 kDa, as expected, after a 3 min exposure (Figure 4.5).

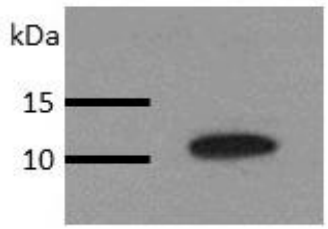

Figure 4.4 Western blot of biotinylated CFP-10 (11.8 kDa).

Blot probed with Streptavidin-HRP.

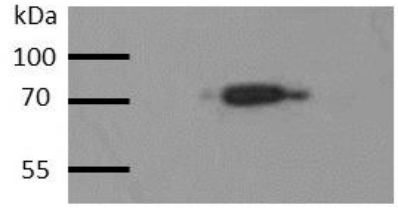

Figure 4.5 Western blot of biotinylated KatG (80 kDa).

Blot probed with Streptavidin-HRP.

LAM

LAM was biotinylated by covalently linking biotin hydrazide to aldehyde groups generated by oxidising carbohydrate moieties on LAM. A faint band between 25 and 35 kDa, pertaining to the biotinylated LAM (H37Rv), was visualised by western Blot using Streptavidin-HRP (Figure 4.6). Although the molecular weight of LAM is ~17-19 kDa, LAM migrates to ~25-35 kDa relative to the bands of a protein ladder (Venisse *et al.*, 1993). In contrast, LAM was more visible in the control blot of biotinylated LAM when probed with CS-40 anti-LAM antibody (Figure 4.7).

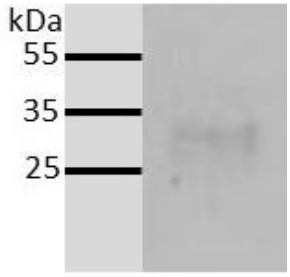

Figure 4.6 Western Blot of Biotinylated LAM

Blot probed with Streptavidin-HRP. Note: LAM runs at about 25-35kDa relative to a protein ladder (Venisse *et al.*, 1993).

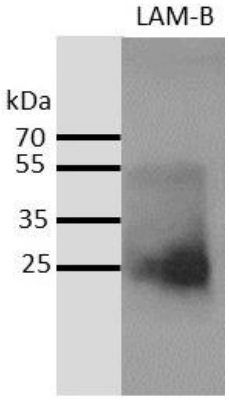

Figure 4.7 Control Western Blot with biotinylated LAM

Blot probed with CS-40 anti-LAM monoclonal antibody. LAM-B: biotinylated LAM

4.3.2 Protein Quantitation

The concentration of the biotinylated proteins was determined to obtain optimal coverage on the streptavidin-coated magnetic beads, and to determine the degree of biotinylation *via* the HABA assay.

The concentration of the biotinylated proteins was estimated by plotting the mean absorbance values on a BSA standard curve (Figure 4.8). The lowest dilution point produced a signal within the noise region, so a linear line was drawn between the origin and the second dilution point (0.125 mg/ml) to estimate the KatG absorbance value that fell within that region. The CFP-10 concentration was also estimated by linear approximation between the second and third dilution points (0.125 mg/ml to 0.5 mg/ml) due to the lack of sufficient valid points in the dilution curve to perform a 4 PL curve fitting analysis. The concentration for biotinylated KatG and CFP-10 were estimated to be 0.048 mg/ml and 0.169 mg/ml respectively (Appendix B:Table A 10 and Table A 11).

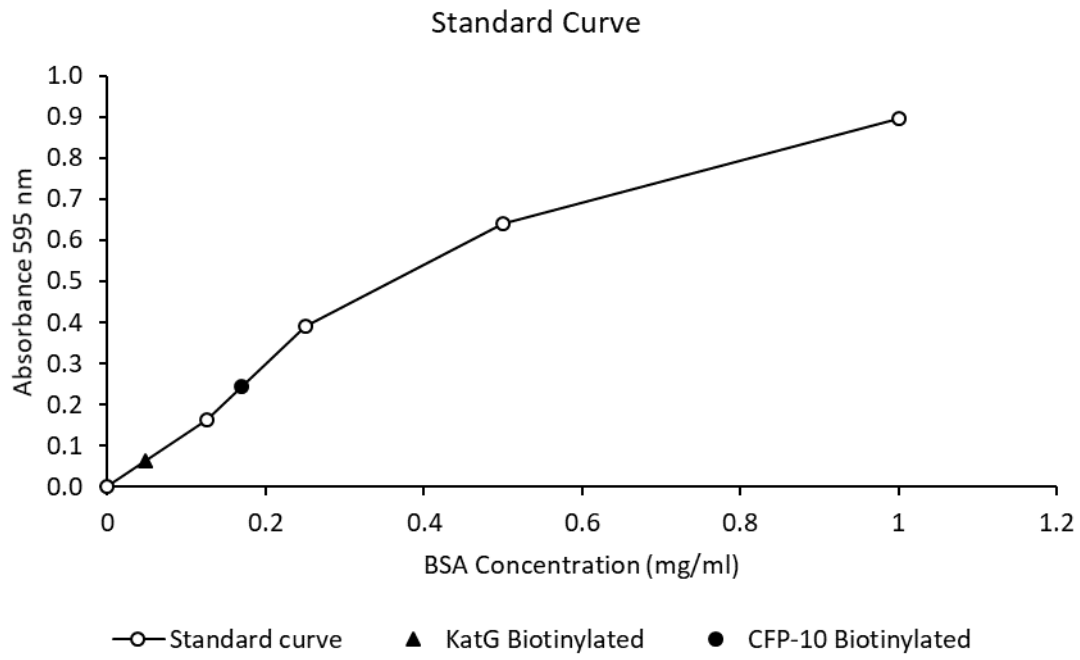

Figure 4.8 Bradford assay standard curve A.

Aliquot 1 of biotinylated KatG and CFP-10 plotted onto the curve. Curve determined using linear approximation. BSA: Bovine Serum Albumin

Given the low concentration of biotinylated KatG and CFP-10 obtained from the first

biotinylation step, a second aliquot of both proteins was biotinylated and the concentration of the biotinylated proteins was determined, as before, using a Bradford assay. A standard curve was generated using a 4PL curve fitting formula and the absorbance readings of KatG and CFP-10 were plotted on the curve (Figure 4.9). The concentration for the second aliquots of biotinylated KatG and CFP-10 were estimated to be 0.238 mg/ml and 0.227 mg/ml, respectively (Appendix B:Table A 10 and Table A 11).

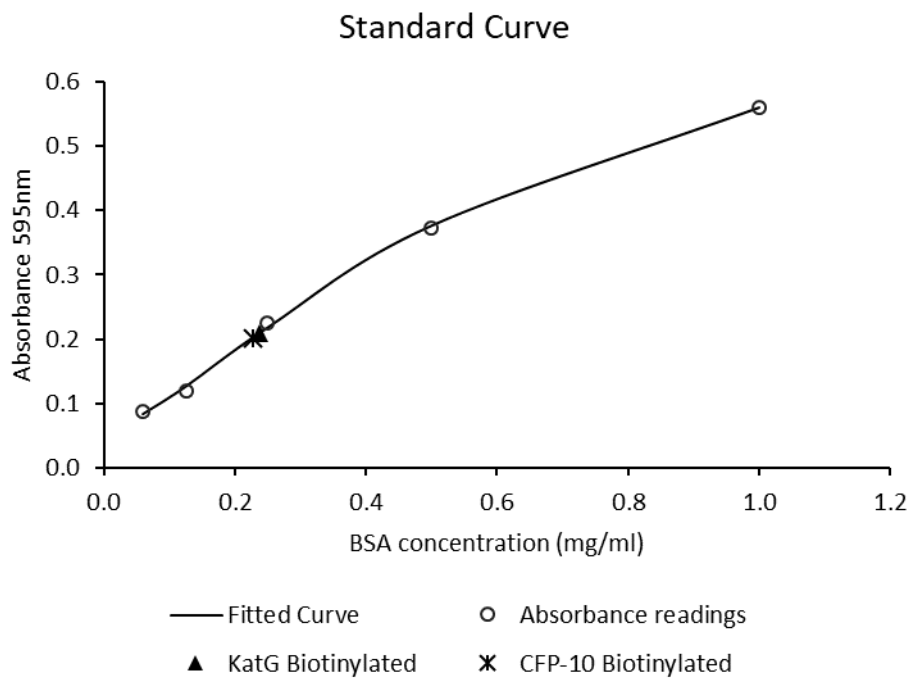

Figure 4.9 Bradford assay standard curve B

Aliquot 2 of biotinylated KatG and CFP-10 plotted onto the curve. Curve determined using 4-PL curve fitting.

4.3.3 HABA Assay

The HABA assay determines the extent of biotinylation based on the degree of displacement of HABA from streptavidin upon addition of the biotinylated target, since biotin has a significantly higher binding affinity than HABA for streptavidin. The displacement of HABA from streptavidin is observed by a proportionate decrease in absorbance at 500 nm, hence the change in absorbance is proportional to the quantity of biotin in the sample. It is important to estimate the mole-to-mole ratio of biotin to protein, because excessive biotinylation of the

protein target could interfere with the aptamer selection process. Aliquot 2 of KatG and CFP-10 was used for the HABA assay (Appendix B: Table A 10 and Table A 11).

The absorbance of the HABA solution (Streptavidin-HABA) is compared to the absorbance of the same solution after addition of the biotinylated molecule (Streptavidin-Biotin + HABA) in Figure 4.10 for all three targets. The biotinylated CFP-10 exhibited a significant decrease in absorbance at 490 nm, which equated to ~3 biotin molecules per CFP-10 molecule (Table 4.4). The biotin: KatG mole ratio could not be calculated due to an increase in background absorbance, which is attributed to the strong absorption of the KatG heme group at 490 nm, potentially masking the displacement of HABA from streptavidin (Lukat-Rodgers *et al.*, 2000). LAM from *M. smegmatis* was used as a proof of principle in this experiment due to a limited supply of *M. tuberculosis* H37Rv LAM. A small decrease in absorbance was noted for the biotinylated LAM (*M. smegmatis*), which equated to approximately every second molecule of LAM being biotinylated (Table 4.4).

Table 4.4 HABA Assay Results

	Mean absorbance at 490 nm			Values for calculating biotin ratio			
Biotinylated molecules	Streptavidin-HABA	Streptavidin-Biotin + HABA	T-test	MW (Da)	mg/ml	Dilution Factor	biotin/mole of protein or LAM
CFP-10-Biotin	0.817	0.787	0.01	11800	0.238	4	3.558
KATG-Biotin	0.800	0.805	0.6	80000	0.227	4	*
LAM-Biotin	0.804	0.795	0.1	17000	0.200	1	0.475
* The biotin/mole of KatG could not be calculated							

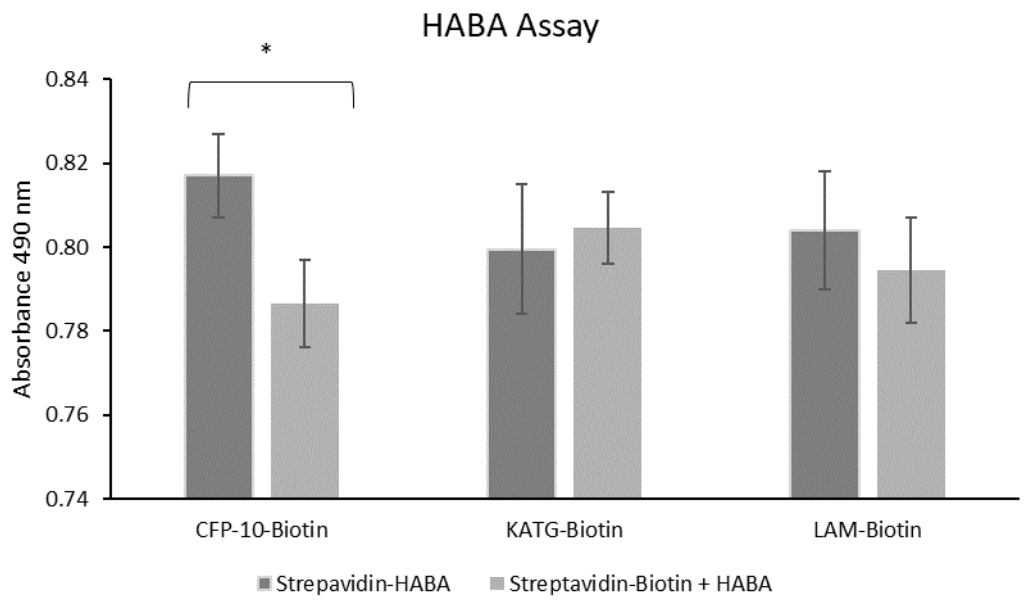

Figure 4.10 HABA assay

A HABA assay was used to measure the extent of biotinylation using the second aliquot of biotinylated proteins and LAM from *M. smegmatis*. Only CFP-10 had a significant shift in absorbance readings *$p \leq 0.05$ according to a t-test. Columns indicate the mean reading of duplicate wells and error bars indicate the minimum and maximum readings taken.

4.3.4 X-Aptamer Selection and PCR Optimisation

Two selections were done using the custom X-Aptamer kit supplied by AM Biotech. For the first selection, KatG, CFP-10 and LAM were used as targets. Due to a low yield of putative aptamers against CFP-10, a second selection was performed against the CFP-10·ESAT-6 heterodimer.

The putative aptamers were amplified by PCR and analysed by separating the PCR products on a native polyacrylamide gel. The expected size of the putative aptamers was approximately 75 base pairs (bp). Bands were compared to the size of the starting pool which served as a positive control. The negative control consisted of any starting library that bound non-specifically to the magnetic beads in the secondary pull-down.

Primer concentration, template concentration and number of cycles were optimised for the PCR to obtain maximal product, and to minimise primer dimers or other spurious products. The optimisation process is summarized in Appendix B: Table A 15 and the figure key is presented

in Table 4.5.

The first PCR was performed as per the AM Biotech protocol (Figure 4.11). While a single band of the desired size (~75 bp) was observed in the positive control, unwanted bands (~60 bp and <50 bp) appeared in all the other samples, including the negative control between 12 and 16 cycles of PCR. Only #2-KatG and #4-LAM had the desired ~75 bp band, which was faint compared to the unwanted bands.

In order to minimise these undesirable bands, the primer concentration was decreased and the template concentration was increased for PCR_1.2. Bands corresponding to the positive control were not observed in any of the other samples in this PCR experiment (Figure 4.12).

A drastic decrease in primer concentration was tested in PCR 1.3, however in this instance, there was insufficient primer to amplify the product, hence no bands were observed on the gel (image not included).

The PCR conditions in PCR_1.4, comprising a primer concentration of 0.1 µM, and 20 µl of template, were found to eliminate the formation of primer dimers (Figure 4.13). However, the yields of the desired PCR products for #2-KatG and #4-LAM were low and barely visible on the gel, and completely absent for #3-CFP-10. Since the quantity of template DNA was limited, which prevented higher starting concentrations of the DNA template being used in the reactions, the number of PCR cycles was instead increased to improve the yield of PCR products.

In PCR_1.5, the PCR product yield improved despite the reappearance of primer dimer products at high cycle numbers (Figure 4.14). At 25 cycles, most targets reached sufficient product yield with minimal or no additional bands. The purified PCR product concentrations were low; therefore an additional PCR was performed to increase the yield of the desired sequences (PCR_1.6: Figure 4.15).

The PCR products were purified as noted in Figure 4.14 and Figure 4.15. The samples with the most product, but least unwanted bands, were purified and putative aptamers for the same target were pooled. The PCR product of #3 CFP-10 was gel purified to minimise the primer dimer contamination since the yield of the true product and the primer dimers were similar.

The PCR yield for the #3-CFP-10 was poor, hence the selection was repeated with the CFP-10·ESAT-6 heterodimer. The optimised conditions were used for PCR_2.1 and resulted in favourable bands (Figure 4.16), however the product yield was suboptimal. Thus, the template concentration and cycle number for PCR_2.2 was increased accordingly (Figure 4.17). The control band in the positive control was faint, which warranted a repeat of the PCR. In the

repeat PCR, a ~75 bp band was observed in all the lanes. A no template control exhibited primer dimers, but not the 75 bp band (Figure 4.17). Since sequences in the #5b tube (negative control) could be excluded after sequencing, the putative aptamers (PCR products) were purified and prepared for shipping (PCR_2.3: Figure 4.18). Each pooled product (50 ng) was separated by PAGE (Figure 4.19), before shipping the DNA to AM Biotech, to ensure that the PCR products were of the correct size, and relatively free of unwanted sequences.

Table 4.5 PCR PAGE Figure Key

Number	**Name**	**Description**
#1	Positive control	Starting pool for secondary pull down amplified by PCR
#2	KatG	Putative aptamers that bound in secondary pulldown to biotinylated KatG amplified by PCR
#3	CFP-10	Putative aptamers that bound in secondary pulldown to biotinylated CFP-10 amplified by PCR
#4	LAM	Putative aptamers that bound in secondary pulldown to biotinylated LAM amplified by PCR
#5	Negative control	DNA that bound in secondary pulldown to magnetic beads amplified by PCR
#1b	Positive control	Starting pool for secondary pull down of second selection.
#3b	CFP-10·ESAT-6	Putative aptamers that bound in secondary pulldown to the CFP-10·ESAT-6 heterodimer amplified by PCR (Only CFP-10 biotinylated)
#5b	Negative control	DNA that bound in secondary pulldown to magnetic beads amplified by PCR
C	No template	Control PCR reaction without any template

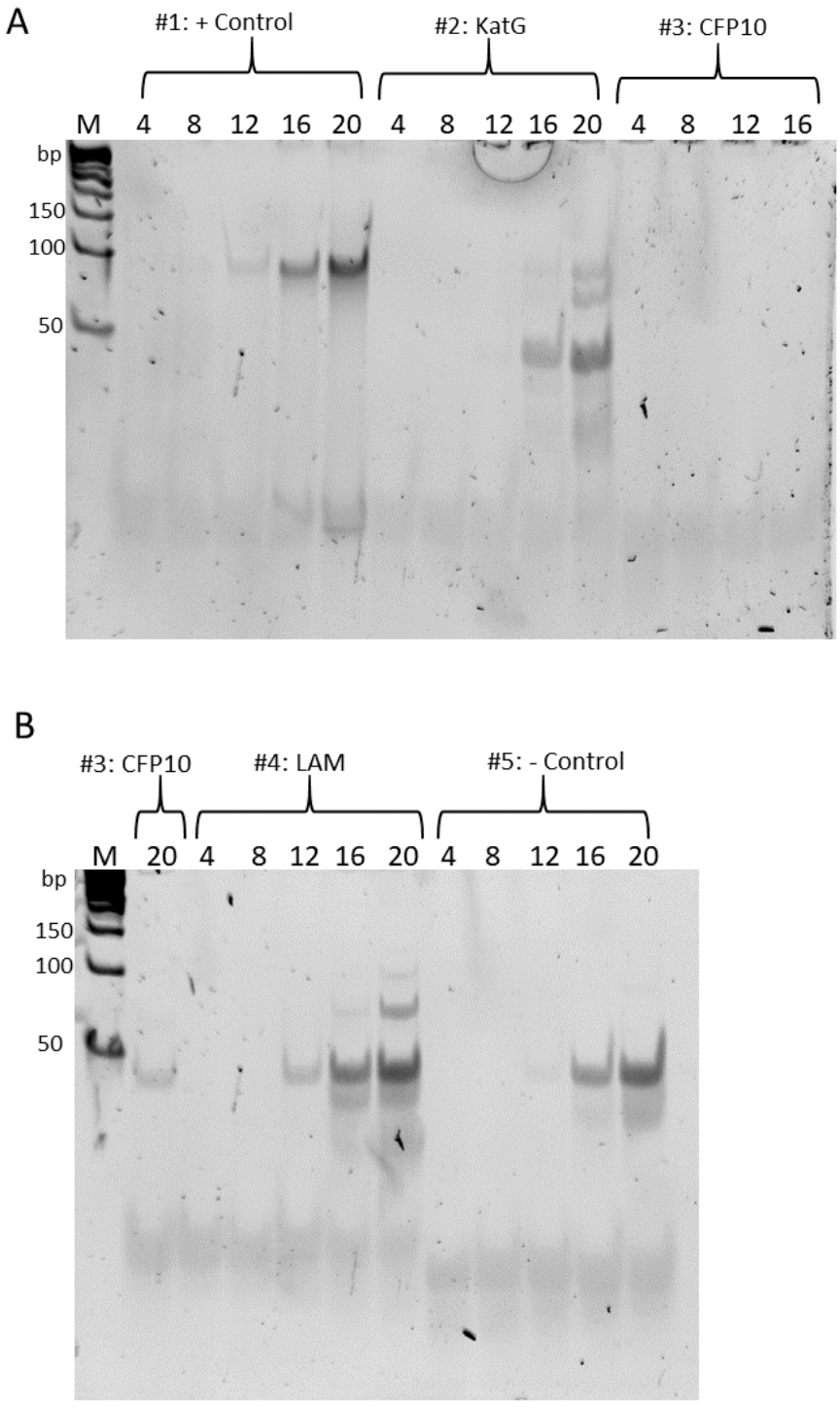

Figure 4.11 PCR _1.1

Parameters: 0.4 µM primer, 10 µl template, and 4-20 PCR cycles. See key above (Table 4.5). M: DNA ladder (bp). Lane numbers indicate number of cycles of PCR.

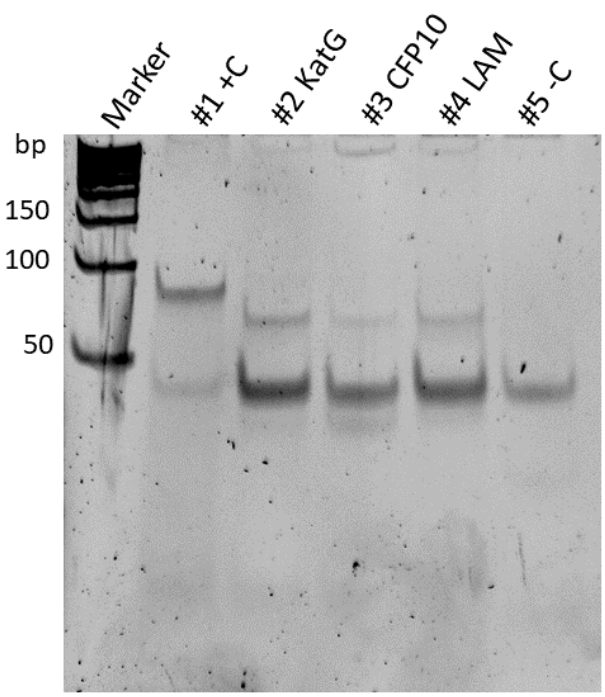

Figure 4.12 PCR_1.2

Parameters: 0.2µM Primer, 20µl template and 16 cycles. See key above (Table 4.5). M: DNA ladder (bp).

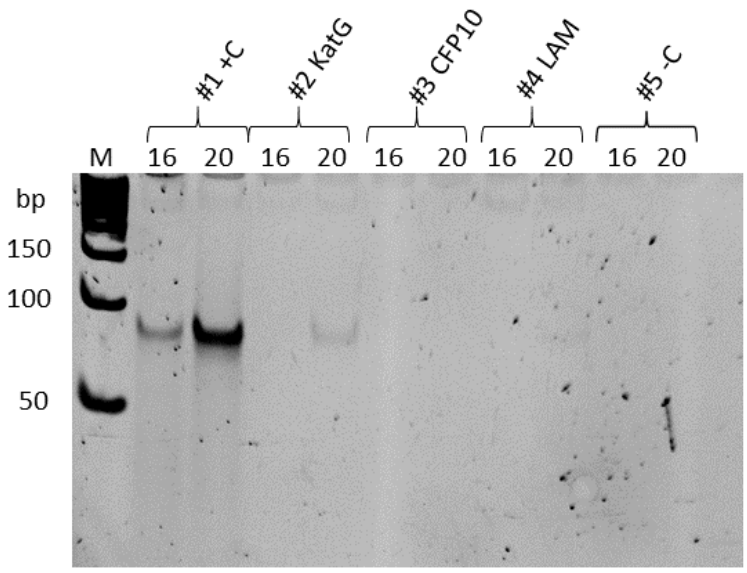

Figure 4.13 PCR_1.4

Parameters: 0.1 µM Primer, 20 µl template, and 16 and 20 cycles. See key above (Table 4.5). Lane numbers indicate number of cycles of PCR. M: DNA ladder (bp).

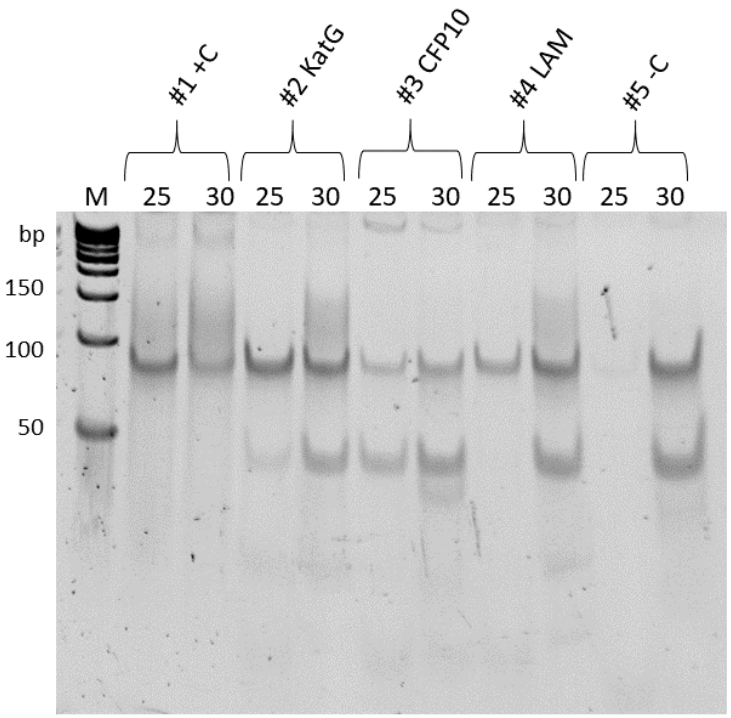

Figure 4.14 PCR_1.5

Parameters: 0.1 µM primer, 20 µl template, and 25 and 30 cycles. See key above (Table 4.5). Lane numbers indicate number of cycles of PCR. PCR products from 25 cycle lanes were purified. #3- CFP-10 products were cut from the gel for purification.

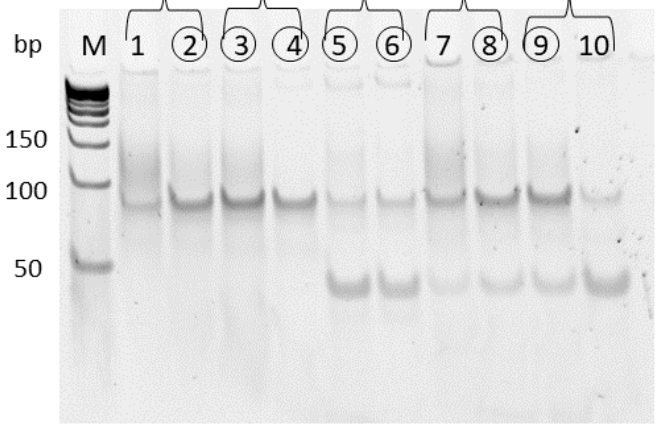

Lane	Sample	(ng/µl)
M	Marker	*
1	#1 + C	27
2	#1 + C	1
3	#2 KatG	6.7
4	#2 KatG	1
5	# 3 CFP-10	12
6	# 3 CFP-10	1
7	#4 LAM	8.9
8	#4 LAM	1
9	#5 - C	26.9
10	#5 - C	1

Figure 4.15 PCR 1.6

Parameters: 0.1 µM primer, 1 µl of template, and 15 cycles. See key above (Table 4.5). PCR products from circled lanes were purified. #3- CFP-10 products were cut from the gel for purification. Concentrations of each template used in the PCR is indicated in the table for each lane.

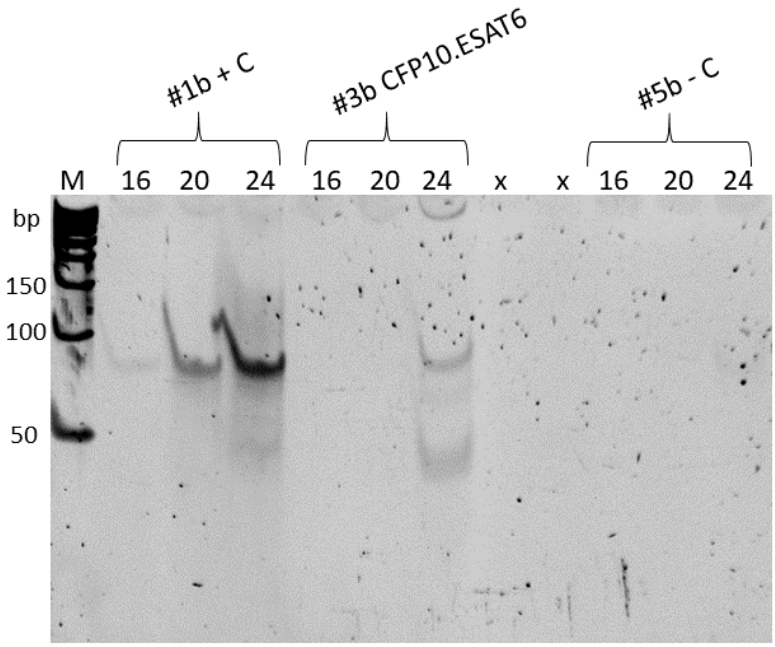

Figure 4.16 PCR 2.1

Parameters: 0.1 µM primer, 20 µl template and 16-24 cycles. See key above (Table 4.5). Lane numbers indicate number of cycles of PCR.

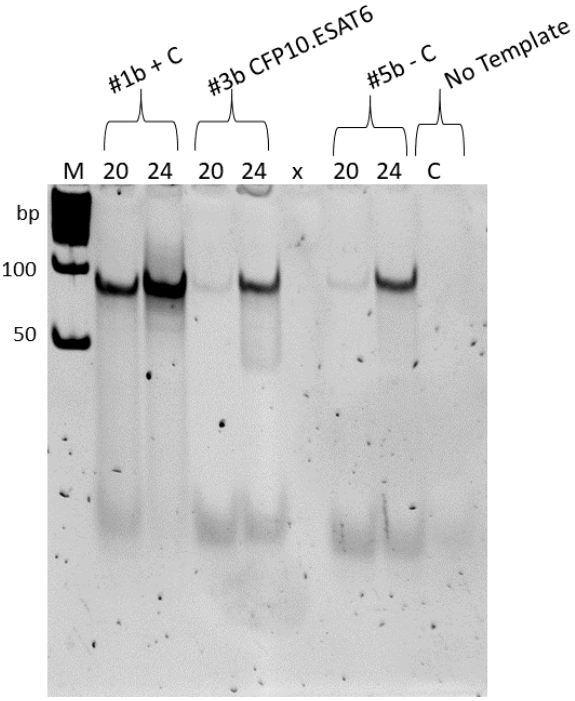

Figure 4.17 PCR 2.2

Parameters: 0.1 µM, 40 µl template, and 20 and 24 cycles. See key above (Table 4.5). Lane numbers indicate number of cycles of PCR.

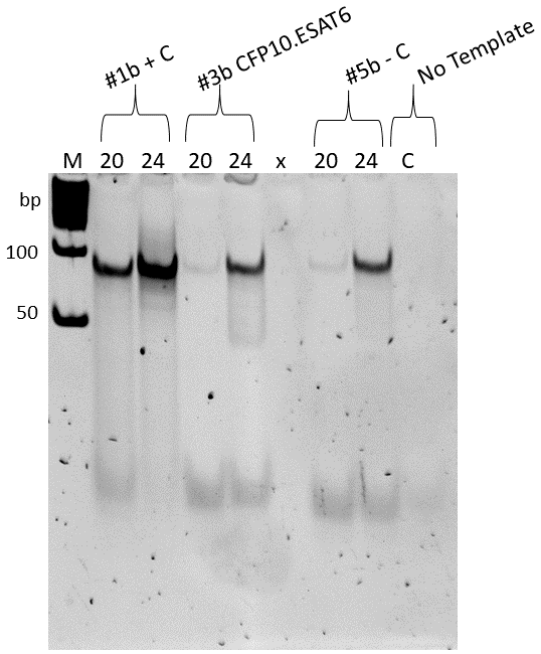

Figure 4.18 PCR_2.3

Parameters: 0.1 µM primer, 20 µl template, and 20 and 24 cycles. See key above (Table 4.5). Lane numbers indicate number of cycles of PCR. PCR products from all lanes were purified. C- No template control, 24 cycles

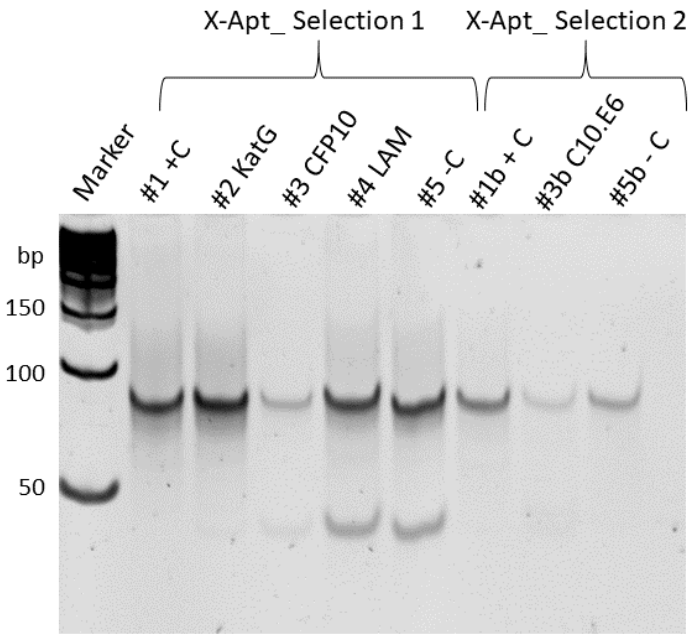

Figure 4.19 Final Gel before shipping putative X-Aptamers.

50 ng of each product was loaded on to the gel as calculated from the nanodrop readings. 100bp band of ladder = 14 ng (7% of 0.2 µg). Expected size is 75 bp. See key above (Table 4.5).

4.3.5 Next Generation Sequencing and Putative X-Aptamer Synthesis

Next generation sequencing, analysis with Aptaligner© and putative X-Aptamers synthesis as described in the Methodology section (4.1.5) was performed by Dr N. Ward at AM Biotech. Aptamers were selected for re-synthesis based on their enrichment in the secondary pull down relative to the start pool, negative control, and to other targets in the selection. Sequences corresponding to the bands in the negative control were removed from the aptamer pool before synthesis of the putative aptamers.

AM Biotechnologies synthesized six to nine biotinylated putative aptamers (Appendix B: Putative X-Aptamer sequences) with the appropriate phenol, indole, boronic acid or hydroxymethyl modifications for each target using a split-pool scheme (Gorenstein *et al.*, 2014). The most common modifications were boronic acid and indole (Figure 4.20).

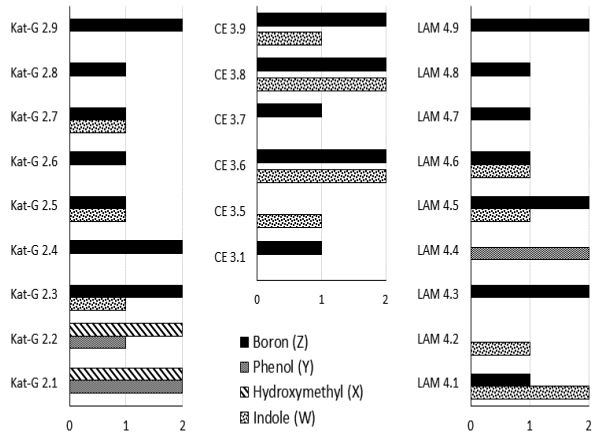

Figure 4.20 Type and number of modifications on each sequence synthesised

4.4 Discussion

The various targets were biotinylated to facilitate their immobilisation onto the streptavidin coated beads. While other forms of immobilisation are possible, the biotin-streptavidin interaction is exceptionally strong ($K_D = 4x10^{-14}$ M), and biotinylation is conveniently optimised since it is widely used in molecular biology applications.

Biotinylation of all three targets was confirmed *via* western blot performed with a Streptavidin-HRP conjugate. Distinct bands were observed at the correct molecular weights for KatG and CFP-10 (Figure 4.4 and Figure 4.5 respectively). The western blot for biotinylated LAM appeared as a weak band suggesting that either the number of biotin molecules per LAM molecule was low, the biotinylation efficiency was low or that there was a loss of material during biotinylation (Figure 4.6). However, a control blot performed with anti-LAM antibodies revealed that biotinylated LAM could be detected with significantly higher sensitivity than observed with streptavidin-HRP, which suggests that the weak signal intensity in the streptavidin-HRP blot was due to low levels of biotinylation (Figure 4.7). The band smearing observed in the control blot is indicative of the heterogeneous nature of the LAM produced by *M. tuberculosis* (Venisse *et al.*, 1993).

When selecting aptamers against biotinylated targets, it is preferable to maintain a low biotin: target molar ratio, since the aim is to select aptamers that recognise native epitopes of the target molecules, and not any excess biotin molecules that may have not bound to streptavidin. Keeping this in mind, a HABA assay was performed to estimate the number of biotin molecules per biomarker target. The HABA assay was performed on the two protein targets, but not on LAM (H37Rv) due to limited stocks of LAM. However, a proof of principle experiment was performed with LAM from *M. smegmatis*. CFP-10 had a favourable biotin-to-target ratio of ~ 3:1, while approximately every second molecule of LAM (*M. smegmatis*) was biotinylated, which is a plausible reason for the low signal intensity observed in the western blot of LAM (H37Rv). The extent of biotinylation for KatG could not be calculated since the heme group of KatG absorbs in the same range as the HABA solution resulting in a high background signal (Table 4.4). Nonetheless, this property of KatG is particularly advantageous for the label-free detection of KatG (Lukat-Rodgers *et al.*, 2000; Kapetanaki *et al.*, 2003).

After the selection process, putative aptamers were amplified by PCR in preparation for sequencing. Various PCR parameters, *i.e.* cycle number, primer concentration and template amount were optimised to reduce primer dimers and obtain maximal yield (Figure 4.11 to Figure 4.18) (Roux, 1995). Due to a low yield of putative aptamers against CFP-10, we repeated

the selection process using the CFP-10·ESAT-6 heterodimer, which is more stable than either of the monomers on their own (Renshaw *et al.*, 2002) (Figure 4.16 to Figure 4.18). It is therefore plausible that an aptamer, which recognises epitopes of either CFP-10, ESAT-6 or some interface of the heterodimer could have been selected.

Initially, it appeared that the concentration of template, which was unknown, was less than the suggested primer concentration of 0.4 μM as primer dimer products (<50 bp) dominated the first PCR (Figure 4.11). Due to limited DNA template available from the selection process, the starting template volume could only be doubled. The primer concentration was reduced to 0.1 μM before primer dimer products were eliminated, or reduced so that the aptamers dominated the final PCR products (Figure 4.13 and Figure 4.14). Except for putative aptamers selected against CFP-10, primer dimers continued to be of similar or greater concentrations than the desired product (Figure 4.14 and Figure 4.15).

The number of PCR cycles was increased to improve the yield of PCR products. However, this should be done with caution when amplifying aptamers as by-products also increase exponentially. Short random DNA sequences are prone to generating spurious by-products due to product-product hybridisation. These by-products can overshadow real products resulting in the original library being lost within five PCR cycles despite ample primers being available for primer-template hybridisation (Musheev and Krylov, 2006).

Stable secondary structures, which are key for aptamer binding ability (Fischer, Tok and Tarasow, 2008) and usually associated with a higher GC content, can be responsible for by-products *via* deletion events. For example, a hairpin-loop that persists during extension results in the polymerase "jumping" over a section of sequence. The outcome is by-products that are shorter than the original template (McDowell, Burns and Parkes, 1998; Viswanathan, Krcmarik and Cianciotto, 1999). This mechanism is a plausible explanation for the ~60 bp band observed in Figure 4.11, Figure 4.13 and Figure 4.16. Agents, such as DMSO or betaine, can be used to minimize stable secondary structures, however they can also destabilise priming during PCR (Kang, Lee and Gorenstein, 2005; Musso *et al.*, 2006).

Enrichment of by-products is minimised in the bead based method (He *et al.*, 2012) as only one round of PCR needs to be performed, whereas in traditional SELEX methods, repeated rounds of PCR expand spurious products to the point that real binders can be lost (Musheev and Krylov, 2006). Another method of preventing product-product hybridisation is emulsion PCR. Each template is amplified in its own compartment, which eliminates the opportunity for complementary random sequences to anneal and produce spurious products. However, the

clean-up process is more tedious and yield is effected with this method (Shao *et al.*, 2011).

The final concern was a 75 bp band that appeared in the #5 tube (negative control) (Figure 4.11, Figure 4.14, Figure 4.17 and Figure 4.18). The source of this 75 bp band could be contamination incurred while preparing the PCR reactions, despite precautions such as, preparing PCR reactions with filter-plugged tips, wearing gloves and preparing reactions in a different location from the thermocycler and electrophoresis apparatus. PCR reactions were performed with a no template control and in these reactions, the 75 bp band was not present (Figure 4.17 and Figure 4.18). It was an oversight to not include this control in all the PCR experiments. An alternative source of the 75 bp sequences is DNA that bound non- specifically in the secondary selection, despite the initial negative selection, which should have excluded most non-specific binders. Sequences from tube #5 were compared to other tubes and excluded from the pool of putative aptamers selected for re-synthesis. If these sequences were a result of contamination rather than non-specific binding, putative aptamers would have been lost in this process.

Although the first and second selections were sent separately for sequencing, the positive controls (#1 and #1b), the CFP-10 and CFP-10·ESAT-6 heterodimer (#3 and #3b) and the negative controls (#5 and #5b) were combined for sequencing, and the subsequent selection of aptamers.

After selecting putative aptamers that were unique to each target and were not present in the negative control (*i.e.* non-specific binders), these sequences were synthesized with the appropriate modifications (Appendix B: Table A 17) (Gorenstein *et al.*, 2014). Boronic acid and indole were the most common modifications since they compromised 68% of the starting library (Figure 4.20).

The putative aptamers against CFP-10 and the CFP-10·ESAT-6 heterodimer had mostly indole and boronic acid modifications. The indole moiety likely interacts with the hydrophobic regions of these proteins. Boronic acid can also interact with hydrophobic amino acids, and any amino acid side chain that can donate a pair of electrons, such as serine (Whyte, Vilar and Woscholski, 2013). The putative aptamers against LAM contained mostly boronic acid and indole moieties, which probably bind to the carbohydrate and lipid parts of LAM, respectively. KatG was the only target to bind putative X-Aptamers containing a hydroxymethyl group, which also contained several boronic acid groups. The active site of KatG contains histidine, which may be one of the epitopes to which a boronic acid aptamer could bind. KatG, being a large protein with several different types of amino acids, probably offers more opportunity for binding aptamers.

4.5 Conclusion

The bead-based SELEX method provides an accelerated means of selecting aptamers against several targets concurrently. Novel modified sequences were selected against KatG, LAM and the CFP-10.ESAT-6 dimer. These putative aptamers could form the basis of a new biosensor for the detection of biomarkers in TB patient samples. Sequences selected after analysis with the Aptaligner® softer were synthesized and will be discussed in the following chapter.

5 CHARACTERISING X-APTAMERS AGAINST TB BIOMARKERS

5.1 Introduction

It is essential to characterise aptamers in order to identify the best candidates for use in a diagnostic biosensor. Diagnostic biosensors should have high analytical sensitivity and specificity to enable detection of biomarkers in complex clinical samples where biomarkers may be in low concentrations. Determining the binding affinities and interrogating the secondary structure of the selected aptamers are two methods to calibrate and optimise a diagnostic platform.

5.1.1 Analytical Sensitivity and Specificity

Analytical sensitivity is determined by measuring the lowest concentration of the biomarker that can be detected by an assay i.e. the limit of detection (Ekins and Chu, 1991). "Analytical specificity is the ability of an assay to exclusively identify a target substance or organism … in a sample or specimen." Note analytical sensitivity and specificity should not be confused with diagnostic sensitivity and specificity (Saah and Hoover, 1997). Binding affinity is a key contributor to the analytical sensitivity and specificity of an assay (Eaton, Gold and Zichi, 1995). Ionic strength and pH of buffers can alter aptamer binding affinity hence buffers should be taken into consideration when designing assays (Baldrich, Restrepo and O'Sullivan, 2004; Hianik *et al.*, 2007). Analyte concentration, assay volume, and complexity of the patient samples will also affect the overall sensitivity and specificity of an assay (Pesce and Michael, 1992). Hence diagnostic assays should be validated with complex samples similar to real samples to determine realistic sensitivity and specificity metrics.

Binding Affinity

Binding affinity is defined at equilibrium by the dissociation equilibrium constant (K_D) which is the quotient of the reactant concentrations and product concentration or the ratio of the dissociation and association rate constants, k_{off} and k_{on} respectively, at equilibrium (See Equations 1). For the purpose of this discussion, when one molecule is immobilised onto a

surface that molecule will be referred to as the ligand, while the molecule in solution will be referred to as the analyte and reactants will be used as a collective term. The smaller the value of the K_D the stronger the binding between a ligand and analyte as the formation of the ligand-analyte complex is favoured ((Pollard, 2010).

Equations 1

$$L + A \leftrightarrow LA \quad (1)$$

Where L is the ligand and A is the analyte and LA is the analyte bound to the ligand. This equation assumes 1:1 stoichiometry

$$\text{Forward Reaction: } Rate = k_{on}\,[L][A] \quad (2)$$

$$\text{Reverse Reaction: } Rate = k_{off}\,[LA] \quad (3)$$

Where $k_{on}$is the association rate constant and $k_{off}$is the dissociation rate constant. [L] is the density of ligand on the surface (mol/m^2) and [A] is the concentration of the analyte in solution (mol/litre), while [LA] is the density of analyte bound to ligand on the surface (mol/m^2).

$$\text{At Equililbrium: } k_{on}[L][A] = k_{off}[LA] \quad (4)$$

$$K_D = \frac{k_{off}}{k_{on}} = \frac{[L][A]}{[LA]} \quad (5)$$

Concentrations of ligand and analyte need to be optimised to determine the binding affinity. Firstly, the fraction bound at equilibrium only varies significantly if the concentration of analyte is within two orders of magnitude from the K_D value (Kuriyan, Konforti and Wemmer, 2009). Secondly, in order to simplify calculations binding should occur under pseudo-first order conditions where either the analyte or ligand is in excess of the other. Pseudo-first order conditions allow for easy calculation of the rate of the reaction since the rate is proportional to the concentration of one of the reactants under these conditions. Lastly, when surface immobilisation became popular there were concerns about the validity of calculating the K_D when a reactant was immobilised on the surface (Goldberg and Djavadi-Ohaniance, 1993). Edwards *et al*. found that K_D values obtained when molecules were immobilised were

comparable to K_D values obtained in solution assays as long as the ligand was not impeded by steric hindrance i.e. crowding on the surface (Edwards, Lowe and Leatherbarrow, 1997). In the context of designing a biosensor the immobilised K_D value is more relevant than an in-solution K_D value and the concentration of immobilised ligand can be optimised to increase analytical sensitivity and specificity.

There are two types of assays to determine the K_D: equilibrium and kinetic assays. Equilibrium assays may be used to determine the K_D but not the rate constants (k_{off} and k_{on}). Kinetic assays are more expensive and complicated, but they yield more useful information including the k_{off} and k_{on} rate constants (Pollard, 2010).

Equilibrium Assays

During an equilibrium assay the two reactants are allowed to reach equilibrium in solution and the concentration of unbound reactant, typically the reactant in excess, is measured without disrupting the equilibrium unless there is a method to remove unbound reactant from the solution (Pollard, 2010). An ELISA or ELONA is an example of an equilibrium assay. An ELONA is similar to an ELISA except antibodies are replaced with aptamers (Drolet, Moon-McDermott and Romig, 1996). When an ELISA is used to measure unbound reactant, a separate aliquot of the other reactant or another molecule becomes the ligand and is immobilised on the surface. This type of assay is often referred to as a "competition assay" since the ligand reactant in solution is "in competition" with itself or another molecule on the surface (Ekins, 1989; Baldrich, Restrepo and O'Sullivan, 2004; Papamichael, Kreuzer and Guilbault, 2007; Martineau, 2010). To maintain the equilibrium less than 10% of the analyte reactant being measured should be involved in the measurement assay. The ELISA (or ELONA) should also be optimised to give a response which is proportional to the total unbound reactant concentration (Friguet *et al.*, 1985, 1995).

ELISAs (or ELONAs) should not be used for determining binding affinity when the equilibrium is between an immobilised ligand and an analyte in solution where there are wash steps before detection of the bound analyte. New equilibria may occur with each subsequent step after the primary ligand-analyte complex formation hence the concentration of the ligand-analyte complex at the initial equilibrium cannot be measured with this method (Venkatesh and Murthy, 1996). However, ELONAs or ELISA-ELONA hybrid assays can be used to screen putative aptamers to find good binders which can be further characterised with kinetic assays.

Kinetic Assays

Kinetic assays yield more information than equilibrium assays including the thermodynamic parameter, the equilibrium constant and the rate constants. (Pollard, 2010). The downfall of kinetic experiments is that they often require more reagents. However, some techniques have become more advanced and minute amounts of a molecule can be detected. A few techniques that have been used to characterise aptamer binding will be highlighted here.

Isothermal titration calorimetry (ITC) has been used in several aptamer studies. The major advantage of this technique is that it does not require immobilisation. However micromolar concentrations are required to perform the analysis (Cooper, 2004). Despite this drawback, studies characterising aptamers and modified aptamers have used this technique (Shum *et al.*, 2011; Wang *et al.*, 2014; Zandarashvili *et al.*, 2015).

Thermophoresis has also been used to characterise binding affinity of aptamers with tweaks such as microscale thermophoresis and optical thermophoresis (Baaske *et al.*, 2010; Reineck, Wienken and Braun, 2010; Wienken *et al.*, 2010). The limitations of this technique is that the thermophoresis of proteins is usually weak and small molecules do not significantly change the charge or size of a molecule (Wienken *et al.*, 2010).

Surface Plasmon Resonance (SPR) is a common method for determining binding affinity and has been used to characterise several aptamers (Murphy *et al.*, 2003; Ostatná *et al.*, 2008; Gong *et al.*, 2012; Miodek *et al.*, 2013). In the Biacore system the ligand is immobilised onto a gold surface via streptavidin, Ni-NTA or liposomal mono- or bi-layers. The analyte, at various dilutions, flows over the immobilised ligand which creates an environment where the analyte is effectively at a constant concentration (Hodnik *et al.*, 2010). The drawbacks of this method are the high maintenance requirements of the equipment and a sensitivity to interfering effects (Homola, 2003; Abdiche *et al.*, 2008).

Biolayer interferometry (BLI) is an "optical analytical technique that measures interference patterns between waves of light" (Figure 5.1). BLI is used by systems such as the Octet® system (ForteBio®) to characterise binding between unlabelled molecules (Tobias and Kumaraswamy, 2013).

The OCTET system has only recently become sensitive enough to detect small molecules such as aptamers as the signal is proportional to the mass of the molecules in the biolayer (Abdiche *et al.*, 2008; Shah and Duncan, 2014). However, recently BLI has been used to characterise RNA aptamers against VEGF and thrombin, and a method has been published in *Current Protocols in*

Nucleic Acid Chemistry (Abeydeera *et al.*, 2016; Lou *et al.*, 2016).

TABLE 2: Biosensors available for kinetic assays on the Octet and BLItz systems.

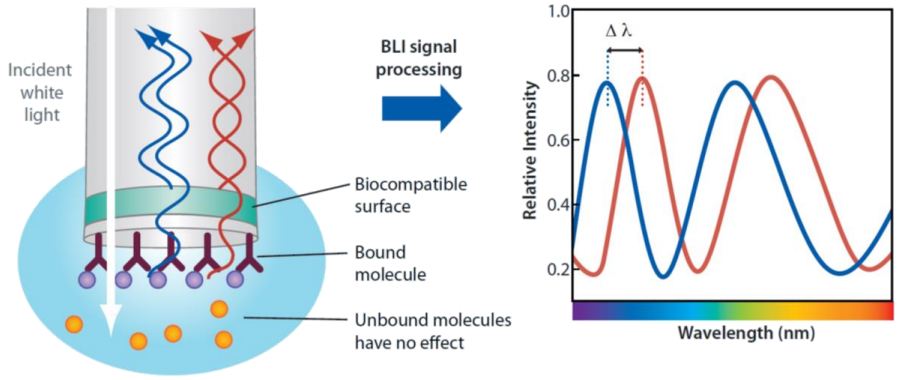

FIGURE 3: BLI is an optical analytical technique that analyzes the interference pattern of white light reflected from two surfaces. Changes in the number of molecules bound to the biosensor causes a shift in the interference pattern that is measured in real time.

Figure 5.1 Forte Bio OCTET System

[Adapted from (Tobias and Kumaraswamy, 2013)]

White light shines through an optic fibre to which a ligand has been immobilised (left). The light reflects and produces constructive and destructive interference depending on the thickness of the biolayer on the optic fiber. Hence as the ligand binds analyte the interference pattern changes and binding can be monitored by a spectrometer (right).

5.1.2 *In Silico* Sequence Analysis

Once the binding affinities of the aptamers have been determined they may be optimised by truncating the sequence. Minimising aptamers has several advantages including reducing the cost of synthesis, improving affinity for the target and understanding aptamer-target interactions. Truncation may be performed empirically or guided by *in silico* secondary structure predictions (Fischer, Tok and Tarasow, 2008; Keefe, Pai and Ellington, 2010; Berezhnoy *et al.*, 2012; Kaur and Yung, 2012).

Secondary structures are associated with key binding regions for example the guanine quadruplex or hairpin structures (Fischer, Tok and Tarasow, 2008; Russo Krauss *et al.*, 2011; Cheung *et al.*, 2013). Constant primer regions do not usually form part of the secondary

structure (Cowperthwaite and Ellington, 2008) whereas consensus sequences may be located within secondary structures (Wilson and Szostak, 1998; Fischer, Tok and Tarasow, 2008; Cho *et al.*, 2013). Some studies have taken advantage of the knowledge that secondary structure plays a key role in selecting high affinity aptamers by designing libraries with built-in secondary structure such as hairpin loops and found better aptamers were selected (Davis and Szostak, 2002; Ruff, Snyder and Liu, 2010).

There are several algorithms available to predict secondary structure (Zuker, 2003, 2010; Mathews, 2004; Afzal *et al.*, 2012). Experimental data assists algorithms in making more accurate predictions (Patel, 1997; Cheung *et al.*, 2013; Tatarinova *et al.*, 2014). Experimental data for modified nucleotides is scarce. Thus, secondary structure prediction for aptamers with modified nucleotides is not commonly supported. An exception is DNA Software Inc. that revealed the Modifieds™ package in a press release which can reportedly include nucleic acid analogues, deoxyribose uracil, purine isomers and deaminated adenosine (DNA Software, 2009). Even without modified nucleotides most software is ill equipped to deal with aptamers. For example Mfold fails to take tertiary interactions into account and neglects kinetically trapped structures i.e. assumes a minimum free energy is the most probable (Zuker, 2010). Despite these limitations a few studies with modified aptamers have used Mfold to predict secondary structures (Kato *et al.*, 2005; He *et al.*, 2012; Gandham *et al.*, 2014). None of these studies discuss the limitations of using Mfold for secondary structure prediction.

5.1.3 Aims and Objectives

Here, modified aptamers against the CFP-10·ESAT-6 dimer, CFP-10 and LAM (H37Rv) were characterised with ELONA-ELISA hybrid assays, BLI and *in silico* structure prediction software. The X-Aptamers selected against KatG were not characterised due to time constraints.

5.2 Methods

5.2.1 ELONA-ELISA Hybrid

Various in-house ELONA-ELISA hybrid assays were developed in our lab to test the ability of putative aptamers to detect CFP-10, ESAT-6 or LAM based on methods described in the following papers (Baldrich, Restrepo and O'Sullivan, 2004; Pan *et al.*, 2014; Tang *et al.*, 2014).

ESAT-6 and CFP-10

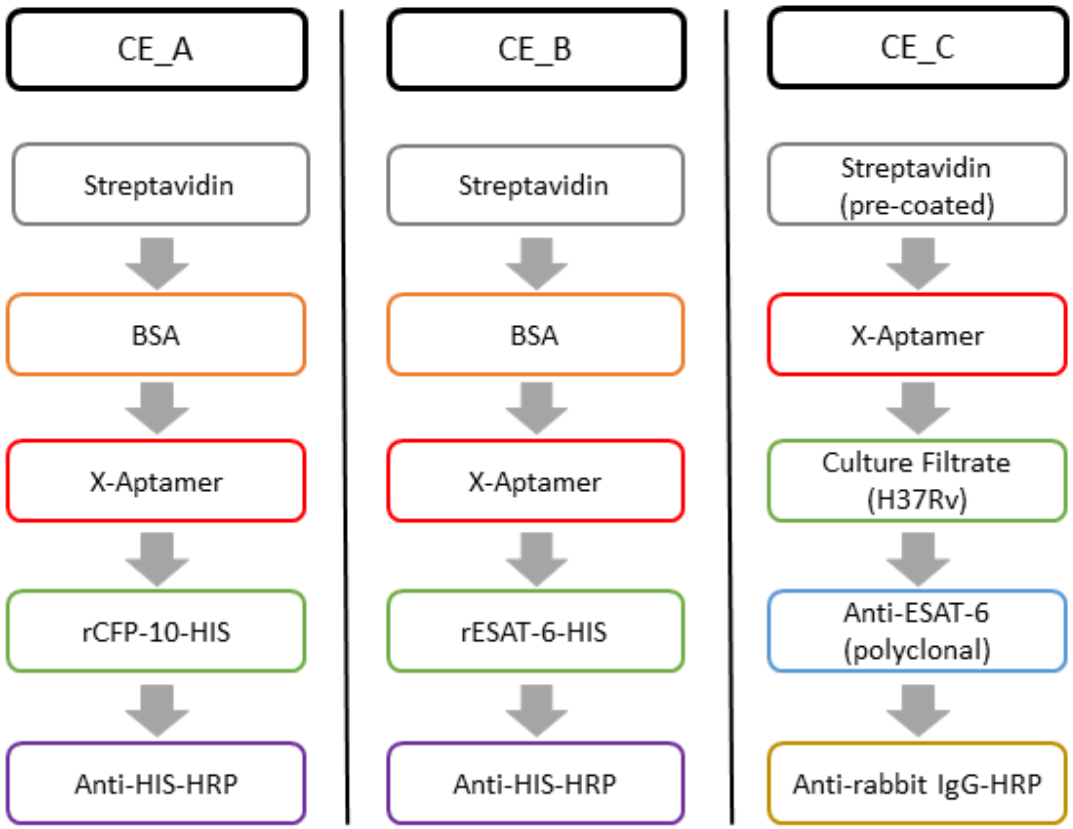

Figure 5.2 CFP-10 and ESAT-6 ELONA-ELISA Hybrid Assay

Workflows: CE_A, CE_B and CE_C

Two different versions of the ELONA-ELISA hybrid assay were used to test the binding of putative X-Aptamers to ESAT-6 and CFP-10 (Figure 5.2). All reagents were resuspended in PBS (Sigma; P4417 or 137 mM NaCl, 2.7 mM KCl, 10 mM $NaHPO_4 \cdot 7\ H_2O$, 1.8 mM KH_2PO_4) at pH 7.4 and this buffer was used as a negative control. All incubations were performed at 37 °C with a plate sealer and the plate was washed three times with wash buffer (PBS containing 0.05% Tween-20) unless otherwise noted. Biotinylated X-Aptamers were immobilised via streptavidin onto the surface.

Binding curves was generated by performing a 1:2 serial dilution of the respective X-Aptamers starting with 0.5 µM. H37Rv cultures were cultured in 7H9 Middlebrook broth (BD Difco™ #271310) and heat killed at 80 °C for 30 min by Dr Z. Mlamla. Cultures were pelleted by centrifugation at 3300 xg for 15-30 min at 4 °C. The culture filtrate was removed and stored at

-20 ºC.

Recombinant ESAT-6 and CFP-10 were detected via their HIS-tags with HRP conjugated Anti-HIS antibodies (Figure 5.2: CE_A and CE_B) (Baldrich, Restrepo and O'Sullivan, 2004). A 96-well plate (Corning® 96-well EIA/RIA plates; CLS3590-100EA) was coated with streptavidin (10 µg/ml) (Prospec; PRO-283) overnight at 4 °C. The plate was washed one to three times with wash buffer before incubating the plate with 200 µl of blocking buffer (PBS containing 1% BSA) for 1-2 h. The plate was washed before adding 75-100 µl of X-Aptamers (0.5 µM) which had been incubated at 95 °C for 10 min and then renatured on ice for 5 min. After washing 75-100 µl of rCFP-10-HIS (5.9 nM) (BEI Resources; NR-14869), rESAT-HIS (5.9 nM) (BEI Resources; NR-14868) or controls in duplicate was added to the plate. Plates were incubated for 1-2 h. After washing HRP-conjugated Anti-HIS (Sigma; A7058-1VL), diluted 1:10000 was added and incubated for 1-2 h. The plate was washed before adding 100 µl of chromogenic substrate TMB (R&D; DY999) and incubated at room temperature for 20 min in the dark. Stop solution (1 M sulphuric acid) was added to terminate the reaction. The absorbance of each well was read at 450 nm with an iMark microplate reader (Bio-Rad).

Native ESAT-6 was detected in H37Rv culture filtrate with anti-ESAT-6 antibodies and HRP conjugated anti-rabbit IgG antibodies (Figure 5.2: CE_C). Pre-coated streptavidin plates (Thermo Scientific Nunc Immobilizer Streptavidin; 436014) were washed before adding 100 µl of X-Aptamers (0.5 µM) which had been incubated at 95 °C for 10 min and then renatured on ice for 5 min. The plate was washed before adding culture filtrate from H37Rv and controls in triplicate. Plates were incubated for 1-2 h. After washing, 100 µl of polyclonal anti-ESAT-6 antibody (BEI resources; NR-13803) diluted 1:5000 was added to the wells. After washing twice, HRP-conjugated Anti-rabbit IgG (R&D systems; HAF008), diluted 1:10000 was added and incubated for 1-2 h. The plate was washed before adding 100 µl of chromogenic substrate TMB and incubated at room temperature for 20 min in the dark. Stop solution (1 M sulphuric acid) was added to terminate the reaction. The absorbance of each well was read at 450 nm with an iMark microplate reader.

LAM

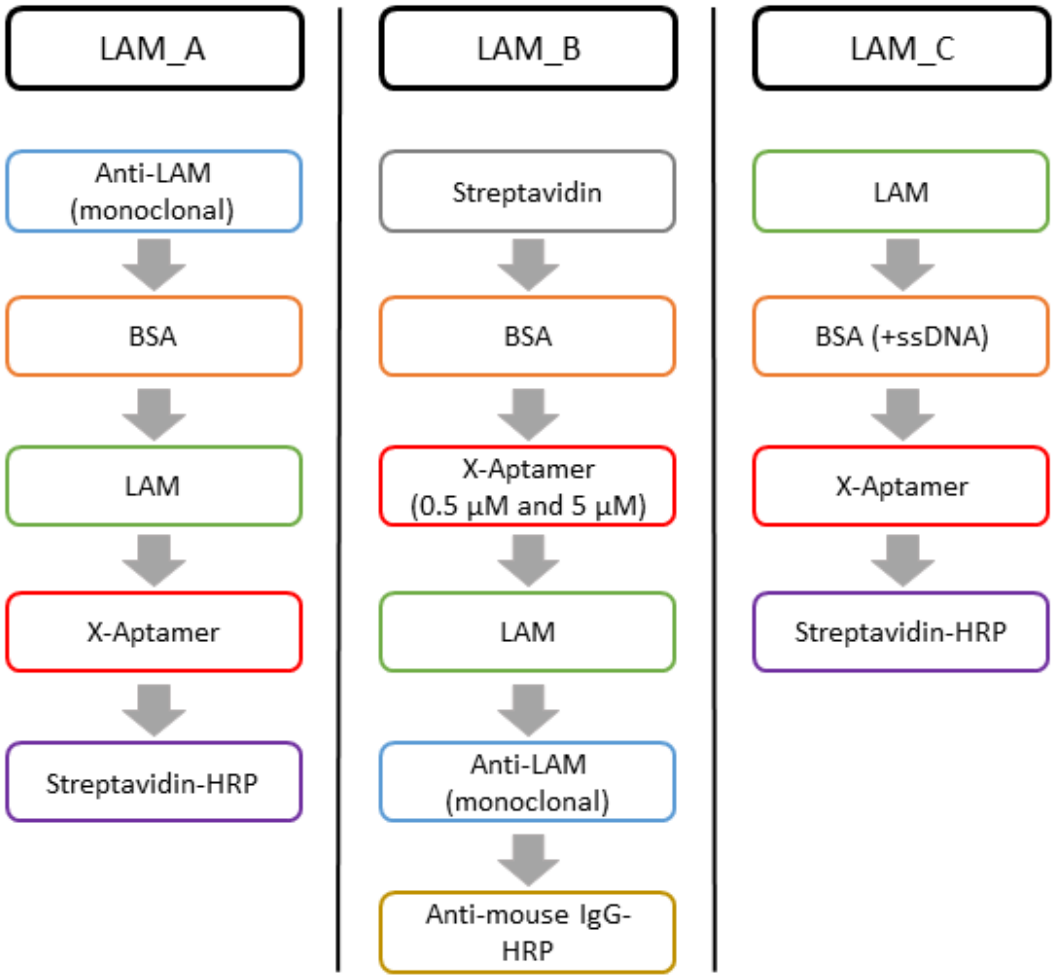

Figure 5.3 LAM ELONA-ELISA Hybrid Assay

Workflows: LAM_A, LAM_B and LAM_C

Three different versions of the ELONA-ELISA hybrid assay were used to test the binding of putative X-Aptamers to LAM (Figure 5.3). All reagents were resuspended in PBS (Sigma; P4417) at pH 7.4 and this buffer was used as a negative control. All incubations were at 37 °C with a plate sealer and the plate was washed three times with wash buffer (PBS containing 0.05% Tween-20) unless otherwise noted. Corning® 96-well EIA/RIA plates (CLS3590-100EA) were used for all the following experiments.

For the first version LAM was immobilised onto the surface via anti-LAM antibodies and detected via the biotinylated X-Aptamers and HRP conjugated streptavidin (Figure 5.3: LAM_A). A 96-well plate was coated with polyclonal Anti-LAM antibodies (BEI Resources; NR-13821)

overnight at 4 °C. The plate was washed once with wash buffer before incubating the plate with 200 µl of blocking buffer (PBS containing 1% BSA) for 1-2 h. The plate was washed before adding 100 µl of LAM (H37Rv) (100 ng/ml or 5.9 nM) (BEI Resources NR-14848) and controls in duplicate. The plate was washed before adding 100 µl of X-Aptamers (0.5 µM) which had been incubated at 95 °C for 10 min and then renatured on ice for 5 min. Plates were incubated for 1-2 h. X-Aptamers were removed but the plate was not washed before adding HRP conjugated streptavidin (#14-20-00 KPL), diluted 1:10000 was added and incubated for 1-2 h. The plate was washed and 100 µl of chromogenic substrate TMB was added and incubated at room temperature for 20 min in the dark. Stop solution (1 M sulphuric acid) was added to terminate the reaction. The absorbance of each well was read at 450 nm with an iMark microplate reader.

A second version of the ELONA-ELISA hybrid, where the biotinylated X-Aptamers were immobilised via streptavidin and the LAM (H37Rv) was detected with antibodies, was also performed (Figure 5.3: LAM_B). A 96-well plate was coated with streptavidin (10 µg/ml) overnight at 4 °C. The plate was washed once with wash buffer before incubating the plate with 200 µl of blocking buffer (PBS containing 1% BSA) for 1-2 h. The plate was washed before adding 100 µl of X-Aptamers (0.5 µM or 5 µM) which had been incubated at 95 °C for 10 min and then renatured on ice for 5 min. The plate was washed before adding 100 µl of LAM (H37RV) (5.9 nM or 1 µM) and controls in duplicate. Plates were incubated for 1-2 h. After washing 100 µl of monoclonal anti-LAM antibody (BEI resources; NR-13812), diluted 1:1000, was added to the wells. After washing, HRP conjugated anti-mouse IgG (R&D systems; HAF007), diluted 1:1000 was added and incubated for 1-2 h. The plate was washed and 100 µl of chromogenic substrate TMB was added and incubated at room temperature for 20 min in the dark. Stop solution (1 M sulphuric acid) was added to terminate the reaction. The absorbance of each well was read at 450 nm with an iMark microplate reader.

Finally, a third assay was performed based on the method described by Pan *et al.* (Figure 5.3: LAM_C) (Pan *et al.*, 2014). LAM was adsorbed directly onto the surface and detected with X-Aptamer and HRP conjugated streptavidin. A 96-well plate was coated with LAM (H37Rv) (20 µg/ml or 1 µM) overnight at 4 °C in triplicate. The plate was washed once with wash buffer before incubating the plate with 200 µl of blocking buffer (100 µg/ml salmon sperm ssDNA (Sigma; D9156-1ML) or salmon sperm ssDNA in 1% BSA) for 1-2 h. The plate was washed before adding 100 µl of X-Aptamers (5 µM) which had been incubated at 95 °C for 10 min and then renatured on ice for 5 min. Plates were incubated for 1-2 h. After washing once, HRP

conjugated streptavidin (#14-20-00 KPL), diluted 1:10000, was added and incubated for 1-2 h. The plate was washed and 100 µl of chromogenic substrate TMB was added and incubated at room temperature for 20 min in the dark. Stop solution (1 M sulphuric acid) was added to terminate the reaction. The absorbance of each well was read at 450 nm with an iMark microplate reader.

5.2.2 Biolayer Interferometry

OCTET RED

Initial BLI analysis of the putative X-Aptamers was done on the OCTET Red system by AmBioTech. Biotinylated X-Aptamers were loaded onto streptavidin coated tips at 500 nM in PBS-TMB buffer (PBS with 0.02% Tween-20, 2 mM $MgCl_2$, 0.1% BSA). X-Aptamers were incubated at 95 °C for 10 min and then renatured on ice for 5 min before loading. The concentration of LAM and rESAT-6 was 500 nM. Tips were loaded with X-Aptamer for 60 s followed by a 30 s wash with PBSTMB buffer for LAM X-Aptamers and a 120 s blocking step for CE X-Aptamers. X-Aptamers were allowed to associate with the target for 300 s before the tips were moved to buffer for a dissociation for 300 s.

Data were processed and analysed using the Octet data analysis software (ForteBio®) using the 1:1 stoichiometric model. Due to poor fitting a custom analysis was performed. The error created by the baseline drift was corrected by subtracting the baseline data from the binding data.

The initial association and dissociation curves were used to estimate the rate constant of the binding reaction between immobilised X-Aptamer and LAM using the initial association and initial dissociation slope expressions. These expressions are derived below.

- The initial slope of association curve is $k_{on}[A]_0[L]_0/\varphi$.
- The initial slope of the dissociation curve is $-R_{sat}k_{off}$.

Definitions

- A: concentration in solution [mol/m^3]
- L: density immobilised on surface [mol/m^2]
- [LA]: analyte-ligand complex on the surface [mol/m^2]
- V: volume of microtitre plate well [m^3]
- S: surface area of microtitre plate well [m^2]
- k_{off}: Dissociation rate constant [1/s]
- k_{on}: Association rate constant [m^3/(mol·s)]
- R: BLI signal [nm shift]

Consider the reversible reaction

$$\mathrm{L} + \mathrm{A} \underset{k_{on}}{\overset{k_{off}}{\leftrightarrows}} \mathrm{LA} \tag{1}$$

Where the forward reaction rate is given by:

$$r_{on} = k_{on}[\mathrm{L}] \cdot [\mathrm{A}] \tag{2}$$

And the reverse reaction rate is:

$$r_{off} = k_{off}[\mathrm{LA}] \tag{3}$$

Where concentration [A] is defined per unit of volume and concentrations [L] and [LA] are defined per unit of surface area. The dynamic mass balance of all the components results in this set of ordinary differential equations:

$$\frac{d[\mathrm{A}]}{dt} = \left(-k_{on}\, C \cdot [\mathrm{L}] \cdot [\mathrm{A}]\right) + \left(k_{off} C \cdot [\mathrm{LA}]\right) \tag{4}$$

$$\frac{d[\mathrm{LA}]}{dt} = \left(\mathrm{k}_{on}[\mathrm{L}] \cdot [\mathrm{A}]\right) - \left(k_{off}[\mathrm{LA}]\right) \tag{5}$$

$$\frac{d[\mathrm{L}]}{dt} = \left(-k_{on}[\mathrm{L}] \cdot [\mathrm{A}]\right) + \left(k_{off}[\mathrm{LA}]\right) \tag{6}$$

Where, C is the ratio of total surface area to the volume.

Since signal R is proportional to the concentration [LA], [LA] can be expressed as [LA] = φR,

where φ is a constant. According to equation (1) stoichiometry, concentrations [L] and [LA] are related via the expression:

$$[L] = [L]_0 - [LA] = [L]_0 - \varphi R \tag{7}$$

Where $[L]_0$ is initial concentration of L. Substituting this expression into the differential equations (4) and (5) results in the following two equations:

$$\frac{d[A]}{dt} = \left(-k_{on}\, C[A]([L]_0 - \varphi R)\right) + \left(k_{off} C \varphi R\right) \tag{8}$$

$$\frac{dR}{\mathrm{d}t} = \frac{k_{on}}{\varphi} \cdot [A]\,([L]_0 - \varphi R) - k_{off} R \tag{9}$$

Equation (6) was excluded as it is not required.

Curve fitting

At initial association (Δt_a), where the curve is almost a straight line the following can be assumed.

Initially, R is small thus assuming R ≈ 0: substitute into equation (8):

$$\frac{d[\mathrm{A}]}{dt} = (-k_{on}\,[\mathrm{A}]C \cdot [\mathrm{L}]_0) \tag{10}$$

This equation can be solved directly, where $[\mathrm{A}]_0$ is the initial concentration of A:

$$[A] = [A]_0 \exp(-k_{on} C [L]_0\, t) \tag{11}$$

Substitute $R \approx 0$ and above expression for [A] into equation (9):

$$\frac{dR}{dt} = \frac{k_{on}}{\varphi}\,([A]_0\, \exp(-k_{on} C [L]_0\, t)) \cdot [L]_0 \tag{12}$$

Integrate equation (12):

$$\mathrm{R} = \frac{[\mathrm{A}]_0}{\varphi C}\,(1 - \exp(-k_{on} C [L]_0\, t)) \tag{13}$$

Since $0 < t < \Delta t_a$ and Δt_a is small, the exponent can be approximated by a linear expression, $e^{-\alpha t} \approx 1 - \alpha t$. Therefore, the expression for the signal R becomes

$$R \approx \frac{k_{on}[A]_0[L]_0}{\varphi} t \tag{14}$$

Thus, the initial slope of the association curve is $k_{on}[A]_0[L]_0/\varphi$.

Similarly, for initial stage of dissociation, $[A] \approx 0$ and equation (6) becomes

$$\frac{dR}{dt} = -k_d R \tag{15}$$

Its integration results in

$$R = R_{sat} \exp\left(-k_{off}(t - t_d)\right) \tag{16}$$

Where t_d is the time at the beginning of dissociation curve and R_{sat} is the signal at time t_d. For small time increments $t - t_d < \Delta t_d$, this simplifies to

$$R \approx R_{sat}\left(1 - k_{off}(t - t_d)\right) \tag{17}$$

Thus, the initial slope of the dissociation curve is $-R_{sat}k_{off}$.

OCTET K2

At a later date an OCTET K2 system became available for use. Due to limited reagents only one aptamer was tested. Previously CE 3.8 had encouraging binding with ELONAs hence it was further characterised. A 2-fold dilution series of rESAT-6 was prepared (1000 to 62.5 nM) in PBS-TM (PBS with 0.05% Tween-20, 1 mM $MgCl_2$). Streptavidin coated tips were equilibrated for 180s in PBS-TM before loading biotinylated X-Aptamers at 100 nM in PBS-TM buffer for 150 s. X-Aptamers were incubated at 95 °C for 10 min and then renatured on ice for 5 min before loading. X-Aptamer coated tips were allowed to associate with the target for 300 s before the tips were moved to PBS-TM buffer for 300 s to dissociate. Reference tips were coated with X-Aptamer but not incubated with rESAT-6. LAM 4.1 was used as an irrelevant aptamer control to assess the analytical specificity of binding.

Data were processed and analysed using the Octet data analysis software (ForteBio®). Curves were fitted using a 1:1 stoichiometric model. Reference traces were subtracted before analysis.

5.2.3 *In silico* Sequence Analysis

The Mfold web server was used to secondary structure analysis of X-Aptamer sequences (http://unafold.rna.albany.edu/?q=mfold/DNA-Folding-Form). All settings were left as default except for folding temperature and sodium concentration ($[Na^+]$). Folding temperature was set at 25 °C and $[Na^+]$ was set at 137 mM since aptamer were suspended in PBS pH ~7.5.

Modified bases were converted from uracil to thymidine since Mfold does not have functionality

for deoxyribose uracil (dUTP) nucleotides.

5.3 Results

5.3.1 ELONA-ELISA Hybrid

In-house ELONA-ELISA hybrid assays were used to screen the binding ability of putative aptamers selected against the CFP-10·ESAT-6 dimer, CFP-10 and LAM. Up to three controls were used in these assays. The aptamer only control assessed non-specific binding of the HRP conjugated antibody to the surface with aptamer. The ESAT-6, CFP-10 or LAM only control assessed non-specific binding of the molecules to the surface without being specifically immobilised by an aptamer or antibody. Lastly, the no aptamer or biomarker assessed baseline non-specific binding of the HRP conjugated antibody to the surface.

ESAT-6 and CFP-10

To screen the aptamers against ESAT-6 and CFP-10, the biotinylated X-Aptamers were immobilised via streptavidin and the recombinant proteins were detected via their HIS-tags with HRP conjugated Anti-HIS antibodies.

X-Aptamer CE 3.8 (Figure 5.4) produced the highest absorbance readings when binding to rESAT-6 and rCFP-10. CE 3.6 and CE 3.9 also had absorbance readings above the pooled X-Aptamer only control for rCFP-10 and control two and three for rESAT-6. There was no detectable binding of rESAT-6 or rCFP-10 for the other X-Aptamers as the absorbance reading was equal to or less than the control for these aptamers (Figure 5.5 and Figure 5.6).

CE 3.8 TTTTT CA TCGT AGCCTAGCCTGWCCCZWAATACTTAZCGGZ TCGT TTTTT
W=INDOLE; Z=BORON

Figure 5.4 X-Aptamer CE 3.8 sequence.

The CE 3.8 sequence was modified at three positions with indole and boron.

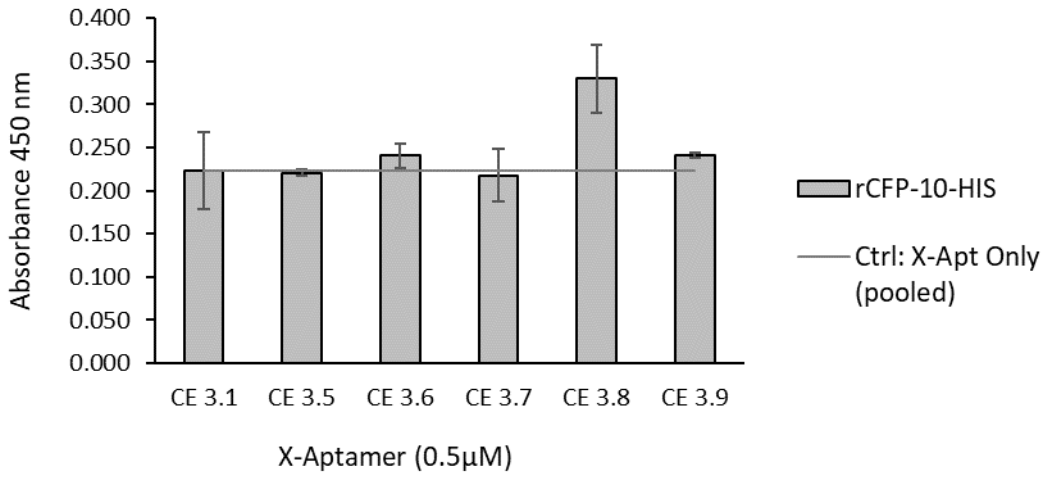

Figure 5.5 CFP-10 ELONA-ELISA Hybrid.

CE 3.1-3.9 were assessed for binding to HIS tagged rCFP-10 (5.9 nM). All wells were performed in duplicate. Columns indicate the mean reading of duplicate or triplicate wells. Error bars indicate the minimum and maximum readings taken.

CE_A: Streptavidin→ BSA→X-Aptamer→rCFP-10-HIS→Anti-HIS-HRP (rCFP-10-HIS)

Control: Streptavidin→BSA→ All X-Aptamers pooled→ PBS→ Anti-HIS-HRP (Ctrl: X-Apt Only)

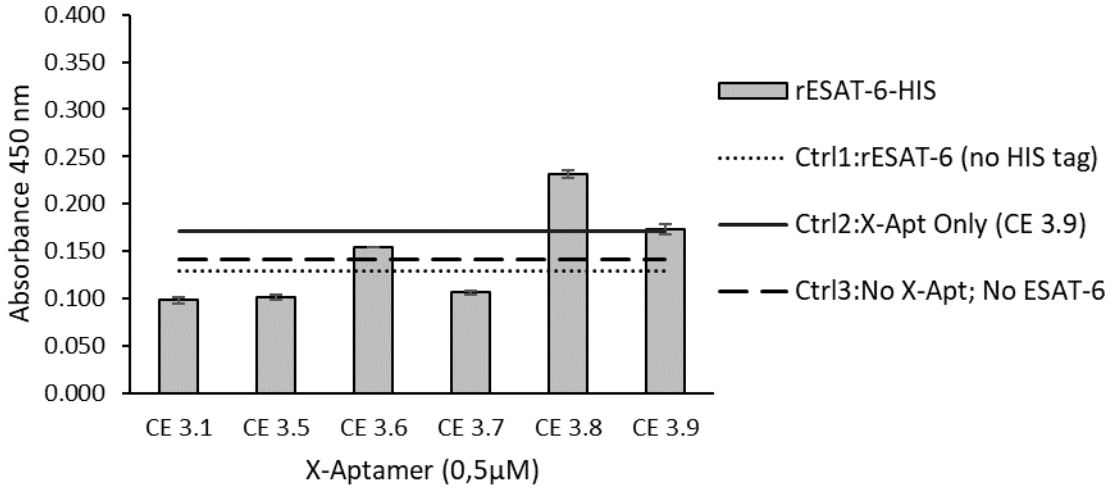

Figure 5.6 ESAT-6 ELONA-ELISA Hybrid.

CE 3.1 to 3.9 were assessed for binding to HIS tagged rESAT-6 (5.9 nM). All wells were in duplicate. Columns indicate the mean reading of duplicate wells. Error bars indicate the minimum and maximum readings taken.

CE_B: Strep→ BSA→X-Aptamer→ rESAT-6-HIS →Anti-HIS-HRP (rESAT-6-HIS)

Control 1: Streptavidin→BSA→ PBS→ rESAT-6 → Anti-HIS-HRP (Ctrl 1: rESAT-6 no HIS tag)

Control 2: Streptavidin→BSA→ X-Aptamer (CE 3.9) → PBS→ Anti-HIS-HRP (Ctrl 2: X-Apt only)

Control 3: Streptavidin→BSA→ PBS→ PBS→ Anti-HIS-HRP (Ctrl 3: No X-Apt; No ESAT-6)

Binding curves were constructed where rESAT-6 and rCFP-10 concentrations were fixed at 1 nM and the X-Aptamers were diluted in a two-fold serial dilution (0.004-0.5 μM). When the concentration of X-Aptamer incubated with the surface was increased the amount of CFP-10 bound at equilibrium did not increase for any of the X-Aptamers tested (Appendix C: Figure A 14 and Figure A 15). Similarly, the amount of rESAT-6 bound did not increase with increasing X-Aptamer immobilised on the surface for X-Aptamers CE3.6 and CE 3.9 (Appendix C: Figure A 16). However, the amount of rESAT-6 bound at equilibrium increased with increasing concentration of X-Aptamer CE 3.8 incubated with the surface which produced a binding curve (Figure 5.7). As little as 4 nM of CE 3.8 could detect 1 nM of rESAT-6. Further experiments were conducted with rESAT-6 and CE 3.8.

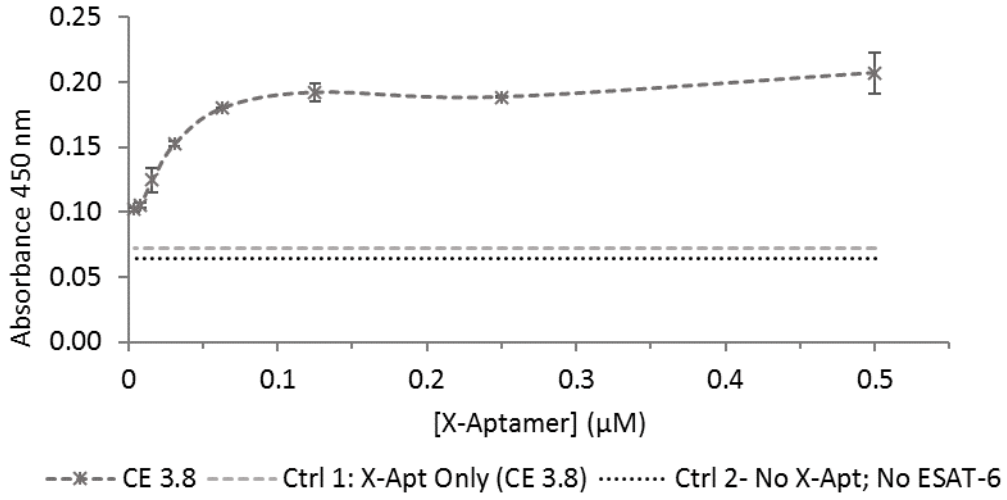

Figure 5.7 Binding Curve with rESAT-6 and CE 3.8.

HIS tagged rESAT-6 (1 nM) and two-fold serial dilutions of X-Aptamer CE 3.8 (0.5-0.004 μM). All wells were performed in duplicate. Columns indicate the mean reading of duplicate wells. Error bars indicate the minimum and maximum readings taken.

CE_B: Streptavidin→ BSA→X-Aptamer→rESAT-6-HIS→Anti-HIS-HRP

Control 1: Streptavidin→BSA→ X-Aptamer (CE 3.9)→ PBS→ Anti-HIS-HRP (Ctrl 1: X-Apt Only)

Control 2: Streptavidin→BSA→ PBS→ PBS→ Anti-HIS-HRP (Ctrl 2: No X-Apt; No ESAT-6)

To detect native ESAT-6 an alternative ELONA-ELISA hybrid was optimised, namely using polyclonal antibodies against ESAT-6 and a secondary HRP conjugated antibody against rabbit IgG. ESAT-6 was detected in H37Rv culture filtrate during mid-log and log phase but not stationary phase (Figure 5.8). Note the X-Aptamer only control gave a high background signal compared to the other controls.

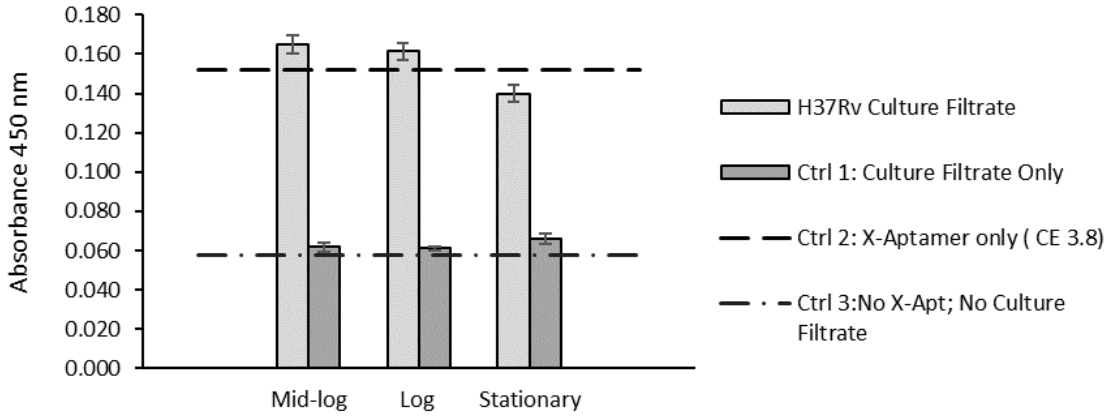

Figure 5.8 ESAT-6 detection in H37Rv Culture Filtrate with CE 3.8.

All wells were performed in triplicate. Columns indicate the mean reading of triplicate wells. Error bars indicate the minimum and maximum readings taken.

ELONA/ELISA: Streptavidin→ X-Aptamer→Culture Filtrate→ Anti-ESAT-6→ Anti-Rabbit IgG-HRP (H37Rv Culture Filtrate)

Control 1: Streptavidin→ PBS→Culture Filtrate→ Anti-ESAT-6→ Anti-Rabbit IgG-HRP

Control 2: Streptavidin→ X-Aptamer→ PBS→ Anti-ESAT-6→ Anti-Rabbit IgG-HRP (Ctrl 2: X-Apt Only)

Control 3: Streptavidin→ PBS→ PBS→ Anti-ESAT-6→ Anti-Rabbit IgG-HRP (Ctrl 3: No X-Apt; No Culture Filtrate)

LAM

To screen aptamers selected against LAM several LAM ELONA-ELISA hybrid assays were performed. For the first experiment LAM was captured onto the surface via anti-LAM antibodies and detected via the biotinylated X-Aptamers and HRP conjugated streptavidin (Figure 5.9 A). Each aptamer was tested with and without LAM present. All wells containing LAM had absorbance readings above the LAM only control, but only LAM 4.3 had an absorbance reading above the respective X-Aptamer only control. When a dilution series of the LAM only control was performed, it appeared that the lower the concentration of LAM the higher the background absorbance reading (Figure 5.9 B).

In the second version of the ELONA-ELISA hybrid assay, biotinylated X-Aptamers were immobilised via streptavidin and the LAM (H37Rv) was detected with a monoclonal anti-LAM antibody and an HRP conjugated anti-mouse IgG. The first experiment was performed with 0.5 µM X-Aptamer and 5.9 nM LAM (Figure 5.10 A). None of the wells had a signal above the controls, thus the concentration of X-Aptamer and LAM were increased to 5 µM and 1 µM respectively in the following experiment (Figure 5.10 B). While the overall signal was low, there were three X-Aptamers (LAM 4.1, 4.4 and 4.7) that had a signal above both the controls.

Finally, a third assay was performed based on the method described by Pan et. al (Pan *et al.*, 2014). LAM (1 µM) was adsorbed directly onto the surface and detected with X-Aptamer and HRP conjugated streptavidin. Salmon sperm ssDNA was used to block the surface in the first version of this assay as reported by Pan *et al.* None of the aptamers binding LAM gave an absorbance reading above the LAM only control (Figure 5.11 A). To improve blocking 1 % BSA was added to the blocking buffer and the previously reported ZXL 1 aptamer was included to test the repeatability of the paper's results. The absorbance readings had low values and the control absorbance reading remained higher than the wells where X-Aptamer was present (Figure 5.11 B).

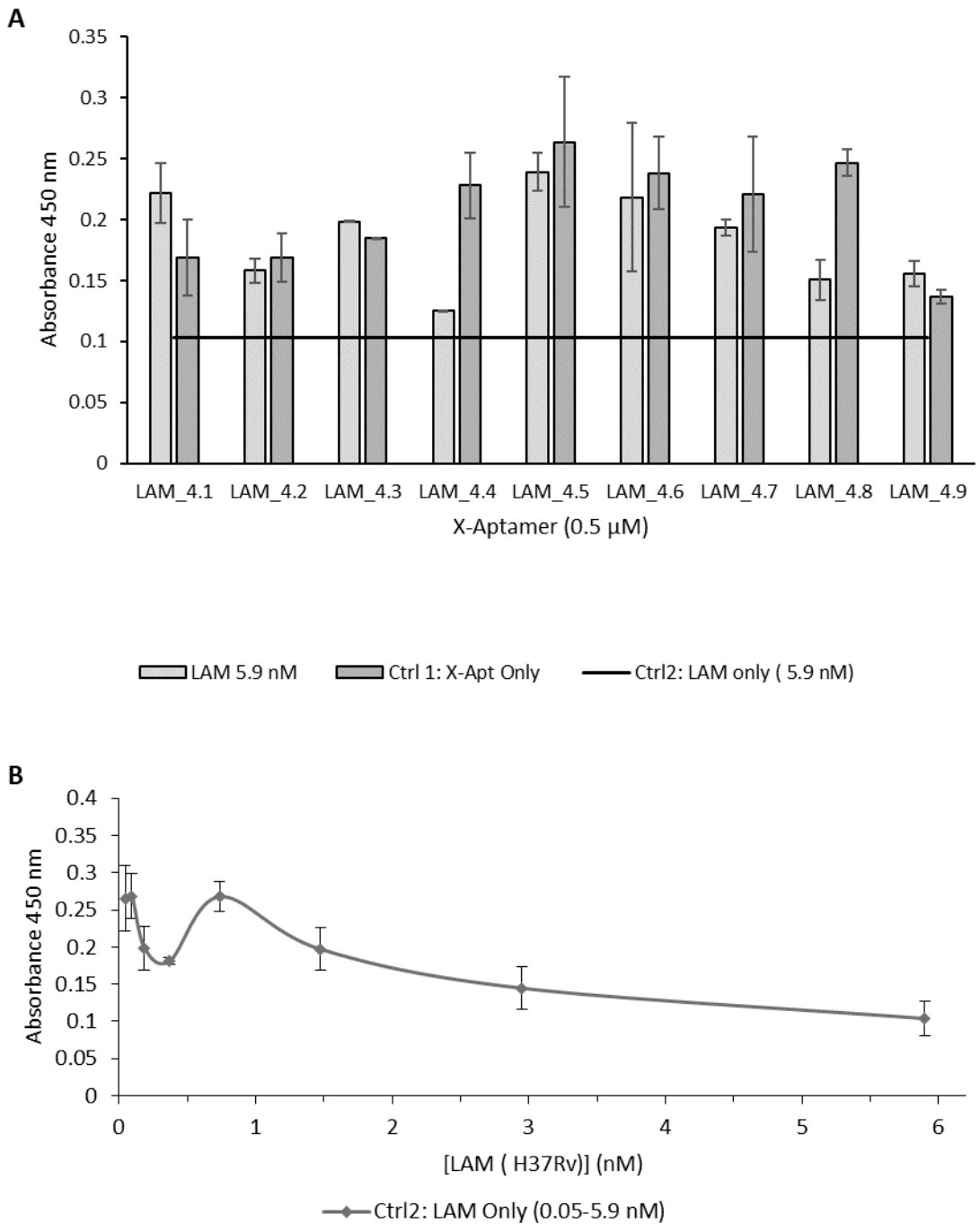

Figure 5.9 LAM ELONA-ELISA hybrid with streptavidin-HRP detection.

A) LAM 4.1-4.9 were assessed for binding to LAM (5.9 nM). B) Serial dilution of LAM only control. All wells were in duplicate. Columns indicate the mean reading of duplicate wells. Error bars indicate the minimum and maximum readings taken.

LAM_A: Anti-LAM (polyclonal) → BSA→LAM → X-Aptamer→Streptavidin-HRP

Control 1: Anti-LAM (polyclonal) →BSA→PBS→ X-Aptamer→Streptavidin-HRP (Ctrl 1: X-Apt only)

Control 2: Anti-LAM (polyclonal) →BSA→LAM→ PBS→Streptavidin-HRP (Ctrl 2: LAM only)

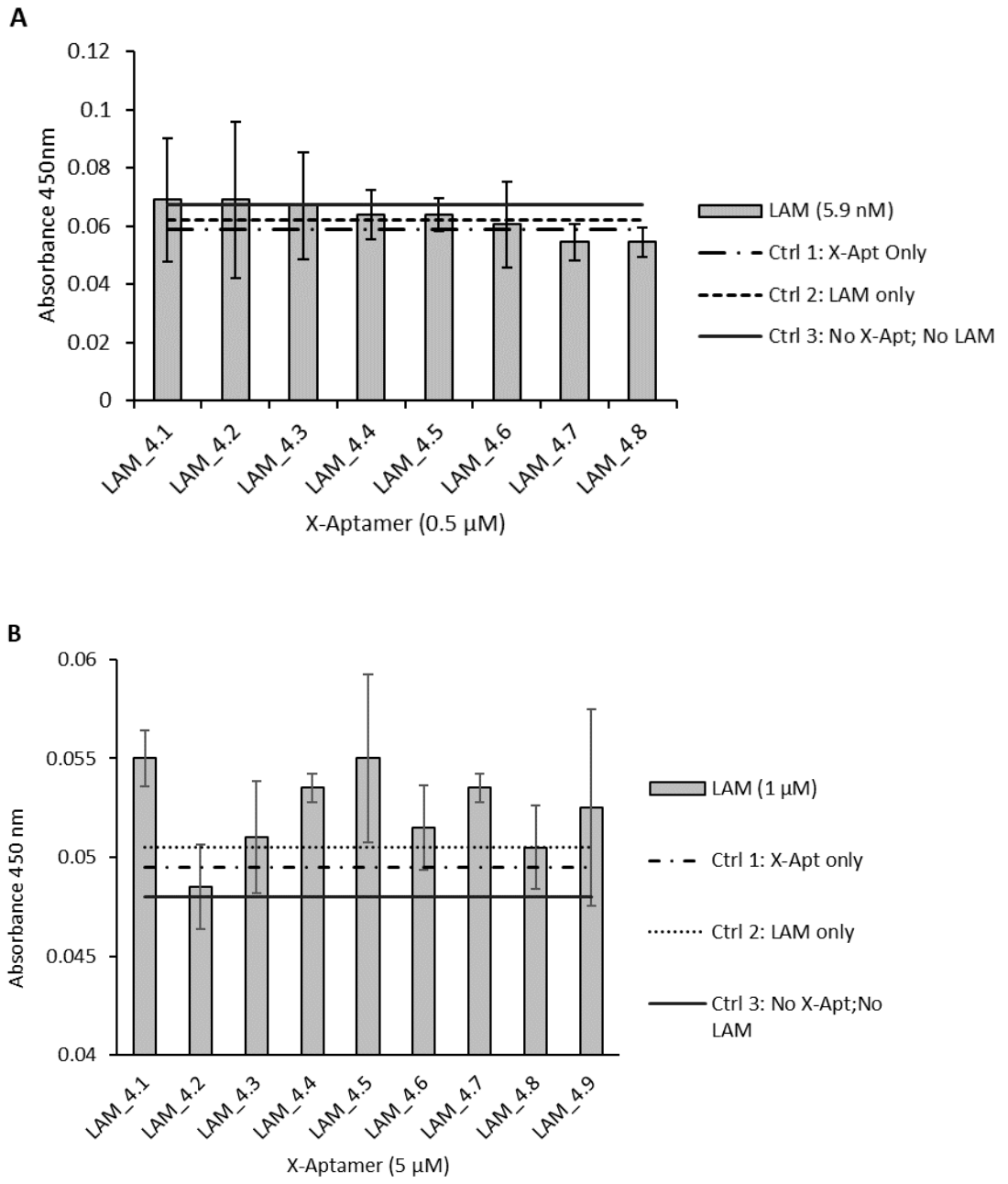

Figure 5.10 ELONA-ELISA Hybrid MAB detection.

A) 0.5 µM X-Aptamer and 5.9 nM LAM B) 5 µM X-Aptamer and 1 µM LAM. All wells were in duplicate. Columns indicate the mean reading of duplicate or triplicate wells. Error bars indicate the minimum and maximum readings taken.

LAM_B: Streptavidin→BSA→ X-Aptamer→ LAM → Anti-LAM (monoclonal)→Anti-mouse IgG-HRP

Control 1: Streptavidin→BSA→ X-Aptamer→ PBS→ Anti-LAM →Anti-mouse IgG-HRP (Ctrl 1: X-Apt only)

Control 2: Streptavidin→BSA→ PBS→ LAM→ Anti-LAM →Anti-mouse IgG-HRP (Ctrl 2: LAM only)

Control 3: Streptavidin→BSA→ PBS→ Anti-LAM →Anti-mouse IgG-HRP (Ctrl 3: No X-Apt; no LAM)

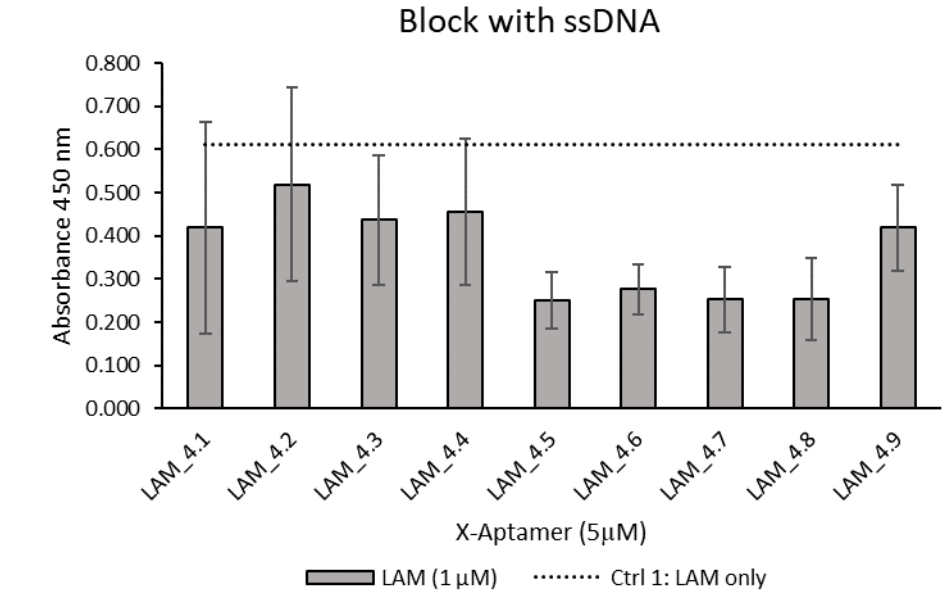

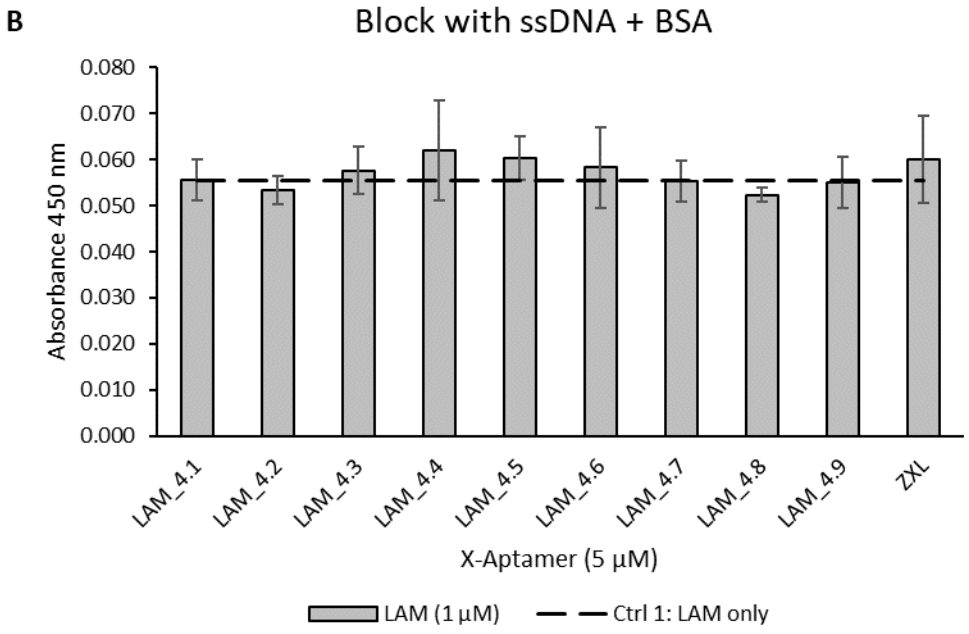

Figure 5.11 LAM ELONA with ssDNA or ssDNA + BSA blocking.

A) Wells blocked with Salmon sperm ssDNA. B) Wells blocked with salmon sperm ssDNA. All wells were in triplicate. Columns indicate the mean reading of duplicate or triplicate wells. Error bars indicate the minimum and maximum readings taken.

LAM_C: LAM→(BSA +) ssDNA→ X-Aptamer→Streptavidin-HRP

Control 1: LAM→(BSA +) ssDNA →PBS→Streptavidin-HRP (Ctrl 1: LAM only)

5.3.2 Biolayer Interferometry

OCTET RED

For analysis with the Octet RED most X-Aptamers did not display binding (Appendix C: Figure A 17 and Figure A 18). Binding to CFP-10 was not tested since ELONA-ELISA assay screening had shown the best binding to ESAT-6.

The exception was LAM 4.1 binding to LAM. ForteBio® Octet software was used to fit a curve to the data assuming 1:1 stoichiometry (Figure 5.12). However, the curve did not fit well with a poor R^2 score (< 0.9). The negative trace of the baseline and dissociation phase is due to alignment artefacts from the software. Equilibrium appears to be reached by 100 s.

Custom curve fitting after correcting the baseline drift was performed using the expressions:

- The initial slope of association curve is $k_{on}[A]_0[L]_0/\varphi$.
- The initial slope of the dissociation curve is $-R_{sat}k_{off}$.

The rate constant value $k_{off} = 0.064$ s^{-1} was found to minimise the error between predicted initial dissociation curve and the experimental data (Figure 5.13). The data from initial stage of association is insufficient to determine rate coefficient k_{on}, since it can only determine the value of the expression $(k_{on}[\mathrm{L}]_0)/\varphi$ and values $[\mathrm{L}]_0$ and φ are unknown.

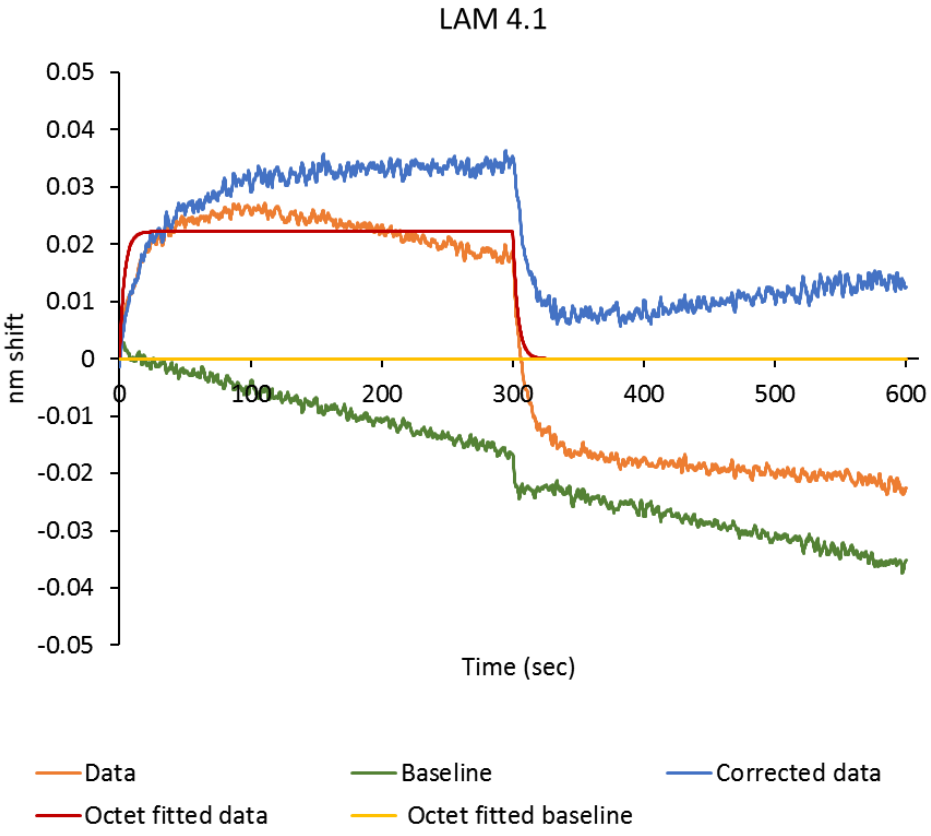

Figure 5.12 BLI data for X-Aptamer LAM 4.1

ForteBio® software fitted curves

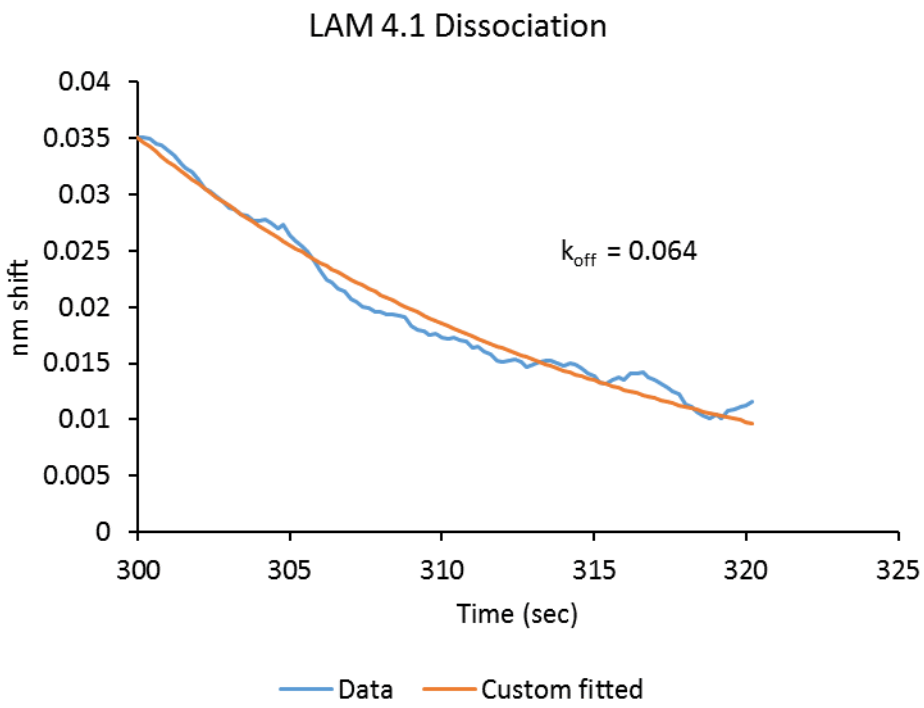

Figure 5.13 Initial dissociation curve of X-Aptamer LAM 4.1 and LAM.

Calculated k_{off} = 0.064 (1/s)

OCTET K2

After optimisation of the ESAT-6 concentration range, X-Aptamer concentration and loading time (Appendix C: Figure A 1) the final experiment was performed as stated in the methods. While signal was weak, it was sufficient. Signal should ideally be > 0.7 nm, but higher signals could not be obtained. Using the ForteBio® software a 1:1 stoichiometric model was used to determine the binding constants. The three highest concentrations of ESAT-6 produced curves that fitted well with a 1:1 model (Figure 5.14 A) X-Aptamer 3.8) and had good R^2 values (> 0.9) (Table 5.1). Small χ^2 values are also desirable. The two lowest concentrations did not have good R^2 values, signal was very low and curves almost appeared flat.

The calculated K_D values for binding between X-Aptamer CE 3.8 and rESAT-6 were between 187 nM and 400 nM. The k_{off} values ranged from 10^{-4} to 10^{-3} (s^{-1}).

An unrelated X-Aptamer was also associated with rESAT-6 to assess non-specific binding. The poor fit to the 1:1 model and (Table 5.2) the sharp dip in signal at the start of dissociation indicates non-specific binding which is most evident at the highest concentration of rESAT-6 (Figure 5.14 B) Unrelated X-Aptamer). Non-specific binding had lower signal than real binding between X-Aptamer CE 3.8 and rESAT-6.

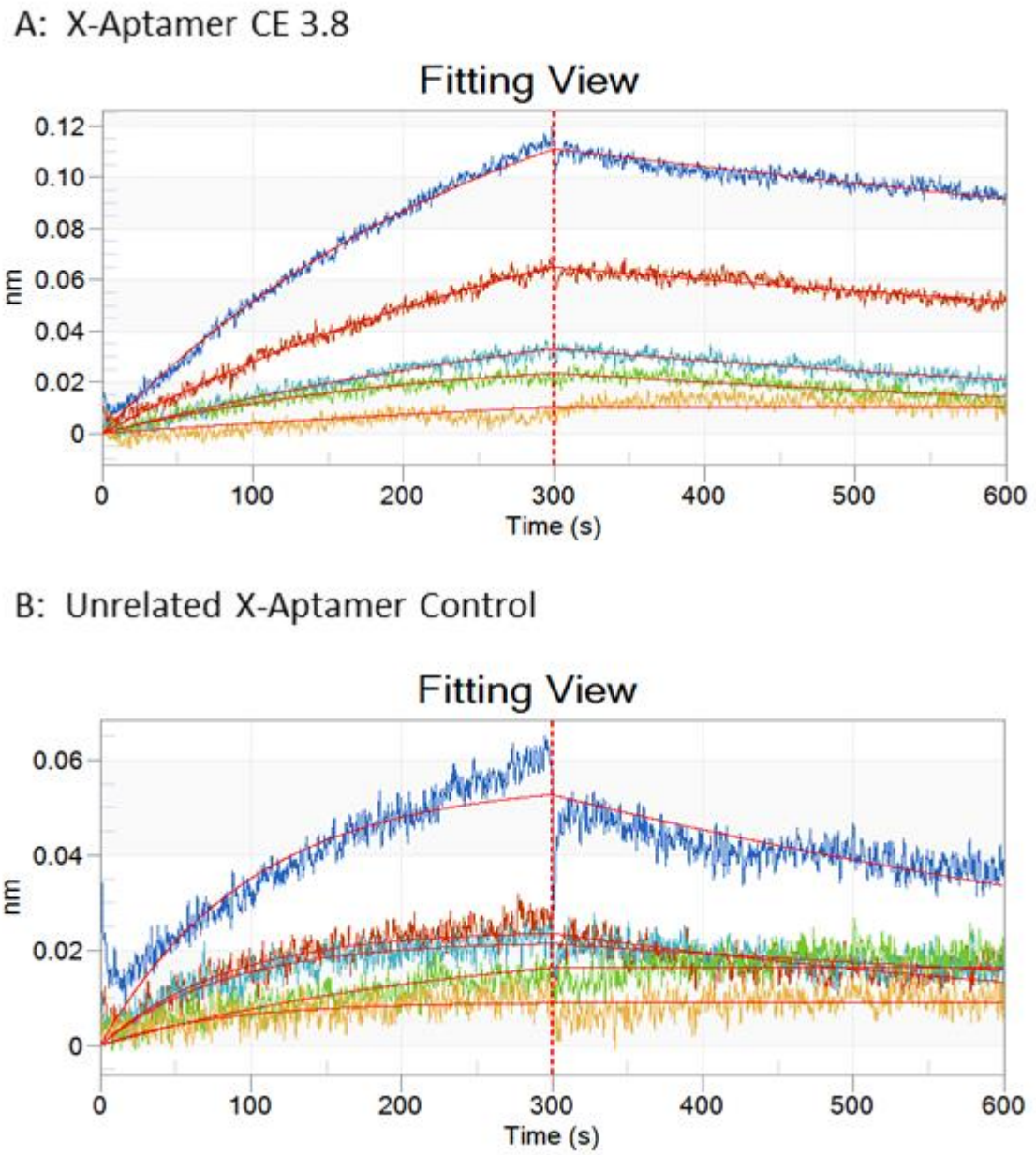

Figure 5.14 Association and Dissociation of rESAT-6 with

A) X-Aptamer CE 3.8 and B) Unrelated X-Aptamer Control (LAM 4.1). rESAT-6 concentrations: Blue- 1000 nM; Red- 500 nM; Light blue- 250 nM; Lime green- 125 nM; Yellow- 62.5 nM. Fitted using a 1: 1 stoichiometric model.

Table 5.1 X-Aptamer CE 3.8 Curve fitting results

rESAT-6 conc. (nM)	K_D(M)	k_{on} (1/Ms)	k_{off} (1/s)	k_{obs} (1/s)	Full X^2	Full R^2
1000	2.04E-07	3.13E+03	6.39E-04	3.77E-03	0.0076	0.992
500	1.87E-07	4.12E+03	7.72E-04	2.83E-03	0.0055	0.985
250	4.06E-07	3.75E+03	1.52E-03	2.46E-03	0.0042	0.951
125	6.73E-08	2.48E+04	1.67E-03	4.76E-03	0.0044	0.886
62.5	<1.0E-12	2.08E+04	<1.0E-07	1.30E-03	0.0093	0.707

Table 5.2 Unrelated X-Aptamer Control Curve fitting results

rESAT-6 conc. (nM)	**K_D (M)**	**k_{on} (1/Ms)**	**k_{off} (1/s)**	**k_{obs} (1/s)**	**Full X^2**	**Full R^2**
1000	1.76E-07	8.54E+03	1.50E-03	1.00E-02	0.0248	0.810
500	9.57E-08	1.99E+04	1.91E-03	1.19E-02	0.0083	0.7493
250	2.25E-08	4.47E+04	1.01E-03	1.22E-02	0.0058	0.7543
125	<1.0E-12	3.17E+04	<1.0E-07	3.96E-03	0.0094	0.7192
62.5	<1.0E-12	2.01E+05	<1.0E-07	1.26E-02	0.0071	0.3196

5.3.3 Secondary Structure Analysis

The two aptamers that showed the most promising binding were subject to *in silico* secondary structure analysis with Mfold software (Zuker, 2003). CE 3.8 produced three structures with hairpin-loops with short stems and minimum free energy (ΔG) values ranging from 0.08 to 1.06 kcal/mol (Figure 5.15 A, B and C). LAM 4.1 had structures with hairpin-loop structures with longer stems and ΔG values from -2.66 to -1.34 kcal/mol (Figure 5.16).

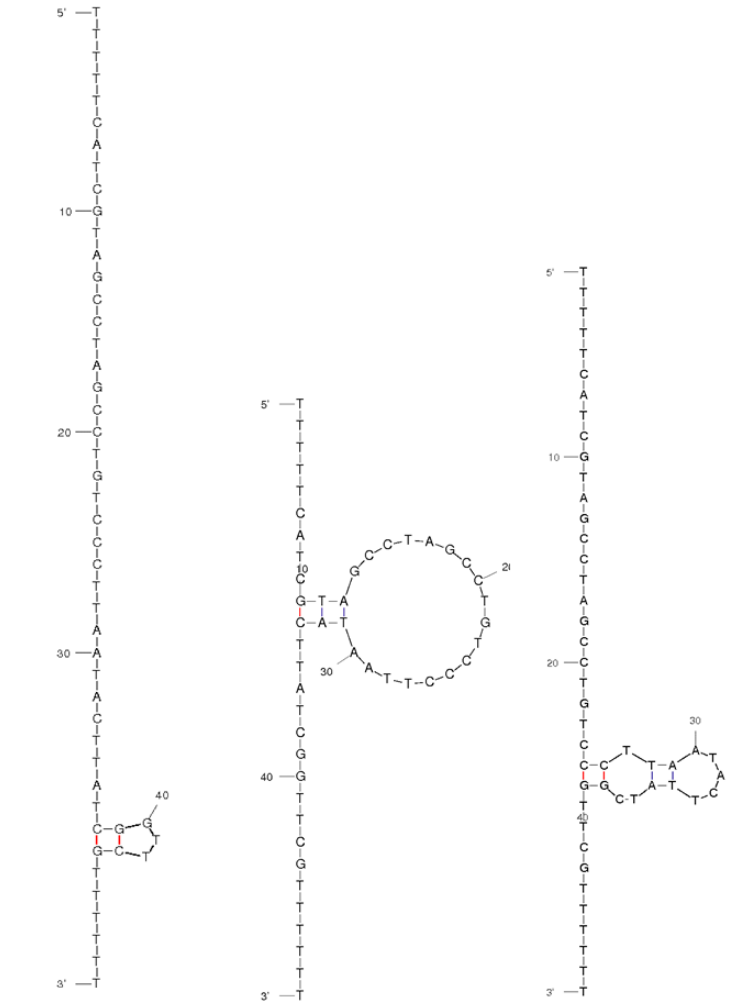

Figure 5.15 X-Aptamer CE 3.8 secondary Structures predicted by Mfold. A) Structure 1; B) Structure 2; C) Structure 3; D) Structure 4.

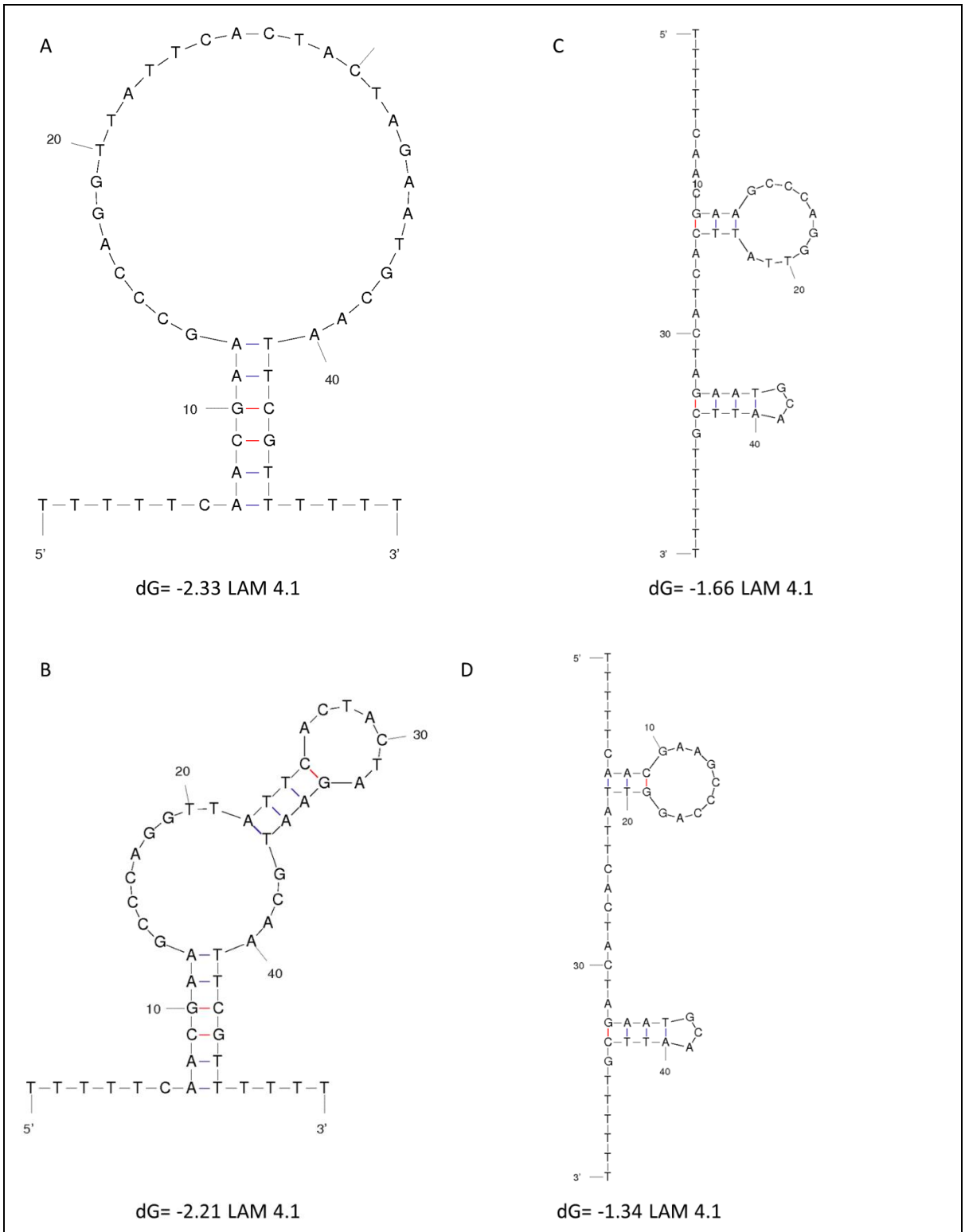

Figure 5.16 X-Aptamer LAM 4.1 secondary structures predicted by Mfold.

A) Structure 1; B) Structure 2; C) Structure 3; D) Structure 4.

5.4 Discussion

5.4.1 ELONA-ELISA hybrid

ESAT-6 and CFP-10

During the initial screening of the X-Aptamers selected against rESAT-6 and rCFP-10 three aptamers were found to bind to rCFP-10 and rESAT-6 with absorbance readings above one or more of the controls (Figure 5.5 and Figure 5.6). The sequence with the best absorbance readings, CE 3.8, had indole and boron modifications which indicate that binding was facilitated by interactions with hydrophobic and nucleophilic amino acid side chains on ESAT-6 (Figure 5.4) (Whyte, Vilar and Woscholski, 2013). CE3.6 and CE 3.9 were included for further investigation with rESAT-6 despite absorbance readings being below the X-Aptamer only control since only X-Aptamer CE 3.9 was used as a control and rCFP-10 had bound to these two aptamers.

In this first experiment X-Aptamers were pooled for the X-Aptamer only control in the assay (Figure 5.5), but since the non-specific binding of the antibodies to the X-Aptamers was not expected to vary greatly from aptamer to aptamer only one X-Aptamer was used as a control in the following experiment to save X-Aptamer stocks (Figure 5.6). This assumption was later withdrawn hence in later experiments, each X-Aptamer investigated had a control well with the respective X-Aptamer only control (Figure 5.7 and Figure A 14 to Figure A 16). The X-Aptamer only control produced a particularly high absorbance reading for the assay with the H37Rv culture filtrate (Figure 5.8) which is likely due to the available antibodies binding non-specifically to the X-Aptamer when there is no protein present, which reiterates the need for better molecular recognition reagents for diagnostic assays.

To explore the parameters of the assay a dilution series of the X-Aptamers was incubated with streptavidin coated surfaces. Streptavidin can bind up to four molecules of biotin with femtomolar affinity ($K_D \sim 10^{-14}$). The density of X-Aptamer on the surface is proportional to the concentration of X-Aptamer incubated with the streptavidin surface until the surface is saturated. Hence the amount of rESAT-6 or rCFP-10 bound should also increase with increasing density of X-Aptamer on the surface.

The dilution series of X-Aptamer CE 3.8 revealed a concentration-dependent binding curve when binding 1 nM of rESAT-6 (Figure 5.7). The other aptamers did not produce a similar curve when binding to rCFP-10 or rESAT-6. The absorbance readings for these aptamers remained constant and low irrespective of the concentration of X-Aptamer immobilised on the surface

(Appendix C: Figure A 14 to Figure A 16). The lack of concentration-dependent binding indicates that the binding observed could be non-specific for these aptamers.

Lastly, the ability of X-Aptamer CE 3.8 to detect ESAT-6 in H37Rv culture filtrate was tested. A common misconception is that ESAT-6 is only present in early stages of growth however it is rather one of the earliest proteins secreted into the culture filtrate (Andersen *et al.*, 1991; Sørensen *et al.*, 1995; Målen *et al.*, 2007). Despite a high background signal from the X-Aptamer only control ESAT-6 was detected in the mid-log and log phase whereas it could not be detected above background, in the stationary phase (Figure 5.8). This assay demonstrates that the CE 3.8 can detect native ESAT-6 in a complex media. Future work would include testing this aptamer in more complex media such as patient samples and testing cross-reactivity with commensal bacteria found in patient samples.

LAM

Since LAM did not have a HIS tag like rESAT-6 and rCFP-10, alternative ELONA-ELISA hybrid assays were explored to assess binding of the putative X-Aptamers against LAM. The first alternative assay captured LAM onto the surface via anti-LAM antibodies and bound X-Aptamers were detected with HRP-conjugated streptavidin (LAM_A: Figure 5.3).

The absorbance values for the X-Aptamer only control wells were higher than wells containing LAM and X-Aptamer, and covered a broad range (0.14 to 0.26) (Figure 5.9 A). This background signal is likely due to the streptavidin-HRP binding non-specifically to the other components of the assay as X-Aptamers used in the control were likely removed during wash steps since no LAM was present for the X-Aptamers to bind. The absorbance readings for this assay were also low which indicates a low concentration of LAM is being retained on the surface. The combination of high background and low assay signal impeded analysis of this assay as it is not clear if binding is due to non-specific binding or if real binding is occurring.

When a dilution series was performed, it was evident that the LAM was acting as a blocking agent; the more LAM that was bound the less non-specific binding there was by the HRP conjugated streptavidin (Figure 5.9 B). When the concentration of LAM is sufficient to block non-specific binding the absorbance values are valid for screening binding. Values should be above the LAM only control.

Given the caveats of the previous assay format another ELONA-ELISA hybrid assay was performed where biotinylated X-Aptamers were immobilised via streptavidin and LAM was detected with a monoclonal anti-LAM antibody and an HRP conjugated anti-mouse IgG (LAM_B:

Figure 5.3). An advantage of this assay format is that the X-Aptamer binds to LAM first. Hence binding is unhindered by a bulky antibody that may obstruct the epitope that the X-Aptamer binds.

Initially the assay was performed with 0.5 µM X-Aptamer and 5.9 nM LAM (Figure 5.10 A) however no binding above the controls was observed. Hence the concentration of X-Aptamer and LAM were increased to 5 µM and 1 µM respectively in the following experiment (Figure 5.10 B). Despite increasing concentrations of LAM and X-Aptamer incubated with the surface, absorbance readings did not increase considerably. The surface could be saturated with 0.5 µM of X-Aptamer hence the amplitude of the signal could not be increased by increasing the concentration to 5 µM. Nevertheless, there were three X-Aptamers (LAM 4.1, LAM 4.4 and LAM 4.7) that had absorbance readings above the controls (Figure 5.10 B).

The last strategy to improve signal was to use different blocking agents to decrease the background absorbance. The third assay was performed based on the method described by Pan *et. al*; LAM was adsorbed directly onto the surface and detected with X-Aptamer and HRP conjugated streptavidin (LAM_C: Figure 5.3)(Pan *et al.*, 2014). Salmon sperm ssDNA was used to block the surface in the first version of this assay as reported by Pan *et al*., however it was not effective at blocking the surface as there were no absorbance readings above the controls (Figure 5.11 A). BSA was added to reduce non-specific binding and one of the aptamers from the Pan *et al*. study (ZXL 1) was synthesized to use as a control (Figure 5.11 B). Overall background binding was reduced 10-fold from 0.6 to 0.06 absorbance units, however the sample signals remained below the background signal including ZXL 1 which had previously been reported to bind to LAM above a LAM only control in a similar experiment (Pan *et al.*, 2014).

In summary, all the X-Aptamers selected against LAM appear to have bound LAM as per the first ELONA-ELISA hybrid assay (Figure 5.9) and LAM 4.1, LAM 4.4, and LAM 4.7 appear to bind more tightly according to the second assay when the concentrations of LAM and X-Aptamer are increased (Figure 5.10).

5.4.2 Biolayer Interferometry

X-Aptamers, LAM and rESAT-6 where sent for analysis by the Octet RED system which employs BLI to measure binding. Poor binding was observed for most the aptamers (Appendix C: Figure A 17 and Figure A 18). The ESAT-6 assays appeared to suffer from non-specific binding of rESAT-6 to the streptavidin tips and blocking strategies did not overcome this.

X-Aptamer LAM 4.1 data showed a clear binding curve, but the Octet software could not fit a curve to the data. Hence a customised approach was used where the initial slope of the dissociation curve was used to estimate k_{off}. The k_{off} value was estimated at 0.064 s^{-1}. Pollard commented that association rate constants for typically sized proteins are often in a narrow range (10^6 to $10^7 M^{-1}s^{-1}$) hence the dissociation rate constant often determines the affinity. Hence micromolar affinity binding reactions have k_{off} values around 1 s^{-1} while nanomolar affinity reactions have k_{off} values around 0.001 s^{-1} (Pollard, 2010). Thus a k_{off} value of 0.064 s^{-1} is an improvement of typical aptamers selected against lipid or carbohydrate moieties which tend to have low micromolar affinity (10^{-5} to 10^{-7} M) (Fukusaki *et al.*, 2000; Betat *et al.*, 2003; Masud *et al.*, 2004; Boese and Breaker, 2007; Low, Hill and Peccia, 2009; Wang *et al.*, 2014).

At a later date a local OCTET K2 system became available. Additional analyses were performed between rESAT-6 and X-Aptamer CE 3.8.

During initial experiments concentrations of rESAT-6 were between 0.7 nM and 250 nM and X-Aptamer concentration was 50 nM. The final rESAT-6 range was 62.5 nM to 1000 nM given the poor signal obtained at lower ranges (data not shown). The concentration of aptamer was also increased to 100 nM to maximise the surface coverage of X-Aptamer on the streptavidin coated surface. ForteBio® recommends concentrations between 50 nM and 100 nM (Tobias and Kumaraswamy, 2013). The loading time of aptamers was increased from 150 s to 300 s in an effort to increase signal. However, increased loading time did not improve signal and excessive loading time or high ligand concentrations can result in steric hindrance (Appendix C: Figure A 2) (Edwards *et al.*, 1995).

BSA and detergents are typical agents used to minimise non-specific binding. BSA is not recommended when characterising aptamers since there is a heating step during aptamer preparation. Hence, Tween-20 or other detergents should be used to mitigate non-specific binding. The ForteBio® Kinetics buffer contains BSA but this is not stated on the data sheet which impeded initial trouble-shooting.

Fitted curves generated K_D values from ~180 to 400 nM (Table 5.1). While this binding affinity is in a modest range the benefits of aptamers coupled with label-free detection could still warrant the use of aptamers over antibodies. Additionally, given the novel method of selection it is bound to improve with time. Hence better aptamers could be selected with more advanced selection methods.

DNA aptamers previously selected against ESAT-6 had a similar K_D value of 160 nM but they did not report k_{off} values (Tang *et al.*, 2014). The k_{off} values for X-Aptamer CE 3.8 ranged from 10^{-3} to 10^{-4} (s^{-1}). This equates to a half-time between ~8-18 min i.e. the amount of time for 50% dissociation. While a K_D value may indicate nano –or micromolar affinity it does not indicate the on- and off-rate. Since the K_D value is the quotient of the rate constants, a reaction with a fast on- and off- rate may have the same K_D value as a reaction with a slower, more favourable off-rate.

Lower concentrations of rESAT-6 had poorly fitted curves and thus poor estimation of the K_D. Lower analyte concentrations may suffer from mass transport issues where binding is dependent on access to the surface rather than affinity between the two molecules. If mass transport is an issue curves tend to be flatter and may appear as flat lines such as observed for the lowest concentration of rESAT-6 (Figure 5.14) (Tobias and Kumaraswamy, 2013).

An unrelated X-Aptamer was also associated with rESAT-6 to assess non-specific binding. The poor fit to the 1:1 model and (Table 5.2) the sharp dip in signal at the start of dissociation indicates non-specific binding which is most evident at the highest concentration of ESAT-6 (Figure 5.14). Non-specific binding had lower signal than real binding between X-Aptamer CE 3.8 and rESAT-6 but should be kept in mind when designing assays.

5.4.3 Secondary Structure Analysis

Despite the caveats discussed above secondary structure analysis was performed on the two best performing X-Aptamers CE 3.8 and LAM 4.1 (Figure 5.15 and Figure 5.16)

CE 3.8 produced three structures with poor ΔG values ranging from 0.08 to 1.06 kcal/mol with short stemmed hairpin loops; hence these predicated structures are unstable and not useful for predicting key binding epitopes of this aptamer (Figure 5.15). LAM 4.1 had more promising predicted structures with ΔG values from -2.66 to -1.34 kcal/mol and longer stems on the hairpin loops which indicates better stability (Figure 5.16). These structures could be used to guide truncation of the X-Aptamer LAM 4.1 for reducing the cost of synthesis, possibly improving affinity for the target and understanding the aptamer-target interaction (Fischer, Tok and Tarasow, 2008; Keefe, Pai and Ellington, 2010; Berezhnoy *et al.*, 2012; Kaur and Yung, 2012).

5.4.4 Conclusion

X-Aptamer CE 3.8 was identified as a good candidate as a molecular recognition unit in a

biosensor to detect ESAT-6 in patient samples. In order to be a viable option for diagnosing tuberculosis, aptamers require further optimisation to improve analytical sensitivity and specificity. Availability and concentration of individual biomarkers is key to the choice of specimen in which to make diagnostic measurements.

6 CONCLUSION

The first aim of this thesis was to determine if LAM could be detected in TB patient urine with conventional methods by concentrating the urine. Concentration of TB patient urine increased the number of patient samples that were LAM positive, including an HIV negative patient. This illustrates that conventional methods are not sensitive enough to detect the low concentration of LAM present in TB patients.

Secondly, urine and sputum were probed for secreted mycobacterial proteins. Initial experiments used an in-house ELISA to detect ESAT-6, but due to cross-reactivity issues an alternative method was employed, namely mass spectrometry. Neither ESAT-6 nor CFP-10 could be detected in urine. Future work should focus on detecting ESAT-6 or CFP-10 in other patient specimens such as sputum.

Lastly, novel X-Aptamers were selected against KatG, ESAT-6 and LAM. A detailed kinetic characterization was carried out for the best aptamer selected against ESAT-6, X-Aptamer CE 3.8. Additionally, this aptamer binds to native ESAT-6 in culture filtrate in a growth state dependent manner. The ability of this aptamer to bind to native ESAT-6 highlights its potential utility in future diagnostic or other assays.

Given that neither CFP-10 nor ESAT-6 were detected in urine by targeted mass spectrometry future work with the selected aptamers should include development of assays for the detection of native biomarkers in biological specimens such as culture filtrate and other patient samples which may contain these biomarkers such as sputum.

The use of aptamers as capture agents for detecting biomarkers in biological specimens thus appears to be a viable option for diagnosing tuberculosis, although availability and concentration of individual biomarkers seems likely to remain key to the choice of specimen in which to make diagnostic measurements.

7 REFERENCES

Abbara, A. and Davidson, R. N. (2011) 'Etiology and management of genitourinary tuberculosis', *Nature Reviews Urology*. Nature Publishing Group, 8(12), pp. 678–688. doi: 10.1038/nrurol.2011.172.

Abdiche, Y. *et al.* (2008) 'Determining kinetics and affinities of protein interactions using a parallel real-time label-free biosensor, the Octet', *Analytical Biochemistry*, 377(2), pp. 209–217. doi: 10.1016/j.ab.2008.03.035.

Abeydeera, N. D. *et al.* (2016) 'Evoking picomolar binding in RNA by a single phosphorodithioate linkage', *Nucleic Acids Research*, 44(17), pp. 8052–8064. doi: 10.1093/nar/gkw725.

Abu-Raddad, L. J. *et al.* (2009) 'Epidemiological benefits of more-effective tuberculosis vaccines, drugs, and diagnostics.', *Proceedings of the National Academy of Sciences of the United States of America*, 106(33), pp. 13980–13985. doi: 10.1073/pnas.0901720106.

Achkar, J. M. *et al.* (2015) 'Host Protein Biomarkers Identify Active Tuberculosis in HIV Uninfected and Co-infected Individuals', *EBioMedicine*. Elsevier B.V., 2(9), pp. 1160–1168. doi: 10.1016/j.ebiom.2015.07.039.

Achkar, J. M., Chan, J. and Casadevall, A. (2015) 'B cells and antibodies in the defense against Mycobacterium tuberculosis infection', *Immunological Reviews*, 264(1), pp. 167–181. doi: 10.1111/imr.12276.

Afzal, M. *et al.* (2012) 'RDNAnalyzer: A tool for DNA secondary structure prediction and sequence analysis.', *Bioinformation*, 8(14), pp. 687–90. doi: 10.6026/97320630008687.

Alland, D. *et al.* (2015) 'Xpert MTB/RIF Ultra: A New Near-Patient TB Test With Sensitivity Equal to Culture', in *Conference on Retroviruses and Opportunistic Infections*. Seattle, Washington, p. 1.

Alsteens, D. *et al.* (2008) 'Organization of the mycobacterial cell wall: a nanoscale view.', *European journal of physiology*, 456(1), pp. 117–125. doi: 10.1007/s00424-007-0386-0.

Altintepe, L. *et al.* (2005) 'Urinary Tuberculosis: Ten Years' Experience', *Renal Failure*, 27(6), pp. 657–661. doi: 10.1080/08860220500234857.

Alves da Cruz, H. L. *et al.* (2011) 'Evaluation of a nested-pcr for Mycobacterium tuberculosis detection in blood and urine samples', *Brazilian Journal of Microbiology*, 42(1), pp. 321–329. doi: 10.1590/S1517-83822011000100041.

Andersen, P. *et al.* (1991) 'Proteins released from Mycobacterium tuberculosis during growth', *Infection and Immunity*, 59(6), pp. 1905–1910.

Andersen, P. *et al.* (1995) 'Recall of long-lived immunity to Mycobacterium tuberculosis infection in mice.', *Journal of Immunology*. American Association of Immunologists, 154(7), pp. 3359–72.

Arend, S. M. *et al.* (2008) 'Double-blind randomized Phase I study comparing rdESAT-6 to tuberculin as skin test reagent in the diagnosis of tuberculosis infection.', *Tuberculosis (Edinburgh, Scotland)*, 88(3), pp. 249–261. doi: 10.1016/j.tube.2007.11.004.

Armand, S. *et al.* (2011) 'Comparison of the Xpert MTB/RIF Test with an IS6110-TaqMan Real-Time PCR Assay for Direct Detection of Mycobacterium tuberculosis in Respiratory and Nonrespiratory Specimens', *Journal of Clinical Microbiology*, 49(5), pp. 1772–1776. doi: 10.1128/JCM.02157-10.

Arnold, S. *et al.* (2012) 'One round of SELEX for the generation of DNA aptamers directed against KLK6', *Biological Chemistry*, 393(5), pp. 343–353. doi: 10.1515/hsz-2011-0253.

Aryan, E. *et al.* (2013) 'Clinical value of IS6110-based loop-mediated isothermal amplification for detection of Mycobacterium tuberculosis complex in respiratory specimens', *Journal of Infection*. W.B. Saunders, 66(6), pp. 487–493. doi: 10.1016/j.jinf.2013.02.005.

Asmar, S. and Drancourt, M. (2015) 'Rapid culture-based diagnosis of pulmonary tuberculosis in developed and developing countries', *Frontiers in Microbiology*, 6(NOV). doi: 10.3389/fmicb.2015.01184.

Atkinson, A. J. *et al.* (2001) 'Biomarkers and surrogate endpoints: Preferred definitions and

conceptual framework', *Clinical Pharmacology and Therapeutics*, 69(3), pp. 89–95. doi: 10.1067/mcp.2001.113989.

Baaske, P. *et al.* (2010) 'Optical Thermophoresis for Quantifying the Buffer Dependence of Aptamer Binding', *Angewandte Chemie International Edition*, 49(12), pp. 2238–2241. doi: 10.1002/anie.200903998.

Baena, A. and Porcelli, S. A. (2009) 'Evasion and subversion of antigen presentation by Mycobacterium tuberculosis', *Tissue Antigens*, 74(3), pp. 189–204. doi: 10.1111/j.1399-0039.2009.01301.x.

Baldrich, E., Restrepo, A. and O'Sullivan, C. K. (2004) 'Aptasensor Development: Elucidation of Critical Parameters for Optimal Aptamer Performance', *Analytical Chemistry*. American Chemical Society, 76(23), pp. 7053–7063. doi: 10.1021/ac049258o.

Bannantine, J. P. *et al.* (2007) 'Development and Characterization of Monoclonal Antibodies and Aptamers against Major Antigens of Mycobacterium avium subsp. paratuberculosis', *Clinical and Vaccine Immunology*, 14(5), pp. 518–526. doi: 10.1128/CVI.00022-07.

Barnard, M. *et al.* (2008) 'Rapid Molecular Screening for Multidrug-Resistant Tuberculosis in a High-Volume Public Health Laboratory in South Africa', *American Journal of Respiratory and Critical Care Medicine*. American Thoracic Society, 177(7), pp. 787–792. doi: 10.1164/rccm.200709-1436OC.

Barratt, J. and Topham, P. (2007) 'Urine proteomics: the present and future of measuring urinary protein components in disease.', *Canadian Medical Association journal*, 177(4), pp. 361–368. doi: 10.1503/cmaj.061590.

Barry, C. E. *et al.* (2009) 'The spectrum of latent tuberculosis: rethinking the biology and intervention strategies', *Nature Reviews Microbiology*. Nature Publishing Group, 7(12), pp. 845–55. doi: 10.1038/nrmicro2236.

Basu, S. K. *et al.* (2006) 'Mycobacterium tuberculosis secreted antigen (MTSA-10) modulates macrophage function by redox regulation of phosphatases.', *The FEBS journal*, 273(24), pp. 5517–5534. doi: 10.1111/j.1742-4658.2006.05543.x.

Battersby, T. R. *et al.* (1999) 'Quantitative analysis of receptors for adenosine nucleotides obtained via in vitro selection from a library incorporating a cationic nucleotide analog', *Journal of the American Chemical Society*, 121(42), pp. 9781–9789. doi: 10.1021/ja9816436.

Beatty, W. L. *et al.* (2000) 'Trafficking and Release of Mycobacterial Lipids from Infected

Macrophages', *Traffic*, 1(3), pp. 235–247. doi: 10.1034/j.1600-0854.2000.010306.x.

Berenguer, J. *et al.* (1992) 'Tuberculous Meningitis in Patients Infected with the Human Immunodeficiency Virus', *New England Journal of Medicine*, 326(10), pp. 668–672. doi: 10.1056/NEJM199203053261004.

Berezhnoy, A. *et al.* (2012) 'Isolation and Optimization of Murine IL-10 Receptor Blocking Oligonucleotide Aptamers Using High-throughput Sequencing', *Molecular Therapy*. Nature Publishing Group, 20(6), pp. 1242–1250. doi: 10.1038/mt.2012.18.

Berry, M. P. R. *et al.* (2010) 'An interferon-inducible neutrophil-driven blood transcriptional signature in human tuberculosis', *Nature*. Nature Publishing Group, 466(7309), pp. 973–977. doi: 10.1038/nature09247.

Berthet, F.-X. *et al.* (1998) 'A Mycobacterium tuberculosis operon encoding ESAT=6 and a novel low-molecular-mass culture filtrate protein (CFP-10)', *Microbiology*, 144(11), pp. 3195–3203. doi: 10.1099/00221287-144-11-3195.

Betat, H. *et al.* (2003) 'Aptamers that recognize the lipid moiety of the antibiotic moenomycin A.', *Biological Chemistry*, 384(10–11), pp. 1497–500. doi: 10.1515/BC.2003.165.

Blakemore, R. *et al.* (2010) 'Evaluation of the analytical performance of the Xpert MTB/RIF assay', *Journal of Clinical Microbiology*, 48(7), pp. 2495–2501. doi: 10.1128/JCM.00128-10.

Bloom, C. I. *et al.* (2013) 'Transcriptional Blood Signatures Distinguish Pulmonary Tuberculosis, Pulmonary Sarcoidosis, Pneumonias and Lung Cancers', *PLoS ONE*. Edited by J. Rengarajan. Public Library of Science, 8(8), p. e70630. doi: 10.1371/journal.pone.0070630.

Boehme, C. *et al.* (2005) 'Detection of mycobacterial lipoarabinomannan with an antigen-capture ELISA in unprocessed urine of Tanzanian patients with suspected tuberculosis.', *Transactions of the Royal Society of Tropical Medicine and Hygiene*, 99(12), pp. 893–900. doi: 10.1016/j.trstmh.2005.04.014.

Boehme, C. C. *et al.* (2011) 'Feasibility, diagnostic accuracy, and effectiveness of decentralised use of the Xpert MTB/RIF test for diagnosis of tuberculosis and multidrug resistance: a multicentre implementation study.', *Lancet*, 377(9776), pp. 1495–1505. doi: 10.1016/S0140-6736(11)60438-8.

Boese, B. J. and Breaker, R. R. (2007) 'In vitro selection and characterization of cellulose-binding DNA aptamers.', *Nucleic Acids Research*, 35(19), pp. 6378–6388. doi: 10.1093/nar/gkm708.

Boiziau, C. and Toulmé, J. J. (2001) 'A method to select chemically modified aptamers directly.',

Antisense and Nucleic Acid Drug Development, 11(6), pp. 379–385. doi: 10.1089/108729001753411344.

Bruins, M. *et al.* (2013) 'Diagnosis of active tuberculosis by e-nose analysis of exhaled air', *Tuberculosis*. Elsevier Ltd, 93(2), pp. 232–238. doi: 10.1016/j.tube.2012.10.002.

Bruno, J. G. *et al.* (2009) 'Plastic-adherent DNA aptamer-magnetic bead and quantum dot sandwich assay for Campylobacter detection.', *Journal of fluorescence*. Springer Netherlands, 19(3), pp. 427–435. doi: 10.1007/s10895-008-0429-8.

Butler, W. R. and Guthertz, L. S. (2001) 'Mycolic Acid Analysis by High-Performance Liquid Chromatography for Identification of Mycobacterium Species', *Clinical Microbiology Reviews*, 14(4), pp. 704–726. doi: 10.1128/CMR.14.4.704-726.2001.

Cambier, C. J., Falkow, S. and Ramakrishnan, L. (2014) 'Host evasion and exploitation schemes of Mycobacterium tuberculosis', *Cell*. Elsevier Inc., 159(7), pp. 1497–1509. doi: 10.1016/j.cell.2014.11.024.

Cegielski, J. P. and McMurray, D. N. (2004) 'The relationship between malnutrition and tuberculosis: Evidence from studies in humans and experimental animals', *International Journal of Tuberculosis and Lung Disease*. International Union Against Tuberculosis and Lung Disease, 8(3), pp. 286–298.

Chan, C. E. *et al.* (2015) 'The diagnostic targeting of a carbohydrate virulence factor from M.Tuberculosis.', *Scientific reports*. Nature Publishing Group, 5, p. 10281. doi: 10.1038/srep10281.

Chan, E. D. *et al.* (2000) 'Diagnosis of tuberculosis by a visually detectable immunoassay for lipoarabinomannan.', *American journal of respiratory and critical care medicine*, 161(5), pp. 1713–1719.

Chan, J. *et al.* (1991) 'Lipoarabinomannan, a possible virulence factor involved in persistence of Mycobacterium tuberculosis within macrophages.', *Infection and Immunity*, 59(5), pp. 1755–1761.

Chanteau, S. *et al.* (2000) '45 / 47 kilodalton (APA) antigen capture and antibody detection assays for the diagnosis of tuberculosis', *International Journal*, 4(4), pp. 377–383.

Chatterjee, D. *et al.* (1991) 'Structural features of the arabinan component of the lipoarabinomannan of Mycobacterium tuberculosis', *Journal of Biological Chemistry*, 266(15), pp. 9652–9660.

Chatterjee, D. *et al.* (1992) 'Lipoarabinomannan. Multiglycosylated form of the mycobacterial mannosylphosphatidylinositols', *Journal of Biological Chemistry*, 267(9), pp. 6228–6233. doi: 10.1017/CBO9781107415324.004.

Chatterjee, D. (1997) 'The mycobacterial cell wall: structure, biosynthesis and sites of drug action.', *Current Opinion in Chemical Biology*, 1(4), pp. 579–588.

Chen, F. *et al.* (2007) 'Aptamer from whole-bacterium SELEX as new therapeutic reagent against virulent Mycobacterium tuberculosis', *Biochemical and Biophysical Research Communications*, 357(3), pp. 743–748. doi: 10.1016/j.bbrc.2007.04.007.

Cheon, S. A. *et al.* (2016) 'Recent tuberculosis diagnosis toward the end TB strategy', *Journal of Microbiological Methods*, 123, pp. 51–61. doi: 10.1016/j.mimet.2016.02.007.

Cheung, Y.-W. *et al.* (2013) 'Structural basis for discriminatory recognition of Plasmodium lactate dehydrogenase by a DNA aptamer.', *Proceedings of the National Academy of Sciences of the United States of America*, 110(40), pp. 15967–72. doi: 10.1073/pnas.1309538110.

Cho, M. *et al.* (2010) 'Quantitative selection of DNA aptamers through microfluidic selection and high-throughput sequencing.', *Proceedings of the National Academy of Sciences of the United States of America*, 107(35), pp. 15373–8. doi: 10.1073/pnas.1009331107.

Cho, M. *et al.* (2013) 'Quantitative selection and parallel characterization of aptamers', *Proceedings of the National Academy of Sciences*, 110(46), pp. 18460–18465. doi: 10.1073/pnas.1315866110.

Choi, J. S. *et al.* (2011) 'Screening and characterization of high-affinity ssDNA aptamers against anthrax protective antigen.', *Journal of biomolecular screening*, 16(2), pp. 266–271. doi: 10.1177/1087057110391787.

Choudhry, V. *et al.* (2002) 'Detection of Mycobacterium tuberculosis Antigens in Urinary Proteins of Tuberculosis Patients', *European Journal of Clinical Microbiology {&} Infectious Diseases*, 21(1), pp. 1–5. doi: 10.1007/s10096-001-0651-7.

Citartan, M. *et al.* (2012) 'Assays for aptamer-based platforms', *Biosensors & Bioelectronics*, 34(1), pp. 1–11. doi: 10.1016/j.bios.2012.01.002.

Colangeli, R. *et al.* (2000) 'MTSA-10, the product of the Rv3874 gene of Mycobacterium tuberculosis, elicits tuberculosis-specific, delayed-type hypersensitivity in guinea pigs.', *Infection and immunity*, 68(2), pp. 990–993.

Cole, S. T. T. *et al.* (1998) 'Deciphering the biology of Mycobacterium tuberculosis from the

complete genome sequence', *Nature*. Nature Publishing Group, 396(6685), pp. 537–544. doi: 10.1038/31159.

Colebunders, R. and Bastian, I. (2000) 'A review of the diagnosis and treatment of smear-negative pulmonary tuberculosis.', *The international journal of tuberculosis and lung disease*, 4(2), pp. 97–107.

Comas, I. *et al.* (2013) 'Out-of-Africa migration and Neolithic coexpansion of Mycobacterium tuberculosis with modern humans', *Nature Genetics*. Nature Publishing Group, a division of Macmillan Publishers Limited. All Rights Reserved., 45(10), pp. 1176–82. doi: 10.1038/ng.2744.

Cooper, M. a (2004) 'Advances in membrane receptor screening and analysis', *Journal of Molecular Recognition*, 17(4), pp. 286–315. doi: 10.1002/jmr.675.

Corbett, E. L. *et al.* (1999) 'Risk factors for pulmonary mycobacterial disease in South African gold miners. A case-control study.', *American journal of respiratory and critical care medicine*, 159(1), pp. 94–99.

Corbett, E. L. *et al.* (2003) 'The Growing Burden of Tuberculosis: Global Trends and Interactions with HIV Epidemic', *Archives of Internal Medicine*, 163, pp. 1009–1021.

Cowperthwaite, M. C. and Ellington, A. D. (2008) 'Bioinformatic Analysis of the Contribution of Primer Sequences to Aptamer Structures', *Journal of Molecular Evolution*. Springer-Verlag, 67(1), pp. 95–102. doi: 10.1007/s00239-008-9130-4.

Cox, E. and Laessig, K. (2014) 'FDA Approval of Bedaquiline — The Benefit–Risk Balance for Drug-Resistant Tuberculosis', *New England Journal of Medicine*, 371(8), pp. 689–691. doi: 10.1056/NEJMp1314385.

Cox, J. *et al.* (2011) 'Andromeda: A Peptide Search Engine Integrated into the MaxQuant Environment', *Journal of Proteome Research*. American Chemical Society, 10(4), pp. 1794–1805. doi: 10.1021/pr101065j.

Cox, J. A. *et al.* (2015) 'Is Urinary Lipoarabinomannan the Result of Renal Tuberculosis? Assessment of the Renal Histology in an Autopsy Cohort of Ugandan HIV-Infected Adults', *PLoS ONE*. Edited by J. M. Sands. Public Library of Science, 10(4), p. e0123323. doi: 10.1371/journal.pone.0123323.

Cox, J. and Mann, M. (2008) 'MaxQuant enables high peptide identification rates, individualized p.p.b.-range mass accuracies and proteome-wide protein quantification', *Nature Biotechnology*.

Nature Publishing Group, 26(12), pp. 1367–1372. doi: 10.1038/nbt.1511.

Crowther, J. R. (2009) 'Basic Systems of ELISA', in *The ELISA Guidebook*. Totowa, NJ: Humana Press Inc., pp. 9–42. doi: 10.1007/978-1-60327-254-4_2.

Daley, C. L. *et al.* (1992) 'An Outbreak of Tuberculosis with Accelerated Progression among Persons Infected with the Human Immunodeficiency Virus', *New England Journal of Medicine*, 326(4), pp. 231–235. doi: 10.1056/NEJM199201233260404.

Daley, P. *et al.* (2009) 'Blinded evaluation of commercial urinary lipoarabinomannan for active tuberculosis: a pilot study', *International Journal of Tuberculosis and Lung Disease*, 13(8), pp. 989–995.

Darmostuk, M. *et al.* (2015) 'Current approaches in SELEX: An update to aptamer selection technology', *Biotechnology Advances*, 33(6), pp. 1141–1161. doi: 10.1016/j.biotechadv.2015.02.008.

Davidow, A. *et al.* (2005) 'Antibody Profiles Characteristic of Mycobacterium tuberculosis Infection State', *Infection and Immunity*, 73(10), pp. 6846–6851. doi: 10.1128/IAI.73.10.6846-6851.2005.

Davies, D. R. *et al.* (2012) 'Unique motifs and hydrophobic interactions shape the binding of modified DNA ligands to protein targets.', *Proceedings of the National Academy of Sciences of the United States of America*. National Academy of Sciences, 109(49), pp. 19971–6. doi: 10.1073/pnas.1213933109.

Davis, J. H. and Szostak, J. W. (2002) 'Isolation of high-affinity GTP aptamers from partially structured RNA libraries.', *Proceedings of the National Academy of Sciences of the United States of America*, 99(18), pp. 11616–11621. doi: 10.1073/pnas.182095699.

Demissie, A. *et al.* (2006) 'Recognition of stage-specific mycobacterial antigens differentiates between acute and latent infections with Mycobacterium tuberculosis.', *Clinical and Vaccine Immunology*, 13(2), pp. 179–186. doi: 10.1128/CVI.13.2.179-186.2006.

Denkinger, C. M. *et al.* (2014) 'Modeling the impact of novel diagnostic tests on pediatric and extrapulmonary tuberculosis', *BMC Infectious Diseases*, 14(1), p. 477. doi: 10.1186/1471-2334-14-477.

Denkinger, C. M. *et al.* (2015) 'Defining the needs for next generation assays for tuberculosis', *Journal of Infectious Diseases*, 211(Suppl 2), pp. S29–S38. doi: 10.1093/infdis/jiu821.

Derrick, S. C. and Morris, S. L. (2007) 'The ESAT6 protein of Mycobacterium tuberculosis

induces apoptosis of macrophages by activating caspase expression', *Cellular Microbiology*, 9(6), pp. 1547–1555. doi: 10.1111/j.1462-5822.2007.00892.x.

Detjen, A. K. *et al.* (2015) 'Xpert MTB/RIF assay for the diagnosis of pulmonary tuberculosis in children: a systematic review and meta-analysis', *The Lancet Respiratory Medicine*. Elsevier Ltd, 3(6), pp. 451–461. doi: 10.1016/S2213-2600(15)00095-8.

Dheda, K. *et al.* (2010) 'Clinical Utility of a Commercial LAM-ELISA Assay for TB Diagnosis in HIV-Infected Patients Using Urine and Sputum Samples', *PLoS ONE*, 5(3), pp. 1–8. doi: 10.1371/journal.pone.0009848.

Diacon, A. H. *et al.* (2009) *The Diarylquinoline TMC207 for Multidrug-Resistant Tuberculosis.*, *The New England Journal of Medicine*. doi: 10.1056/NEJMoa0808427.

Diacon, A. H. *et al.* (2012) 'Randomized pilot trial of eight weeks of bedaquiline (TMC207) treatment for multidrug-resistant tuberculosis: Long-term outcome, tolerability, and effect on emergence of drug resistance', *Antimicrobial Agents and Chemotherapy*, 56(6), pp. 3271–3276. doi: 10.1128/AAC.06126-11.

Diafa, S. and Hollenstein, M. (2015) 'Generation of Aptamers with an Expanded Chemical Repertoire', *Molecules*. Multidisciplinary Digital Publishing Institute, 20(9), pp. 16643–16671. doi: 10.3390/molecules200916643.

Digiuseppe Champion, P. A. and Cox, J. S. (2007) 'Protein secretion systems in Mycobacteria', *Cellular Microbiology*, 9(6), pp. 1376–1384. doi: 10.1111/j.1462-5822.2007.00943.x.

Dillon, D. C. *et al.* (2000) 'Molecular and immunological characterization of Mycobacterium tuberculosis CFP-10, an immunodiagnostic antigen missing in Mycobacterium bovis BCG.', *Journal of Clinical Microbiology*, 38(9), pp. 3285–3290.

DNA Software (2009) *DNA Software, Inc. Awarded NIH Funding to Develop Pioneering Nucleic Acid-Based Technologies*.

Doherty, T. M. *et al.* (2002) 'Immune Responses to the Mycobacterium tuberculosis-Specific Antigen ESAT-6 Signal Subclinical Infection among Contacts of Tuberculosis Patients', *Journal of Clinical Microbiology*, 40(2), pp. 704–706. doi: 10.1128/JCM.40.2.704-706.2002.

Donald, P. R. and Diacon, A. H. (2008) 'The early bactericidal activity of anti-tuberculosis drugs: a literature review', *Tuberculosis*, 88(SUPPL. 1), pp. S75--83. doi: 10.1016/S1472-9792(08)70038-6.

Driver, E. R. *et al.* (2012) 'Evaluation of a Mouse Model of Necrotic Granuloma Formation Using

C3HeB/FeJ Mice for Testing of Drugs against Mycobacterium tuberculosis', *Antimicrobial Agents and Chemotherapy*, 56(6), pp. 3181–3195. doi: 10.1128/AAC.00217-12.

Drolet, D. W., Moon-McDermott, L. and Romig, T. S. (1996) 'An enzyme-linked oligonucleotide assay.', *Nature biotechnology*, 14(8), pp. 1021–5. doi: 10.1038/nbt0896-1021.

Duan, N. *et al.* (2013) 'In vitro selection of a DNA aptamer targeted against Shigella dysenteriae', *Journal of Microbiological Methods*, 94(3), pp. 170–4. doi: 10.1016/j.mimet.2013.06.016.

Eaton, B. E., Gold, L. and Zichi, D. A. (1995) 'Let's get specific: the relationship between specificity and affinity', *Chemistry and Biology*, 2(10), pp. 633–638. doi: 10.1016/1074-5521(95)90023-3.

Edwards, P. R. *et al.* (1995) 'Kinetics of Protein-Protein Interactions at the Surface of an Optical Biosensor', *Analytical Biochemistry*, 231(1), pp. 210–217. doi: 10.1006/abio.1995.1522.

Edwards, P. R., Lowe, P. a and Leatherbarrow, R. J. (1997) 'Ligand loading at the surface of an optical biosensor and its effect upon the kinetics of protein–protein interactions', *Journal of Molecular Recognition*, 10(3), pp. 128–134. doi: 10.1002/(SICI)1099-1352(199705/06)10:3<128::AID-JMR357>3.0.CO;2-Y.

Ekins, R. P. (1989) 'Multi-analyte immunoassay', *Journal of Pharmaceutical and Biomedical Analysis*. Sollentuna, Sweden: Pergamon Press, 7(2), pp. 155–168. doi: 10.1016/0731-7085(89)80079-2.

Ekins, R. P. and Chu, F. W. (1991) 'Immunoassay-Microanalytical " Compact Disk " of the Future', *Clinical Chemistry*, 37(11), pp. 1955–1967.

Elhay, M. J., Oettinger, T. and Andersen, P. (1998) 'Delayed-type hypersensitivity responses to ESAT-6 and MPT64 from Mycobacterium tuberculosis in the guinea pig', *Infection and Immunity*, 66(7), pp. 3454–6.

Elias, J. E. and Gygi, S. P. (2007) 'Target-decoy search strategy for increased confidence in large-scale protein identifications by mass spectrometry.', *Nature methods*. Nature Publishing Group, 4(3), pp. 207–14. doi: 10.1038/nmeth1019.

Ellington, A. D. and Szostak, J. W. (1990) 'In vitro selection of RNA molecules that bind specific ligands', *Nature*, 346, pp. 818–822. doi: 10.1038/346818a0.

Ellington, A. D. and Szostak, J. W. (1992) 'Selection in vitro of single-stranded DNA molecules that fold into specific ligand-binding structures.', *Nature*. Nature Publishing Group, 355(6363), pp. 850–2. doi: 10.1038/355850a0.

Elliott, A. M. *et al.* (1993) 'The impact of human immunodeficiency virus on presentation and diagnosis of tuberculosis in a cohort study in Zambia.', *The Journal of tropical medicine and hygiene*, 96(1), pp. 1–11.

Ellner, J. J. (1997) 'Regulation of the human immune response during tuberculosis', *Journal of Laboratory and Clinical Medicine*, 130(5), pp. 469–475. doi: 10.1016/S0022-2143(97)90123-2.

Eng, J. K., McCormack, A. L. and Yates, J. R. (1994) 'An approach to correlate tandem mass spectral data of peptides with amino acid sequences in a protein database', *Journal of the American Society for Mass Spectrometry*, 5(11), pp. 976–989. doi: 10.1016/1044-0305(94)80016-2.

Engvall, E. and Perlmann, P. (1971) 'Enzyme-linked immunosorbent assay (ELISA) quantitative assay of immunoglobulin G', *Immunochemistry*, 8(9), pp. 871–874. doi: 10.1016/0019-2791(71)90454-X.

Esteban, B. *et al.* (2013) 'Determinants of the Detection Limit and Speci fi city of Surface-Based Biosensors', *Analytical chemistry*, i, pp. 1–5. doi: 10.1021/ac4012123.

Fan, M. *et al.* (2008) 'Aptamer selection express: A novel method for rapid single-step selection and sensing of aptamers', *Journal of Biomolecular Techniques*, 19(5), pp. 311–321.

Feng, T.-T. *et al.* (2011) 'Novel monoclonal antibodies to ESAT-6 and CFP-10 antigens for ELISA-based diagnosis of pleural tuberculosis', *The International Journal of Tuberculosis and Lung Disease*, 15(6), pp. 804–810. doi: 10.5588/ijtld.10.0393.

Feng, X. *et al.* (2014) 'IgG, IgM and IgA antibodies against the novel polyprotein in active tuberculosis.', *BMC Infectious Diseases*. BioMed Central, 14(1), pp. 1–19.

Fischer, N. O., Tok, J. B. H. and Tarasow, T. M. (2008) 'Massively parallel interrogation of aptamer sequence, structure and function', *PLoS ONE*, 3(7), pp. 1–9. doi: 10.1371/journal.pone.0002720.

Flores, L. L. *et al.* (2011) 'Systematic Review and Meta-Analysis of Antigen Detection Tests for the Diagnosis of Tuberculosis', *Clinical and Vaccine Immunology*, 18(10), pp. 1616–1627. doi: 10.1128/CVI.05205-11.

Foundation for Innovative New Diagnostics (FIND) (2017) *Report for WHO: A multicentre non-inferiority diagnostic accuracy study of the Ultra assay compared to Xpert MTB/RIF assay. Geneva: Foundation for Innovative New Diagnostics (FIND); 2017.*

Fox, H. H. (1961) 'Synthetic Tuberculostats. 111. Isonicotinaldehyde Thiosemicarbazone and Some Related Compounds', *Reseasch Labratories of Hoffmann-la Roche INC.*, (242), pp. 555–562.

Friguet, B. *et al.* (1985) 'Measurements of the true affinity constant in solution of antigen-antibody complexes by enzyme-linked immunosorbent assay', *Journal of Immunological Methods*, 77(2), pp. 305–319. doi: 10.1016/0022-1759(85)90044-4.

Friguet, B. *et al.* (1995) 'Under proper experimental conditions the solid-phase antigen does not disrupt the liquid phase equilibrium when measuring dissociation constants by competition ELISA', *J Immunol Methods*, 182(1), pp. 145–150. doi: 002217599500065I [pii].

Fukusaki, E. *et al.* (2000) 'DNA aptamers that bind to chitin.', *Bioorganic & medicinal chemistry letters*, 10(5), pp. 423–5.

Gagneux, S. *et al.* (2006) 'Variable host-pathogen compatibility in Mycobacterium tuberculosis', *Proceedings of the National Academy of Sciences*. National Academy of Sciences, 103(8), pp. 2869–2873. doi: 10.1073/pnas.0511240103.

Gallagher, S. (2004) 'Immunoblotting and Immunodetection', in *Current Protocols in Molecular Biology*. Hoboken, NJ, USA: John Wiley & Sons, Inc., p. 8.10.1-8.10.36.

Gallien, S., Duriez, E. and Domon, B. (2011) 'Selected reaction monitoring applied to proteomics', *Journal of Mass Spectrometry*, 46(January), pp. 298–312. doi: 10.1002/jms.1895.

Gandham, S. H. A. *et al.* (2014) 'Thioaptamers targeting dengue virus type-2 envelope protein domain III', *Biochemical and Biophysical Research Communications*. Elsevier Inc., 453(3), pp. 309–315. doi: 10.1016/j.bbrc.2014.09.053.

Ganguly, N., Siddiqui, I. and Sharma, P. (2008) 'Role of M. tuberculosis RD-1 region encoded secretory proteins in protective response and virulence', *Tuberculosis*, 88(6), pp. 510–517. doi: 10.1016/j.tube.2008.05.002.

Getahun, H. *et al.* (2007) 'Diagnosis of smear-negative pulmonary tuberculosis in people with HIV infection or AIDS in resource-constrained settings: informing urgent policy changes', *Lancet*, 369(9578), pp. 2042–2049. doi: 10.1016/S0140-6736(07)60284-0.

Gey Van Pittius, N. C. *et al.* (2001) 'The ESAT-6 gene cluster of Mycobacterium tuberculosis and other high G+C Gram-positive bacteria.', *Genome biology*, 2(10), p. RESEARCH0044.

Gibson, K. J. C. *et al.* (2004) 'Tsukamurella paurometabola lipoglycan, a new lipoarabinomannan variant with pro-inflammatory activity.', *The Journal of biological chemistry*, 279(22), pp. 22973–22982. doi: 10.1074/jbc.M310906200.

Gilleron, M. *et al.* (1997) 'Mycobacterium smegmatis Phosphoinositols-Glyceroarabinomannans', *Journal of Biological Chemistry*, 272(1), pp. 117–124. doi:

10.1074/jbc.272.1.117.

Gilleron, M. *et al.* (2000) 'Mycobacterium tuberculosis H37Rv parietal and cellular lipoarabinomannans. Characterization of the acyl- and glyco-forms.', *The Journal of Biological Chemistry*, 275(1), pp. 677–684.

Gold, L. *et al.* (2010) 'Aptamer-Based Multiplexed Proteomic Technology for Biomarker Discovery.', *PLoS ONE*. Public Library of Science, 5(12), pp. 1–17. doi: 10.1371/journal.pone.0015004.

Goldberg, M. E. and Djavadi-Ohaniance, L. (1993) 'Methods for measurement of antibody/antigen affinity based on ELISA and RIA', *Current Opinion in Immunology*, 5(2), pp. 278–281. doi: 10.1016/0952-7915(93)90018-N.

Gong, Q. *et al.* (2012) 'Selection strategy to generate aptamer pairs that bind to distinct sites on protein targets', *Analytical Chemistry*. NIH Public Access, 84(12), pp. 5365–5371. doi: 10.1021/ac300873p.

Gonzalez, J. M. *et al.* (2014) 'Development of a POC Test for TB Based on Multiple Immunodominant Epitopes of M. tuberculosis Specific Cell-Wall Proteins.', *PLoS ONE*. Public Library of Science, 9(9), pp. 1–10. doi: 10.1371/journal.pone.0106279.

Gorenstein, D. G. *et al.* (2014) 'Methods of x-aptamer generation and compositions thereof (patent)'.

Green, R. *et al.* (1991) 'In vitro genetic analysis: Selection and amplification of rare functional nucleic acids', *Methods*, 2(1), pp. 75–86. doi: 10.1016/S1046-2023(05)80127-6.

Grimme, S. (2008) 'Do special noncovalent pi-pi stacking interactions really exist?', *Angewandte Chemie (International ed. in English)*, 47(18), pp. 3430–4. doi: 10.1002/anie.200705157.

Guerardel, Y. *et al.* (2002) 'Structural study of lipomannan and lipoarabinomannan from Mycobacterium chelonae. Presence of unusual components with alpha 1,3-mannopyranose side chains.', *The Journal of Biological Chemistry*, 277(34), pp. 30635–30648. doi: 10.1074/jbc.M204398200.

Guinn, K. M. *et al.* (2004) 'Individual RD1-region genes are required for export of ESAT-6/CFP-10 and for virulence of Mycobacterium tuberculosis.', *Molecular Microbiology*, 51(2), pp. 359–70. doi: 10.1046/j.1365-2958.2003.03844.x.

Gülbakan, B. (2015) 'Oligonucleotide aptamers: emerging affinity probes for bioanalytical mass spectrometry and biomarker discovery', *Anal. Methods*, 7(18), pp. 7416–7430. doi:

10.1039/C5AY00650C.

Guo, S. *et al.* (2012) 'The CFP10/ESAT6 complex of Mycobacterium tuberculosis may function as a regulator of macrophage cell death at different stages of tuberculosis infection', *Medical Hypotheses*, 78(3), pp. 389–392. doi: 10.1016/j.mehy.2011.11.022.

Haas, C. T. *et al.* (2016) 'Diagnostic "omics" for active tuberculosis', *BMC Medicine*. BMC Medicine, 14(1), p. 37. doi: 10.1186/s12916-016-0583-9.

Hamasur, B. *et al.* (2001) 'Rapid diagnosis of tuberculosis by detection of mycobacterial lipoarabinomannan in urine', *Journal of microbiological methods*, 45, pp. 41–52. doi: 10.1016/S0167-7012(01)00239-1.

Hamasur, B. *et al.* (2015) 'A sensitive urinary lipoarabinomannan test for tuberculosis.', *PLoS ONE*. Public Library of Science, 10(4), p. e0123457. doi: 10.1371/journal.pone.0123457.

Harboe, M. *et al.* (1996) 'Evidence for occurrence of the ESAT-6 protein in Mycobacterium tuberculosis and virulent Mycobacterium bovis and for its absence in Mycobacterium bovis BCG.', *Infection and immunity*, 64(1), pp. 16–22.

Harpole, M., Davis, J. and Espina, V. (2016) 'Current state of the art for enhancing urine biomarker discovery', *Expert Review of Proteomics*, 13(6), pp. 609–626. doi: 10.1080/14789450.2016.1190651.

Harroun, S. G. (2014) *Development of an electrochemical surface-enhanced Raman spectroscopy DNA aptamer biosensor for rapid detection of protein biomarkers of disease*. Halifax, N.S. : Saint Mary's University.

He, W. *et al.* (2012) 'X-aptamers: A bead-based selection method for random incorporation of druglike moieties onto next-generation aptamers for enhanced binding', *Biochemistry*, 51(42), pp. 8321–8323. doi: 10.1021/bi300471d.

Helb, D. *et al.* (2010) 'Rapid detection of Mycobacterium tuberculosis and rifampin resistance by use of on-demand, near-patient technology.', *Journal of Clinical Microbiology*, 48(1), pp. 229–237.

Hermann, T. and Patel, D. J. (2000) 'Adaptive Recognition by Nucleic Acid Aptamers', *Science*, 287(5454), pp. 820–825. doi: 10.1126/science.287.5454.820.

Hianik, T. *et al.* (2007) 'Influence of ionic strength, pH and aptamer configuration for binding affinity to thrombin', *Bioelectrochemistry*, 70(1), pp. 127–133. doi: 10.1016/j.bioelechem.2006.03.012.

Hiatt, L. A. and Cliffel, D. E. (2012) 'Real-time Recognition of Mycobacterium tuberculosis and Lipoarabinomannan using the Quartz Crystal Microbalance.', *Sensors and actuators. B, Chemical*, 174, pp. 245–252. doi: 10.1016/j.snb.2012.06.095.

Hodnik, V. *et al.* (2010) *Surface Plasmon Resonance*, *Methods in Molecular Biology*. Edited by N. J. Mol and M. J. E. Fischer. Totowa, NJ: Humana Press (Methods in Molecular Biology). doi: 10.1007/978-1-60761-670-2.

Hoffmann, E. de. *et al.* (2007) *Mass spectrometry: Principles and Applications*. 3rd ed. Chichester, UK, UK: J. Wiley {&} Sons.

Homola, J. (2003) 'Present and future of surface plasmon resonance biosensors', *Analytical and Bioanalytical Chemistry*, 377(3), pp. 528–539. doi: 10.1007/s00216-003-2101-0.

Hong, K. L. and Sooter, L. J. (2015) 'Single-Stranded DNA Aptamers against Pathogens and Toxins: Identification and Biosensing Applications', *BioMed Research International*. Hindawi Publishing Corporation, 2015, pp. 1–31. doi: 10.1155/2015/419318.

Hong, S. C. *et al.* (2011) 'Clinical immunosensing of tuberculosis CFP-10 in patient urine by surface plasmon resonance spectroscopy', *Sensors and Actuators, B: Chemical*. Elsevier B.V., 160(1), pp. 1434–1438. doi: 10.1016/j.snb.2011.10.006.

Horvati, K. *et al.* (2016) 'Population tailored modification of tuberculosis specific interferon-gamma release assay', *Journal of Infection*, 72(2), pp. 179–188. doi: 10.1016/j.jinf.2015.10.012.

Hsu, T. *et al.* (2003) 'The primary mechanism of attenuation of bacillus Calmette-Guerin is a loss of secreted lytic function required for invasion of lung interstitial tissue.', *Proceedings of the National Academy of Sciences of the United States of America*, 100(21), pp. 12420–12425. doi: 10.1073/pnas.1635213100.

Huh, Y. S. and Erickson, D. (2010) 'Aptamer based surface enhanced Raman scattering detection of vasopressin using multilayer nanotube arrays.', *Biosensors {&} Bioelectronics*, 25(5), pp. 1240–1243. doi: 10.1016/j.bios.2009.09.040.

Hulsen, T., de Vlieg, J. and Alkema, W. (2008) 'BioVenn - a web application for the comparison and visualization of biological lists using area-proportional Venn diagrams.', *BMC genomics*. BioMed Central, 9(1), p. 488. doi: 10.1186/1471-2164-9-488.

Hunter, S. W. *et al.* (1990) 'Evidence for the Presence of a Phosphatidylinositol Anchor on the Lipoarabinomannan and Lipomannan of Mycobacterium tuberculosis', *The Journal of Biological Chemistry*, 265(16), pp. 9272–9279.

Hunter, S. W., Gaylord, H. and Brennan, P. J. (1986) 'Structure and antigenicity of the phosphorylated lipopolysaccharide antigens from the leprosy and tubercle bacilli', *Journal of Biological Chemistry*, 261(26), pp. 12345–12351.

Janssen, K. *et al.* (2012) 'Multiplexed protein detection using an affinity aptamer amplification assay.', *Analytical & Bioanalytical Chemistry*. Springer Science & Business Media B.V., 404(6/7), pp. 2073–2081.

Janssens, J.-P. *et al.* (2007) 'Quantitative scoring of an interferon- assay for differentiating active from latent tuberculosis', *European Respiratory Journal*, 30(4), pp. 722–728. doi: 10.1183/09031936.00028507.

de Jonge, M. I. *et al.* (2007) 'ESAT-6 from Mycobacterium tuberculosis Dissociates from Its Putative Chaperone CFP-10 under Acidic Conditions and Exhibits Membrane-Lysing Activity', *Journal of Bacteriology*, 189(16), pp. 6028–6034. doi: 10.1128/JB.00469-07.

Kaforou, M. *et al.* (2013) 'Detection of Tuberculosis in HIV-Infected and -Uninfected African Adults Using Whole Blood RNA Expression Signatures: A Case-Control Study', *PLoS Medicine*. Edited by A. Cattamanchi. Public Library of Science, 10(10), p. e1001538. doi: 10.1371/journal.pmed.1001538.

Kalsdorf, B. *et al.* (2009) 'HIV-1 infection impairs the bronchoalveolar T-cell response to mycobacteria.', *American journal of respiratory and critical care medicine*, 180(12), pp. 1262–1270. doi: 10.1164/rccm.200907-1011OC.

Kang, J., Lee, M. S. and Gorenstein, D. G. (2005) 'The enhancement of PCR amplification of a random sequence DNA library by DMSO and betaine: application to in vitro combinatorial selection of aptamers.', *Journal of biochemical and biophysical methods*, 64(2), pp. 147–151. doi: 10.1016/j.jbbm.2005.06.003.

Kapetanaki, S. *et al.* (2003) 'Conformational differences in Mycobacterium tuberculosis catalase-peroxidase KatG and its S315T mutant revealed by resonance raman spectroscopy', *Biochemistry*, 42(13), pp. 3835–3845. doi: 10.1021/bi026992y.

Kase, D. *et al.* (2004) 'Affinity Selection of Peptide Phage Libraries against Single-Wall Carbon Nanohorns Identifies a Peptide Aptamer with Conformational Variability', *Langmuir*, 20(20), pp. 8939–8941. doi: 10.1021/la048968m.

Kashino, S. S. *et al.* (2008) 'Identification and characterization of Mycobacterium tuberculosis antigens in urine of patients with active pulmonary tuberculosis: an innovative and alternative

approach of antigen discovery of useful microbial molecules.', *Clinical and experimental immunology*, 153(1), pp. 56–62. doi: 10.1111/j.1365-2249.2008.03672.x.

Kashyap, R. S. *et al.* (2009) 'Diagnostic Value of Early Secreted Antigenic Target-6 for the Diagnosis of Tuberculous Meningitis Patients', *Infection*, 37(6), pp. 508–513. doi: 10.1007/s15010-009-8261-x.

Kato, Y. *et al.* (2005) 'New NTP analogs: the synthesis of 4'-thioUTP and 4'-thioCTP and their utility for SELEX.', *Nucleic Acids Research*, 33(9), pp. 2942–51. doi: 10.1093/nar/gki578.

Kaur, H. and Yung, L. Y. L. (2012) 'Probing high affinity sequences of DNA aptamer against VEGF 165', *PLoS ONE*, 7(2), pp. 19–26. doi: 10.1371/journal.pone.0031196.

Keefe, A. D., Pai, S. and Ellington, A. (2010) 'Aptamers as therapeutics.', *Nature reviews. Drug discovery*. Nature Publishing Group, 9(7), pp. 537–550. doi: 10.1038/nrd3249.

Keeler, E. *et al.* (2006) 'Reducing the global burden of tuberculosis: the contribution of improved diagnostics.', *Nature*, 444 Suppl, pp. 49–57. doi: 10.1038/nature05446.

Kemeny, D. M. *et al.* (1985) 'Increased sensitivity and specificity of a sandwich ELISA for measurement of IgE antibodies.', *Journal of immunological methods*, 78(2), pp. 217–26.

Khatkhatay, M. I. and Desai, M. (1999) 'A comparison of performances of four enzymes used in ELISA with special reference to beta-lactamase.', *Journal of immunoassay*. Taylor & Francis Group, 20(3), pp. 151–83. doi: 10.1080/01971529909349349.

Khoo, K. *et al.* (1995) 'Inositol Phosphate Capping of the Nonreducing Termini of Lipoarabinomannan from Rapidly Growing Strains of Mycobacterium', *The Journal of biological chemistry*, 270(21), pp. 12380–12389.

Khoo, K. H., Tang, J. B. and Chatterjee, D. (2001) 'Variation in mannose-capped terminal arabinan motifs of lipoarabinomannans from clinical isolates of Mycobacterium tuberculosis and Mycobacterium avium complex.', *The Journal of biological chemistry*, 276(6), pp. 3863–3871. doi: 10.1074/jbc.M004010200.

Kik, S. V. *et al.* (2015) 'Potential Market for Novel Tuberculosis Diagnostics: Worth the Investment?', *Journal of Infectious Diseases*, 211(suppl 2), pp. S58--S66. doi: 10.1093/infdis/jiu817.

Kim, J. *et al.* (2013) 'Rapid monitoring of CFP-10 during culture of Mycobacterium tuberculosis by using a magnetophoretic immunoassay', *Sensors and Actuators B: Chemical*, 177, pp. 327–333. doi: 10.1016/j.snb.2012.11.011.

Kim, J. *et al.* (2015) 'Clinical immunosensing of tuberculosis CFP-10 antigen in urine using interferometric optical fiber array', *Sensors and Actuators B: Chemical*, 216, pp. 184–191. doi: 10.1016/j.snb.2015.04.046.

Kimoto, M. *et al.* (2013) 'Generation of high-affinity DNA aptamers using an expanded genetic alphabet.', *Nature Biotechnology*. Nature Publishing Group, 31(5), pp. 453–457.

Kirby, R. *et al.* (2004) 'Aptamer-Based Sensor Arrays for the Detection and Quantitation of Proteins', *Analytical Chemistry*, 76(14), pp. 4066–4075. doi: 10.1021/ac049858n.

Klein, J. *et al.* (2013) 'Proteasix: A tool for automated and large-scale prediction of proteases involved in naturally occurring peptide generation', *Proteomics*, 13(7), pp. 1077–1082. doi: 10.1002/pmic.201200493.

Knutson, K. L. *et al.* (1998) 'Lipoarabinomannan of Mycobacterium tuberculosis Promotes Protein Tyrosine Dephosphorylation and Inhibition of Mitogen-activated Protein Kinase in Human Mononuclear Phagocytes', *The Journal of Biological Chemistry*, 273(1), pp. 645–652.

Koch, R. (1890) 'Aetiology of Tuberculosis', p. 97.

Kolk, A. *et al.* (2010) 'Electronic-nose technology using sputum samples in diagnosis of patients with tuberculosis', *Journal of Clinical Microbiology*, 48(11), pp. 4235–4238. doi: 10.1128/JCM.00569-10.

Koul, A. *et al.* (2011) 'The challenge of new drug discovery for tuberculosis', *Nature*. Nature Publishing Group, 469(7331), pp. 483–490. doi: 10.1038/nature09657.

Kruh-Garcia, N. A. *et al.* (2014) 'Detection of Mycobacterium tuberculosis Peptides in the Exosomes of Patients with Active and Latent M. tuberculosis Infection Using MRM-MS.', *PLoS ONE*. Public Library of Science, 9(7), pp. 1–11.

Kumar, P. *et al.* (2012) 'ESAT6 differentially inhibits IFN-γ-inducible class II transactivator isoforms in both a TLR2-dependent and -independent manner', *Immunology and Cell Biology*, 90(4), pp. 411–420. doi: 10.1038/icb.2011.54.

Kuriyan, Konforti and Wemmer (2009) 'Molecular Recognition : The Thermodynamics of Binding', in *The Molecules of Life*. Garland Publishing, pp. 1–58.

Lalvani, A. *et al.* (2001) 'Enumeration of T cells specific for RD1-encoded antigens suggests a high prevalence of latent Mycobacterium tuberculosis infection in healthy urban Indians.', *The Journal of Infectious Diseases*, 183(3), pp. 469–77. doi: 10.1086/318081.

Lamont, E. A. *et al.* (2014) 'A Combined Enrichment and Aptamer Pulldown Assay for Francisella tularensis Detection in Food and Environmental Matrices', *PLoS ONE*. Edited by K. Kourentzi. Public Library of Science, 9(12), p. e114622. doi: 10.1371/journal.pone.0114622.

Langley, I. *et al.* (2014) 'Assessment of the patient, health system, and population effects of Xpert MTB/RIF and alternative diagnostics for tuberculosis in Tanzania: An integrated modelling approach', *The Lancet Global Health*. Langley et al. Open Access article distributed under the terms of CC BY-NC-SA, 2(10), pp. e581–e591. doi: 10.1016/S2214-109X(14)70291-8.

Larguinho, M. *et al.* (2015) 'DNA adduct identification using gold-aptamer nanoprobes.', *IET Nanobiotechnology*. Institution of Engineering & Technology, 9(2), pp. 95–101.

Lato, S. M. *et al.* (2002) 'Boron-containing aptamers to ATP.', *Nucleic Acids Research*, 30(6), pp. 1401–7. doi: 10.1093/nar/30.6.1401.

Lawn, S. D. *et al.* (2009) 'Urine lipoarabinomannan assay for tuberculosis screening before antiretroviral therapy diagnostic yield and association with immune reconstitution disease', *Aids*, 23(14), pp. 1875–1880. doi: 10.1097/QAD.0b013e32832e05c8.

Lawn, S. D. *et al.* (2012) 'High diagnostic yield of tuberculosis from screening urine samples from HIV-infected patients with advanced immunodeficiency using the Xpert MTB/RIF assay', *J Acquir Immune Defic Syndr*, 60(3), pp. 289–294. doi: 10.1097/QAI.0b013e318258c6af.

Lee, S.-W. *et al.* (2016) 'Gene expression profiling identifies candidate biomarkers for active and latent tuberculosis', *BMC Bioinformatics*, 17(3), pp. 27–39. doi: 10.1186/s12859-015-0848-x.

Legesse, M. *et al.* (2013) 'IgA Response to ESAT-6/ CFP-10 and Rv2031 Antigens Varies in Patients With Culture-Confirmed Pulmonary Tuberculosis, Healthy Mycobacterium tuberculosis-Infected and Non-Infected Individuals in a Tuberculosis Endemic Setting, Ethiopia.', *Scandinavian Journal of Immunology*. Wiley-Blackwell, 78(3), pp. 266–274.

Lewis, K. N. *et al.* (2003) 'Deletion of RD1 from Mycobacterium tuberculosis mimics bacille Calmette-Guérin attenuation.', *The Journal of Infectious Diseases*, 187(1), pp. 117–23. doi: 10.1086/345862.

Li, M. *et al.* (2008) 'Selecting aptamers for a glycoprotein through the incorporation of the boronic acid moiety.', *Journal of the American Chemical Society*, 130(38), pp. 12636–12638. doi: 10.1021/ja801510d.

Liss, M. *et al.* (2002) 'An Aptamer-Based Quartz Crystal Protein Biosensor', *Analytical Chemistry*.

American Chemical Society, 74(17), pp. 4488–4495. doi: 10.1021/ac011294p.

Liu, M. *et al.* (2014) 'Increased genetic diversity of the Mycobacterium tuberculosis W-Beijing genotype that predominates in eastern China', *Infection, Genetics and Evolution*. Elsevier B.V., 22, pp. 23–29. doi: 10.1016/j.meegid.2013.12.023.

Liu, Q. *et al.* (2010) 'Serum protein profiling of smear-positive and smear-negative pulmonary tuberculosis using SELDI-TOF mass spectrometry', *Lung*. Springer-Verlag, 188(1), pp. 15–23. doi: 10.1007/s00408-009-9199-6.

Liu, Y. *et al.* (2015) 'Detecting multiple cell-secreted cytokines from the same aptamer-functionalized electrode.', *Biosensors & Bioelectronics*, 64, pp. 43–50. doi: 10.1016/j.bios.2014.08.034.

Lokesh, G. L. *et al.* (2017) 'X-Aptamer selection and validation', *Methods in Molecular Biology*, 1632, pp. 151–174. doi: 10.1007/978-1-4939-7138-1_10.

Lopez, P. H. H. and Schnaar, R. L. (2006) 'Determination of glycolipid-protein interaction specificity.', *Methods in enzymology*, 417(06), pp. 205–220. doi: 10.1016/S0076-6879(06)17015-9.

Lou, X. *et al.* (2016) 'Determining Functional Aptamer-Protein Interaction by Biolayer Interferometry', *Current Protocols in Nucleic Acid Chemistry*. Hoboken, NJ, USA: John Wiley & Sons, Inc., (December), p. 7.25.1-7.25.15. doi: 10.1002/cpnc.18.

Low, S. Y., Hill, J. E. and Peccia, J. (2009) 'DNA aptamers bind specifically and selectively to (1→3)-β-d-glucans', *Biochemical and Biophysical Research Communications*, 378(4), pp. 701–705. doi: 10.1016/j.bbrc.2008.11.087.

Lu, E. *et al.* (2014) 'Aptaligner: Automated software for aligning pseudorandom DNA X-aptamers from next-generation sequencing data', *Biochemistry*. American Chemical Society, 53(22), pp. 3523–3525. doi: 10.1021/bi500443e.

Lukat-Rodgers, G. S. *et al.* (2000) 'Spectroscopic Comparison of the Heme Active Sites in WT KatG and Its S315T Mutant †', *Biochemistry*. American Chemical Society, 39(32), pp. 9984–9993. doi: 10.1021/bi0006870.

Madigan, M. T. *et al.* (2012) *Brock Biology of Microorganisms*.

Maertzdorf, J. *et al.* (2012) 'Enabling biomarkers for tuberculosis control', *International Journal of Tuberculosis and Lung Disease*, 16(9), pp. 1140–1148. doi: 10.5588/ijtld.12.0246.

Makarov, A. (2000) 'Electrostatic Axially Harmonic Orbital Trapping: A High-Performance Technique of Mass Analysis', *Analytical Chemistry*, 72(6), pp. 1156–1162. doi: 10.1021/ac991131p.

Målen, H. *et al.* (2007) 'Comprehensive analysis of exported proteins from Mycobacterium tuberculosis H37Rv', *Proteomics*, 7(10), pp. 1702–1718. doi: 10.1002/pmic.200600853.

Mandalakas, A. M. *et al.* (2008) 'High level of discordant IGRA results in HIV-infected adults and children.', *The International Journal of Tuberculosis and Lung Disease*. International Union Against Tuberculosis and Lung Disease, 12(4), pp. 417–23.

Mann, A. P. *et al.* (2010) 'Identification of thioaptamer ligand against E-selectin: potential application for inflamed vasculature targeting.', *PLoS ONE*. Public Library of Science, 5(9), pp. 1–11. doi: 10.1371/journal.pone.0013050.

Marlowe, E. M. *et al.* (2011) 'Evaluation of the cepheid xpert MTB/RIF assay for direct detection of mycobacterium tuberculosis complex in respiratory specimens', *Journal of Clinical Microbiology*, 49(4), pp. 1621–1623. doi: 10.1128/JCM.02214-10.

Martineau, P. (2010) 'Affinity Measurements by Competition ELISA', in Kontermann, R. and Dübel, S. (eds) *Antibody Engineering*. Berlin, Heidelberg: Springer Berlin Heidelberg, pp. 657–665. doi: 10.1007/978-3-642-01144-3_41.

Masud, M. M. *et al.* (2004) 'Sialyllactose-binding modified DNA aptamer bearing additional functionality by SELEX.', *Bioorganic {&} Medicinal Chemistry*, 12(5), pp. 1111–1120. doi: 10.1016/j.bmc.2003.12.009.

Mataija-Botelho, D. *et al.* (2009) 'A qualitative proteome investigation of the sediment portion of human urine: Implications in the biomarker discovery process', *Proteomics - Clinical Applications*, 3(1), pp. 95–105. doi: 10.1002/prca.200800019.

Math Works (2017) *Visualizing and Preprocessing Hyphenated Mass Spectrometry Data Sets for Metabolite and Protein/Peptide Profiling*.

Mathema, B. *et al.* (2006) 'Molecular epidemiology of tuberculosis: current insights.', *Clinical microbiology reviews*, 19(4), pp. 658–685. doi: 10.1128/CMR.00061-05.

Mathews, D. H. (2004) 'Using an RNA secondary structure partition function to determine confidence in base pairs predicted by free energy minimization', *RNA*, 10(8), pp. 1178–1190. doi: 10.1261/rna.7650904.

McDowell, D. G., Burns, N. A. and Parkes, H. C. (1998) 'Localised sequence regions possessing

high melting temperatures prevent the amplification of a DNA mimic in competitive PCR', *Nucleic Acids Research*, 26(14), pp. 3340–3347. doi: 10.1093/nar/26.14.3340.

McLafferty, F. W. (1981) 'Tandem Mass Spectrometry', *Science*, 214(4518), pp. 280–287.

McNerney, R. *et al.* (2012) 'Tuberculosis diagnostics and biomarkers: Needs, challenges, recent advances, and opportunities', *Journal of Infectious Diseases*, 205(SUPPL. 2), pp. 147–158. doi: 10.1093/infdis/jir860.

McNerney, R. *et al.* (2015) 'New tuberculosis diagnostics and rollout', *International Journal of Infectious Diseases*. International Society for Infectious Diseases, 32, pp. 81–86. doi: 10.1016/j.ijid.2015.01.012.

McNerney, R. and Daley, P. (2011) 'Towards a point-of-care test for active tuberculosis: obstacles and opportunities.', *Nature reviews. Microbiology*, 9(3), pp. 204–213. doi: 10.1038/nrmicro2521.

Meher, A. K. *et al.* (2006) 'Mycobacterium tuberculosis H37Rv ESAT-6-CFP-10 complex formation confers thermodynamic and biochemical stability.', *The FEBS journal*, 273(7), pp. 1445–1462. doi: 10.1111/j.1742-4658.2006.05166.x.

Mendelboum Raviv, S. *et al.* (2008) '4-Thio-deoxyuridylate-modified thrombin aptamer and its inhibitory effect on fibrin clot formation, platelet aggregation and thrombus growth on subendothelial matrix', *Journal of Thrombosis and Haemostasis*. Wiley-Blackwell, 6(10), pp. 1764–1771. doi: 10.1111/j.1538-7836.2008.03106.x.

Michalski, A. *et al.* (2011) 'Mass Spectrometry-based Proteomics Using Q Exactive, a High-performance Benchtop Quadrupole Orbitrap Mass Spectrometer.', *Molecular & cellular proteomics : MCP*, 10(9), p. M111.011015. doi: 10.1074/mcp.M111.011015.

Miller, P. E. and Denton, M. B. (1986) 'The quadrupole mass filter: Basic operating concepts', *Journal of Chemical Education*, 63(7), p. 617. doi: 10.1021/ed063p617.

Min, K. *et al.* (2008) 'A simple and direct electrochemical detection of interferon-gamma using its RNA and DNA aptamers.', *Biosensors {&} Bioelectronics*, 23(12), pp. 1819–1824. doi: 10.1016/j.bios.2008.02.021.

Minion, J. *et al.* (2011) 'Diagnosing tuberculosis with urine lipoarabinomannan: systematic review and meta-analysis.', *The European Respiratory Journal*, 38(6), p. 09031936.00025711-. doi: 10.1183/09031936.00025711.

Miodek, A. *et al.* (2013) 'Binding kinetics of human cellular prion detection by DNA aptamers

immobilized on a conducting polypyrrole.', *Analytical & Bioanalytical Chemistry*. Springer Science & Business Media B.V., 405(8), pp. 2505–2514.

Mukadi, Y. D., Maher, D. and Harries, A. (2001) 'Tuberculosis case fatality rates in high HIV prevalence populations in sub-Saharan Africa.', *AIDS (London, England)*, 15(June 2000), pp. 143–152. doi: 10.1097/00002030-200101260-00002.

Mukundan, H. *et al.* (2012) 'Rapid detection of Mycobacterium tuberculosis biomarkers in a sandwich immunoassay format using a waveguide-based optical biosensor', *Tuberculosis*. Elsevier Ltd, 92(5), pp. 407–416. doi: 10.1016/j.tube.2012.05.009.

Murphy, M. B. *et al.* (2003) 'An improved method for the in vitro evolution of aptamers and applications in protein detection and purification.', *Nucleic acids research*. Oxford University Press, 31(18), p. e110. doi: 10.1093/nar/gng110.

Murray, K. K. *et al.* (2013) 'Definitions of terms relating to mass spectrometry (IUPAC Recommendations 2013)*', *Pure Appl. Chem*, 85(7), pp. 1515–1609. doi: 10.1351/PAC-REC-06-04-06.

Musheev, M. U. and Krylov, S. N. (2006) 'Selection of aptamers by systematic evolution of ligands by exponential enrichment: addressing the polymerase chain reaction issue.', *Analytica Chimica Acta*, 564(1), pp. 91–6. doi: 10.1016/j.aca.2005.09.069.

Musso, M. *et al.* (2006) 'Betaine, dimethyl sulfoxide, and 7-deaza-dGTP, a powerful mixture for amplification of GC-rich DNA sequences.', *The Journal of Molecular Diagnostics*. American Society for Investigative Pathology and Association for Molecular Pathology, 8(5), pp. 544–550. doi: 10.2353/jmoldx.2006.060058.

Nahid, P. *et al.* (2016) 'Executive Summary: Official American Thoracic Society/Centers for Disease Control and Prevention/Infectious Diseases Society of America Clinical Practice Guidelines: Treatment of Drug-Susceptible Tuberculosis', *Clinical Infectious Diseases*, 63(7), pp. 853–867. doi: 10.1093/cid/ciw566.

Namba, Y. (2013) 'Immunodetection assay for Mycobacterium tuberculosis complex'. Google Patents.

Napolitano, D. R. *et al.* (2008) 'Identification of Mycobacterium tuberculosis ornithine carboamyltransferase in urine as a possible molecular marker of active pulmonary tuberculosis.', *Clinical and Vaccine Immunology*, 15(4), pp. 638–643. doi: 10.1128/CVI.00010-08.

Nathan, C. and Shiloh, M. U. (2000) 'Reactive oxygen and nitrogen intermediates in the relationship between mammalian hosts and microbial pathogens', *Proceedings of the National Academy of Sciences*, 97(16), pp. 8841–8848. doi: 10.1073/pnas.97.16.8841.

Ng, V. H. *et al.* (2004) 'Role of KatG catalase-peroxidase in mycobacterial pathogenisis: Countering the phagocyte oxidative burst', *Molecular Microbiology*, 52, pp. 1291–1302. doi: 10.1111/j.1365-2958.2004.04078.x.

Nigou, J. *et al.* (2001) 'Mannosylated Lipoarabinomannans Inhibit IL-12 Production by Human Dendritic Cells: Evidence for a Negative Signal Delivered Through the Mannose Receptor', *The Journal of Immunology*, 166, pp. 7477–7485.

Nigou, J., Vercellone, A. and Puzo, G. (2000) 'New structural insights into the molecular deciphering of mycobacterial lipoglycan binding to C-type lectins: lipoarabinomannan glycoform characterization and quantification by capillary electrophoresis at the subnanomole level', *Journal of Molecular Biology*, 299(5), pp. 1353–1362. doi: 10.1006/jmbi.2000.3821.

Nitsche, A. *et al.* (2007) 'One-step selection of Vaccinia virus-binding DNA aptamers by MonoLEX', *BMC Biotechnology*, 7(1), p. 48. doi: 10.1186/1472-6750-7-48.

Oliphant, A. R. and Struhl, K. (1987) *The use of random-sequence oligonucleotides for determining consensus sequences*, *Methods in Enzymology*. Elsevier (Methods in Enzymology). doi: 10.1016/0076-6879(87)55037-6.

Olsen, J. V *et al.* (2007) 'Higher-energy C-trap dissociation for peptide modification analysis', *Nature Methods*, 4(9), pp. 709–712. doi: 10.1038/nmeth1060.

Orme, I. M. (2014) 'A new unifying theory of the pathogenesis of tuberculosis', *Tuberculosis*. Elsevier Ltd, 94(1), pp. 8–14. doi: 10.1016/j.tube.2013.07.004.

Ostatná, V. *et al.* (2008) 'Effect of the immobilisation of DNA aptamers on the detection of thrombin by means of surface plasmon resonance', *Analytical and Bioanalytical Chemistry*, 391(5), pp. 1861–1869. doi: 10.1007/s00216-008-2133-6.

Palomino, J. C. *et al.* (2008) 'Rapid culture-based methods for drug-resistance detection in Mycobacterium tuberculosis.', *Journal of microbiological methods*, 75(2), pp. 161–166. doi: 10.1016/j.mimet.2008.06.015.

Pan, Q. *et al.* (2014) 'Aptamer against mannose-capped lipoarabinomannan inhibits virulent Mycobacterium tuberculosis infection in mice and rhesus monkeys.', *Molecular therapy : the journal of the American Society of Gene Therapy*, 22(5), pp. 940–951. doi: 10.1038/mt.2014.31.

Pan, S.-J. *et al.* (2015) 'Biomarkers for Tuberculosis Based on Secreted, Species-Specific, Bacterial Small Molecules', *Journal of Infectious Diseases*, 212(11), pp. 1827–1834. doi: 10.1093/infdis/jiv312.

Pantoja, A., Kik, S. V and Denkinger, C. M. (2015) 'Costs of novel tuberculosis diagnostics--will countries be able to afford it?', *The Journal of Infectious Diseases*, 211 Suppl(suppl{_}2), pp. S67--77. doi: 10.1093/infdis/jiu820.

Papamichael, K. I., Kreuzer, M. P. and Guilbault, G. G. (2007) 'Viability of allergy (IgE) detection using an alternative aptamer receptor and electrochemical means', *Sensors and Actuators, B: Chemical*, 121(1), pp. 178–186. doi: 10.1016/j.snb.2006.09.024.

Park, M. Y. *et al.* (2009) 'Evaluation of an immunochromatographic assay kit for rapid identification of Mycobacterium tuberculosis complex in clinical isolates.', *Journal of Clinical Microbiology*, 47(2), pp. 481–484. doi: 10.1128/JCM.01253-08.

Parsons, L. M. *et al.* (2011) 'Laboratory diagnosis of tuberculosis in resource-poor Countries: Challenges and opportunities', *Clinical Microbiology Reviews*, 24(2), pp. 314–350. doi: 10.1128/CMR.00059-10.

Parwati, I., van Crevel, R. and van Soolingen, D. (2010) 'Possible underlying mechanisms for successful emergence of the Mycobacterium tuberculosis Beijing genotype strains', *The Lancet Infectious Diseases*. Elsevier, 10(2), pp. 103–111. doi: 10.1016/S1473-3099(09)70330-5.

Patel, D. (1997) 'Structural analysis of nucleic acid aptamers', *Current Opinion in Chemical Biology*, 1(1), pp. 32–46. doi: 10.1016/S1367-5931(97)80106-8.

Patel, V. B. *et al.* (2009) 'Utility of a novel lipoarabinomannan assay for the diagnosis of tuberculous meningitis in a resource-poor high-HIV prevalence setting.', *Cerebrospinal fluid research*, 6, p. 13. doi: 10.1186/1743-8454-6-13.

Pathak, S. K. *et al.* (2007) 'Direct extracellular interaction between the early secreted antigen ESAT-6 of Mycobacterium tuberculosis and TLR2 inhibits TLR signaling in macrophages.', *Nature immunology*. Nature Publishing Group, 8(6), pp. 610–8. doi: 10.1038/ni1468.

Pathan, A. A. *et al.* (2001) 'Direct Ex Vivo Analysis of Antigen-Specific IFN- -Secreting CD4 T Cells in Mycobacterium tuberculosis-Infected Individuals: Associations with Clinical Disease State and Effect of Treatment', *The Journal of Immunology*. American Association of Immunologists, 167(9), pp. 5217–5225. doi: 10.4049/jimmunol.167.9.5217.

Pesce, A. J. and Michael, J. G. (1992) 'Artifacts and limitations of enzyme immunoassay', *Journal*

of Immunological Methods, 150(1–2), pp. 111–119. doi: 10.1016/0022-1759(92)90070-A.

Peter, J. G. *et al.* (2012) 'Diagnostic accuracy of induced sputum LAM ELISA for tuberculosis diagnosis in sputum-scarce patients', *International Journal of Tuberculosis and Lung Disease*, 16(8), pp. 1108–1112. doi: 10.5588/ijtld.11.0614.

Peter, J. G. *et al.* (2012) 'The Diagnostic Accuracy of Urine-Based Xpert MTB/RIF in HIV-Infected Hospitalized Patients Who Are Smear-Negative or Sputum Scarce.', *PLoS ONE*. Public Library of Science, 7(7), pp. 1–8. doi: 10.1371/journal.pone.0039966.

Peter, J. G. *et al.* (2014) 'Sputum induction to aid diagnosis of smear-negative or sputum-scarce tuberculosis in adults in HIV-endemic settings', *European Respiratory Journal*, 43, pp. 185–194. doi: 10.1183/09031936.00198012.

Peter, J. G., Theron, G. and Dheda, K. (2013) 'Can Point-of-Care Urine LAM Strip Testing for Tuberculosis Add Value to Clinical Decision Making in Hospitalised HIV-Infected Persons?', *PLoS ONE*. Public Library of Science, 8(2), pp. 1–9.

Peters, J. S. *et al.* (2016) 'Identification of Quantitative Proteomic Differences between Mycobacterium tuberculosis Lineages with Altered Virulence', *Frontiers in Microbiology*. Frontiers, 7, p. 813. doi: 10.3389/fmicb.2016.00813.

Peterson, A. C. *et al.* (2012) 'Parallel Reaction Monitoring for High Resolution and High Mass Accuracy Quantitative, Targeted Proteomics', *Molecular & Cellular Proteomics*, 11(11), pp. 1475–1488. doi: 10.1074/mcp.O112.020131.

Petzold, C. J., Stanton, L. H. and Leary, J. a (2005) 'Structural characterization of Lipoarabinomannans from Mycobacterium tuberculosis and Mycobacterium smegmatis by ESI mass spectrometry.', *Journal of the American Society for Mass Spectrometry*, 16(7), pp. 1109–1116. doi: 10.1016/j.jasms.2005.02.023.

Phillips, M. *et al.* (2010) 'Breath biomarkers of active pulmonary tuberculosis.', *Tuberculosis*, 90(2), pp. 145–151. doi: 10.1016/j.tube.2010.01.003.

Ping, J. *et al.* (2015) 'Recent advances in aptasensors based on graphene and graphene-like nanomaterials', *Biosensors and Bioelectronics*, 64, pp. 373–385. doi: 10.1016/j.bios.2014.08.090.

van Pinxteren, L. a *et al.* (2000) 'Diagnosis of tuberculosis based on the two specific antigens ESAT-6 and CFP10.', *Clinical and Diagnostic Laboratory Immunology*, 7(2), pp. 155–160.

Pirmoradian, M. *et al.* (2013) 'Rapid and Deep Human Proteome Analysis by Single-dimension

Shotgun Proteomics', *Molecular & Cellular Proteomics*, 12(11), pp. 3330–3338. doi: 10.1074/mcp.O113.028787.

Pollard, T. D. (2010) 'A guide to simple and informative binding assays.', *Molecular biology of the cell*, 21(23), pp. 4061–7. doi: 10.1091/mbc.E10-08-0683.

Pollock, N. R. *et al.* (2013) 'Validation of Mycobacterium tuberculosis Rv1681 protein as a diagnostic marker of active pulmonary tuberculosis.', *Journal of Clinical Microbiology*, 51(5), pp. 1367–1373. doi: 10.1128/JCM.03192-12.

Posthuma-Trumpie, G. A., Korf, J. and Van Amerongen, A. (2009) 'Lateral flow (immuno)assay: Its strengths, weaknesses, opportunities and threats. A literature survey', *Analytical and Bioanalytical Chemistry*, 393(2), pp. 569–582. doi: 10.1007/s00216-008-2287-2.

Pym, A. S. *et al.* (2002) 'Loss of RD1 contributed to the attenuation of the live tuberculosis vaccines Mycobacterium bovis BCG and Mycobacterium microti.', *Molecular Microbiology*, 46(3), pp. 709–717.

Pym, A. S. *et al.* (2016) 'Bedaquiline in the treatment of multidrug- and extensively drugresistant tuberculosis', *European Respiratory Journal*, 47(2), pp. 564–574. doi: 10.1183/13993003.00724-2015.

Qin, L. *et al.* (2009) 'The selection and application of ssDNA aptamers against MPT64 protein in Mycobacterium tuberculosis.', *Clinical chemistry and laboratory medicine : CCLM / FESCC*, 47(4), pp. 405–411. doi: 10.1515/CCLM.2009.097.

Radom, F. *et al.* (2013) 'Aptamers: Molecules of great potential', *Biotechnology Advances*, 31(8), pp. 1260–1274. doi: 10.1016/j.biotechadv.2013.04.007.

Rangaka, M. X. *et al.* (2012) 'Predictive value of interferon-γ release assays for incident active tuberculosis: A systematic review and meta-analysis', *The Lancet Infectious Diseases*. Elsevier Ltd, 12(1), pp. 45–55. doi: 10.1016/S1473-3099(11)70210-9.

Rappsilber, J., Ishihama, Y. and Mann, M. (2003) 'Stop and Go Extraction Tips for Matrix-Assisted Laser Desorption/Ionization, Nanoelectrospray, and LC/MS Sample Pretreatment in Proteomics', *Analytical Chemistry*. American Chemical Society, 75(3), pp. 663–670. doi: 10.1021/ac026117i.

Ravn, P. *et al.* (1999) 'Human T cell responses to the ESAT-6 antigen from Mycobacterium tuberculosis.', *The Journal of Infectious Diseases*, 179(3), pp. 637–45. doi: 10.1086/314640.

Ravn, P. *et al.* (2005) 'Prospective evaluation of a whole-blood test using Mycobacterium

tuberculosis-specific antigens ESAT-6 and CFP-10 for diagnosis of active tuberculosis.', *Clinical and Diagnostic Laboratory Immunology*, 12(4), pp. 491–496. doi: 10.1128/CDLI.12.4.491-496.2005.

Raynaud, C. *et al.* (1998) 'Extracellular enzyme activities potentially involved in the pathogenicity of Mycobacterium tuberculosis', *Microbiology*, 144 (Pt 2(1 998), pp. 577–587.

Reid, M. J. and Shah, N. S. (2009) 'Approaches to tuberculosis screening and diagnosis in people with HIV in resource-limited settings', *Lancet Infect Dis*. 2009/02/28, 9(3), pp. 173–184. doi: S1473-3099(09)70043-X [pii] 10.1016/S1473-3099(09)70043-X.

Reineck, P., Wienken, C. J. and Braun, D. (2010) 'Thermophoresis of single stranded DNA.', *Electrophoresis*, 31(2), pp. 279–286. doi: 10.1002/elps.200900505.

Reither, K. *et al.* (2009) 'Low sensitivity of a urine LAM-ELISA in the diagnosis of pulmonary tuberculosis.', *BMC Infectious Diseases*. BioMed Central, 9(1), p. 141. doi: 10.1186/1471-2334-9-141.

Reither, K. *et al.* (2010) 'Evaluation of Diagnos TB AG, a flow-through immunoassay for rapid detection of pulmonary tuberculosis.', *The International Journal of Tuberculosis and Lung Disease*, 14(2), pp. 238–40.

Renshaw, P. S. *et al.* (2002) 'Conclusive evidence that the major T-cell antigens of the Mycobacterium tuberculosis complex ESAT-6 and CFP-10 form a tight, 1:1 complex and characterization of the structural properties of ESAT-6, CFP-10, and the ESAT-6*CFP-10 complex. Implications for p', *The Journal of biological chemistry*, 277(24), pp. 21598–21603. doi: 10.1074/jbc.M201625200.

Renshaw, P. S. *et al.* (2005) 'Structure and function of the complex formed by the tuberculosis virulence factors CFP-10 and ESAT-6.', *The EMBO journal*, 24(14), pp. 2491–2498. doi: 10.1038/sj.emboj.7600732.

Reverberi, R. and Reverberi, L. (2007) 'Factors affecting the antigen-antibody reaction.', *Blood transfusion*, 5(4), pp. 227–40. doi: 10.2450/2007.0047-07.

Rodrigues, L. C. *et al.* (2005) 'Effect of BCG revaccination on incidence of tuberculosis in school-aged children in Brazil: the BCG-REVAC cluster-randomised trial.', *Lancet*, 366(9493), pp. 1290–5.

Rogerson, B. J. *et al.* (2006) 'Expression levels of Mycobacterium tuberculosis antigen-encoding genes versus production levels of antigen-specific T cells during stationary level lung infection

in mice', *Immunology*, 118(2), pp. 195–201. doi: 10.1111/j.1365-2567.2006.02355.x.

Rotherham, L. S. (2012) *Isolation and characterization of novel aptamers against the CFP-10 / ESAT-6 heterodimer for the development of TB diagnostic tools*. University of Pretoria.

Rotherham, L. S. *et al.* (2012) 'Selection and Application of ssDNA Aptamers to Detect Active TB from Sputum Samples.', *PLoS ONE*, 7(10), p. e46862. doi: 10.1371/journal.pone.0046862.

Roux, K. H. (1995) 'Optimization and troubleshooting in PCR.', *Genome Research*, 4(5), pp. S185–S194. doi: 10.1101/gr.4.5.S185.

Rowe, A. A., Miller, E. A. and Plaxco, K. W. (2010) 'Reagentless measurement of aminoglycoside antibiotics in blood serum via an electrochemical, ribonucleic acid aptamer-based biosensor', *Analytical Chemistry*, 82(17), pp. 7090–7095. doi: 10.1021/ac101491d.

Ruff, K. M., Snyder, T. M. and Liu, D. R. (2010) 'Enhanced functional potential of nucleic acid aptamer libraries patterned to increase secondary structure', *Journal of the American Chemical Society*. American Chemical Society, 132(27), pp. 9453–9464. doi: 10.1021/ja103023m.

Russo Krauss, I. *et al.* (2011) 'Thrombin-aptamer recognition: a revealed ambiguity', *Nucleic Acids Research*, 39(17), pp. 7858–7867. doi: 10.1093/nar/gkr522.

Saah, A. J. and Hoover, D. R. (1997) '"Sensitivity" and "specificity" reconsidered: The meaning of these terms in analytical and diagnostic settings', *Annals of Internal Medicine*. American College of Physicians, 126(1), pp. 91–94. doi: 10.7326/0003-4819-126-1-199701010-00026.

Sada, E. *et al.* (1990) 'Evaluation of Lipoarabinomannan for the Serological Diagnosis of Tuberculosis', *Journal of Clinical Microbiology*, 28(12), pp. 2587–2590.

Sada, E. *et al.* (1992) 'Detection of Lipoarabinomannan as a Diagnostic Test for Tuberculosis', *Journal of Clinical Microbiology*, 30(9), pp. 2415–2418.

Sakamuri, R. M. *et al.* (2013) 'Association of lipoarabinomannan with high density lipoprotein in blood: implications for diagnostics.', *Tuberculosis*, 93(3), pp. 301–7. doi: 10.1016/j.tube.2013.02.015.

Sanghavi, B. J. *et al.* (2015) 'Ultrafast immunoassays by coupling dielectrophoretic biomarker enrichment in nanoslit channel with electrochemical detection on graphene', *Lab Chip*, 15, p. 22904. doi: 10.1039/C5LC00840A.

Sarkar, P. *et al.* (2014) 'Application of lipoarabinomannan antigen in tuberculosis diagnostics: current evidence.', *Postgraduate medical journal*, 90(1061), pp. 155–63. doi:

10.1136/postgradmedj-2013-132053.

Savolainen, L. *et al.* (2013) 'Modification of clearview tuberculosis (TB) enzyme-linked immunosorbent assay for TB patients not infected with HIV.', *Clinical and Vaccine Immunology*, 20(9), pp. 1479–82. doi: 10.1128/CVI.00375-13.

Savolainen, L. (2014) *Characterization of diagnostic biomarkers for Mycobacterium tuberculosis infection*. University of Helsinki.

Schägger, H. (2006) 'Tricine-SDS-PAGE.', *Nature protocols*, 1(1), pp. 16–22. doi: 10.1038/nprot.2006.4.

Schmidt, R. *et al.* (2011) 'Single-Molecule Detection on a Protein-Array Assay Platform for the Exposure of a Tuberculosis Antigen', *Journal of Proteome Research*, 10(3), pp. 1316–1322. doi: 10.1021/pr101070j.

Schubert, O. T. *et al.* (2013) 'The Mtb Proteome Library: A Resource of Assays to Quantify the Complete Proteome of Mycobacterium tuberculosis', *Cell Host & Microbe*. NIH Public Access, 13(5), pp. 602–612. doi: 10.1016/j.chom.2013.04.008.

Scott, L. E. *et al.* (2011) 'Comparison of Xpert MTB/RIF with other nucleic acid technologies for diagnosing pulmonary tuberculosis in a high HIV prevalence setting: A prospective study', *PLoS Medicine*, 8(7). doi: 10.1371/journal.pmed.1001061.

Sester, M. *et al.* (2014) 'Risk assessment of tuberculosis in immunocompromised patients: A TBNET study', *American Journal of Respiratory and Critical Care Medicine*. American Thoracic Society, 190(10), pp. 1168–1176. doi: 10.1164/rccm.201405-0967OC.

Shah, M. *et al.* (2010) 'Quantitative Analysis of a Urine-Based Assay for Detection of Lipoarabinomannan in Patients with Tuberculosis', *Journal of Clinical Microbiology*, 48(8), pp. 2972–2974. doi: 10.1128/JCM.00363-10.

Shah, M. *et al.* (2016) 'Lateral flow urine lipoarabinomannan assay for detecting active tuberculosis in HIV-positive adults', in Shah, M. (ed.) *Cochrane Database of Systematic Reviews*. Chichester, UK: John Wiley {&} Sons, Ltd, p. CD011420. doi: 10.1002/14651858.CD011420.pub2.

Shah, N. B. and Duncan, T. M. (2014) 'Bio-layer Interferometry for Measuring Kinetics of Protein-protein Interactions and Allosteric Ligand Effects', *Journal of Visualized Experiments*, (84), pp. 1–7. doi: 10.3791/51383.

Shao, K. *et al.* (2011) 'Emulsion PCR: a high efficient way of PCR amplification of random DNA

libraries in aptamer selection.', *PLoS ONE*, 6(9), p. e24910. doi: 10.1371/journal.pone.0024910.

Shen, G.-H. G.-H. *et al.* (2011) 'Rapid Identification of the Mycobacterium tuberculosis Complex by Combining the ESAT-6/CFP-10 Immunochromatographic Assay and Smear Morphology', *Journal of Clinical Microbiology*, 49(3), pp. 902–907. doi: 10.1128/JCM.00592-10.

Sherman, D. R. *et al.* (1996) 'Compensatory ahpC gene expression in isoniazid-resistant Mycobacterium tuberculosis.', *Science*. American Association for the Advancement of Science, 272(April), pp. 1641–1643. doi: 10.1126/science.272.5268.1641.

Shevchenko, A. *et al.* (2007) 'In-gel digestion for mass spectrometric characterization of proteins and proteomes', *Nature Protocols*, 1(6), pp. 2856–2860. doi: 10.1038/nprot.2006.468.

Shi, L., North, R. and Gennaro, M. L. (2004) 'Effect of Growth State on Transcription Levels of Genes Encoding Major Secreted Antigens of Mycobacterium tuberculosis in the Mouse Lung', *Infection and Immunity*, 72(4), pp. 2420–2424. doi: 10.1128/IAI.72.4.2420-2424.2004.

Shui, G. *et al.* (2012) 'Mycolic acids as diagnostic markers for tuberculosis case detection in humans and drug efficacy in mice', *EMBO Molecular Medicine*, 4(1), pp. 27–37. doi: 10.1002/emmm.201100185.

Shum, K. T. *et al.* (2011) 'Aptamer-mediated inhibition of mycobacterium tuberculosis polyphosphate kinase 2', *Biochemistry*, 50(15), pp. 3261–3271. doi: 10.1021/bi2001455.

Silva, V. M. C. *et al.* (2003) 'Factors associated with humoral response to ESAT-6, 38 kDa and 14 kDa in patients with a spectrum of tuberculosis', *International Journal of Tubberculosis and Lung Disease*, 7(July 2002), pp. 478–484.

Šimundić, A.-M. (2008) 'Measures of diagnostic accuracy: Basic definitions.', *Medical {&} Biological Science*, pp. 1–9.

Smith, J. *et al.* (2008) 'Evidence for pore formation in host cell membranes by ESX-1-secreted ESAT-6 and its role in Mycobacterium marinum escape from the vacuole.', *Infection and immunity*, 76(12), pp. 5478–5487. doi: 10.1128/IAI.00614-08.

Sohn, H. (2016) *Improving tuberculosis diagnosis in vulnerable populations : impact and cost-effectiveness of novel , rapid molecular assays*.

Sonnenberg, M. G. and Belisle, J. T. (1997) 'Definition of Mycobacterium tuberculosis culture filtrate proteins by two-dimensional polyacrylamide gel electrophoresis, N-terminal amino acid sequencing, and electrospray mass spectrometry.', *Infection and immunity*, 65(11), pp. 4515–4524.

Sørensen, A. L. *et al.* (1995) 'Purification and Characterization of a Low-Molecular-Mass T-Cell Antigen Secreted by Mycobacterium tuberculosis', *Infection and Immunity*, 63(5), pp. 1710–1717.

Sreevatsan, S. *et al.* (1997) 'Restricted structural gene polymorphism in the Mycobacterium tuberculosis complex indicates evolutionarily recent global dissemination', *Proceedings of the National Academy of Sciences*, 94(18), pp. 9869–9874. doi: 10.1073/pnas.94.18.9869.

St John, A. and Price, C. P. (2014) 'Existing and Emerging Technologies for Point-of-Care Testing.', *The Clinical biochemist. Reviews / Australian Association of Clinical Biochemists*, 35(3), pp. 155–67.

Stanley, S. A. *et al.* (2003) 'Acute infection and macrophage subversion by Mycobacterium tuberculosis require a specialized secretion system.', *Proceedings of the National Academy of Sciences of the United States of America*, 100(22), pp. 13001–13006. doi: 10.1073/pnas.2235593100.

Stedtfeld, R. D. *et al.* (2012) 'Gene-Z: a device for point of care genetic testing using a smartphone.', *Lab on a chip*, pp. 1454–1462. doi: 10.1039/c2lc21226a.

Steingart, K. R., Henry, M., *et al.* (2006) 'Fluorescence versus conventional sputum smear microscopy for tuberculosis: a systematic review', *The Lancet Infectious Diseases*, 6(9), pp. 570–581. doi: 10.1016/S1473-3099(06)70578-3.

Steingart, K. R., Ng, V., *et al.* (2006) 'Sputum processing methods to improve the sensitivity of smear microscopy for tuberculosis: a systematic review', *The Lancet Infectious Diseases*, 6(10), pp. 664–674. doi: 10.1016/S1473-3099(06)70602-8.

Steingart, K. R. *et al.* (2007) 'Commercial serological antibody detection tests for the diagnosis of pulmonary tuberculosis: A systematic review', *PLoS Medicine*, 4(6), pp. 1041–1060.

Steingart, K. R. *et al.* (2011) 'Commercial Serological tests for the diagnosis of active pulmonary and extrapulmonary tuberculosis: An updated systematic review and Meta-Analysis', *PLoS Medicine*, 8(8), p. e1001062. doi: 10.1371/journal.pmed.1001062.

Stoltenburg, R., Reinemann, C. and Strehlitz, B. (2007) 'SELEX--a (r)evolutionary method to generate high-affinity nucleic acid ligands.', *Biomolecular Engineering*, 24(4), pp. 381–403. doi: 10.1016/j.bioeng.2007.06.001.

Sutcliffe, I. C. (1995) 'Identification of a lipoarabinomannan-like lipoglycan in Corynebacterium matruchotii', *Archives of Oral Biology*, 40(12), pp. 1119–1124. doi: 10.1016/0003-

9969(95)00086-0.

Szewczyk, R. *et al.* (2013) 'Rapid method for Mycobacterium tuberculosis identification using electrospray ionization tandem mass spectrometry analysis of mycolic acids', *Diagnostic Microbiology and Infectious Disease*, 76(3), pp. 298–305. doi: 10.1016/j.diagmicrobio.2013.03.025.

Tan, T. *et al.* (2006) 'The ESAT-6/CFP-10 secretion system of Mycobacterium marinum modulates phagosome maturation', *Cellular Microbiology*, 8(9), pp. 1417–1429.

Tang, X.-L. *et al.* (2014) 'CFP10 and ESAT6 aptamers as effective Mycobacterial antigen diagnostic reagents', *Journal of Infection*. Elsevier Ltd, 69(6), pp. 569–580. doi: 10.1016/j.jinf.2014.05.015.

Tang, X.-L. *et al.* (2016) 'Generation and application of ssDNA aptamers against glycolipid antigen ManLAM of Mycobacterium tuberculosis for TB diagnosis.', *The Journal of Infection*, 72(5), pp. 573–586. doi: 10.1016/j.jinf.2016.01.014.

Tang, X. J., Thibault, P. and Boyd, R. K. (1993) 'Fragmentation reactions of multiply-protonated peptides and implications for sequencing by tandem mass spectrometry with low-energy collision-induced dissociation', *Analytical Chemistry*, 65(20), pp. 2824–2834. doi: 10.1021/ac00068a020.

Tatarinova, O. *et al.* (2014) 'Comparison of the "Chemical" and "Structural" Approaches to the Optimization of the Thrombin-Binding Aptamer.', *PLoS ONE*. Public Library of Science, 9(2), pp. 1–9.

TB Diagnostics Market Analysis Consortium (2014) 'Market Assessment of Tuberculosis Diagnostics in Brazil in 2012', *PLoS ONE*. Edited by O. Sued. Public Library of Science, 9(8), p. e104105. doi: 10.1371/journal.pone.0104105.

TB Diagnostics Market Analysis Consortium (2015) 'Market assessment of tuberculosis diagnostics in South Africa, 2012-2013', *International Journal of Tuberculosis and Lung Disease*. International Union Against Tuberculosis and Lung Disease, 19(2), pp. 216–222. doi: 10.5588/ijtld.14.0565.

Tessema, T. A. *et al.* (2001) 'Diagnostic Evaluation of Urinary Lipoarabinomannan at an Ethiopian Tuberculosis Centre', *Scandinavian Journal of Infectious Diseases*. Taylor & Francis Ltd, 33(4), pp. 279–284.

Teutschbein, J. *et al.* (2009) 'A protein linkage map of the ESAT-6 secretion system 1 (ESX-1) of

Mycobacterium tuberculosis.', *Microbiological research*, 164(3), pp. 253–9. doi: 10.1016/j.micres.2006.11.016.

The UniProt Consortium (2014) 'UniProt: a hub for protein information', *Nucleic Acids Research*, 43(Database issue), pp. D204-12. doi: 10.1093/nar/gku989.

Tijssen, P. (1985) 'The immobilization of immunoreactants on solid phases', in *Practice and Theory of Enzyme Immunoassays*, pp. 297–321.

Tobias, R. and Kumaraswamy, S. (2013) 'Application Note 14: Biomolecular Binding Kinetics Assays on the Octet Platform', *ForteBio a Division of Pall Life Sciences:*, pp. 1–66.

Tu, H.-Z. *et al.* (2015) 'Cost-effective identification of Mycobacterium tuberculosis complex using microscopic morphology and rapid tests.', *The international journal of tuberculosis and lung disease*, 19(10), pp. 1204–1208. doi: 10.5588/ijtld.15.0781.

Tucci, P., González-Sapienza, G. and Marin, M. (2014) 'Pathogen-derived biomarkers for active tuberculosis diagnosis.', *Frontiers in microbiology*, 5, p. 549. doi: 10.3389/fmicb.2014.00549.

Tuerk, C. and Gold, L. (1990) 'Systematic evolution of ligands by exponential enrichment: RNA ligands to bacteriophage T4 DNA polymerase', *Science*, 249(4968), pp. 505–510. doi: 10.1126/science.2200121.

Turner, O. C., Basaraba, R. J. and Orme, I. M. (2003) 'Immunopathogenesis of pulmonary granulomas in the guinea pig after infection with Mycobacterium tuberculosis.', *Infection and immunity*, 71(2), pp. 864–71. doi: 10.1128/IAI.71.2.864.

Ueno, Y. *et al.* (2015) 'On-chip graphene oxide aptasensor for multiple protein detection', *Analytica Chimica Acta*. Elsevier B.V., 866, pp. 1–9. doi: 10.1016/j.aca.2014.10.047.

Ukwaja, K. N. *et al.* (2012) 'The economic burden of tuberculosis care for patients and households in Africa: a systematic review', *The International Journal of Tuberculosis and Lung Disease*. International Union Against Tuberculosis and Lung Disease, 16(6), pp. 733–9. doi: 10.5588/ijtld.11.0193.

Ulrichs, T. *et al.* (2000) 'Increased numbers of ESAT-6- and purified protein derivative-specific gamma interferon-producing cells in subclinical and active tuberculosis infection', *Infection and Immunity*, 68(10), pp. 6073–6076. doi: 10.1128/IAI.68.10.6073-6076.2000.

Urdahl, K. B., Shafiani, S. and Ernst, J. D. (2011) 'Initiation and regulation of T-cell responses in tuberculosis.', *Mucosal immunology*. Nature Publishing Group, 4(3), pp. 288–293. doi: 10.1038/mi.2011.10.

Van't Hoog, A. H. *et al.* (2013) 'Optimal triage test characteristics to improve the cost-effectiveness of the Xpert MTB/RIF assay for TB diagnosis: A decision analysis', *PLoS ONE*, 8(12). doi: 10.1371/journal.pone.0082786.

Vandal, O. H., Nathan, C. F. and Ehrt, S. (2009) 'Acid resistance in Mycobacterium tuberculosis.', *Journal of Bacteriology*, 191(15), pp. 4714–21. doi: 10.1128/JB.00305-09.

Vaught, J. D. *et al.* (2010) 'Expanding the Chemistry of DNA for in Vitro Selection', *Journal of the American Chemical Society*, 132(12), pp. 4141–4151. doi: 10.1021/ja908035g.

Venisse, A. *et al.* (1993) 'Structural features of lipoarabinomannan from Mycobacterium bovis BCG. Determination of molecular mass by laser desorption mass spectrometry.', *The Journal of Biological Chemistry*, 268(17), pp. 12401–12411.

Venisse, A. *et al.* (1995) 'Mannosylated Lipoarabinomannan Interacts with Phagocytes', *European Journal of Biochemistry*, 231(2), pp. 440–447. doi: 10.1111/j.1432-1033.1995.tb20717.x.

Venkatesh, N. and Murthy, G. S. (1996) 'Dissociation of monoclonal antibody-antigen complexes: Implications for ELISA procedures', *Journal of Immunological Methods*, 199(2), pp. 167–174. doi: 10.1016/S0022-1759(96)00179-2.

Viswanathan, V. K., Krcmarik, K. and Cianciotto, N. P. (1999) 'Template secondary structure promotes polymerase jumping during PCR amplification', *BioTechniques*, 27(3), pp. 508–11.

Vizcaíno, C. *et al.* (2010) 'Computational prediction and experimental assessment of secreted/surface proteins from Mycobacterium tuberculosis H37Rv', *PLoS Computational Biology*, 6(6), pp. 1–14. doi: 10.1371/journal.pcbi.1000824.

Volkman, H. E. *et al.* (2010) 'Tuberculous granuloma induction via interaction of a bacterial secreted protein with host epithelium.', *Science (New York, N.Y.)*, 327(5964), pp. 466–9. doi: 10.1126/science.1179663.

Wallis, R. S. *et al.* (2009) 'Biomarkers for tuberculosis disease activity, cure, and relapse', *The Lancet Infectious Diseases*. Elsevier Ltd, 9(3), pp. 162–172. doi: 10.1016/S1473-3099(09)70042-8.

Walzl, G. *et al.* (2008) 'Biomarkers for TB treatment response: challenges and future strategies.', *The Journal of Infection*, 57(2), pp. 103–109. doi: 10.1016/j.jinf.2008.06.007.

Walzl, G. *et al.* (2011) 'Immunological biomarkers of tuberculosis', *Nature Reviews Immunology*. Nature Publishing Group, 11(5), pp. 343–354. doi: 10.1038/nri2960.

Wang, C.-Y. *et al.* (2014) 'Sequence-constructive SELEX: A new strategy for screening DNA aptamer binding to Globo H', *Biochemical and Biophysical Research Communications*, 452(3), pp. 484–489. doi: 10.1016/j.bbrc.2014.08.086.

Wang, J.-T. *et al.* (2002) 'Prognosis of tuberculous meningitis in adults in the era of modern antituberculous chemotherapy.', *Journal of microbiology, immunology, and infection*, 35(4), pp. 215–22.

Wards, B. J., de Lisle, G. W. and Collins, D. M. (2000) 'An esat6 knockout mutant of Mycobacterium bovis produced by homologous recombination will contribute to the development of a live tuberculosis vaccine', *Tubercle and Lung Disease*, 80(4–5), pp. 185–189. doi: 10.1054/tuld.2000.0244.

Wayne, L. G. and Sohaskey, C. D. (2001) 'Nonreplicating persistence of mycobacterium tuberculosis.', *Annual review of microbiology*, 55(1), pp. 139–63. doi: 10.1146/annurev.micro.55.1.139.

Wehrli, W. (1983) 'Rifampin: Mechanisms of Action and Resistance', *Clinical Infectious Diseases*. Oxford University Press, 5(Supplement_3), pp. S407–S411. doi: 10.1093/clinids/5.Supplement_3.S407.

van der Wel, N. *et al.* (2007) 'M. tuberculosis and M. leprae Translocate from the Phagolysosome to the Cytosol in Myeloid Cells', *Cell*, 129(7), pp. 1287–1298. doi: 10.1016/j.cell.2007.05.059.

Whelan, A. O. *et al.* (2010) 'Development of a skin test for bovine tuberculosis for differentiating infected from vaccinated animals.', *Journal of Clinical Microbiology*, 48(9), pp. 3176–81. doi: 10.1128/JCM.00420-10.

WHO (2011a) 'Commercial serodiagnostic tests for diagnosis of tuberculosis: policy statement', *Geneva: WHO*, p. 26 p. doi: WHO/HTM/TB/2011.8.

WHO (2011b) *Fluorescent light-emitting diode (LED) microscopy for diagnosis of tuberculosis Policy statement*. doi: WHO/HTM/TB/2011.8.

WHO (2011c) *Rapid implementation of the Xpert MTB/RIF diagnostic test. Technical and operational 'How to' practical considerations*. doi: WHO/HTM/TB/2011.2.

WHO (2011d) *Use of tuberculosis release assays (IGRAs) in low and middle-income countries*, *World Health Organization Policy Statement*. doi: WHO/HTM/TB/2011.18.

WHO (2011e) *WHO Report Global Tuberculosis Control 2011*. doi: WHO/HTM/TB/2011.16.

WHO (2013a) *Automated Real-Time Nucleic Acid Amplification Technology for Rapid and Simultaneous Detection of Tuberculosis and Rifampicin Resistance: Xpert MTB/RIF Assay for the Diagnosis of Pulmonary and Extrapulmonary TB in Adults and Children: Policy update*. doi: ISBN 978 92 4 150633 5.

WHO (2013b) *Global Tuberculosis Report 2013*. Geneva, Switzerland. doi: WHO/HTM/TB/2013.11.

WHO (2014a) *Global tuberculosis report 2014*. Geneva, Switzerland. doi: WHO/HTM/TB/2014.08.

WHO (2014b) *High-priority target product profiles for new tuberculosis diagnostics: report of a consensus meeting*, *WHO Meeting Report*. Geneva, Switzerland. doi: WHO/HTM/TB/2014.18.

WHO (2015a) *Guidelines on the management of latent tuberculosis infection*. doi: WHO/HTM/TB/2015.01.

WHO (2015b) *The use of lateral flow urine lipoarabinomannan assay (LF-LAM) for the diagnosis and screening of active tuberculosis in people living with HIV: policy*. Geneva, Switzerland: WHO Press. doi: WHO/HTM/TB/2015.25.

WHO (2016a) *Global Tuberculosis Report 2016*. WHO Press.

WHO (2016b) *The use of loop-mediated isothermal amplification (TB-LAMP) for the diagnosis of pulmonary tuberculosis*. doi: WHO/HTM/TB/2016.11.

Whyte, G. F., Vilar, R. and Woscholski, R. (2013) 'Molecular recognition with boronic acids-applications in chemical biology', *Journal of Chemical Biology*, 6(4), pp. 161–174. doi: 10.1007/s12154-013-0099-0.

Wienken, C. J. *et al.* (2010) 'Protein-binding assays in biological liquids using microscale thermophoresis.', *Nature Communications*, 1(May), p. 100. doi: 10.1038/ncomms1093.

Wilson, C. and Szostak, J. W. (1998) 'Isolation of a fluorophore-specific DNA aptamer with weak redox activity', *Chemistry & Biology*, 5(11), pp. 609–617. doi: 10.1016/S1074-5521(98)90289-7.

Wood, R. *et al.* (2012) 'Lipoarabinomannan in urine during tuberculosis treatment: association with host and pathogen factors and mycobacteriuria', *BMC Infectious Diseases*. BioMed Central Ltd, 12(1), p. 47. doi: 10.1186/1471-2334-12-47.

Wu, Y. *et al.* (2008) 'Vaccine-elicited 10-kilodalton culture filtrate protein-specific CD8+ T cells

are sufficient to mediate protection against Mycobacterium tuberculosis infection.', *Infection and immunity*, 76(5), pp. 2249–2255. doi: 10.1128/IAI.00024-08.

Xie, H. *et al.* (2012) 'Rapid point-of-care detection of the tuberculosis pathogen using a BlaC-specific fluorogenic probe', *Nature Chemistry*. Nature Publishing Group, 4(10), pp. 802–809. doi: 10.1038/nchem.1435.

Xu, D.-D. *et al.* (2015) 'Serum protein S100A9, SOD3, and MMP9 as new diagnostic biomarkers for pulmonary tuberculosis by iTRAQ-coupled two-dimensional LC-MS/MS.', *Proteomics*, 15(1), pp. 58–67. doi: 10.1002/pmic.201400366.

Xu, S. *et al.* (1994) 'Intracellular trafficking in Mycobacterium tuberculosis and Mycobacterium avium-infected macrophages.', *Journal of Immunology*. American Association of Immunologists, 153(6), pp. 2568–2578.

Yanez, M. A. *et al.* (1986) 'Determination of Mycobacterial Antigens in Sputum by Enzyme Immunoassay', *Journal of Clinical Microbiology*, 23(5), pp. 822–825.

Youmans, G. (1979) *Tuberculosis*. Philadelphia: Saunders.

Young, B. L. *et al.* (2014) 'The identification of tuberculosis biomarkers in human urine samples.', *The European Respiratory Journal*, 43(6), pp. 1719–1729. doi: 10.1183/09031936.00175113.

Young, C. C. (1924) 'Public Health Laboratory Notes', *The American Journal of Public Health*, 14(2), p. 153. doi: 10.2105/AJPH.14.2.152.

Young, D. B., Gideon, H. P. and Wilkinson, R. J. (2009) 'Eliminating latent tuberculosis', *Trends in Microbiology*, 17(5), pp. 183–188. doi: 10.1016/j.tim.2009.02.005.

Zahnd, C., Amstutz, P. and Plückthun, A. (2007) 'Ribosome display: selecting and evolving proteins in vitro that specifically bind to a target', *Nature Methods*, 4(3), pp. 269–279. doi: 10.1038/nmeth1003.

Zak, D. E. *et al.* (2016) 'A blood RNA signature for tuberculosis disease risk: a prospective cohort study', *Lancet*, 387(10035), pp. 2312–2322. doi: 10.1016/S0140-6736(15)01316-1.

Zámocký, M. *et al.* (2014) 'Turning points in the evolution of peroxidase–catalase superfamily: molecular phylogeny of hybrid heme peroxidases', *Cellular and Molecular Life Sciences*, 71(23), pp. 4681–4696. doi: 10.1007/s00018-014-1643-y.

Zandarashvili, L. *et al.* (2015) 'Entropic Enhancement of Protein-DNA Affinity by Oxygen-to-

Sulfur Substitution in DNA Phosphate', *Biophysical Journal*, 109(5), pp. 1026–1037. doi: 10.1016/j.bpj.2015.07.032.

Zar, H. J. *et al.* (2005) 'Induced sputum versus gastric lavage for microbiological confirmation of pulmonary tuberculosis in infants and young children: a prospective study', *The Lancet*, 365(9454), pp. 130–134. doi: 10.1016/S0140-6736(05)17702-2.

Zar, H. J., Workman, L. and Nicol, M. (2017) 'Diagnosis Of Pulmonary Tuberculosis In Hiv-Infected And Uninfected Children Using Xpert Mtb / rif Ultra', in *American Thoracic Society 2017 International Conference*, p. 7610.

Zhang, H. *et al.* (2014) 'Identification of Serum microRNA Biomarkers for Tuberculosis Using RNA-seq', *PLoS ONE*. Edited by T. J. Scriba, 9(2), p. e88909. doi: 10.1371/journal.pone.0088909.

Zhang, Y. (2003) 'Mode of action of pyrazinamide: disruption of Mycobacterium tuberculosis membrane transport and energetics by pyrazinoic acid', *Journal of Antimicrobial Chemotherapy*. Oxford University Press, 52(5), pp. 790–795. doi: 10.1093/jac/dkg446.

Zheng, Y. *et al.* (2015) 'A label-free electrochemical aptasensor based on the catalysis of manganese porphyrins for detection of thrombin.', *Biosensors & Bioelectronics*, 66, pp. 585–9. doi: 10.1016/j.bios.2014.12.022.

Zhou, J., Battig, M. R. and Wang, Y. (2010) 'Aptamer-based molecular recognition for biosensor development', *Analytical and Bioanalytical Chemistry*, 398(6), pp. 2471–2480. doi: 10.1007/s00216-010-3987-y.

Zuker, M. (2003) 'Mfold web server for nucleic acid folding and hybridization prediction', *Nucleic Acids Research*. Oxford University Press, 31(13), pp. 3406–3415. doi: 10.1093/nar/gkg595.

Zuker, M. (2010) 'Mfold © : RNA modeling program', *GERF Bulletin of Biosciences*.

APPENDIX A

Binding curve results

Table A2 Mean absorbance readings for ESAT-6 ELISA binding curves. Each point is the mean of triplicate wells except for rESAT-6 10 ng/ml and 5 ng/ml in PBS which were in duplicate. The estimated limit of detection in each medium is shaded with grey.

rESAT-6 (ng/ml)	PBS	Lyophilised Urine	Neat Urine
10.00	0.420	0.694	0.414
5.00	0.397	0.566	0.367
2.50	0.331	0.478	0.286
1.25	0.272	0.418	0.211
0.63	0.199	0.380	0.177
0.31	0.168	0.373	0.168
0.15	0.151	0.355	0.157
Negative Control	0.140	0.347	0.131
Cut-off	0.206	0.377	0.159

ELISA Patient Sample Information and Results

Table A3 Urine sample patient details

Patient	HIV Status	CD4+ cells/µl	TB Status	Renal disease	Protein in Urine	Assay
UA133	Positive	17	TB +	No	*	ELISA
UA141	Positive	54	TB +	No	*	ELISA
UA158	Positive	6	TB +	No	*	ELISA
UA215	Positive	84	TB +	Yes	1+	ELISA
UA310	Positive	164	TB +	Yes	*	ELISA
UA120	Positive	112	TB +	No	trace	MS; WB
UA127	Positive	146	TB +	No	1+	MS; WB
UA211	Positive	5	TB +	No	trace	MS; WB
UA268	Negative	*	TB +	No	*	MS; WB
UA137	Positive	17	TB +	No	*	WB
UA144	Positive	*	TB +	No	*	WB
UA167	Positive	*	TB +	No	*	WB

*Data not available; *M. tuberculosis* detected by culturing sputum (TB +); Protein in urine grading: negative (less than 10 mg per dL), trace (10 to 20 mg per dL), 1+ (30 mg per dL), 2+ (100 mg per dL), 3+ (300 mg per dL) or 4+ (1,000 mg per dL); Western Blot (WB); Enzyme linked immunoassay (ELISA); Mass Spectrometry (MS)

Table A4 Mean absorbance readings from in-house ESAT 6 ELISA using urine samples

Sample numbers	**5 kDa MWCO filter**	**Lyophilised**	**Neat**
UA133	0.105	0.122	0.089
UA141	0.387*	0.146	0.078
UA158	0.116	0.081	0.094
UA215	0.548*	0.144	0.087
UA310	0.108	0.092	0.084
H1	0.096	0.094	0.084
H2	0.171	0.150	0.085
H3	0.111	0.312*	0.098
H4	0.106	0.098	0.089
H5	0.315*	0.153	0.094
Negative Control	0.125	0.125	0.125
Cut-off	0.258	0.258	0.258
*Absorbance reading above the cut-off			

Table A5 Sputum sample patient details and absorbance readings from in-house ESAT-6 ELISA

Patient	**#Absorbance**	**TB Status**	**Culture**	**T-SPOT®. TB**
TBN58	0.111	TB+	+	*
TBN59	0.108	TB+	+	*
TBN141	0.125	TB+	+	*
TBN145	0.113	TB+	+	*
TBN162	0.143	TB+	+	*
TBN274	0.148	TB+	+	*
TBN73	0.170	LTBI	-	+
TBN113	0.210	LTBI	-	+
TBN146	0.115	LTBI	-	+
TBN164	0.260	LTBI	-	+
TBN282	0.548	LTBI	-	+
TBN35	0.106	TB-	-	-
TBN397	0.155	TB-	-	-
TBN399	0.140	TB-	-	-
TBN465	0.317	TB-	-	-
TBN468	0.270	TB-	-	-
Negative control	0,117	n/a	n/a	n/a

*Data not available or test not performed; *M. tuberculosis* detected by culturing sputum (TB +); positive T-SPOT®.TB and negative culture (LTBI); negative T-SPOT®.TB and negative culture (TB -).

Max Quant

MaxQuant Settings

Table A6 MaxQuant Parameters

Parameter	Value
Version	1.5.3.12
Fixed modifications	Carbamidomethyl (C)
Decoy mode	revert
Special AAs	KR
Include contaminants	TRUE
MS/MS toll. (FTMS)	20 ppm
Top MS/MS peaks per 100 Da. (FTMS)	12
MS/MS deisotoping (FTMS)	TRUE
MS/MS tol. (ITMS)	0.5 Da
Top MS/MS peaks per 100 Da. (ITMS)	8
MS/MS deisotoping (ITMS)	FALSE
MS/MS tol. (TOF)	40 ppm
Top MS/MS peaks per 100 Da. (TOF)	10
MS/MS deisotoping (TOF)	TRUE
MS/MS tol. (Unknown)	0.5 Da
Top MS/MS peaks per 100 Da. (Unknown)	8
MS/MS deisotoping (Unknown)	FALSE
PSM FDR	0.01
Protein FDR	0.01
Site FDR	0.01
Use Normalized Ratios For Occupancy	TRUE

Parameter	**Value**
Min. peptide Length	7
Min. score for unmodified peptides	0
Min. score for modified peptides	40
Min. delta score for unmodified peptides	0
Min. delta score for modified peptides	6
Min. unique peptides	0
Min. razor peptides	1
Min. peptides	1
Use only unmodified peptides and	TRUE
Modifications included in protein quantification	Oxidation (M); Acetyl (Protein N-term)
Peptides used for protein quantification	Razor
Discard unmodified counterpart peptides	TRUE
Min. ratio count	2
Use delta score	FALSE
iBAQ	FALSE
iBAQ log fit	FALSE
Match between runs	FALSE
Find dependent peptides	FALSE
Fasta file	E:\2016\Protein_databases_2016\Uniprot_human_proteome_Feb2016.fasta OR *M. tuberculosis* (strain ATCC 25618 / H37Rv) _ UP000001584_Feb2016.fasta
Labelled amino acid filtering	TRUE
Site tables	Oxidation (M)Sites.txt
Decoy mode	revert

Parameter	Value
Special AAs	KR
Include contaminants	TRUE
RT shift	FALSE
Advanced ratios	TRUE
AIF correlation	0
First pass AIF correlation	0
AIF topx	0
AIF min mass	0
AIF SIL weight	0
AIF ISO weight	0
AIF iterative	FALSE
AIF threshold FDR	0

MaxQuant Results

Table A7 MaxQuant Results (majority protein IDs are displayed for simplicity). Protein IDs which had at least one unique peptide in each patient for each gel slice respectively is indicated by 25-35 kDa and 130-250 kDa unique peptides. Majority proteins with one or more Ig or Ig-like domain are indicated in the last column. Decimal separator in this table are commas.

Majority protein IDs	Protein names	Score	Intensity overall	Mass	25-35 kDa unique peptides	130-250 kDa unique peptides	Ig related
A0A087WV47	Ig gamma-1 chain C region	323,31	3,13E+11	51,154	No	No	No
P02760	Protein AMBP [Cleaved into: Alpha-1-microglobulin (Protein HC) (Alpha-1 microglycoprotein) (Complex-forming glycoprotein heterogeneous in charge); Inter-alpha-trypsin inhibitor light chain (ITI-LC) (Bikunin) (EDC1) (HI-30) (Uronic-acid-rich protein); Trypstatin]	323,31	1,58E+11	38,999	Yes	Yes	No
A0A087WZW8	Ig kappa chain C region	323,31	1,30E+11	12,997	Yes	Yes	Yes
A0A024R6I7	Alpha-1-antitrypsin (Serpin peptidase inhibitor, clade A (Alpha-1 antiproteinase, antitrypsin), member 1, isoform CRA_a)	323,31	6,76E+10	46,708	Yes	Yes	No
P01876	Ig alpha-1 chain C region	323,31	3,56E+10	37,655	No	Yes	Yes
A0A0G2JN06	Ig gamma-2 chain C region (Fragment)	323,31	2,82E+10	35,901	No	Yes	Yes
A0A087WXL8	Ig gamma-3 chain C region	323,31	2,42E+10	56,89	No	No	No
P00915	Carbonic anhydrase 1 (EC 4.2.1.1) (Carbonate dehydratase I) (Carbonic anhydrase B) (CAB) (Carbonic anhydrase I) (CA-I)	323,31	1,96E+10	28,87	No	No	No
E9PFZ2	Ceruloplasmin	323,31	1,83E+10	108,82	No	No	No
P01011	Alpha-1-antichymotrypsin (ACT) (Cell growth-inhibiting gene 24/25 protein) (Serpin A3) [Cleaved into: Alpha-1-antichymotrypsin His-Pro-less]	323,31	1,82E+10	47,651	Yes	Yes	No

Majority protein IDs	Protein names	Score	Intensity overall	Mass	25-35 kDa unique peptides	130-250 kDa unique peptides	Ig related
P02750	Leucine-rich alpha-2-glycoprotein (LRG)	323,31	1,62E+10	38,178	Yes	Yes	Yes
B4E1Z4	Uncharacterized protein (cDNA FLJ55673, highly similar to Complement factor B (EC 3.4.21.47))	323,31	1,57E+10	140,943	Yes	No	No
A0A075B6L0	Ig lambda-3 chain C regions (Fragment)	142,05	1,35E+10	11,32	No	No	No
P01024	Complement C3 (C3 and PZP-like alpha-2-macroglobulin domain-containing protein 1) [Cleaved into: Complement C3 beta chain; C3-beta-c (C3bc); Complement C3 alpha chain; C3a anaphylatoxin; Acylation stimulating protein (ASP) (C3adesArg); Complement C3b alpha' chain; Complement C3c alpha' chain fragment 1; Complement C3dg fragment; Complement C3g fragment; Complement C3d fragment; Complement C3f fragment; Complement C3c alpha' chain fragment 2]	323,31	1,27E+10	187,148	Yes	Yes	No
P0C0L5	Complement C4-B (Basic complement C4) (C3 and PZP-like alpha-2-macroglobulin domain-containing protein 3) [Cleaved into: Complement C4 beta chain; Complement C4-B alpha chain; C4a anaphylatoxin; C4b-B; C4d-B; Complement C4 gamma chain]	323,31	1,23E+10	192,751	No	No	No
P01623	Ig kappa chain V-III region WOL	323,31	1,17E+10	11,746	No	No	No
P02763	Alpha-1-acid glycoprotein 1 (AGP 1) (Orosomucoid-1) (OMD 1)	323,31	8,76E+09	23,512	Yes	Yes	No
P00738	Haptoglobin (Zonulin) [Cleaved into: Haptoglobin alpha chain; Haptoglobin beta chain]	295,10	8,14E+09	45,205	Yes	Yes	No
P18135	Ig kappa chain V-III region HAH	287,23	7,16E+09	14,073	No	No	No
A0A0G2JPD4	Ig gamma-4 chain C region (Fragment)	233,96	6,92E+09	35,941	No	Yes	Yes
A0A0A0MS51	Gelsolin	323,31	6,82E+09	82,526	Yes	No	No

Majority protein IDs	Protein names	Score	Intensity overall	Mass	25-35 kDa unique peptides	130-250 kDa unique peptides	Ig related
P08571	Monocyte differentiation antigen CD14 (Myeloid cell-specific leucine-rich glycoprotein) (CD antigen CD14) [Cleaved into: Monocyte differentiation antigen CD14, urinary form; Monocyte differentiation antigen CD14, membrane-bound form]	323,31	6,48E+09	40,076	Yes	No	No
B7ZKJ8	ITIH4 protein (Inter-alpha-trypsin inhibitor heavy chain H4)	323,31	6,41E+09	103,881	Yes	No	No
P01019	Angiotensinogen (Serpin A8) [Cleaved into: Angiotensin-1 (Angiotensin 1-10) (Angiotensin I) (Ang I); Angiotensin-2 (Angiotensin 1-8) (Angiotensin II) (Ang II); Angiotensin-3 (Angiotensin 2-8) (Angiotensin III) (Ang III) (Des-Asp[1]-angiotensin II); Angiotensin-4 (Angiotensin 3-8) (Angiotensin IV) (Ang IV); Angiotensin 1-9; Angiotensin 1-7; Angiotensin 1-5; Angiotensin 1-4]	323,31	5,91E+09	53,154	Yes	Yes	No
C9JF17	Apolipoprotein D (Fragment)	323,31	5,55E+09	24,158	Yes	No	No
P41222	Prostaglandin-H2 D-isomerase (EC 5.3.99.2) (Beta-trace protein) (Cerebrin-28) (Glutathione-independent PGD synthase) (Lipocalin-type prostaglandin-D synthase) (Prostaglandin-D2 synthase) (PGD2 synthase) (PGDS) (PGDS2)	148,96	5,11E+09	21,029	Yes	No	No
P80748	Ig lambda chain V-III region LOI	266,75	4,84E+09	11,935	Yes	Yes	Yes
P02790	Hemopexin (Beta-1B-glycoprotein)	323,31	4,71E+09	51,676	Yes	Yes	No
P04264	Keratin, type II cytoskeletal 1 (67 kDa cytokeratin) (Cytokeratin-1) (CK-1) (Hair alpha protein) (Keratin-1) (K1) (Type-II keratin Kb1)	323,31	4,21E+09	66,039	Yes	Yes	No
A0A087WW89	Protein IGHV3-72	225,05	4,19E+09	11,167	No	No	No
P01625	Ig kappa chain V-IV region Len	188,03	3,54E+09	12,64	No	Yes	Yes
D6RBV2	Vesicular integral-membrane protein VIP36	323,31	3,36E+09	36,543	Yes	No	No
P01621	Ig kappa chain V-III region NG9 (Fragment)	43,04	3,33E+09	10,729	Yes	Yes	Yes

Majority protein IDs	Protein names	Score	Intensity overall	Mass	25-35 kDa unique peptides	130-250 kDa unique peptides	Ig related
P25311	Zinc-alpha-2-glycoprotein (Zn-alpha-2-GP) (Zn-alpha-2-glycoprotein)	323,31	3,05E+09	34,259	Yes	No	Yes
Q9UBR2	Cathepsin Z (EC 3.4.18.1) (Cathepsin P) (Cathepsin X)	155,70	2,93E+09	33,868	Yes	No	No
P02787	Serotransferrin (Transferrin) (Beta-1 metal-binding globulin) (Siderophilin)	323,31	2,89E+09	77,064	Yes	Yes	No
P01779	Ig heavy chain V-III region TUR	151,70	2,32E+09	12,431	No	No	No
A0A0A0MTQ6	Protein IGKV2D-28	112,62	2,24E+09	11,043	No	Yes	Yes
P05155	Plasma protease C1 inhibitor (C1 Inh) (C1Inh) (C1 esterase inhibitor) (C1-inhibiting factor) (Serpin G1)	257,37	2,19E+09	55,154	Yes	Yes	No
P01714	Ig lambda chain V-III region SH	112,04	1,95E+09	11,393	Yes	Yes	Yes
P59666	Neutrophil defensin 3 (Defensin, alpha 3) (HNP-3) (HP-3) (HP3) [Cleaved into: HP 3-56; Neutrophil defensin 2 (HNP-2) (HP-2) (HP2)]	79,60	1,72E+09	10,245	Yes	Yes	No
A0A0C4DH40	Protein IGHV4-59 (Fragment)	268,56	1,60E+09	12,936	No	No	No
A0A087WYJ9	Ig mu chain C region	12,78	1,56E+09	65,701	No	Yes	Yes
P60709	Actin, cytoplasmic 1 (Beta-actin) [Cleaved into: Actin, cytoplasmic 1, N-terminally processed]	237,36	1,41E+09	41,737	Yes	Yes	No
P01610	Ig kappa chain V-I region WEA	264,72	1,34E+09	11,84	No	No	No
X6RBG4	Uromodulin	214,33	1,29E+09	75,663	No	Yes	No
A0A087X130	Ig kappa chain C region (Fragment)	208,02	1,24E+09	11,72	No	No	No
A0A0J9YY99	Uncharacterized protein (Fragment)	262,75	1,24E+09	12,965	No	No	No
A0A075B6I5	Protein IGLV1-51 (Fragment)	62,63	1,23E+09	12,619	Yes	No	Yes
P07339	Cathepsin D (EC 3.4.23.5) [Cleaved into: Cathepsin D light chain; Cathepsin D heavy chain]	130,56	1,22E+09	44,552	Yes	No	No
P01598	Ig kappa chain V-I region EU	201,84	1,08E+09	11,788	No	No	No

Majority protein IDs	Protein names	Score	Intensity overall	Mass	25-35 kDa unique peptides	130-250 kDa unique peptides	Ig related
A0A087X0S5	Collagen alpha-1(VI) chain	309,35	1,05E+09	108,339	Yes	Yes	No
P01008	Antithrombin-III (ATIII) (Serpin C1)	281,12	1,02E+09	52,602	Yes	Yes	No
P15144	Aminopeptidase N (AP-N) (hAPN) (EC 3.4.11.2) (Alanyl aminopeptidase) (Aminopeptidase M) (AP-M) (Microsomal aminopeptidase) (Myeloid plasma membrane glycoprotein CD13) (gp150) (CD antigen CD13)	246,64	9,98E+08	109,54	No	Yes	No
A0A075B6I0	Protein IGLV8-61 (Fragment)	37,45	9,26E+08	12,901	No	Yes	Yes
A0A087WTX5	Ig kappa chain C region	46,12	9,13E+08	26,096	No	No	No
Q99459	Cell division cycle 5-like protein (Cdc5-like protein) (Pombe cdc5-related protein)	6,84	9,11E+08	92,251	No	Yes	No
A0A087X2C0	Ig mu chain C region	238,99	8,38E+08	64,106	No	No	No
O95336	6-phosphogluconolactonase (6PGL) (EC 3.1.1.31)	188,66	7,93E+08	27,547	No	No	No
P05543	Thyroxine-binding globulin (Serpin A7) (T4-binding globulin)	284,31	7,89E+08	46,325	No	No	No
Q9BYE9	Cadherin-related family member 2 (Protocadherin LKC) (PC-LKC) (Protocadherin-24)	293,74	7,67E+08	141,543	No	Yes	No
A0A087WYC5	Ig gamma-1 chain C region	93,90	7,67E+08	52,426	No	No	No
P04004	Vitronectin (VN) (S-protein) (Serum-spreading factor) (V75) [Cleaved into: Vitronectin V65 subunit; Vitronectin V10 subunit; Somatomedin-B]	167,04	7,31E+08	54,306	No	No	No
P35908	Keratin, type II cytoskeletal 2 epidermal (Cytokeratin-2e) (CK-2e) (Epithelial keratin-2e) (Keratin-2 epidermis) (Keratin-2e) (K2e) (Type-II keratin Kb2)	185,59	7,25E+08	65,433	Yes	Yes	No

Majority protein IDs	Protein names	Score	Intensity overall	Mass	25-35 kDa unique peptides	130-250 kDa unique peptides	Ig related
P06702	Protein S100-A9 (Calgranulin-B) (Calprotectin L1H subunit) (Leukocyte L1 complex heavy chain) (Migration inhibitory factor-related protein 14) (MRP-14) (p14) (S100 calcium-binding protein A9)	127,12	7,09E+08	13,242	Yes	Yes	No
P36955	Pigment epithelium-derived factor (PEDF) (Cell proliferation-inducing gene 35 protein) (EPC-1) (Serpin F1)	148,04	6,95E+08	46,312	No	No	No
P69905	Hemoglobin subunit alpha (Alpha-globin) (Hemoglobin alpha chain)	48,07	6,91E+08	15,258	Yes	Yes	No
P19320	Vascular cell adhesion protein 1 (V-CAM 1) (VCAM-1) (INCAM-100) (CD antigen CD106)	130,17	6,84E+08	81,276	Yes	No	Yes
A0A0B4J1Z4	Protein IGKV1-17 (Fragment)	195,52	6,74E+08	12,779	No	Yes	Yes
E9PIT3	Prothrombin	323,31	6,63E+08	65,409	No	No	No
D6RF35	Vitamin D-binding protein	271,65	6,41E+08	53,021	Yes	No	No
A0A0C4DH25	Protein IGKV3D-20 (Fragment)	23,93	6,40E+08	12,515	No	No	No
Q92820	Gamma-glutamyl hydrolase (EC 3.4.19.9) (Conjugase) (GH) (Gamma-Glu-X carboxypeptidase)	136,15	6,09E+08	35,964	Yes	No	No
Q12805	EGF-containing fibulin-like extracellular matrix protein 1 (Extracellular protein S1-5) (Fibrillin-like protein) (Fibulin-3) (FIBL-3)	226,84	6,03E+08	54,641	No	No	No
A0A087WZH9	Protein IGKV1-33 (Protein IGKV1D-33)	85,51	6,03E+08	11,842	No	No	No
P98164	Low-density lipoprotein receptor-related protein 2 (LRP-2) (Glycoprotein 330) (gp330) (Megalin)	323,31	6,01E+08	521,958	No	Yes	No
P07195	L-lactate dehydrogenase B chain (LDH-B) (EC 1.1.1.27) (LDH heart subunit) (LDH-H) (Renal carcinoma antigen NY-REN-46)	120,22	5,89E+08	36,638	No	No	No
P04217	Alpha-1B-glycoprotein (Alpha-1-B glycoprotein)	170,74	5,77E+08	54,254	Yes	Yes	Yes

Majority protein IDs	Protein names	Score	Intensity overall	Mass	25-35 kDa unique peptides	130-250 kDa unique peptides	Ig related
P00747	Plasminogen (EC 3.4.21.7) [Cleaved into: Plasmin heavy chain A; Activation peptide; Angiostatin; Plasmin heavy chain A, short form; Plasmin light chain B]	171,62	5,65E+08	90,569	Yes	No	No
P68871	Hemoglobin subunit beta (Beta-globin) (Hemoglobin beta chain) [Cleaved into: LVV-hemorphin-7; Spinorphin]	176,21	5,64E+08	15,998	Yes	Yes	No
P01042	Kininogen-1 (Alpha-2-thiol proteinase inhibitor) (Fitzgerald factor) (High molecular weight kininogen) (HMWK) (Williams-Fitzgerald-Flaujeac factor) [Cleaved into: Kininogen-1 heavy chain; T-kinin (Ile-Ser-Bradykinin); Bradykinin (Kallidin I); Lysyl-bradykinin (Kallidin II); Kininogen-1 light chain; Low molecular weight growth-promoting factor]	152,29	5,61E+08	71,957	Yes	Yes	No
P06331	Ig heavy chain V-II region ARH-77	21,35	5,48E+08	16,228	No	Yes	Yes
C9JEU5	Fibrinogen gamma chain	279,84	5,46E+08	50,322	No	No	No
A0A0C4DH38	Protein IGHV5-51 (Fragment)	51,23	5,32E+08	12,675	No	No	No
P02748	Complement component C9 [Cleaved into: Complement component C9a; Complement component C9b]	108,12	5,17E+08	63,173	No	No	No
A0A0C4DGN4	Uncharacterized protein (Zymogen granule protein 16 homolog B)	292,24	5,06E+08	19,6	Yes	No	No
P02671	Fibrinogen alpha chain [Cleaved into: Fibrinopeptide A; Fibrinogen alpha chain]	298,28	5,05E+08	94,973	Yes	Yes	No
P13473	Lysosome-associated membrane glycoprotein 2 (LAMP-2) (Lysosome-associated membrane protein 2) (CD107 antigen-like family member B) (CD antigen CD107b)	33,07	5,03E+08	44,961	Yes	No	No
P01767	Ig heavy chain V-III region BUT	32,06	4,85E+08	12,379	No	No	No

Majority protein IDs	Protein names	Score	Intensity overall	Mass	25-35 kDa unique peptides	130-250 kDa unique peptides	Ig related
P01009	Alpha-1-antitrypsin (Alpha-1 protease inhibitor) (Alpha-1-antiproteinase) (Serpin A1) [Cleaved into: Short peptide from AAT (SPAAT)]	206,14	4,82E+08	46,737	Yes	Yes	No
P01717	Ig lambda chain V-IV region Hil	54,79	4,81E+08	11,517	No	Yes	Yes
A0A0B4J1X5	Protein IGHV3-74 (Fragment)	18,47	4,72E+08	12,84	No	Yes	Yes
P08697	Alpha-2-antiplasmin (Alpha-2-AP) (Alpha-2-plasmin inhibitor) (Alpha-2-PI) (Serpin F2)	135,93	4,72E+08	54,566	No	No	No
P18428	Lipopolysaccharide-binding protein (LBP)	132,36	4,58E+08	53,384	No	No	No
P02751	Fibronectin (FN) (Cold-insoluble globulin) (CIG) [Cleaved into: Anastellin; Ugl-Y1; Ugl-Y2; Ugl-Y3]	160,37	4,51E+08	262,625	Yes	Yes	Yes
P04208	Ig lambda chain V-I region WAH	28,62	4,43E+08	11,725	No	No	No
P00748	Coagulation factor XII (EC 3.4.21.38) (Hageman factor) (HAF) [Cleaved into: Coagulation factor XIIa heavy chain; Beta-factor XIIa part 1; Coagulation factor XIIa light chain (Beta-factor XIIa part 2)]	148,16	4,41E+08	67,792	No	No	No
A0A087X0D5	Pro-cathepsin H	91,03	4,35E+08	36,269	Yes	No	No
P00450	Ceruloplasmin (EC 1.16.3.1) (Ferroxidase)	104,45	4,27E+08	122,205	No	No	No
P19652	Alpha-1-acid glycoprotein 2 (AGP 2) (Orosomucoid-2) (OMD 2)	251,21	4,17E+08	23,603	Yes	No	No
P01602	Ig heavy chain V-I region 5 (Ig kappa chain V-I region HK102) (Immunoglobulin kappa variable 1-5) (Fragment)	35,57	4,13E+08	12,782	No	No	No
P01824	Ig heavy chain V-II region WAH	28,30	4,13E+08	14,117	No	Yes	Yes
Q08380	Galectin-3-binding protein (Basement membrane autoantigen p105) (Lectin galactoside-binding soluble 3-binding protein) (Mac-2-binding protein) (MAC2BP) (Mac-2 BP) (Tumor-associated antigen 90K)	108,52	4,11E+08	65,331	No	Yes	No
A0A087WU91	Protein IGHV3-49	42,83	4,07E+08	12,332	No	No	No

Majority protein IDs	Protein names	Score	Intensity overall	Mass	25-35 kDa unique peptides	130-250 kDa unique peptides	Ig related
P08758	Annexin A5 (Anchorin CII) (Annexin V) (Annexin-5) (Calphobindin I) (CBP-I) (Endonexin II) (Lipocortin V) (Placental anticoagulant protein 4) (PP4) (Placental anticoagulant protein I) (PAP-I) (Thromboplastin inhibitor) (Vascular anticoagulant-alpha) (VAC-alpha)	233,40	4,06E+08	35,937	No	No	No
Q5VY30	Retinol binding protein 4, plasma, isoform CRA_b (Retinol-binding protein 4)	163,69	4,02E+08	22,974	No	Yes	No
A0A087WSY6	Protein IGKV3D-15 (Fragment)	8,17	3,99E+08	12,631	No	No	No
P62805	Histone H4	40,11	3,93E+08	11,367	Yes	Yes	No
P05109	Protein S100-A8 (Calgranulin-A) (Calprotectin L1L subunit) (Cystic fibrosis antigen) (CFAG) (Leukocyte L1 complex light chain) (Migration inhibitory factor-related protein 8) (MRP-8) (p8) (S100 calcium-binding protein A8) (Urinary stone protein band A) [Cleaved into: Protein S100-A8, N-terminally processed]	72,12	3,79E+08	10,835	Yes	Yes	No
P01608	Ig kappa chain V-I region Roy	-2,00	3,73E+08	11,782	No	Yes	Yes
Q13228	Selenium-binding protein 1 (56 kDa selenium-binding protein) (SBP56) (SP56)	158,48	3,72E+08	52,391	Yes	No	No
P02766	Transthyretin (ATTR) (Prealbumin) (TBPA)	125,99	3,63E+08	15,887	No	No	No
A0A0A0MTL4	Neuron navigator 2	6,51	3,62E+08	261,862	No	No	No
A0A0J9YVU5	Protein IGHV2-70 (Fragment)	6,77	3,61E+08	13,359	No	No	No
A0A075B6J0	Protein IGLV1-40 (Fragment)	45,06	3,51E+08	12,389	Yes	No	Yes
H7C3P4	N-acetylglucosamine-6-sulfatase (EC 3.1.6.14) (Glucosamine-6-sulfatase)	74,56	3,46E+08	56,374	Yes	No	No
A0A0C4DH68	Protein IGKV2-24 (Fragment)	101,61	3,32E+08	13,079	No	No	No

Majority protein IDs	Protein names	Score	Intensity overall	Mass	25-35 kDa unique peptides	130-250 kDa unique peptides	Ig related
P04207	Ig kappa chain V-III region CLL (Rheumatoid factor)	85,29	3,27E+08	14,275	Yes	No	Yes
A0A0G2JMB2	Ig alpha-2 chain C region (Fragment)	161,33	3,26E+08	36,508	No	No	No
Q5T985	Inter-alpha-trypsin inhibitor heavy chain H2	91,67	3,20E+08	105,216	No	No	No
A0A075B6J8	Protein IGLV3-19 (Fragment)	28,82	3,15E+08	12,042	No	No	No
A0A087WW43	Inter-alpha-trypsin inhibitor heavy chain H3	93,99	3,14E+08	75,078	No	No	No
P10153	Non-secretory ribonuclease (EC 3.1.27.5) (Eosinophil-derived neurotoxin) (RNase UpI-2) (Ribonuclease 2) (RNase 2) (Ribonuclease US)	40,88	3,13E+08	18,354	Yes	No	No
O96009	Napsin-A (EC 3.4.23.-) (Aspartyl protease 4) (ASP4) (Asp 4) (Napsin-1) (TA01/TA02)	58,46	3,12E+08	45,387	No	No	No
P24387	Corticotropin-releasing factor-binding protein (CRF-BP) (CRF-binding protein) (Corticotropin-releasing hormone-binding protein) (CRH-BP)	137,37	3,02E+08	36,144	No	No	No
Q9HCU0	Endosialin (Tumor endothelial marker 1) (CD antigen CD248)	86,23	3,01E+08	80,859	Yes	No	No
A0A075B6J4	Protein IGLV3-25 (Fragment)	24,02	2,98E+08	12,011	No	No	No
Q16270	Insulin-like growth factor-binding protein 7 (IBP-7) (IGF-binding protein 7) (IGFBP-7) (IGFBP-rP1) (MAC25 protein) (PGI2-stimulating factor) (Prostacyclin-stimulating factor) (Tumor-derived adhesion factor) (TAF)	100,63	2,97E+08	29,13	Yes	No	Yes
P61769	Beta-2-microglobulin [Cleaved into: Beta-2-microglobulin form pI 5.3]	55,03	2,87E+08	13,715	No	Yes	Yes
A0A075B7B8	Protein IGHV3OR16-12 (Fragment)	67,70	2,86E+08	12,875	No	No	No
P01699	Ig lambda chain V-I region VOR	6,96	2,84E+08	11,515	No	Yes	Yes
A0A075B6S3	Protein IGKV2-30 (Fragment)	58,40	2,82E+08	13,185	No	No	No
P15085	Carboxypeptidase A1 (EC 3.4.17.1)	202,59	2,80E+08	47,14	No	No	No

Majority protein IDs	Protein names	Score	Intensity overall	Mass	25-35 kDa unique peptides	130-250 kDa unique peptides	Ig related
P01612	Ig kappa chain V-I region Mev	6,56	2,73E+08	11,87	No	No	No
P0C0L4	Complement C4-A (Acidic complement C4) (C3 and PZP-like alpha-2-macroglobulin domain-containing protein 2) [Cleaved into: Complement C4 beta chain; Complement C4-A alpha chain; C4a anaphylatoxin; C4b-A; C4d-A; Complement C4 gamma chain]	26,66	2,71E+08	192,785	No	No	No
P01133	Pro-epidermal growth factor (EGF) [Cleaved into: Epidermal growth factor (Urogastrone)]	112,62	2,67E+08	133,994	No	No	No
Q99972	Myocilin (Myocilin 55 kDa subunit) (Trabecular meshwork-induced glucocorticoid response protein) [Cleaved into: Myocilin, N-terminal fragment (Myocilin 20 kDa N-terminal fragment); Myocilin, C-terminal fragment (Myocilin 35 kDa N-terminal fragment)]	107,89	2,64E+08	56,972	No	No	No
P01597	Ig kappa chain V-I region DEE	14,58	2,57E+08	11,661	No	No	No
P23083	Ig heavy chain V-I region V35	10,18	2,56E+08	13,009	No	No	No
E7EQB2	Lactotransferrin (Fragment)	119,24	2,53E+08	76,626	Yes	No	No
A0A0A0MT74	Protein IGKV1-16 (Fragment)	66,92	2,52E+08	12,618	No	Yes	Yes
O75882	Attractin (DPPT-L) (Mahogany homolog)	197,82	2,51E+08	158,537	No	Yes	No
Q07075	Glutamyl aminopeptidase (EAP) (EC 3.4.11.7) (Aminopeptidase A) (AP-A) (Differentiation antigen gp160) (CD antigen CD249)	123,51	2,48E+08	109,244	No	No	No
P01781	Ig heavy chain V-III region GAL	56,63	2,47E+08	12,731	No	No	No
A0A075B6N7	Ig alpha-2 chain C region (Fragment)	108,98	2,46E+08	36,591	No	No	No
Q9NUQ9	Protein FAM49B (L1)	132,20	2,39E+08	36,748	No	No	No
P01619	Ig kappa chain V-III region B6	47,72	2,33E+08	11,636	No	No	No

Majority protein IDs	Protein names	Score	Intensity overall	Mass	25-35 kDa unique peptides	130-250 kDa unique peptides	Ig related
O60494	Cubilin (460 kDa receptor) (Intestinal intrinsic factor receptor) (Intrinsic factor-cobalamin receptor) (Intrinsic factor-vitamin B12 receptor)	169,71	2,26E+08	398,736	No	Yes	No
A0A0C4DGZ9	Tripeptidyl-peptidase 1	46,61	2,25E+08	60,458	No	No	No
C9J0D1	Histone H2A	18,29	2,24E+08	13,163	Yes	Yes	No
P04746	Pancreatic alpha-amylase (PA) (EC 3.2.1.1) (1,4-alpha-D-glucan glucanohydrolase)	118,41	2,10E+08	57,707	No	No	No
P01620	Ig kappa chain V-III region SIE	55,56	2,07E+08	11,775	No	No	No
P12111	Collagen alpha-3(VI) chain	173,33	2,05E+08	343,669	No	No	No
A0A087X0K0	Collagen alpha-1(XV) chain	36,39	1,99E+08	140,059	No	No	No
E7ESB3	NAD(P)(+)--arginine ADP-ribosyltransferase (EC 2.4.2.31) (Mono(ADP-ribosyl)transferase) (Fragment)	85,66	1,89E+08	23,179	No	No	No
P01703	Ig lambda chain V-I region NEWM	8,65	1,85E+08	10,904	No	No	No
P02743	Serum amyloid P-component (SAP) (9.5S alpha-1-glycoprotein) [Cleaved into: Serum amyloid P-component(1-203)]	118,42	1,84E+08	25,387	No	No	No
A0A0B4J2D9	Protein IGKV1D-13 (Fragment)	61,39	1,82E+08	12,569	No	Yes	Yes
O94919	Endonuclease domain-containing 1 protein (EC 3.1.30.-)	100,54	1,80E+08	55,017	No	No	No
Q16651	Prostasin (EC 3.4.21.-) (Channel-activating protease 1) (CAP1) (Serine protease 8) [Cleaved into: Prostasin light chain; Prostasin heavy chain]	100,13	1,79E+08	36,431	No	No	No
P24855	Deoxyribonuclease-1 (EC 3.1.21.1) (Deoxyribonuclease I) (DNase I) (Dornase alfa)	71,28	1,75E+08	31,434	No	No	No
P04430	Ig kappa chain V-I region BAN	141,93	1,74E+08	11,84	No	No	No
A0A075B6I8	Protein IGLV1-47 (Fragment)	30,34	1,72E+08	12,284	No	No	No

Majority protein IDs	Protein names	Score	Intensity overall	Mass	25-35 kDa unique peptides	130-250 kDa unique peptides	Ig related
P29508	Serpin B3 (Protein T4-A) (Squamous cell carcinoma antigen 1) (SCCA-1)	117,69	1,69E+08	44,565	No	No	No
O00560	Syntenin-1 (Melanoma differentiation-associated protein 9) (MDA-9) (Pro-TGF-alpha cytoplasmic domain-interacting protein 18) (TACIP18) (Scaffold protein Pbp1) (Syndecan-binding protein 1)	81,79	1,69E+08	32,444	Yes	No	No
P01772	Ig heavy chain V-III region KOL	30,56	1,69E+08	13,718	No	Yes	Yes
X6R8F3	Neutrophil gelatinase-associated lipocalin	186,51	1,69E+08	22,788	Yes	No	No
A0A087WUS7	Ig delta chain C region	84,41	1,63E+08	42,353	No	No	No
P0DJD9	Pepsin A-5 (EC 3.4.23.1) (Pepsinogen-5)	31,19	1,63E+08	41,993	No	No	No
U3KPS2	Myeloblastin	30,66	1,61E+08	23,611	No	No	No
A0A0B4J1X8	Protein IGHV3-43 (Fragment)	60,48	1,60E+08	13,077	No	No	No
A0A075B6I9	Protein IGLV7-46 (Fragment)	16,29	1,56E+08	12,468	No	No	No
A0A0B4J1Z7	Protein IGKV1-39 (Fragment)	10,60	1,52E+08	12,737	No	No	No
P10451	Osteopontin (Bone sialoprotein 1) (Nephropontin) (Secreted phosphoprotein 1) (SPP-1) (Urinary stone protein) (Uropontin)	201,11	1,49E+08	35,423	No	No	No
A0A0G2JRQ6	Uncharacterized protein (Fragment)	17,41	1,49E+08	12,846	No	No	No
P08185	Corticosteroid-binding globulin (CBG) (Serpin A6) (Transcortin)	36,42	1,48E+08	45,141	No	No	No
B2R4S9	Histone H2B	6,52	1,46E+08	13,906	Yes	Yes	No
E7ER45	Maltase-glucoamylase, intestinal	122,72	1,44E+08	312,022	No	Yes	No
Q16769	Glutaminyl-peptide cyclotransferase (EC 2.3.2.5) (Glutaminyl cyclase) (QC) (sQC) (Glutaminyl-tRNA cyclotransferase) (Glutamyl cyclase) (EC)	98,44	1,43E+08	40,877	No	No	No
A0A0A0MT36	Protein IGKV6D-21 (Fragment)	42,39	1,42E+08	12,34	No	No	No

Majority protein IDs	Protein names	Score	Intensity overall	Mass	25-35 kDa unique peptides	130-250 kDa unique peptides	Ig related
P07355	Annexin A2 (Annexin II) (Annexin-2) (Calpactin I heavy chain) (Calpactin-1 heavy chain) (Chromobindin-8) (Lipocortin II) (Placental anticoagulant protein IV) (PAP-IV) (Protein I) (p36)	158,50	1,41E+08	38,604	No	No	No
P46952	3-hydroxyanthranilate 3,4-dioxygenase (EC 1.13.11.6) (3-hydroxyanthranilate oxygenase) (3-HAO) (3-hydroxyanthranilic acid dioxygenase) (HAD)	89,38	1,40E+08	32,556	No	No	No
P10253	Lysosomal alpha-glucosidase (EC 3.2.1.20) (Acid maltase) (Aglucosidase alfa) [Cleaved into: 76 kDa lysosomal alpha-glucosidase; 70 kDa lysosomal alpha-glucosidase]	93,34	1,39E+08	105,324	No	No	No
P04209	Ig lambda chain V-II region NIG-84	16,87	1,38E+08	11,581	No	No	No
H0YD13	CD44 antigen	31,70	1,38E+08	22,683	Yes	Yes	No
X6R3L3	MOB kinase activator 3C	6,41	1,37E+08	31,726	No	No	No
A0A0G2JMI3	Uncharacterized protein (Fragment)	40,31	1,35E+08	12,871	No	No	No
P09525	Annexin A4 (35-beta calcimedin) (Annexin IV) (Annexin-4) (Carbohydrate-binding protein p33/p41) (Chromobindin-4) (Endonexin I) (Lipocortin IV) (P32.5) (PP4-X) (Placental anticoagulant protein II) (PAP-II) (Protein II)	89,02	1,35E+08	35,883	No	No	No
A0A0C4DGZ8	Glycoprotein Ib (Platelet), alpha polypeptide (Platelet glycoprotein Ib alpha chain)	41,29	1,33E+08	68,955	No	No	No
P01023	Alpha-2-macroglobulin (Alpha-2-M) (C3 and PZP-like alpha-2-macroglobulin domain-containing protein 5)	94,37	1,32E+08	163,291	No	No	No
Q14573	Inositol 1,4,5-trisphosphate receptor type 3 (IP3 receptor isoform 3) (IP3R 3) (InsP3R3) (Type 3 inositol 1,4,5-trisphosphate receptor) (Type 3 InsP3 receptor)	6,62	1,31E+08	304,106	No	No	No
A0A0C4DH34	Protein IGHV4-28 (Fragment)	15,65	1,29E+08	13,124	No	No	No

Majority protein IDs	Protein names	Score	Intensity overall	Mass	25-35 kDa unique peptides	130-250 kDa unique peptides	Ig related
Q15848	Adiponectin (30 kDa adipocyte complement-related protein) (Adipocyte complement-related 30 kDa protein) (ACRP30) (Adipocyte, C1q and collagen domain-containing protein) (Adipose most abundant gene transcript 1 protein) (apM-1) (Gelatin-binding protein)	22,17	1,25E+08	26,414	No	No	No
P04083	Annexin A1 (Annexin I) (Annexin-1) (Calpactin II) (Calpactin-2) (Chromobindin-9) (Lipocortin I) (Phospholipase A2 inhibitory protein) (p35)	200,48	1,23E+08	38,714	No	No	No
P98160	Basement membrane-specific heparan sulfate proteoglycan core protein (HSPG) (Perlecan) (PLC) [Cleaved into: Endorepellin; LG3 peptide]	62,92	1,23E+08	468,83	No	No	No
F8WE04	Heat shock protein beta-1	38,50	1,22E+08	20,406	No	No	No
P01833	Polymeric immunoglobulin receptor (PIgR) (Poly-Ig receptor) (Hepatocellular carcinoma-associated protein TB6) [Cleaved into: Secretory component]	79,55	1,20E+08	83,284	No	No	No
P01613	Ig kappa chain V-I region Ni	32,16	1,19E+08	12,246	No	No	No
P07737	Profilin-1 (Epididymis tissue protein Li 184a) (Profilin I)	42,80	1,17E+08	15,054	No	No	No
A0A075B6H9	Protein IGLV4-69 (Fragment)	21,55	1,11E+08	12,773	No	No	No
C9J6H2	Insulin-like growth factor-binding protein 1	31,85	1,10E+08	22,886	No	No	No
A0A075B6S5	Protein IGKV1-27 (Fragment)	19,60	1,09E+08	12,712	No	No	No
P01034	Cystatin-C (Cystatin-3) (Gamma-trace) (Neuroendocrine basic polypeptide) (Post-gamma-globulin)	67,24	1,08E+08	15,799	No	No	No
A0A0A0MS11	Protein IGHV3-13 (Fragment)	36,10	1,08E+08	12,506	No	No	No
P05062	Fructose-bisphosphate aldolase B (EC 4.1.2.13) (Liver-type aldolase)	90,87	1,08E+08	39,473	No	No	No

Majority protein IDs	Protein names	Score	Intensity overall	Mass	25-35 kDa unique peptides	130-250 kDa unique peptides	Ig related
Q5JS37	NHL repeat-containing protein 3	34,73	1,07E+08	38,283	Yes	No	No
C9JR67	Epsilon-sarcoglycan (Sarcoglycan epsilon isoform 2)	74,18	1,05E+08	48,751	No	No	No
P62258	14-3-3 protein epsilon (14-3-3E)	44,04	1,05E+08	29,174	No	No	No
P01742	Ig heavy chain V-I region EU	7,69	1,05E+08	12,472	No	Yes	Yes
P63104	14-3-3 protein zeta/delta (Protein kinase C inhibitor protein 1) (KCIP-1)	103,64	1,04E+08	27,745	No	No	No
I3L145	Sex hormone-binding globulin (Sex hormone-binding globulin, isoform CRA_a)	76,01	1,04E+08	37,488	No	No	No
P14543	Nidogen-1 (NID-1) (Entactin)	139,74	1,02E+08	136,377	No	No	No
Q5TEC6	Histone H3	26,68	1,01E+08	15,43	Yes	Yes	No
Q14165	Malectin	62,21	9,90E+07	32,234	No	No	No
P04431	Ig kappa chain V-I region Walker	45,70	9,89E+07	14,069	No	No	No
O75594	Peptidoglycan recognition protein 1 (Peptidoglycan recognition protein short) (PGRP-S)	149,79	9,78E+07	21,731	No	No	No
P83593	Ig kappa chain V-IV region STH (Fragment)	7,89	9,78E+07	12,06	No	No	No
P05154	Plasma serine protease inhibitor (Acrosomal serine protease inhibitor) (Plasminogen activator inhibitor 3) (PAI-3) (PAI3) (Protein C inhibitor) (PCI) (Serpin A5)	64,25	9,62E+07	45,675	No	No	No
E9PIM6	Thy-1 membrane glycoprotein (Fragment)	31,82	9,50E+07	17,041	Yes	No	Yes
C9JV77	Alpha-2-HS-glycoprotein	73,42	9,48E+07	39,412	No	No	No
A0A0G2JM94	Leukocyte-associated immunoglobulin-like receptor 1	162,85	9,47E+07	15,143	Yes	No	Yes
Q9Y5Z4	Heme-binding protein 2 (Placental protein 23) (PP23) (Protein SOUL)	178,52	9,39E+07	22,875	No	No	No
P01611	Ig kappa chain V-I region Wes	76,73	9,20E+07	11,608	No	No	No

Majority protein IDs	Protein names	Score	Intensity overall	Mass	25-35 kDa unique peptides	130-250 kDa unique peptides	Ig related
A0A0B4J2H0	Protein IGHV1-69-2 (Fragment)	8,28	9,15E+07	12,66	No	No	No
P00441	Superoxide dismutase [Cu-Zn] (EC 1.15.1.1) (Superoxide dismutase 1) (hSod1)	52,72	9,01E+07	15,936	No	No	No
P01594	Ig kappa chain V-I region AU	45,89	8,96E+07	11,939	No	No	No
O15230	Laminin subunit alpha-5 (Laminin-10 subunit alpha) (Laminin-11 subunit alpha) (Laminin-15 subunit alpha)	6,80	8,94E+07	399,737	No	No	No
A0A0C4DH31	Protein IGHV1-18 (Fragment)	35,90	8,92E+07	12,82	No	No	No
Q14118	Dystroglycan (Dystrophin-associated glycoprotein 1) [Cleaved into: Alpha-dystroglycan (Alpha-DG); Beta-dystroglycan (Beta-DG)]	33,93	8,89E+07	97,441	No	No	No
P53634	Dipeptidyl peptidase 1 (EC 3.4.14.1) (Cathepsin C) (Cathepsin J) (Dipeptidyl peptidase I) (DPP-I) (DPPI) (Dipeptidyl transferase) [Cleaved into: Dipeptidyl peptidase 1 exclusion domain chain (Dipeptidyl peptidase I exclusion domain chain); Dipeptidyl peptidase 1 heavy chain (Dipeptidyl peptidase I heavy chain); Dipeptidyl peptidase 1 light chain (Dipeptidyl peptidase I light chain)]	47,51	8,85E+07	51,854	No	No	No
P00338	L-lactate dehydrogenase A chain (LDH-A) (EC 1.1.1.27) (Cell proliferation-inducing gene 19 protein) (LDH muscle subunit) (LDH-M) (Renal carcinoma antigen NY-REN-59)	55,93	8,81E+07	36,689	No	No	No
A0A087WXI5	Cadherin-1	65,02	8,73E+07	100,027	No	No	No
P00491	Purine nucleoside phosphorylase (PNP) (EC 2.4.2.1) (Inosine phosphorylase) (Inosine-guanosine phosphorylase)	67,36	8,71E+07	32,118	No	No	No
J3QS39	Polyubiquitin-B (Fragment)	81,70	8,65E+07	10,469	Yes	Yes	No
A0A087WVJ0	Mucin-1 (Fragment)	37,23	8,57E+07	25,566	Yes	No	No
Q6EMK4	Vasorin (Protein slit-like 2)	97,09	8,48E+07	71,713	No	No	No
F8VYK9	Insulin-like growth factor-binding protein 6	275,61	8,38E+07	25,152	No	No	No

Majority protein IDs	Protein names	Score	Intensity overall	Mass	25-35 kDa unique peptides	130-250 kDa unique peptides	Ig related
P10909	Clusterin (Aging-associated gene 4 protein) (Apolipoprotein J) (Apo-J) (Complement cytolysis inhibitor) (CLI) (Complement-associated protein SP-40,40) (Ku70-binding protein 1) (NA1/NA2) (Testosterone-repressed prostate message 2) (TRPM-2) [Cleaved into: Clusterin beta chain (ApoJalpha) (Complement cytolysis inhibitor a chain); Clusterin alpha chain (ApoJbeta) (Complement cytolysis inhibitor b chain)]	51,21	8,32E+07	52,495	No	No	No
E9PHH3	Syndecan-1	56,05	8,14E+07	17,782	No	No	No
A0A024QZX5	Serpin B6 (Serpin peptidase inhibitor, clade B (Ovalbumin), member 6, isoform CRA_d)	29,52	8,14E+07	43,024	No	No	No
A0A0C4DH35	Protein IGHV3-35 (Fragment)	18,51	8,00E+07	12,81	No	No	No
P27487	Dipeptidyl peptidase 4 (EC 3.4.14.5) (ADABP) (Adenosine deaminase complexing protein 2) (ADCP-2) (Dipeptidyl peptidase IV) (DPP IV) (T-cell activation antigen CD26) (TP103) (CD antigen CD26) [Cleaved into: Dipeptidyl peptidase 4 membrane form (Dipeptidyl peptidase IV membrane form); Dipeptidyl peptidase 4 soluble form (Dipeptidyl peptidase IV soluble form)]	59,74	7,92E+07	88,279	No	No	No
Q9UKU9	Angiopoietin-related protein 2 (Angiopoietin-like protein 2)	54,33	7,65E+07	57,104	No	No	No
A4UGR9	Xin actin-binding repeat-containing protein 2 (Beta-xin) (Cardiomyopathy-associated protein 3) (Xeplin)	10,59	7,50E+07	382,3	No	No	No
Q96S96	Phosphatidylethanolamine-binding protein 4 (PEBP-4) (hPEBP4) (Protein cousin-of-RKIP 1)	29,00	7,37E+07	25,733	No	No	No
Q9Y490	Talin-1	58,15	7,33E+07	269,767	No	No	No
A0A075B6J9	HCG1782423 (Protein IGLV2-18) (Fragment)	13,53	7,28E+07	12,705	No	No	No

Majority protein IDs	Protein names	Score	Intensity overall	Mass	25-35 kDa unique peptides	130-250 kDa unique peptides	Ig related
Q96FE7	Phosphoinositide-3-kinase-interacting protein 1 (Kringle domain-containing protein HGFL)	19,34	7,16E+07	28,248	Yes	No	No
P98172	Ephrin-B1 (EFL-3) (ELK ligand) (ELK-L) (EPH-related receptor tyrosine kinase ligand 2) (LERK-2)	48,30	7,12E+07	38,007	No	No	No
Q6PK18	2-oxoglutarate and iron-dependent oxygenase domain-containing protein 3 (EC 1.14.11.-)	75,57	7,07E+07	35,646	No	No	No
B0QYF8	Myoglobin (Fragment)	29,67	7,07E+07	15,989	No	No	No
Q71U36	Tubulin alpha-1A chain (Alpha-tubulin 3) (Tubulin B-alpha-1) (Tubulin alpha-3 chain)	69,52	7,06E+07	50,136	No	No	No
P56537	Eukaryotic translation initiation factor 6 (eIF-6) (B(2)GCN homolog) (B4 integrin interactor) (CAB) (p27(BBP))	30,72	7,02E+07	26,599	No	No	No
A0A0C4DH33	Protein IGHV1-24 (Fragment)	10,71	6,96E+07	12,824	No	No	No
G3XAM2	Complement factor I (Complement factor I, isoform CRA_b)	29,30	6,87E+07	65,06	No	No	No
P18669	Phosphoglycerate mutase 1 (EC 3.1.3.13) (EC 5.4.2.11) (EC 5.4.2.4) (BPG-dependent PGAM 1) (Phosphoglycerate mutase isozyme B) (PGAM-B)	39,68	6,86E+07	28,804	No	No	No
A0A075B6J7	Protein IGLV3-21 (Fragment)	38,66	6,69E+07	12,446	No	No	No
Q9UHI8	A disintegrin and metalloproteinase with thrombospondin motifs 1 (ADAM-TS 1) (ADAM-TS1) (ADAMTS-1) (EC 3.4.24.-) (METH-1)	48,36	6,60E+07	105,358	No	No	No
P01615	Ig kappa chain V-II region FR	12,91	6,60E+07	12,66	No	No	No
P01593	Ig kappa chain V-I region AG	12,51	6,58E+07	11,992	No	No	No
P06311	Ig kappa chain V-III region IARC/BL41	8,37	6,57E+07	14,07	No	No	No
P01604	Ig kappa chain V-I region Kue	7,03	6,57E+07	12,127	No	No	No

Majority protein IDs	Protein names	Score	Intensity overall	Mass	25-35 kDa unique peptides	130-250 kDa unique peptides	Ig related
Q9UNN8	Endothelial protein C receptor (Activated protein C receptor) (APC receptor) (Endothelial cell protein C receptor) (CD antigen CD201)	15,35	6,52E+07	26,671	No	No	No
P06733	Alpha-enolase (EC 4.2.1.11) (2-phospho-D-glycerate hydro-lyase) (C-myc promoter-binding protein) (Enolase 1) (MBP-1) (MPB-1) (Non-neural enolase) (NNE) (Phosphopyruvate hydratase) (Plasminogen-binding protein)	44,43	6,43E+07	47,169	No	No	No
P06727	Apolipoprotein A-IV (Apo-AIV) (ApoA-IV) (Apolipoprotein A4)	68,87	6,33E+07	45,399	No	No	No
D6REQ6	Ribonuclease T2 (Ribonuclease T2, isoform CRA_c)	14,87	6,31E+07	25,309	No	No	No
P05164	Myeloperoxidase (MPO) (EC 1.11.2.2) [Cleaved into: Myeloperoxidase; 89 kDa myeloperoxidase; 84 kDa myeloperoxidase; Myeloperoxidase light chain; Myeloperoxidase heavy chain]	24,71	6,20E+07	83,869	Yes	No	No
F8WE65	Peptidyl-prolyl cis-trans isomerase (EC 5.2.1.8)	12,36	6,20E+07	13,022	Yes	No	No
Q9UBN7	Histone deacetylase 6 (HD6) (EC 3.5.1.98)	6,77	6,19E+07	131,419	No	No	No
P01622	Ig kappa chain V-III region Ti	20,14	6,08E+07	11,788	No	No	No
P40926	Malate dehydrogenase, mitochondrial (EC 1.1.1.37)	32,89	6,02E+07	35,503	No	No	No
P63267	Actin, gamma-enteric smooth muscle (Alpha-actin-3) (Gamma-2-actin) (Smooth muscle gamma-actin)	8,38	6,01E+07	41,877	No	No	No
A0A0C4DH24	Protein IGKV6-21 (Fragment)	7,56	6,00E+07	12,43	No	No	No
P01708	Ig lambda chain V-II region BUR	12,18	5,96E+07	11,506	No	No	No
Q15113	Procollagen C-endopeptidase enhancer 1 (Procollagen COOH-terminal proteinase enhancer 1) (PCPE-1) (Procollagen C-proteinase enhancer 1) (Type 1 procollagen C-proteinase enhancer protein) (Type I procollagen COOH-terminal proteinase enhancer)	105,29	5,93E+07	47,972	No	No	No

Majority protein IDs	Protein names	Score	Intensity overall	Mass	25-35 kDa unique peptides	130-250 kDa unique peptides	Ig related
P04406	Glyceraldehyde-3-phosphate dehydrogenase (GAPDH) (EC 1.2.1.12) (Peptidyl-cysteine S-nitrosylase GAPDH) (EC 2.6.99.-)	59,74	5,89E+07	36,053	Yes	Yes	No
A0A0G2JL54	Complement C4-B	16,05	5,86E+07	187,716	No	No	No
P35606	Coatomer subunit beta' (Beta'-coat protein) (Beta'-COP) (p102)	40,39	5,69E+07	102,487	No	No	No
P07858	Cathepsin B (EC 3.4.22.1) (APP secretase) (APPS) (Cathepsin B1) [Cleaved into: Cathepsin B light chain; Cathepsin B heavy chain]	34,32	5,66E+07	37,822	No	No	No
P14550	Alcohol dehydrogenase [NADP(+)] (EC 1.1.1.2) (Aldehyde reductase) (Aldo-keto reductase family 1 member A1)	49,07	5,51E+07	36,573	No	No	No
P10643	Complement component C7	29,36	5,26E+07	93,518	No	No	No
P08294	Extracellular superoxide dismutase [Cu-Zn] (EC-SOD) (EC 1.15.1.1)	27,74	5,18E+07	25,851	No	No	No
P78417	Glutathione S-transferase omega-1 (GSTO-1) (EC 2.5.1.18) (Glutathione S-transferase omega 1-1) (GSTO 1-1) (Glutathione-dependent dehydroascorbate reductase) (EC 1.8.5.1) (Monomethylarsonic acid reductase) (MMA(V) reductase) (EC 1.20.4.2) (S-(Phenacyl)glutathione reductase) (SPG-R)	24,44	5,12E+07	27,566	No	No	No
F8WDW9	Endothelial cell-selective adhesion molecule	27,21	5,11E+07	26,701	No	No	No
F8VV32	Lysozyme C	22,57	5,11E+07	11,488	Yes	No	No
A0A0B4J1Y8	Protein IGLV9-49	22,19	5,08E+07	13,024	No	No	No
A0A087X0M8	Neural cell adhesion molecule L1-like protein	62,79	5,06E+07	130,795	No	No	No
G3V357	Ribonuclease pancreatic	24,21	4,84E+07	13,05	No	No	No
A0A075B6I2	Protein IGLV6-57	77,88	4,79E+07	15,95	No	No	No
O95865	N(G),N(G)-dimethylarginine dimethylaminohydrolase 2 (DDAH-2) (Dimethylarginine dimethylaminohydrolase 2) (EC 3.5.3.18) (DDAHII) (Dimethylargininase-2) (Protein G6a) (S-phase protein)	29,32	4,78E+07	29,644	No	No	No

Majority protein IDs	Protein names	Score	Intensity overall	Mass	25-35 kDa unique peptides	130-250 kDa unique peptides	Ig related
P30048	Thioredoxin-dependent peroxide reductase, mitochondrial (EC 1.11.1.15) (Antioxidant protein 1) (AOP-1) (HBC189) (Peroxiredoxin III) (Prx-III) (Peroxiredoxin-3) (Protein MER5 homolog)	22,21	4,65E+07	27,693	No	No	No
P09467	Fructose-1,6-bisphosphatase 1 (FBPase 1) (EC 3.1.3.11) (D-fructose-1,6-bisphosphate 1-phosphohydrolase 1) (Liver FBPase)	36,50	4,62E+07	36,842	No	No	No
P04206	Ig kappa chain V-III region GOL (Rheumatoid factor)	17,74	4,60E+07	11,83	No	No	No
P06870	Kallikrein-1 (EC 3.4.21.35) (Kidney/pancreas/salivary gland kallikrein) (Tissue kallikrein)	16,57	4,57E+07	28,89	No	No	No
O00187	Mannan-binding lectin serine protease 2 (EC 3.4.21.104) (MBL-associated serine protease 2) (Mannose-binding protein-associated serine protease 2) (MASP-2) [Cleaved into: Mannan-binding lectin serine protease 2 A chain; Mannan-binding lectin serine protease 2 B chain]	23,03	4,53E+07	75,702	No	No	No
P48595	Serpin B10 (Bomapin) (Peptidase inhibitor 10) (PI-10)	35,66	4,52E+07	45,403	No	No	No
P11021	78 kDa glucose-regulated protein (GRP-78) (Endoplasmic reticulum lumenal Ca(2+)-binding protein grp78) (Heat shock 70 kDa protein 5) (Immunoglobulin heavy chain-binding protein) (BiP)	40,89	4,51E+07	72,333	No	No	No
P01596	Ig kappa chain V-I region CAR	7,35	4,48E+07	11,704	No	No	No
A0A087WVW2	Ig gamma-3 chain C region	17,80	4,46E+07	57,156	No	No	No
P01701	Ig lambda chain V-I region NEW	12,82	4,46E+07	11,453	No	No	No
A0A075B7D4	Protein IGKV1OR2-108 (Fragment)	6,52	4,45E+07	12,535	No	No	No
Q9H6B4	CXADR-like membrane protein (Adipocyte adhesion molecule) (Coxsackie- and adenovirus receptor-like membrane protein) (CAR-like membrane protein)	22,52	4,45E+07	41,281	No	No	No
A0A0B4J1V0	Protein IGHV3-15 (Fragment)	24,26	4,44E+07	12,926	No	No	No

Majority protein IDs	Protein names	Score	Intensity overall	Mass	25-35 kDa unique peptides	130-250 kDa unique peptides	Ig related
P30740	Leukocyte elastase inhibitor (LEI) (Monocyte/neutrophil elastase inhibitor) (EI) (M/NEI) (Peptidase inhibitor 2) (PI-2) (Serpin B1)	26,31	4,33E+07	42,742	No	No	No
X6R868	Carboxylic ester hydrolase (EC 3.1.1.-)	36,02	4,21E+07	79,667	No	No	No
K7EJB9	Calreticulin (Fragment)	26,97	4,19E+07	28,432	No	No	No
P08246	Neutrophil elastase (EC 3.4.21.37) (Bone marrow serine protease) (Elastase-2) (Human leukocyte elastase) (HLE) (Medullasin) (PMN elastase)	18,97	4,06E+07	28,518	Yes	No	No
P07686	Beta-hexosaminidase subunit beta (EC 3.2.1.52) (Beta-N-acetylhexosaminidase subunit beta) (Hexosaminidase subunit B) (Cervical cancer proto-oncogene 7 protein) (HCC-7) (N-acetyl-beta-glucosaminidase subunit beta) [Cleaved into: Beta-hexosaminidase subunit beta chain B; Beta-hexosaminidase subunit beta chain A]	46,80	4,03E+07	63,111	No	No	No
P31431	Syndecan-4 (SYND4) (Amphiglycan) (Ryudocan core protein)	38,71	4,01E+07	21,642	No	No	No
B4DQI4	Alpha/beta hydrolase domain-containing protein 14B (cDNA FLJ52723, highly similar to Abhydrolase domain-containing protein 14B)	26,25	4,01E+07	19,756	No	No	No
B1AH49	Sulfurtransferase	47,10	3,99E+07	24,982	No	No	No
P35030	Trypsin-3 (EC 3.4.21.4) (Brain trypsinogen) (Mesotrypsinogen) (Serine protease 3) (Serine protease 4) (Trypsin III) (Trypsin IV)	13,93	3,96E+07	32,529	No	No	No
Q9H3G5	Probable serine carboxypeptidase CPVL (EC 3.4.16.-) (Carboxypeptidase, vitellogenic-like) (Vitellogenic carboxypeptidase-like protein) (VCP-like protein) (hVLP)	25,89	3,85E+07	54,164	No	No	No
A0A0J9YXX1	Uncharacterized protein (Fragment)	-2,00	3,85E+07	12,773	No	No	No

Majority protein IDs	Protein names	Score	Intensity overall	Mass	25-35 kDa unique peptides	130-250 kDa unique peptides	Ig related
Q9Y4E8	Ubiquitin carboxyl-terminal hydrolase 15 (EC 3.4.19.12) (Deubiquitinating enzyme 15) (Ubiquitin thioesterase 15) (Ubiquitin-specific-processing protease 15) (Unph-2) (Unph4)	33,04	3,82E+07	112,419	No	No	No
O00462	Beta-mannosidase (EC 3.2.1.25) (Lysosomal beta A mannosidase) (Mannanase) (Mannase)	54,21	3,81E+07	100,895	No	No	No
O14498	Immunoglobulin superfamily containing leucine-rich repeat protein	26,42	3,78E+07	45,997	No	No	No
B0YJC4	Vimentin (Vimentin variant 3)	39,43	3,70E+07	49,653	No	No	No
Q92692	Nectin-2 (Herpes virus entry mediator B) (Herpesvirus entry mediator B) (HveB) (Poliovirus receptor-related protein 2) (CD antigen CD112)	31,44	3,69E+07	57,742	No	No	No
P02649	Apolipoprotein E (Apo-E)	51,55	3,65E+07	36,154	No	No	No
P06889	Ig lambda chain V-IV region MOL	7,97	3,60E+07	11,272	No	No	No
P01778	Ig heavy chain V-III region ZAP	31,60	3,57E+07	12,582	No	No	No
P01763	Ig heavy chain V-III region WEA	-2,00	3,57E+07	12,256	No	No	No
Q01459	Di-N-acetylchitobiase (EC 3.2.1.-)	13,02	3,50E+07	43,76	Yes	No	No
Q12860	Contactin-1 (Glycoprotein gp135) (Neural cell surface protein F3)	35,05	3,49E+07	113,32	No	No	No
Q14019	Coactosin-like protein	28,18	3,43E+07	15,945	No	No	No
A0A075B708	Protein TRAJ61 (Fragment)	6,89	3,42E+07	2,35	No	No	No
P04066	Tissue alpha-L-fucosidase (EC 3.2.1.51) (Alpha-L-fucosidase I) (Alpha-L-fucoside fucohydrolase 1) (Alpha-L-fucosidase 1)	26,57	3,42E+07	53,689	No	No	No
Q06323	Proteasome activator complex subunit 1 (11S regulator complex subunit alpha) (REG-alpha) (Activator of multicatalytic protease subunit 1) (Interferon gamma up-regulated I-5111 protein) (IGUP I-5111) (Proteasome activator 28 subunit alpha) (PA28a) (PA28alpha)	33,06	3,38E+07	28,723	No	No	No

Majority protein IDs	Protein names	Score	Intensity overall	Mass	25-35 kDa unique peptides	130-250 kDa unique peptides	Ig related
P22792	Carboxypeptidase N subunit 2 (Carboxypeptidase N 83 kDa chain) (Carboxypeptidase N large subunit) (Carboxypeptidase N polypeptide 2) (Carboxypeptidase N regulatory subunit)	26,01	3,37E+07	60,557	No	No	No
P12110	Collagen alpha-2(VI) chain	20,66	3,34E+07	108,579	No	No	No
P00918	Carbonic anhydrase 2 (EC 4.2.1.1) (Carbonate dehydratase II) (Carbonic anhydrase C) (CAC) (Carbonic anhydrase II) (CA-II)	32,42	3,30E+07	29,246	No	No	No
H0Y5H9	Serpin B4 (Fragment)	18,15	3,29E+07	42,499	No	No	No
A0A075B6K1	Protein IGLV2-14 (Fragment)	30,00	3,23E+07	12,597	No	No	No
E5RFN6	ATP-binding cassette sub-family A member 10	7,59	3,22E+07	150,865	No	No	No
P16152	Carbonyl reductase [NADPH] 1 (EC 1.1.1.184) (15-hydroxyprostaglandin dehydrogenase [NADP(+)]) (EC 1.1.1.197) (NADPH-dependent carbonyl reductase 1) (Prostaglandin 9-ketoreductase) (Prostaglandin-E(2) 9-reductase) (EC 1.1.1.189) (Short chain dehydrogenase/reductase family 21C member 1)	35,32	3,20E+07	30,375	No	No	No
A0A0A0MS12	Protein IGHV4-34 (Fragment)	6,67	3,17E+07	13,815	No	No	No
C9JEE0	Immunoglobulin lambda-like polypeptide 1 (Fragment)	11,87	3,17E+07	19,227	No	No	No
Q9UHL4	Dipeptidyl peptidase 2 (EC 3.4.14.2) (Dipeptidyl aminopeptidase II) (Dipeptidyl peptidase 7) (Dipeptidyl peptidase II) (DPP II) (Quiescent cell proline dipeptidase)	45,88	3,15E+07	54,341	No	No	No
P08603	Complement factor H (H factor 1)	40,93	3,14E+07	139,096	No	No	No
P00558	Phosphoglycerate kinase 1 (EC 2.7.2.3) (Cell migration-inducing gene 10 protein) (Primer recognition protein 2) (PRP 2)	24,96	3,11E+07	44,615	No	No	No
E7EMM4	Acid ceramidase	17,35	3,07E+07	41,796	No	No	No
Q96RW7	Hemicentin-1 (Fibulin-6) (FIBL-6)	14,96	3,03E+07	613,39	No	No	No

Majority protein IDs	Protein names	Score	Intensity overall	Mass	25-35 kDa unique peptides	130-250 kDa unique peptides	Ig related
P13796	Plastin-2 (L-plastin) (LC64P) (Lymphocyte cytosolic protein 1) (LCP-1)	42,53	3,02E+07	70,288	No	No	No
C9JGG1	Paired immunoglobulin-like type 2 receptor alpha (Fragment)	49,54	2,95E+07	18,888	No	No	No
Q86VQ0	Lebercilin (Leber congenital amaurosis 5 protein)	10,67	2,93E+07	80,554	No	No	No
Q13421	Mesothelin (CAK1 antigen) (Pre-pro-megakaryocyte-potentiating factor) [Cleaved into: Megakaryocyte-potentiating factor (MPF); Mesothelin, cleaved form]	28,91	2,93E+07	68,986	No	No	No
A0A0B4J1U1	Protein IGLV1-44 (Fragment)	12,23	2,87E+07	12,299	No	No	No
P11279	Lysosome-associated membrane glycoprotein 1 (LAMP-1) (Lysosome-associated membrane protein 1) (CD107 antigen-like family member A) (CD antigen CD107a)	19,20	2,86E+07	44,882	No	No	No
P01616	Ig kappa chain V-II region MIL	11,14	2,82E+07	12,057	No	No	No
P27105	Erythrocyte band 7 integral membrane protein (Protein 7.2b) (Stomatin)	36,89	2,81E+07	31,731	No	No	No
P39060	Collagen alpha-1(XVIII) chain [Cleaved into: Endostatin]	34,24	2,77E+07	178,188	No	No	No
E7EQ29	Beta-galactosidase	23,88	2,77E+07	60,483	No	No	No
A0A087WTK0	Receptor-type tyrosine-protein phosphatase eta	41,34	2,76E+07	146,073	No	No	No
P01780	Ig heavy chain V-III region JON	10,40	2,71E+07	12,564	No	No	No
Q5JP53	Tubulin beta chain	18,06	2,67E+07	47,767	Yes	Yes	No
J3QRN2	Beta-2-glycoprotein 1 (Fragment)	12,94	2,62E+07	19,907	No	No	No
A0A0A0MSI0	Peroxiredoxin-1 (Fragment)	13,43	2,61E+07	18,976	No	No	No
Q86UY0	TXNDC5 protein	25,71	2,60E+07	40,369	No	No	No
P04080	Cystatin-B (CPI-B) (Liver thiol proteinase inhibitor) (Stefin-B)	18,77	2,60E+07	11,14	No	No	No

Majority protein IDs	Protein names	Score	Intensity overall	Mass	25-35 kDa unique peptides	130-250 kDa unique peptides	Ig related
Q9BTY2	Plasma alpha-L-fucosidase (EC 3.2.1.51) (Alpha-L-fucoside fucohydrolase 2) (Alpha-L-fucosidase 2)	16,89	2,56E+07	54,067	No	No	No
P01775	Ig heavy chain V-III region LAY	24,94	2,55E+07	12,858	No	No	No
A0A087WT99	Ester hydrolase C11orf54	19,35	2,50E+07	28,683	No	No	No
F6TLX2	Glyoxalase domain-containing protein 4	23,04	2,42E+07	54,72	No	No	No
Q8WUM0	Nuclear pore complex protein Nup133 (133 kDa nucleoporin) (Nucleoporin Nup133)	6,38	2,40E+07	128,979	No	No	No
G5E968	Chromogranin A (Parathyroid secretory protein 1), isoform CRA_b (Chromogranin-A)	23,98	2,39E+07	34,269	No	No	No
P07237	Protein disulfide-isomerase (PDI) (EC 5.3.4.1) (Cellular thyroid hormone-binding protein) (Prolyl 4-hydroxylase subunit beta) (p55)	28,28	2,33E+07	57,116	No	No	No
A0A075B6K4	HCG2043238 (Protein IGLV3-10) (Fragment)	13,18	2,33E+07	12,629	No	No	No
P16188	HLA class I histocompatibility antigen, A-30 alpha chain (MHC class I antigen A*30)	29,64	2,29E+07	40,905	No	No	No
A0A0A0MS14	Protein IGHV1-45 (Fragment)	6,77	2,27E+07	13,508	No	No	No
A0A0J9YVT0	Protein IGHV3-33 (Fragment)	8,55	2,26E+07	12,989	No	No	No
V9GYE7	Complement factor H-related protein 2	23,04	2,23E+07	28,912	No	No	No
A0A087WUS4	Aminopeptidase B (Fragment)	6,52	2,18E+07	16,322	No	No	No
S4R3C6	Transforming growth factor-beta-induced protein ig-h3 (Fragment)	12,27	2,18E+07	23,497	No	No	No
P43251	Biotinidase (Biotinase) (EC 3.5.1.12)	14,67	2,16E+07	61,133	No	No	No
A0A0C4DFZ2	Arylsulfatase A	13,23	2,10E+07	53,806	No	No	No
O95861	3'(2'),5'-bisphosphate nucleotidase 1 (EC 3.1.3.7) (Bisphosphate 3'-nucleotidase 1) (PAP-inositol 1,4-phosphatase) (PIP)	19,83	2,10E+07	33,392	No	No	No
J3QLM0	T-cell antigen CD7	14,59	2,07E+07	23,041	No	No	No

Majority protein IDs	Protein names	Score	Intensity overall	Mass	25-35 kDa unique peptides	130-250 kDa unique peptides	Ig related
P01601	Ig kappa chain V-ID region 16 (Ig kappa chain V-I region HK101) (Fragment)	36,48	2,06E+07	12,73	No	No	No
P08238	Heat shock protein HSP 90-beta (HSP 90) (Heat shock 84 kDa) (HSP 84) (HSP84)	23,46	2,04E+07	83,264	No	No	No
Q13011	Delta(3,5)-Delta(2,4)-dienoyl-CoA isomerase, mitochondrial (EC 5.3.3.-)	21,83	2,04E+07	35,816	No	No	No
A0A075B6S4	Protein IGKV1D-17 (Fragment)	7,41	2,03E+07	12,835	No	No	No
J3QSE5	Phosphatidylcholine-sterol acyltransferase (Fragment)	49,25	2,00E+07	29,387	No	No	No
C9JC71	Low affinity immunoglobulin gamma Fc region receptor III-A (Fragment)	6,90	1,98E+07	11,823	No	No	No
A0A0B4J227	Neuroblastoma breakpoint family member 6 (Fragment)	6,36	1,94E+07	64,812	No	No	No
O00391	Sulfhydryl oxidase 1 (hQSOX) (EC 1.8.3.2) (Quiescin Q6)	39,57	1,93E+07	82,578	No	No	No
Q08830	Fibrinogen-like protein 1 (HP-041) (Hepassocin) (Hepatocyte-derived fibrinogen-related protein 1) (HFREP-1) (Liver fibrinogen-related protein 1) (LFIRE-1)	18,64	1,87E+07	36,379	No	No	No
A0A0A0MTR1	Cadherin-13	30,13	1,85E+07	76,969	No	No	No
F2Z393	Transaldolase (EC 2.2.1.2)	18,92	1,85E+07	35,329	No	No	No
Q15485	Ficolin-2 (37 kDa elastin-binding protein) (Collagen/fibrinogen domain-containing protein 2) (EBP-37) (Ficolin-B) (Ficolin-beta) (Hucolin) (L-ficolin) (Serum lectin p35)	15,29	1,85E+07	34,001	No	No	No
P01764	Ig heavy chain V-III region 23 (Ig heavy chain V-III region VH26) (Immunoglobulin heavy variable 3-23)	18,80	1,84E+07	12,582	No	No	No
P01605	Ig kappa chain V-I region Lay	8,80	1,83E+07	11,834	No	No	No
Q9HAT2	Sialate O-acetylesterase (EC 3.1.1.53) (H-Lse) (Sialic acid-specific 9-O-acetylesterase)	7,67	1,81E+07	58,315	No	No	No

Majority protein IDs	Protein names	Score	Intensity overall	Mass	25-35 kDa unique peptides	130-250 kDa unique peptides	Ig related
Q9BXP8	Pappalysin-2 (EC 3.4.24.-) (Pregnancy-associated plasma protein A2) (PAPP-A2) (Pregnancy-associated plasma protein E1) (PAPP-E)	9,53	1,80E+07	198,539	No	No	No
P07711	Cathepsin L1 (EC 3.4.22.15) (Cathepsin L) (Major excreted protein) (MEP) [Cleaved into: Cathepsin L1 heavy chain; Cathepsin L1 light chain]	17,90	1,78E+07	37,564	No	No	No
P20142	Gastricsin (EC 3.4.23.3) (Pepsinogen C)	27,88	1,78E+07	42,426	No	No	No
A6NI73	Leukocyte immunoglobulin-like receptor subfamily A member 5 (CD85 antigen-like family member F) (Immunoglobulin-like transcript 11) (ILT-11) (Leukocyte immunoglobulin-like receptor 9) (LIR-9) (CD antigen CD85f)	24,07	1,73E+07	32,755	No	No	No
P21695	Glycerol-3-phosphate dehydrogenase [NAD(+)], cytoplasmic (GPD-C) (GPDH-C) (EC 1.1.1.8)	20,46	1,71E+07	37,568	No	No	No
A0A0G2JQJ0	Protein IGKV1D-8 (Fragment)	12,58	1,70E+07	12,962	No	No	No
A0M8Q6	Ig lambda-7 chain C region	8,50	1,68E+07	11,303	No	No	No
P30039	Phenazine biosynthesis-like domain-containing protein (EC 5.1.-.-) (MAWD-binding protein) (MAWDBP) (Unknown protein 32 from 2D-page of liver tissue)	42,96	1,67E+07	31,785	No	No	No
Q8WZ75	Roundabout homolog 4 (Magic roundabout)	11,28	1,65E+07	107,457	No	No	No
P46926	Glucosamine-6-phosphate isomerase 1 (EC 3.5.99.6) (Glucosamine-6-phosphate deaminase 1) (GNPDA 1) (GlcN6P deaminase 1) (Oscillin)	18,00	1,65E+07	32,669	No	No	No
P61981	14-3-3 protein gamma (Protein kinase C inhibitor protein 1) (KCIP-1) [Cleaved into: 14-3-3 protein gamma, N-terminally processed]	78,94	1,63E+07	28,303	No	No	No

Majority protein IDs	Protein names	Score	Intensity overall	Mass	25-35 kDa unique peptides	130-250 kDa unique peptides	Ig related
Q6UX06	Olfactomedin-4 (OLM4) (Antiapoptotic protein GW112) (G-CSF-stimulated clone 1 protein) (hGC-1) (hOLfD)	33,50	1,61E+07	57,28	No	No	No
Q9Y279	V-set and immunoglobulin domain-containing protein 4 (Protein Z39Ig)	6,47	1,61E+07	43,987	No	No	No
F8WC59	Aminoacylase-1	18,12	1,60E+07	22,709	No	No	No
H3BMU8	Group XV phospholipase A2 (Fragment)	14,52	1,59E+07	33,878	No	No	No
Q9H257	Caspase recruitment domain-containing protein 9 (hCARD9)	7,55	1,58E+07	62,241	No	No	No
B1AKQ8	Guanine nucleotide-binding protein G(I)/G(S)/G(T) subunit beta-1 (Fragment)	90,26	1,57E+07	12,285	No	No	No
P17050	Alpha-N-acetylgalactosaminidase (EC 3.2.1.49) (Alpha-galactosidase B)	15,17	1,49E+07	46,565	No	No	No
P01603	Ig kappa chain V-I region Ka	13,31	1,48E+07	11,9	No	No	No
P01719	Ig lambda chain V-V region DEL	29,27	1,46E+07	11,343	No	No	No
A0A0C4DGY8	Enolase-phosphatase E1	15,73	1,45E+07	16,533	No	No	No
Q7Z7M0	Multiple epidermal growth factor-like domains protein 8 (Multiple EGF-like domains protein 8) (Epidermal growth factor-like protein 4) (EGF-like protein 4)	13,58	1,42E+07	303,1	No	No	No
P17174	Aspartate aminotransferase, cytoplasmic (cAspAT) (EC 2.6.1.1) (EC 2.6.1.3) (Cysteine aminotransferase, cytoplasmic) (Cysteine transaminase, cytoplasmic) (cCAT) (Glutamate oxaloacetate transaminase 1) (Transaminase A)	21,80	1,41E+07	46,248	No	No	No
P31946	14-3-3 protein beta/alpha (Protein 1054) (Protein kinase C inhibitor protein 1) (KCIP-1) [Cleaved into: 14-3-3 protein beta/alpha, N-terminally processed]	19,75	1,41E+07	28,082	No	No	No
A0A0B4J1U9	Protein IGHV3-11 (Fragment)	10,14	1,40E+07	12,909	No	No	No

Majority protein IDs	Protein names	Score	Intensity overall	Mass	25-35 kDa unique peptides	130-250 kDa unique peptides	Ig related
A0A087WXL1	Folate receptor gamma	20,10	1,31E+07	27,885	No	No	No
E9PKP4	Macrophage colony-stimulating factor 1 (Fragment)	12,10	1,27E+07	13,253	No	No	No
A0A087WWP7	Receptor-type tyrosine-protein phosphatase gamma	19,01	1,26E+07	151,539	No	No	No
P01624	Ig kappa chain V-III region POM	9,95	1,24E+07	11,922	No	No	No
A0A087WWY0	Apolipoprotein(a)	32,93	1,24E+07	62,554	No	No	No
E5RHP7	Carbonic anhydrase 1 (Fragment)	7,88	1,23E+07	27,754	No	No	No
P15814	Immunoglobulin lambda-like polypeptide 1 (CD179 antigen-like family member B) (Ig lambda-5) (Immunoglobulin omega polypeptide) (Immunoglobulin-related protein 14.1) (CD antigen CD179b)	6,82	1,23E+07	22,963	No	No	No
P01609	Ig kappa chain V-I region Scw	16,28	1,23E+07	11,764	No	No	No
H0YMZ1	Proteasome subunit alpha type (EC 3.4.25.1) (Fragment)	12,99	1,22E+07	24,583	No	No	No
Q9BS40	Latexin (Endogenous carboxypeptidase inhibitor) (ECI) (Protein MUM) (Tissue carboxypeptidase inhibitor) (TCI)	13,12	1,21E+07	25,75	No	No	No
P20160	Azurocidin (Cationic antimicrobial protein CAP37) (Heparin-binding protein) (HBP) (hHBP)	17,50	1,19E+07	26,886	No	No	No
A0A075B6K3	Protein IGLV2-11 (Fragment)	-2,00	1,19E+07	12,644	No	No	No
Q96KP4	Cytosolic non-specific dipeptidase (EC 3.4.13.18) (CNDP dipeptidase 2) (Glutamate carboxypeptidase-like protein 1) (Peptidase A)	18,52	1,16E+07	52,878	No	No	No
E9PSE5	Palmitoyl-protein thioesterase 1	8,04	1,16E+07	10,016	No	No	No
Q9BRF8	Serine/threonine-protein phosphatase CPPED1 (EC 3.1.3.16) (Calcineurin-like phosphoesterase domain-containing protein 1) (Complete S-transactivated protein 1)	13,90	1,16E+07	35,548	No	No	No
D6RAR4	Hepatocyte growth factor activator	18,83	1,14E+07	71,483	No	No	No
F5GWF3	Complement C1r subcomponent-like protein	14,02	1,14E+07	33,679	No	No	No

Majority protein IDs	Protein names	Score	Intensity overall	Mass	25-35 kDa unique peptides	130-250 kDa unique peptides	Ig related
X6R5C5	Carboxypeptidase (EC 3.4.16.-)	15,35	1,11E+07	54,256	No	No	No
O00299	Chloride intracellular channel protein 1 (Chloride channel ABP) (Nuclear chloride ion channel 27) (NCC27) (Regulatory nuclear chloride ion channel protein) (hRNCC)	12,90	1,10E+07	26,923	No	No	No
H3BPE1	Microtubule-actin cross-linking factor 1, isoforms 1/2/3/5	6,51	1,09E+07	856,879	No	No	No
P32004	Neural cell adhesion molecule L1 (N-CAM-L1) (NCAM-L1) (CD antigen CD171)	25,57	1,09E+07	140,003	No	No	No
O15144	Actin-related protein 2/3 complex subunit 2 (Arp2/3 complex 34 kDa subunit) (p34-ARC)	14,73	1,08E+07	34,333	No	No	No
A0A087WX97	Bcl-2-like protein 13	6,94	1,07E+07	54,389	No	No	No
A0A087X1Z3	Proteasome activator complex subunit 2	27,41	1,06E+07	29,127	No	No	No
A0A0A0MRJ7	Coagulation factor V	6,46	1,06E+07	252,236	No	No	No
A0A075B6Q5	Protein IGHV3-64 (Fragment)	11,57	1,03E+07	12,891	No	No	No
P11597	Cholesteryl ester transfer protein (Lipid transfer protein I)	16,84	1,02E+07	54,756	No	No	No
Q08ET2	Sialic acid-binding Ig-like lectin 14 (Siglec-14)	12,40	1,01E+07	43,97	No	No	No
P17900	Ganglioside GM2 activator (Cerebroside sulfate activator protein) (GM2-AP) (Sphingolipid activator protein 3) (SAP-3) [Cleaved into: Ganglioside GM2 activator isoform short]	17,34	9,94E+06	20,838	No	No	No
R4GNC0	N-acylethanolamine-hydrolyzing acid amidase (Fragment)	13,53	9,90E+06	24,836	No	No	No
A0A087X0P6	Protein IGKV2D-29	9,11	9,88E+06	11,192	No	No	No
A6NIW5	Peroxiredoxin 2, isoform CRA_a (Peroxiredoxin-2)	12,36	9,87E+06	15,138	No	No	No
Q14112	Nidogen-2 (NID-2) (Osteonidogen)	12,46	9,81E+06	151,254	No	No	No

Majority protein IDs	Protein names	Score	Intensity overall	Mass	25-35 kDa unique peptides	130-250 kDa unique peptides	Ig related
P01031	Complement C5 (C3 and PZP-like alpha-2-macroglobulin domain-containing protein 4) [Cleaved into: Complement C5 beta chain; Complement C5 alpha chain; C5a anaphylatoxin; Complement C5 alpha' chain]	12,32	9,71E+06	188,305	No	No	No
P22492	Histone H1t (Testicular H1 histone)	6,32	9,36E+06	22,019	No	No	No
Q9NUM4	Transmembrane protein 106B	11,79	9,25E+06	31,127	No	No	No
O95154	Aflatoxin B1 aldehyde reductase member 3 (EC 1.-.-.-) (AFB1 aldehyde reductase 2) (AFB1-AR 2)	7,23	9,22E+06	37,206	No	No	No
P54802	Alpha-N-acetylglucosaminidase (EC 3.2.1.50) (N-acetyl-alpha-glucosaminidase) (NAG) [Cleaved into: Alpha-N-acetylglucosaminidase 82 kDa form; Alpha-N-acetylglucosaminidase 77 kDa form]	17,63	9,14E+06	82,266	No	No	No
H0Y5U1	Agrin (Fragment)	12,02	9,09E+06	28,773	No	No	No
Q5H9B4	Metalloproteinase inhibitor 1 (Fragment)	6,53	9,05E+06	10,707	No	No	No
P02675	Fibrinogen beta chain [Cleaved into: Fibrinopeptide B; Fibrinogen beta chain]	17,94	9,02E+06	55,928	No	No	No
P07360	Complement component C8 gamma chain	13,41	9,00E+06	22,277	No	No	No
A0A0C4DGX4	Cullin-1	-2,00	8,94E+06	87,388	No	No	No
P23142	Fibulin-1 (FIBL-1)	11,01	8,86E+06	77,214	No	No	No
J3KSN0	Secreted and transmembrane protein 1 (Fragment)	7,65	8,71E+06	15,958	No	No	No
A0A0G2JNK4	Ig gamma-1 chain C region	8,49	8,65E+06	50,916	No	No	No
F6X2W2	Neuronal growth regulator 1	12,23	8,59E+06	32,85	No	No	No
E9PKE3	Heat shock cognate 71 kDa protein	23,10	8,37E+06	68,806	No	No	No
A0A087X2E2	Carcinoembryonic antigen-related cell adhesion molecule 8	6,88	8,22E+06	37,528	No	No	No

Majority protein IDs	Protein names	Score	Intensity overall	Mass	25-35 kDa unique peptides	130-250 kDa unique peptides	Ig related
E9PIF4	Sialidase-1	16,76	8,14E+06	29	No	No	No
Q14126	Desmoglein-2 (Cadherin family member 5) (HDGC)	9,76	8,10E+06	122,294	No	No	No
P17066	Heat shock 70 kDa protein 6 (Heat shock 70 kDa protein B')	23,52	8,06E+06	71,028	No	No	No
P17931	Galectin-3 (Gal-3) (35 kDa lectin) (Carbohydrate-binding protein 35) (CBP 35) (Galactose-specific lectin 3) (Galactoside-binding protein) (GALBP) (IgE-binding protein) (L-31) (Laminin-binding protein) (Lectin L-29) (Mac-2 antigen)	10,57	7,91E+06	26,152	No	No	No
P13727	Bone marrow proteoglycan (BMPG) (Proteoglycan 2) [Cleaved into: Eosinophil granule major basic protein (EMBP) (MBP) (Pregnancy-associated major basic protein)]	7,19	7,81E+06	25,206	No	No	No
A0A0G2JQF3	Mucin-20 (Fragment)	9,04	7,80E+06	13,357	No	No	No
H3BNH4	Protein ADGRG1 (Fragment)	10,91	7,80E+06	22,299	No	No	No
P51688	N-sulphoglucosamine sulphohydrolase (EC 3.10.1.1) (Sulfoglucosamine sulfamidase) (Sulphamidase)	11,85	7,69E+06	56,695	No	No	No
A0A087WY82	Junctional adhesion molecule A	7,31	7,61E+06	30,197	No	No	No
H3BS70	Enoyl-CoA delta isomerase 1, mitochondrial (Fragment)	12,10	7,41E+06	24,705	No	No	No
D6RA82	Annexin	12,07	7,39E+06	32,119	No	No	No
P08311	Cathepsin G (CG) (EC 3.4.21.20)	17,15	7,39E+06	28,837	No	No	No
A0A0A0MR14	Osteoclast-associated immunoglobulin-like receptor	12,14	7,36E+06	27,603	No	No	No
A0A0B4J1R6	Transketolase	6,51	7,18E+06	49,91	No	No	No
Q9HB40	Retinoid-inducible serine carboxypeptidase (EC 3.4.16.-) (Serine carboxypeptidase 1)	12,36	7,16E+06	50,831	No	No	No
Q93088	Betaine--homocysteine S-methyltransferase 1 (EC 2.1.1.5)	13,31	6,97E+06	44,998	No	No	No
A0A075B7D0	Protein IGHV1OR15-1 (Uncharacterized protein) (Fragment)	6,96	6,84E+06	13,012	No	No	No

Majority protein IDs	Protein names	Score	Intensity overall	Mass	25-35 kDa unique peptides	130-250 kDa unique peptides	Ig related
Q8NBJ4	Golgi membrane protein 1 (Golgi membrane protein GP73) (Golgi phosphoprotein 2)	14,17	6,80E+06	45,333	No	No	No
Q03591	Complement factor H-related protein 1 (FHR-1) (H factor-like protein 1) (H-factor-like 1) (H36)	12,06	6,79E+06	37,651	No	No	No
E5RJD2	2,4-dienoyl-CoA reductase, mitochondrial (Fragment)	8,67	6,72E+06	15,898	No	No	No
Q10567	AP-1 complex subunit beta-1 (Adaptor protein complex AP-1 subunit beta-1) (Adaptor-related protein complex 1 subunit beta-1) (Beta-1-adaptin) (Beta-adaptin 1) (Clathrin assembly protein complex 1 beta large chain) (Golgi adaptor HA1/AP1 adaptin beta subunit)	11,11	6,50E+06	104,637	No	No	No
A0A0J9YX35	Uncharacterized protein (Fragment)	-2,00	6,39E+06	12,823	No	No	No
O00592	Podocalyxin (GCTM-2 antigen) (Gp200) (Podocalyxin-like protein 1) (PC) (PCLP-1)	11,68	6,34E+06	58,635	No	No	No
O43490	Prominin-1 (Antigen AC133) (Prominin-like protein 1) (CD antigen CD133)	17,54	6,33E+06	97,202	No	No	No
Q8NHP8	Putative phospholipase B-like 2 (EC 3.1.1.-) (76 kDa protein) (p76) (LAMA-like protein 2) (Lamina ancestor homolog 2) (Phospholipase B domain-containing protein 2) [Cleaved into: Putative phospholipase B-like 2 32 kDa form; Putative phospholipase B-like 2 45 kDa form]	11,83	6,32E+06	65,472	No	No	No
A0A0A0MSN4	Angiotensin-converting enzyme	6,54	6,27E+06	142,42	No	No	No
Q9HD89	Resistin (Adipose tissue-specific secretory factor) (ADSF) (C/EBP-epsilon-regulated myeloid-specific secreted cysteine-rich protein) (Cysteine-rich secreted protein A12-alpha-like 2) (Cysteine-rich secreted protein FIZZ3)	7,19	6,21E+06	11,419	No	No	No
P18510	Interleukin-1 receptor antagonist protein (IL-1RN) (IL-1ra) (IRAP) (ICIL-1RA) (IL1 inhibitor) (Anakinra)	6,59	6,13E+06	20,055	No	No	No

Majority protein IDs	Protein names	Score	Intensity overall	Mass	25-35 kDa unique peptides	130-250 kDa unique peptides	Ig related
D6RAX3	Protocadherin-1	10,76	6,06E+06	41,443	No	No	No
Q9NZH0	G-protein coupled receptor family C group 5 member B (A-69G12.1) (Retinoic acid-induced gene 2 protein) (RAIG-2)	19,86	5,86E+06	44,795	No	No	No
I3NI28	Chymotrypsin-like protease CTRL-1 (Fragment)	12,34	5,86E+06	20,086	No	No	No
Q29940	HLA class I histocompatibility antigen, B-59 alpha chain (MHC class I antigen B*59)	10,31	5,69E+06	40,584	No	No	No
Q9Y646	Carboxypeptidase Q (EC 3.4.17.-) (Lysosomal dipeptidase) (Plasma glutamate carboxypeptidase)	11,65	5,67E+06	51,888	No	No	No
Q5TFQ8	Signal-regulatory protein beta-1 isoform 3 (SIRP-beta-1 isoform 3)	11,68	5,58E+06	43,359	No	No	No
P49257	Protein ERGIC-53 (ER-Golgi intermediate compartment 53 kDa protein) (Gp58) (Intracellular mannose-specific lectin MR60) (Lectin mannose-binding 1)	9,02	5,48E+06	57,549	No	No	No
Q9Y2S2	Lambda-crystallin homolog (EC 1.1.1.45) (L-gulonate 3-dehydrogenase) (Gul3DH)	17,15	5,41E+06	35,419	No	No	No
H0YLJ2	Solute carrier family 12 member 1 (Fragment)	11,31	5,32E+06	70,369	No	No	No
A0A087X243	Glutathione S-transferase P (Fragment)	6,34	5,30E+06	7,449	No	No	No
Q9NQR4	Omega-amidase NIT2 (EC 3.5.1.3) (Nitrilase homolog 2)	12,34	5,18E+06	30,608	No	No	No
C9JA05	Immunoglobulin J chain (Fragment)	7,52	5,17E+06	8,168	No	No	No
P05451	Lithostathine-1-alpha (Islet cells regeneration factor) (ICRF) (Islet of Langerhans regenerating protein) (REG) (Pancreatic stone protein) (PSP) (Pancreatic thread protein) (PTP) (Regenerating islet-derived protein 1-alpha) (REG-1-alpha) (Regenerating protein I alpha)	11,80	5,09E+06	18,731	No	No	No
P25788	Proteasome subunit alpha type-3 (EC 3.4.25.1) (Macropain subunit C8) (Multicatalytic endopeptidase complex subunit C8) (Proteasome component C8)	14,15	5,08E+06	28,433	No	No	No

Majority protein IDs	Protein names	Score	Intensity overall	Mass	25-35 kDa unique peptides	130-250 kDa unique peptides	Ig related
P12955	Xaa-Pro dipeptidase (X-Pro dipeptidase) (EC 3.4.13.9) (Imidodipeptidase) (Peptidase D) (Proline dipeptidase) (Prolidase)	6,72	5,05E+06	54,548	No	No	No
Q96L35	EPH receptor B4, isoform CRA_b (Ephrin type-B receptor 4) (Receptor protein tyrosine kinase variant EphB4v1)	7,09	4,97E+06	102,558	No	No	No
A0A024R644	Ceroid-lipofuscinosis neuronal protein 5 (Ceroid-lipofuscinosis, neuronal 5, isoform CRA_a)	6,39	4,84E+06	46,339	No	No	No
Q496F6	CMRF35-like molecule 2 (CLM-2) (CD300 antigen-like family member E) (CMRF35-A5) (Immune receptor expressed on myeloid cells 2) (IREM-2) (Polymeric immunoglobulin receptor 2) (PIgR-2) (PIgR2) (Poly-Ig receptor 2) (CD antigen CD300e)	6,64	4,82E+06	22,918	No	No	No
Q9H6X2	Anthrax toxin receptor 1 (Tumor endothelial marker 8)	12,70	4,79E+06	62,789	No	No	No
D6REY1	Chitotriosidase-1	11,35	4,79E+06	40,239	No	No	No
J3KS60	Rho GDP-dissociation inhibitor 1	7,51	4,69E+06	9,944	No	No	No
A0A0B4J1V6	Protein IGHV3-73 (Fragment)	7,06	4,53E+06	12,858	No	No	No
B1AHL2	Fibulin-1	9,39	4,47E+06	78,329	No	No	No
I3L297	Adapter molecule crk	7,30	4,41E+06	25,504	No	No	No
A0A087WWY3	Filamin-A	10,91	4,32E+06	245,851	No	No	No
O75636	Ficolin-3 (Collagen/fibrinogen domain-containing lectin 3 p35) (Collagen/fibrinogen domain-containing protein 3) (Hakata antigen)	10,90	4,31E+06	32,903	No	No	No
F5GWG3	Retinoic acid-induced protein 3 (Fragment)	6,76	4,28E+06	30,618	No	No	No
P15086	Carboxypeptidase B (EC 3.4.17.2) (Pancreas-specific protein) (PASP)	12,48	4,05E+06	47,368	No	No	No
M0QYG8	Glia maturation factor gamma	11,53	4,04E+06	10,99	No	No	No
Q5T0R7	Adenylyl cyclase-associated protein (Fragment)	6,59	3,64E+06	19,202	No	No	No

Majority protein IDs	Protein names	Score	Intensity overall	Mass	25-35 kDa unique peptides	130-250 kDa unique peptides	Ig related
D6RGG3	Collagen alpha-1(XII) chain	12,03	3,58E+06	333,202	No	No	No
Q8IY13	FBLN7 protein (Fibulin-7) (Fragment)	10,65	3,57E+06	28,038	No	No	No
A0A087WVQ9	Elongation factor 1-alpha 1	11,21	3,57E+06	47,883	No	No	No
Q9H8L6	Multimerin-2 (EMILIN-3) (Elastin microfibril interface located protein 3) (Elastin microfibril interfacer 3) (EndoGlyx-1 p125/p140 subunit)	6,31	3,48E+06	104,409	No	No	No
E9PJ29	Out at first protein homolog	6,67	3,43E+06	18,092	No	No	No
A0A075B6J1	Protein IGLV5-37 (Fragment)	7,77	3,41E+06	13,277	No	No	No
Q96NY8	Nectin-4 (Ig superfamily receptor LNIR) (Poliovirus receptor-related protein 4) [Cleaved into: Processed poliovirus receptor-related protein 4]	11,60	3,41E+06	55,454	No	No	No
P06681	Complement C2 (EC 3.4.21.43) (C3/C5 convertase) [Cleaved into: Complement C2b fragment; Complement C2a fragment]	6,38	3,37E+06	83,268	No	No	No
P00505	Aspartate aminotransferase, mitochondrial (mAspAT) (EC 2.6.1.1) (EC 2.6.1.7) (Fatty acid-binding protein) (FABP-1) (Glutamate oxaloacetate transaminase 2) (Kynurenine aminotransferase 4) (Kynurenine aminotransferase IV) (Kynurenine--oxoglutarate transaminase 4) (Kynurenine--oxoglutarate transaminase IV) (Plasma membrane-associated fatty acid-binding protein) (FABPpm) (Transaminase A)	12,82	3,27E+06	47,518	No	No	No
P29622	Kallistatin (Kallikrein inhibitor) (Peptidase inhibitor 4) (PI-4) (Serpin A4)	10,81	3,25E+06	48,542	No	No	No
F8W0P7	ATP synthase subunit beta, mitochondrial (Fragment)	7,21	3,09E+06	28,393	No	No	No
Q99574	Neuroserpin (Peptidase inhibitor 12) (PI-12) (Serpin I1)	6,60	3,04E+06	46,427	No	No	No

Majority protein IDs	Protein names	Score	Intensity overall	Mass	25-35 kDa unique peptides	130-250 kDa unique peptides	Ig related
Q9H3H3	UPF0696 protein C11orf68 (Basophilic leukemia-expressed protein Bles03) (Protein p5326)	6,60	3,03E+06	27,355	No	No	No
Q15181	Inorganic pyrophosphatase (EC 3.6.1.1) (Pyrophosphate phospho-hydrolase) (PPase)	6,99	2,98E+06	32,66	No	No	No
Q9UGN4	CMRF35-like molecule 8 (CLM-8) (CD300 antigen-like family member A) (CMRF-35-H9) (CMRF35-H9) (CMRF35-H) (IRC1/IRC2) (Immunoglobulin superfamily member 12) (IgSF12) (Inhibitory receptor protein 60) (IRp60) (NK inhibitory receptor) (CD antigen CD300a)	7,09	2,89E+06	33,201	No	No	No
A0A096LPE1	Vinculin	6,76	2,68E+06	6,087	No	No	No
A0A0B4J1R4	4-hydroxyphenylpyruvate dioxygenase	6,39	2,39E+06	44,964	No	No	No
E9PHY0	Lysosomal acid phosphatase	10,63	2,09E+06	40,99	No	No	No
P08572	Collagen alpha-2(IV) chain [Cleaved into: Canstatin]	17,78	1,91E+06	167,553	No	No	No
C9JPK6	HMG box-containing protein 1 (Fragment)	-2,00	9,25E+05	3,219	No	No	No
A0A0C4DH72	Protein IGKV1-6 (Fragment)	7,47	0,00E+00	12,697	No	No	No

Targeted Proteomics

PRM Patient Information

Table A 8 Patient information for urine samples for PRM experiments

Sample number	Protein conc (µg/µl)	TB status	HIV status
17	0.41	Positive	Negative
27	1.31	Positive	Negative
30	0.45	Positive	Negative
32	6.11	Positive	Negative
36	1.00	Positive	Negative
37	0.75	Positive	Negative
39	0.99	Positive	Negative
55	7.89	Positive	Negative
64	3.24	Positive	Negative
105	0.82	Positive	Negative
1204	7.94	Positive	Positive
1244	8.40	Positive	Positive
1245	1.24	Positive	Positive
1250	7.86	Positive	Positive
1259	13.42	Positive	Positive
1275	1.78	Positive	Positive
1291	3.19	Positive	Positive
1350	10.82	Positive	Positive
1397	9.71	Positive	Positive
1475	10.70	Positive	Positive
1100	11.36	Negative	Positive
1102	1.53	Negative	Positive
1103	0.56	Negative	Positive
1104	6.05	Negative	Positive
1107	1.77	Negative	Positive
1113	1.52	Negative	Positive
1123	0.58	Negative	Positive
1136	0.74	Negative	Positive
1180	28.62	Negative	Positive

Sample number	Protein conc (µg/µl)	TB status	HIV status
1070	0.68	Negative	Negative
1073	1.02	Negative	Negative
1075	0.60	Negative	Negative
1083	1.17	Negative	Negative
1091	0.98	Negative	Negative
1119	0.56	Negative	Negative
2031	0.60	Negative	Negative
2064	0.25	Negative	Negative
2102*	1.10	Negative	Negative

* miss labelled as 2101

Isolation List for Targeted Proteomics

Table A 9 Isolation list for targeted proteomics (ESAT-6 and CFP-10)

Mass [m/z]	CS [z]	Polarity	NCE	Comment
1002.492692	2	Positive	27	TQIDQVESTAGSLQGQWR (light)
668.66422	3	Positive	27	TQIDQVESTAGSLQGQWR (light)
501.749984	4	Positive	27	TQIDQVESTAGSLQGQWR (light)
571.817461	2	Positive	27	GAAGTAAQAAVVR (light)
381.547399	3	Positive	27	GAAGTAAQAAVVR (light)
286.412368	4	Positive	27	GAAGTAAQAAVVR (light)
659.335881	2	Positive	27	QELDEISTNIR (light)
439.893012	3	Positive	27	QELDEISTNIR (light)
330.171578	4	Positive	27	QELDEISTNIR (light)
454.732866	2	Positive	27	QAGVQYSR (light)
303.491002	3	Positive	27	QAGVQYSR (light)
227.870071	4	Positive	27	QAGVQYSR (light)
834.862134	2	Positive	27	ADEEQQQALSSQMGF (light)
556.910514	3	Positive	27	ADEEQQQALSSQMGF (light)
417.934705	4	Positive	27	ADEEQQQALSSQMGF (light)
954.465946	2	Positive	27	LAAAWGGSGSEAYQGVQQK (light)
636.646389	3	Positive	27	LAAAWGGSGSEAYQGVQQK (light)
477.736611	4	Positive	27	LAAAWGGSGSEAYQGVQQK (light)
950.979221	2	Positive	27	WDATATELNNALQNLAR (light)
634.321906	3	Positive	27	WDATATELNNALQNLAR (light)
475.993248	4	Positive	27	WDATATELNNALQNLAR (light)
1036.966804	2	Positive	27	TISEAGQAMASTEGNVTGMFA (light)
691.646961	3	Positive	27	TISEAGQAMASTEGNVTGMFA (light)
518.98704	4	Positive	27	TISEAGQAMASTEGNVTGMFA (light)

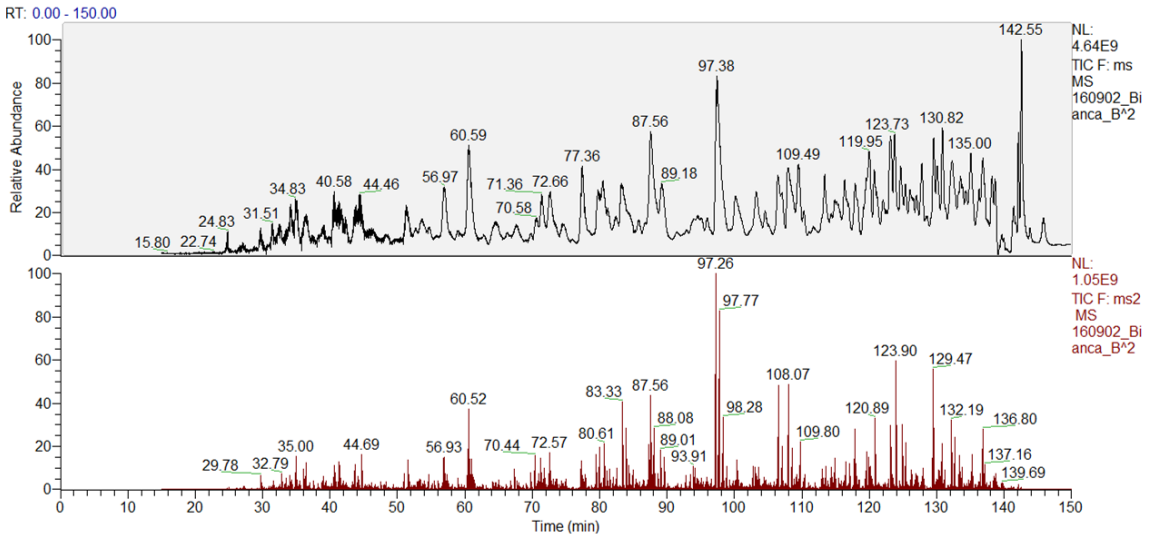

Figure A 3 Total Ion Chromatogram (TIC) for MS1 and MS2 spectra for rESAT-6 and rCFP-10 spiked into a healthy volunteer urine sample.

Targeted Proteomics Results

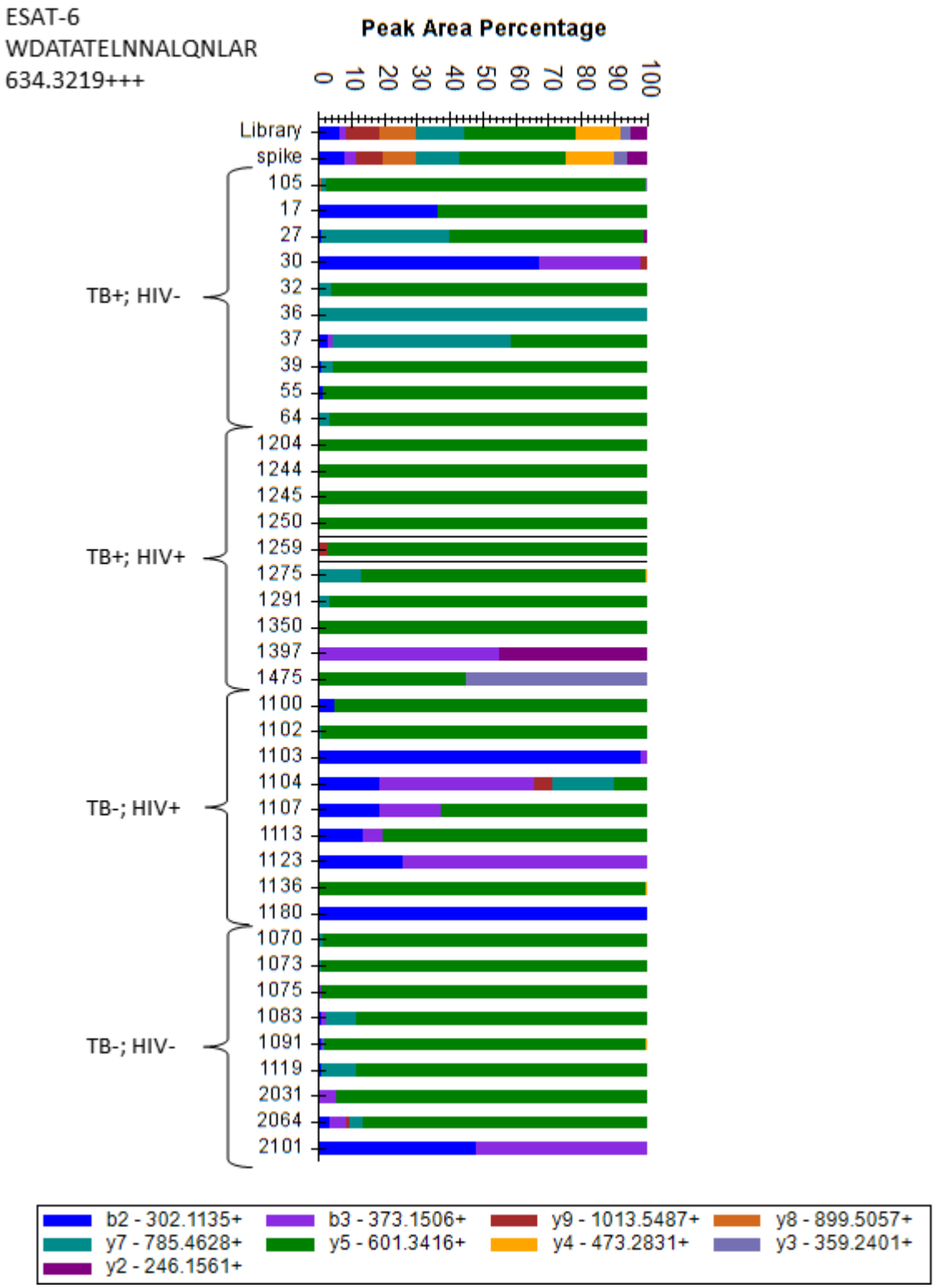

Figure A 4 Comparison of peak areas for transition peaks of WDATATELNNALQNLAR between the spectral library, the rESAT-6 control spike and patient samples.

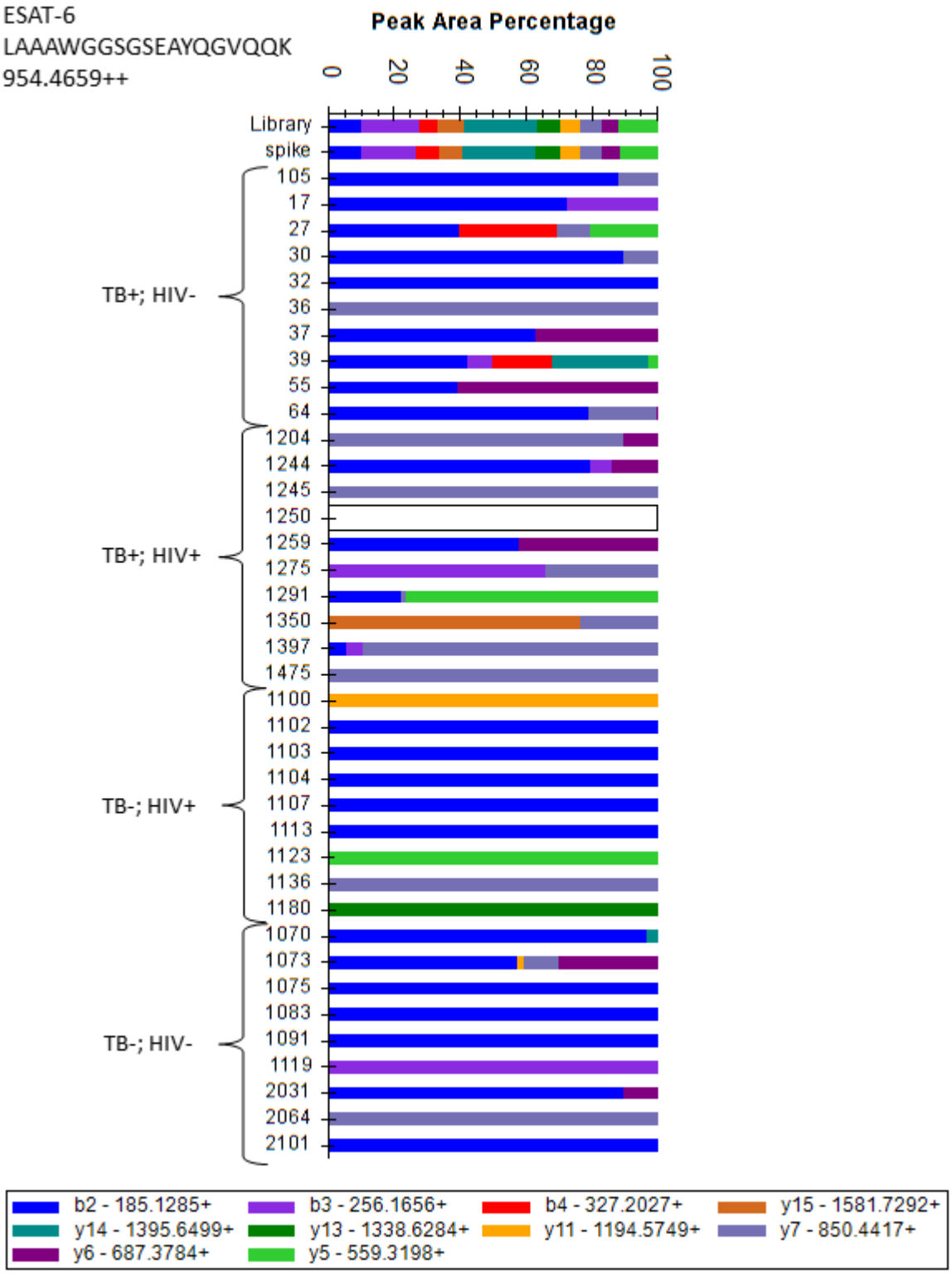

Figure A 5 Comparison of peak areas for transition peaks of peptide LAAAWGGSGSEAYQGVQQK between the spectral library, the rESAT-6 control spike and patient samples.

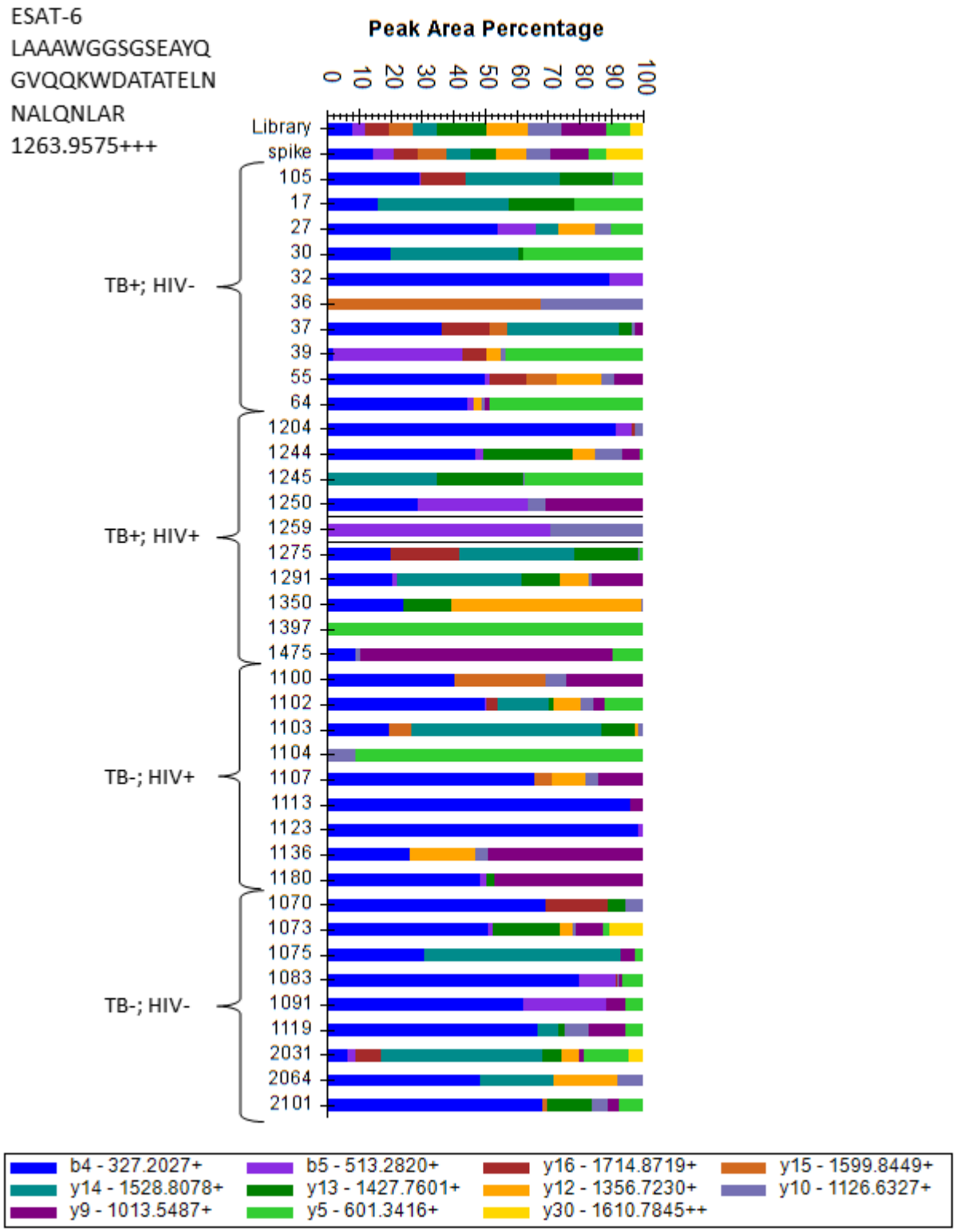

Figure A 6 Comparison of peak areas for transition peaks of peptide LAAAWGGSGSEAYQGVQQKWDATATELNNALQNLAR between the spectral library, the rESAT-6 control spike and patient samples.

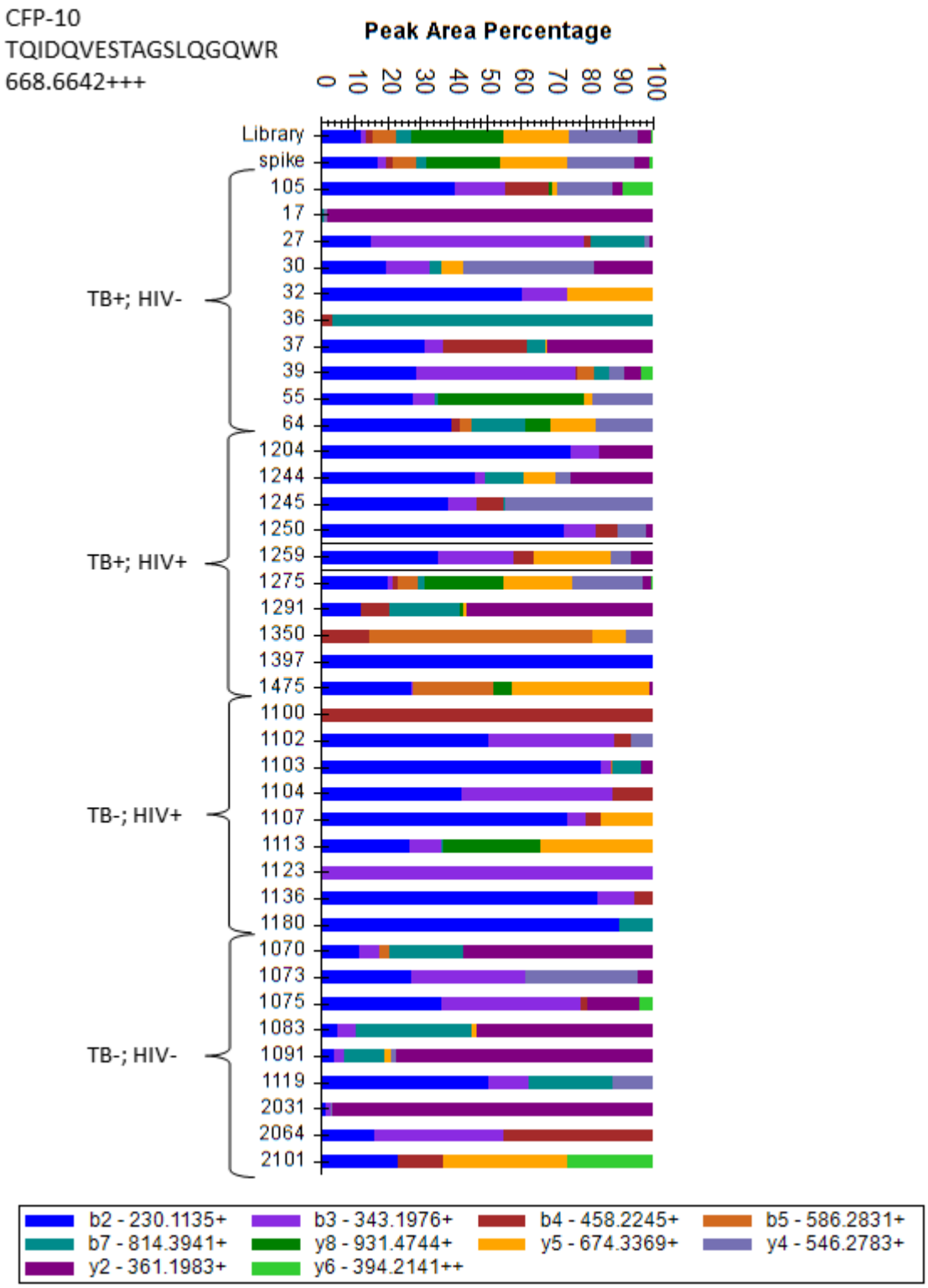

Figure A 7 Comparison of peak areas for transition peaks of peptide TQIDQVESTAGSLQGQWR between the spectral library, the rCFP-10 control spike and patient samples.

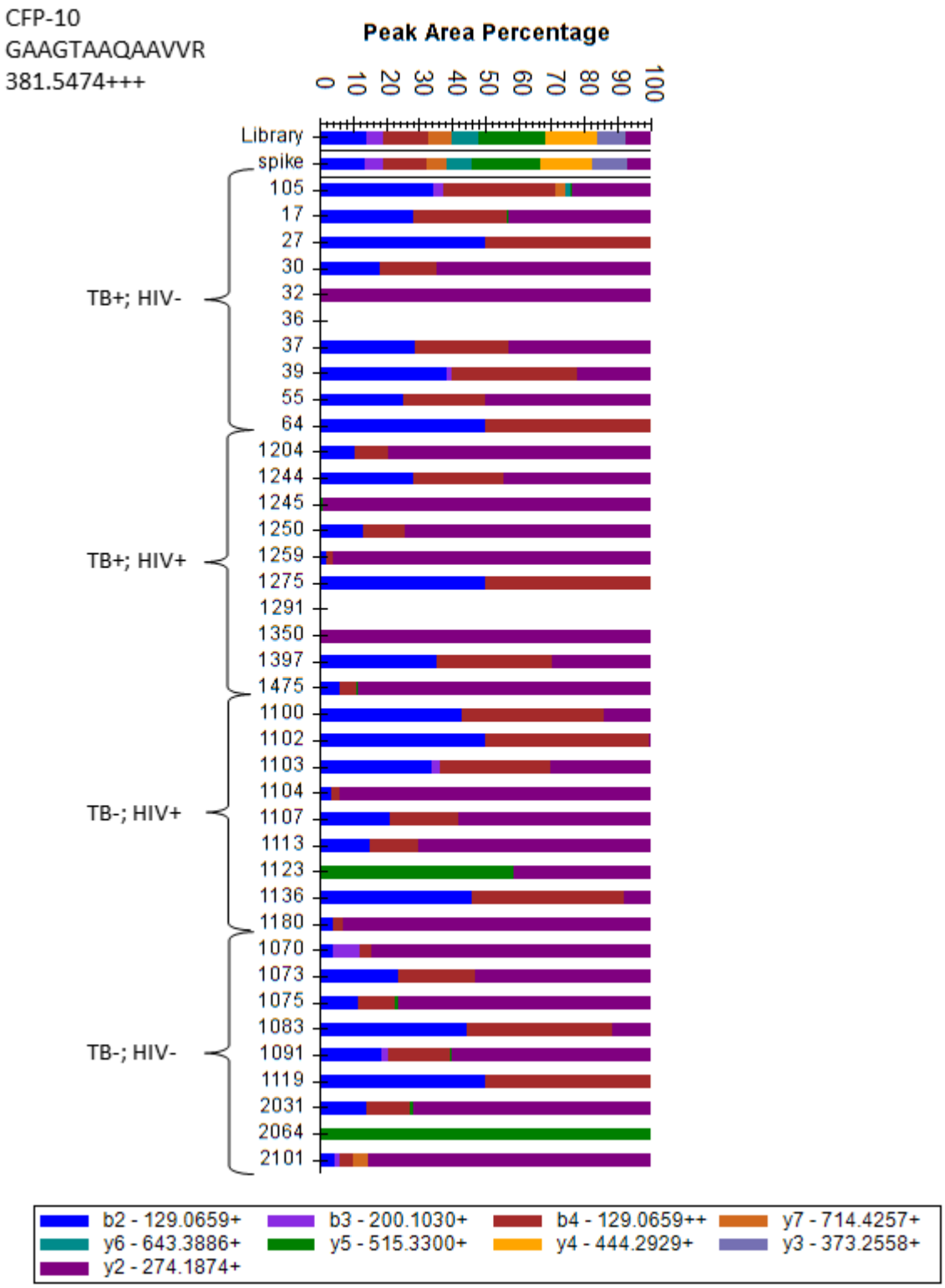

Figure A 8 Comparison of peak areas for transition peaks of peptide GAAGTAAQAAVVR between the spectral library, the rCFP-10 control spike and patient samples.

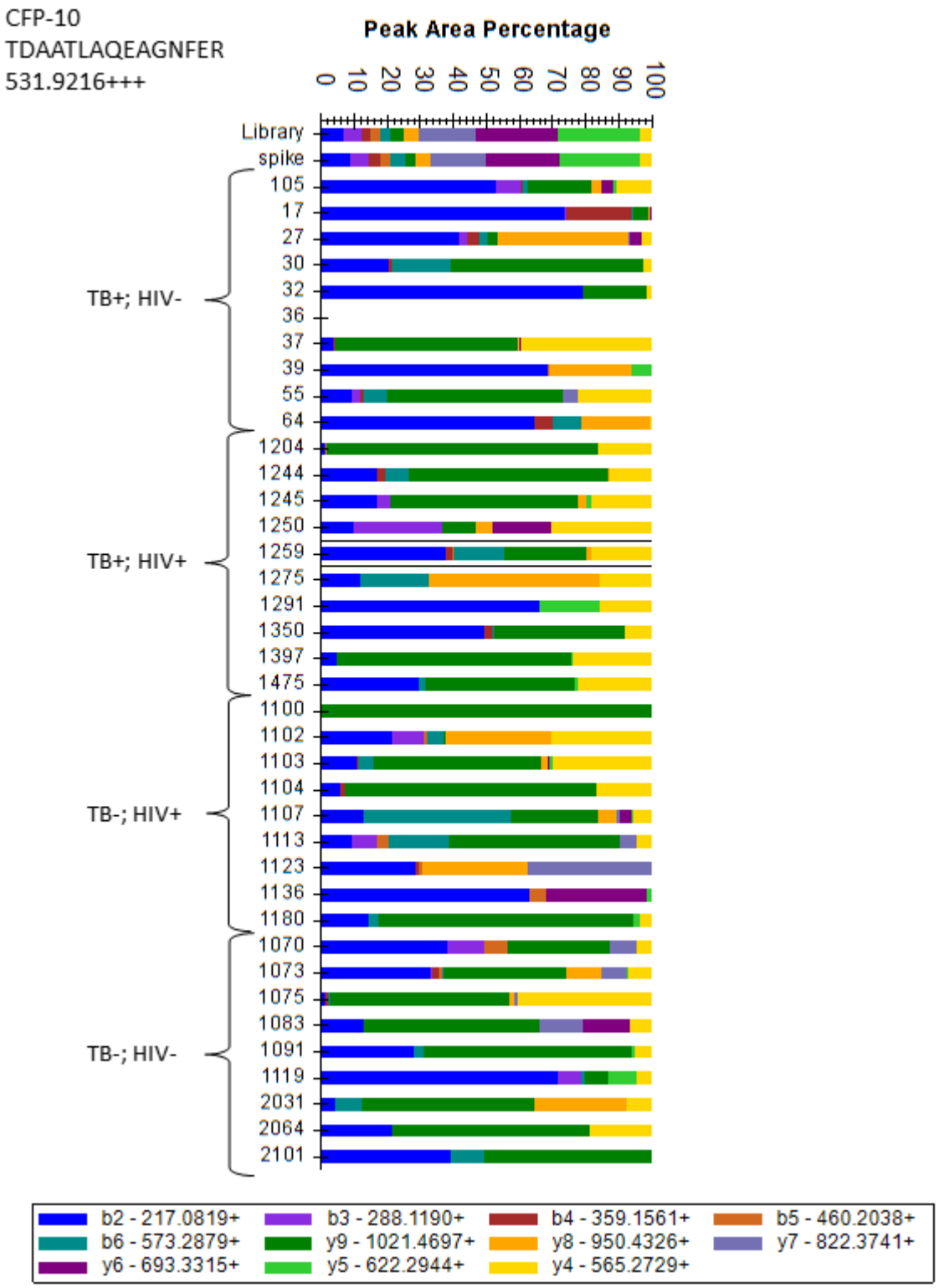

Figure A 9 Comparison of peak areas for transition peaks of peptide TDAATLAQEAGNFER between the spectral library, the rCFP-10 control spike and patient samples.

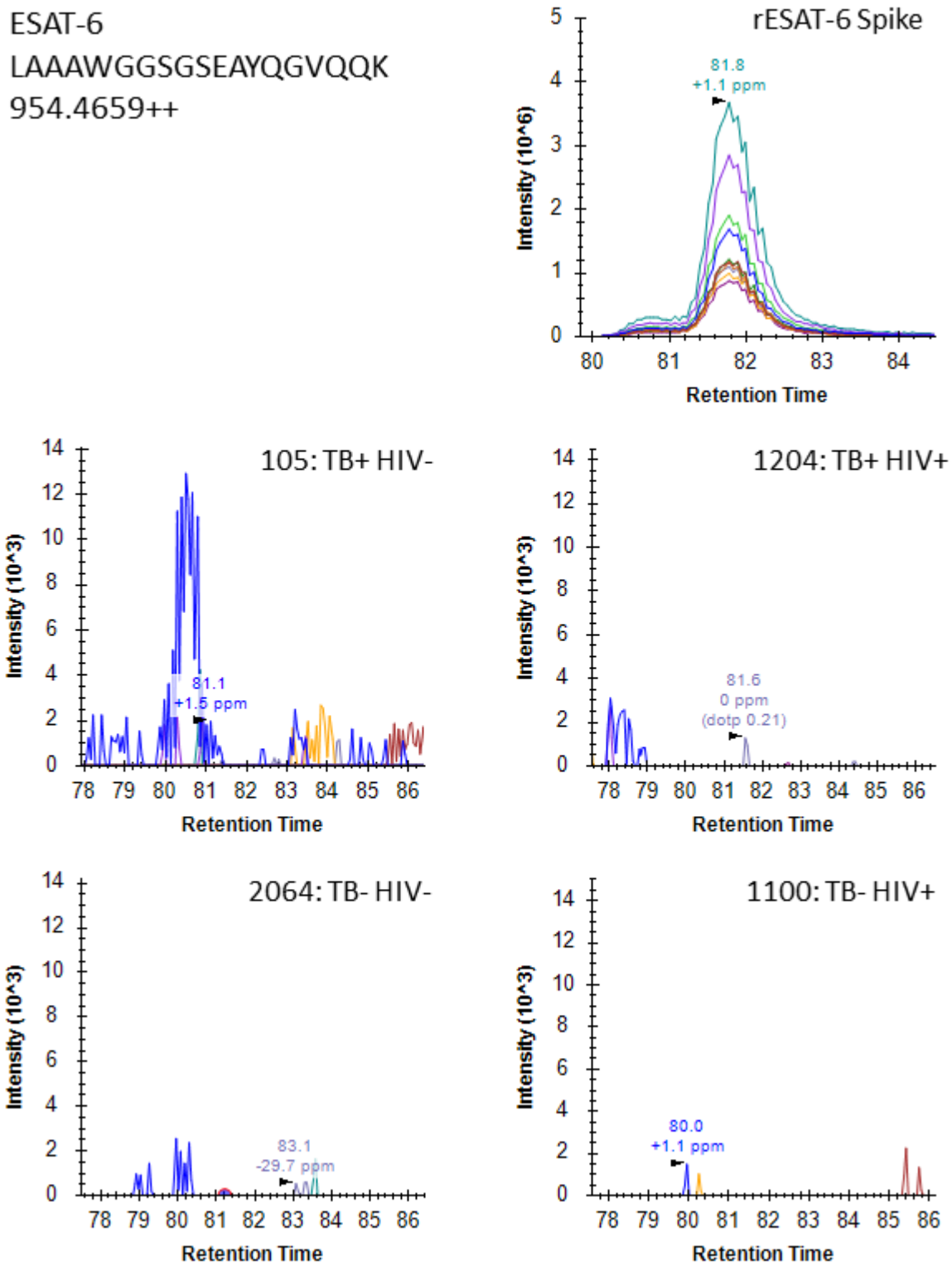

Figure A 10 Transition chromatogram of the rESAT-6 control spike for peptide LAAAWGGSGSEAYQGVQQK and four representative patient chromatograms from each patient group at the same retention time.

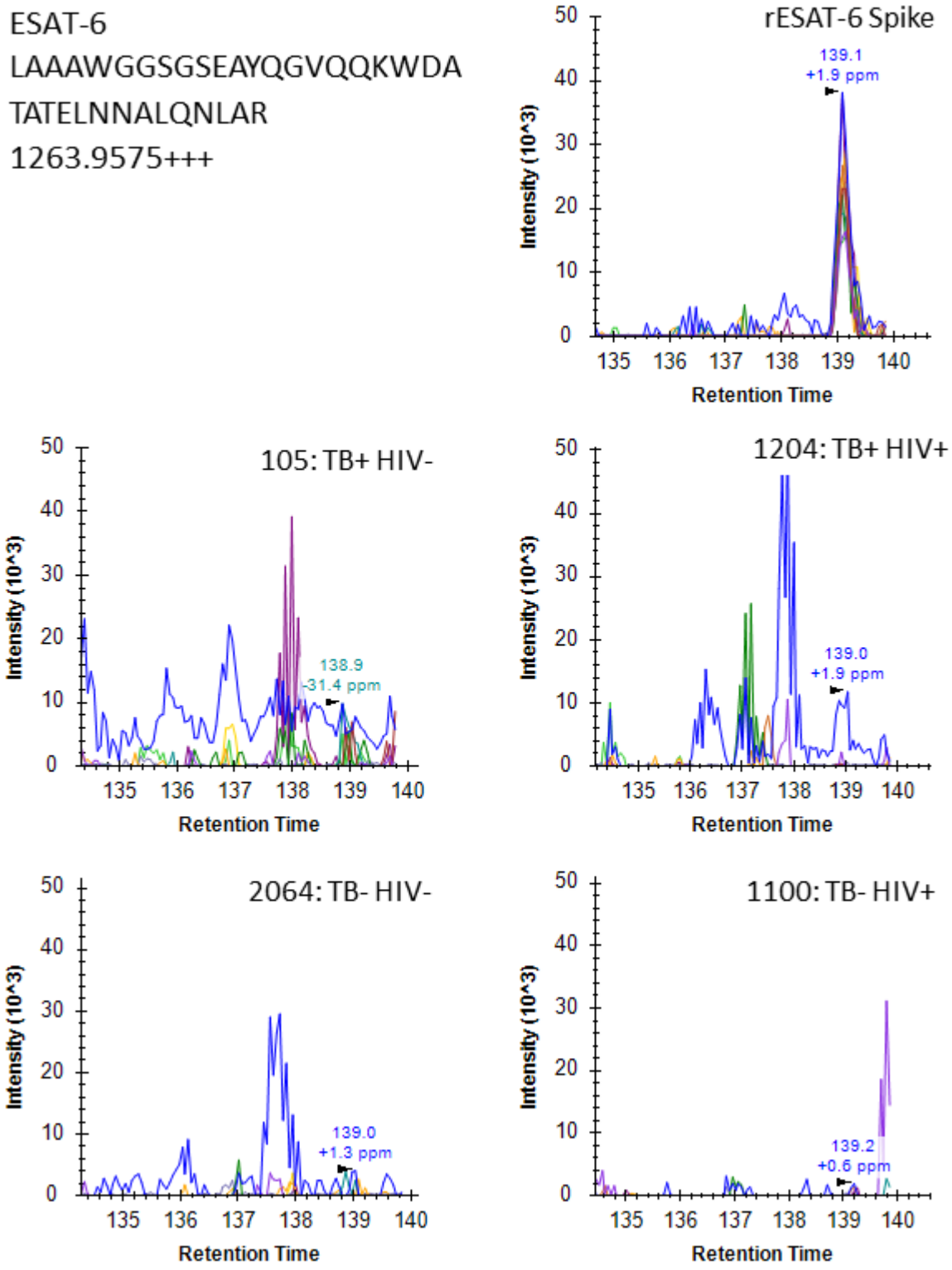

Figure A 11 Transition chromatogram of the rESAT-6 control spike for peptide LAAAWGGSGSEAYQGVQQKWDATATELNNALQNLAR and four representative patient chromatograms from each patient group at the same retention time.

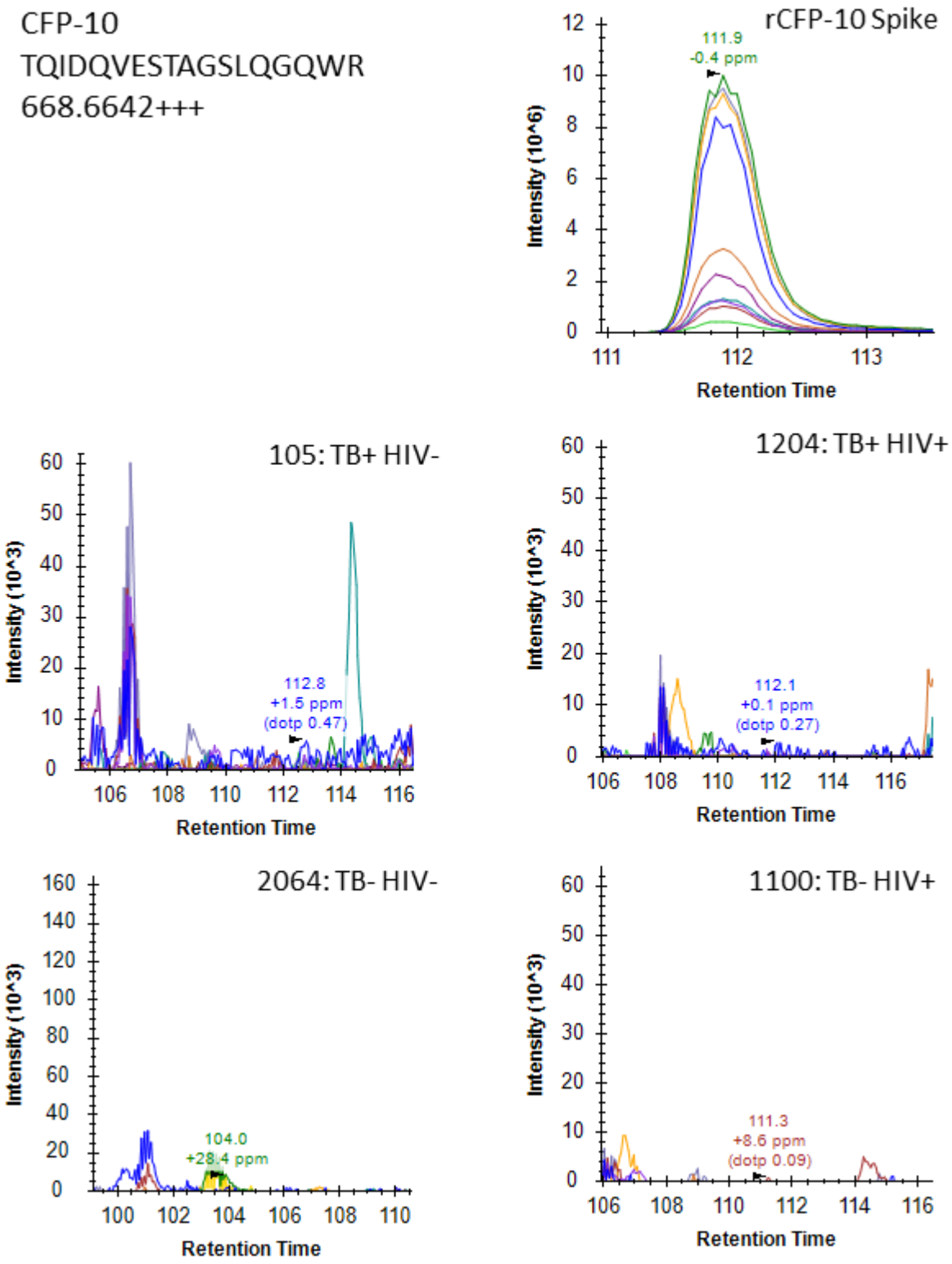

Figure A 12 Transition chromatogram of the rCFP-10 control spike for peptide TQIDQVESTAGSLQGQWR and four representative patient chromatograms from each patient group at the same retention time.

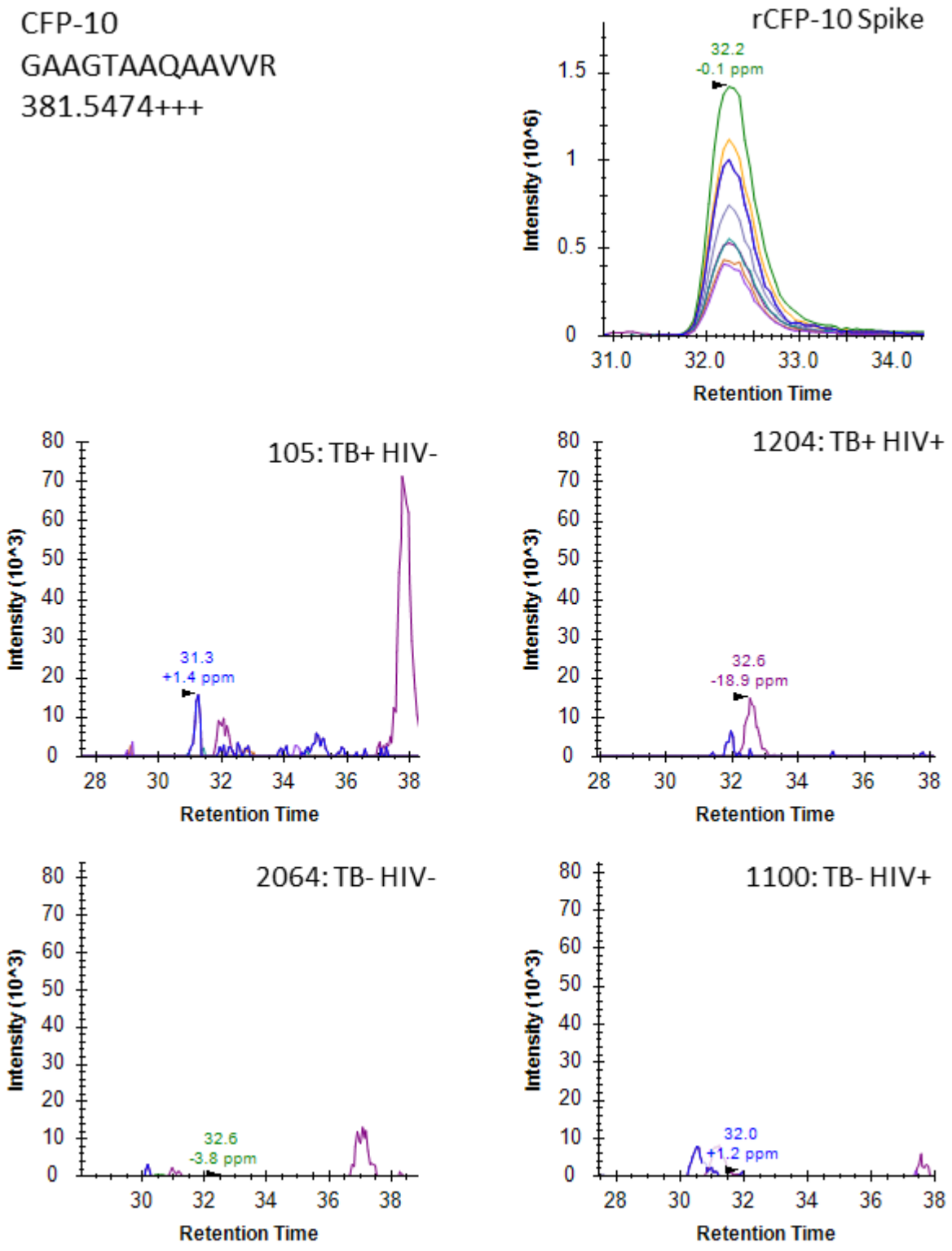

Figure A 13 Transition chromatogram of the rCFP-10 control spike for peptide GAAGTAAQAAVVR and four representative patient chromatograms from each patient group at the same retention time.

APPENDIX B

Protein Sequences

CFP-10 from *M. tuberculosis (H37Rv)*

UniProt: P0A566

Mass (Da): 10,794

HIS tagged recombinant protein: MW: 10,794 + ~1 kDa (6x HIS tag) = 11.8 kDa

>sp|P9WNK5|ESXB_MYCTU ESAT-6-like protein EsxB OS=Mycobacterium tuberculosis (strain ATCC 25618 / H37Rv) GN=esxB PE=1 SV=1

MAEMKTDAATLAQEAGNFERISGDLKTQIDQVESTAGSLQGQWRGAAGTAAQAAVVRFQEAANKQK
QELDEISTNIRQAGVQYSRADEEQQQALSSQMGF

ESAT-6 from *M. tuberculosis (H37Rv)*

UniProt: P9WNK7

Mass (Da): 9,904

HIS tagged recombinant protein: MW: 9,904+ ~1 kDa (6x HIS tag) = 10.9 kDa

>sp|P9WNK7|ESXA_MYCTU 6 kDa early secretory antigenic target OS=Mycobacterium tuberculosis (strain ATCC 25618 / H37Rv) GN=esxA PE=1 SV=1

MTEQQWNFAGIEAAASAIQGNVTSIHSLLDEGKQSLTKLAAAWGGSGSEAYQGVQQKWDA

TATELNNALQNLARTISEAGQAMASTEGNVTGMFA

KatG from *M. tuberculosis (H37Rv)*

UniProt: P9WIE5

Mass (Da): 80,605

HIS tagged recombinant protein: MW: 80,605 + ~1 kDa (6x HIS tag) = 81.6 kDa

>sp|P9WIE5|KATG_MYCTU Catalase-peroxidase OS=Mycobacterium tuberculosis (strain ATCC 25618 / H37Rv) GN=katG PE=1 SV=1

MPEQHPPITETTTGAASNGCPVVGHMKYPVEGGGNQDWWPNRLNLKVLHQNPAVADPMGA
AFDYAAEVATIDVDALTRDIEEVMTTSQPWWPADYGHYGPLFIRMAWHAAGTYRIHDGRG
GAGGGMQRFAPLNSWPDNASLDKARRLLWPVKKKYGKKLSWADLIVFAGNCALESMGFKT
FGFGFGRVDQWEPDEVYWGKEATWLGDERYSGKRDLENPLAAVQMGLIYVNPEGPNGNPD
PMAAAVDIRETFRRMAMNDVETAALIVGGHTFGKTHGAGPADLVGPEPEAAPLEQMGLGW
KSSYGTGTGKDAITSGIEVVWTNTPTKWDNSFLEILYGYEWELTKSPAGAWQYTAKDGAG
AGTIPDPFGGPGRSPTMLATDLSLRVDPIYERITRRWLEHPEELADEFAKAWYKLIHRDM
GPVARYLGPLVPKQTLLWQDPVPAVSHDLVGEAEIASLKSQIRASGLTVSQLVSTAWAAA
SSFRGSDKRGGANGGRIRLQPQVGWEVNDPDGDLRKVIRTLEEIQESFNSAAPGNIKVSF
ADLVVLGGCAAIEKAAKAAGHNITVPFTPGRTDASQEQTDVESFAVLEPKADGFRNYLGK
GNPLPAEYMLLDKANLLTLSAPEMTVLVGGLRVLGANYKRLPLGVFTEASESLTNDFFVN
LLDMGITWEPSPADDGTYQGKDGSGKVKWTGSRVDLVFGSNSELRALVEVYGADDAQPKF
VQDFVAAWDKVMNLDRFDVR

Target concentrations

Table A 10 Bradford assay absorbance readings and estimated concentrations for KatG aliquots

KatG-biotin	Mean absorbance	mg/ml	µl	µg	µM
Aliquot 1	0.063	0.048	165	7.88	0.60
Aliquot 2	0.209	0.238	20	4.75	2.99
Combined (Final)	*	0.068	185	12.63	0.85

Table A 11 Bradford assay absorbance readings and estimated concentrations CFP-10

CFP-10-biotin	Mean absorbance	mg/ml	µl	µg	µM
Aliquot 1	0.244	0.169	50	8.43	14.28
Aliquot 2	0.202	0.227	185	42.08	19.27
Combined (Final)	*	0.215	235	50.51	18.21

Table A 12 Estimated concentrations of biotinylated LAM

LAM-biotin	mg/ml	µl	µg	µM
Final	0.1	900	90	5,88

Table A 13 Amounts of targets loaded onto the PAGE gel

Target	(µg)
Biotinylated KatG	0.24
Biotinylated CFP-10	0.34
Biotinylated LAM	~2

Table A 14 Concentrations of targets incubated with magnetic beads.

Target	**(µM)**
KatG	0.85
CFP-10	19.91
CFP-10·ESAT-6	5.00
LAM	5.88

PCR

Table A 15 PCR Optimisation Summary

	Primer (µM)	**Template (µl)**	**Cycle number**
PCR_1.1	0.4	10	4-20
PCR_1.2	0.2	20	16
PCR_1.3	0.01	20	16 & 20
PCR_1.4	0.1	20	16 & 20
PCR_1.5	0.1	20	25 & 30
PCR_1.6	0.1	1 (1ng/µl)	15
PCR_2.1	0.1	20	16, 20 & 24
PCR_2.2	0.1	40	20 & 24
PCR_2.3	0.1	20	20 & 24

Table A 16 Final nanodrop readings of pooled putative aptamers and amounts aliquoted for sequencing

Tube	Nanodrop Reading Concentration (ng/µl)	Aliquoted for Sequencing 100 ng (µl)	200 ng (µl)	300 ng (µl)
#1 Positive Control	19.9	5.03	*	*
#2 KatG	31.8	3.14	*	*
#3 CFP-10	12.3	*	*	24.4
# 4 LAM	17.3	5.78	*	*
#5 Negative Control	23.5	4.26	*	*
#1b Positive Control	68.3	*	2.93	*
#3b CFP-10· ESAT-6	54.2	1.85	*	5.54
#5b Negative Control	22.9	*	8.73	*

Putative X-Aptamer Sequences

Table A 17 Putative X-Aptamer Sequences

W=INDOLE; X=HYDROXYMETHYL; Y=PHENOL; Z=BORON

KatG (corresponding to enrichment in fraction 2)

KATG.2.1 TTTTT AC ACGA GYXCCTAACAGTCTAAACTXGCCTGTYTTG TCGT TTTTT
KATG.2.2 TTTTT AC TCGT GYXCCTGAATGTGCCGCTGCCTAACCTG TCGT TTTTT
KATG.2.3 TTTTT CA ACGA CGTTCZGGTTATCCGTWACZGAAAGAACAT TCGT TTTTT
KATG.2.4 TTTTT CA ACGA CGGATAGGTTATCTCZATCZGATTCTACAT TCGT TTTTT
KATG.2.5 TTTTT CA TCGT AGCCAWTGCTATCTAAATCGTATCGACAGZ TCGT TTTTT
KATG.2.6 TTTTT CA ACGA CGCCCTACATATACTCCTCGGZ TCGT TTTTT
KATG.2.7 TTTTT CA TCGT CGGACZGGCCAGCCAAWAAAACTTCTCACA TCGT TTTTT
KATG.2.8 TTTTT CA ACGA AGGGCZGGGTATCCACATCGACTA ACGA TTTTT
KATG.2.9 TTTTT CA TCGT AGGGTAGGCCCACCCZATATGATCAZACTA TCGT TTTTT

CFP-10·ESAT-6 + CFP-10 only (corresponding to enrichment in fraction 3)

CE.3.1 TTTTT CA TCGT CGGGCAGGCCCATCAATCCZAGTCCTCGTA TCGT TTTTT
CE.3.5 TTTTT CA ACGA GWGGTAGCTTAGTAACTCATTATCGAACCA ACGA TTTTT
CE.3.6 TTTTT CA ACGA AGGGCAACCCCATACZWACZAGAAWGCATA TCGT TTTTT
CE.3.7 TTTTT CA ACGA CGTTCAGGCTAGCTGTTCATAGTCAZACTA TCGT TTTTT
CE.3.8 TTTTT CA TCGT AGCCTAGCCTGWCCCZWAATACTTAZCGGZ TCGT TTTTT
CE.3.9 TTTTT CA TCGT CGGATAACCCAGCCCZWACZTATCGAACTA TCGT TTTTT

LAM (corresponding to enrichment in fraction 4)

LAM.4.1 TTTTT CA ACGA AGCCCAGGTTATTCACWACZAGAAWGCAAT TCGT TTTTT
LAM.4.2 TTTTT CA TCGT CGCCTAGGTTAGCTACWAATTATTGAACTA TCGT TTTTT
LAM.4.3 TTTTT CA ACGA ZGGACZGCCTATTCGTATCZTATCGAACTA TCGT TTTTT
LAM.4.4 TTTTT AC ACGA GYGCAGGATGGTTCCCYAAAGCAGGTGT TCGT TTTTT
LAM.4.5 TTTTT CA TCGT GWCCCZGGTTATCCACTCCZACTCAZCATA TCGT TTTTT
LAM.4.6 TTTTT CA TCGT AGGATAGGTTAGCTACTTCZACTTWGCGAT TCGT TTTTT
LAM.4.7 TTTTT CA ACGA AGTTCATGCTCACCACATCZACCGCTCATA TCGT TTTTT
LAM.4.8 TTTTT CA ACGA AGGGCZTGCTATTCACATAAAGTCGACATA TCGT TTTTT
LAM.4.9 TTTTT CA TCGT AGGGCAGGCTAGTCAATCCZACAACTACGZ TCGT TTTTT

APPENDIX C

X-Aptamer binding curves: CFP-10

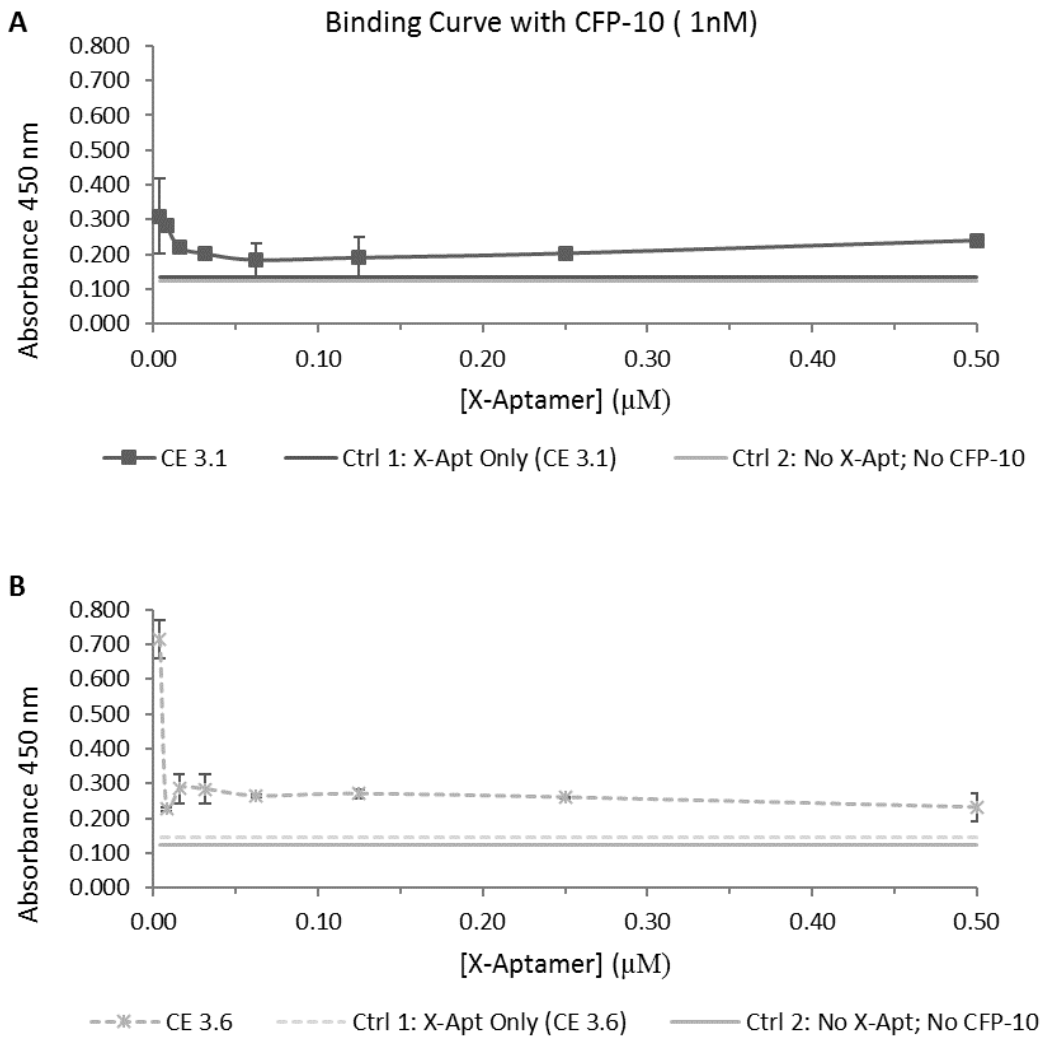

Figure A 14 Binding Curves with rCFP-10 (1 nM) and two-fold serial dilutions of X-Aptamers (0.004-0.5 µM). A) CE 3.1 B) CE 3.6. All wells were performed in duplicate.

ELONA: Streptavidin→ BSA→X-Aptamer→rCFP-10-HIS→Anti-HIS-HRP

Control 1: Streptavidin→BSA→ X-Aptamer→ PBS→ Anti-HIS-HRP (Ctrl 1: X-Apt Only)

Control 2: Streptavidin→BSA→ PBS→ PBS→ Anti-HIS-HRP (Ctrl 2: No X-Apt; No CFP-10)

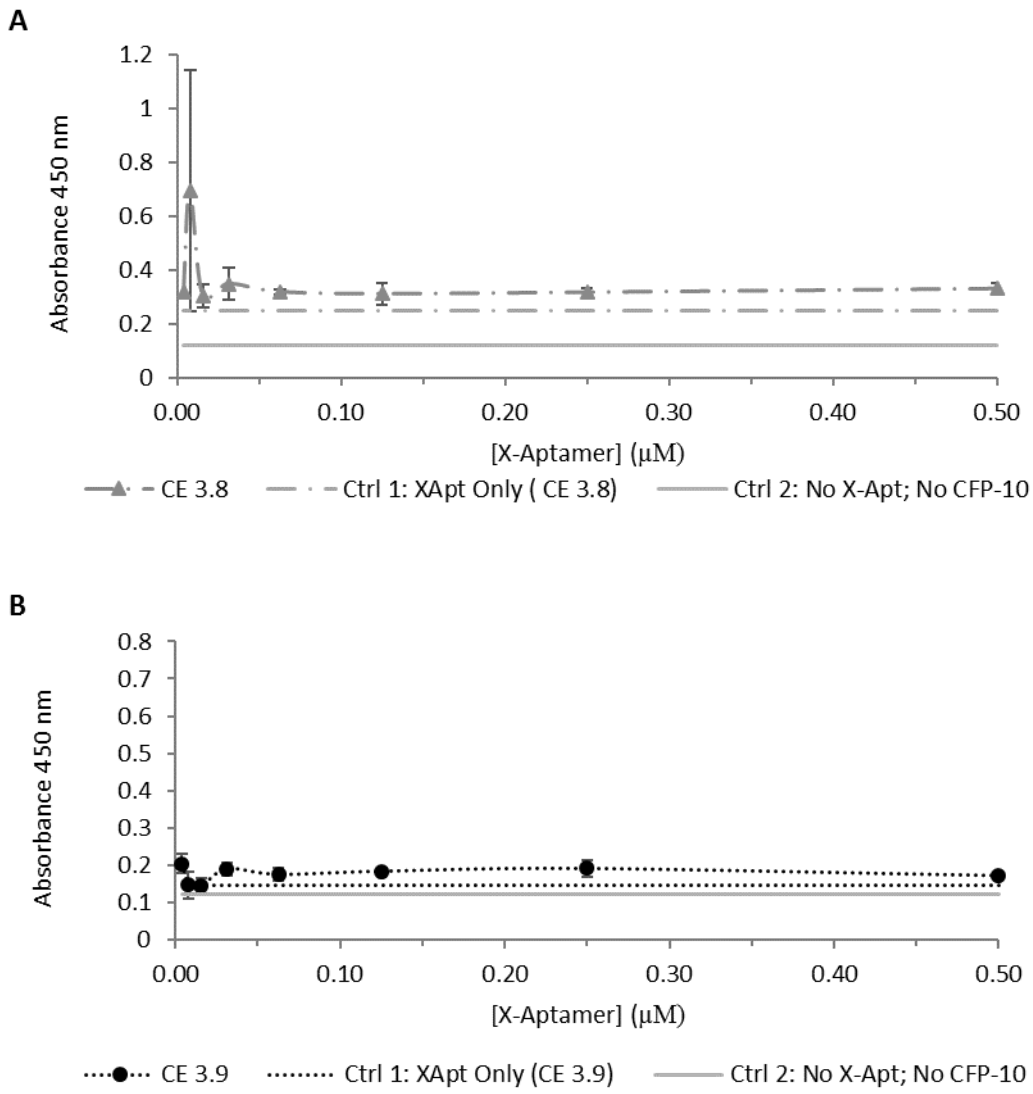

Figure A 15 Binding Curves with rCFP-10 (1 nM) and two-fold serial dilutions of X-Aptamers (0.5-0.004 µM). A) CE 3.8 B) CE 3.9. All wells were performed in duplicate.

ELONA: Streptavidin→ BSA→X-Aptamer→rCFP-10-HIS→Anti-HIS-HRP

Control 1: Streptavidin→BSA→ X-Aptamer→ PBS→ Anti-HIS-HRP (Ctrl 1: X-Apt Only)

Control 2: Streptavidin→BSA→ PBS→ PBS→ Anti-HIS-HRP (Ctrl 3: No X-Apt; No ESAT-6)

X-Aptamer binding curves: ESAT-6

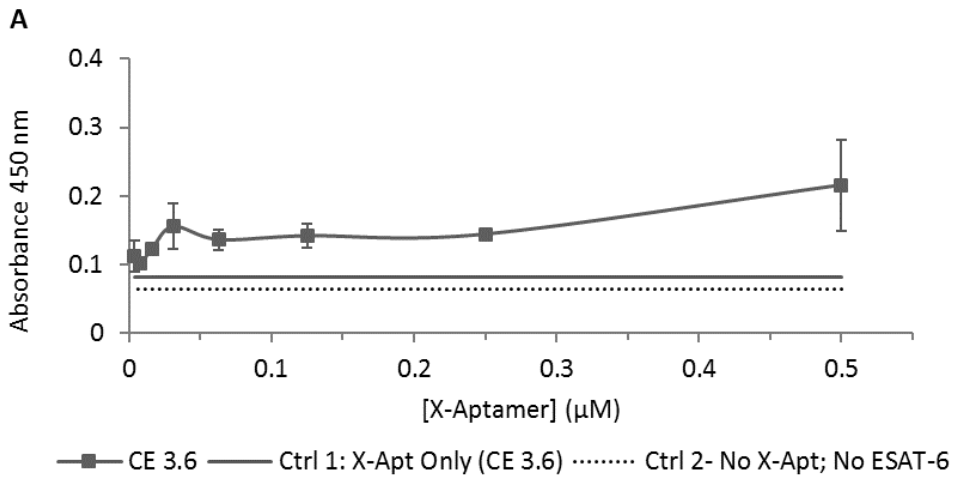

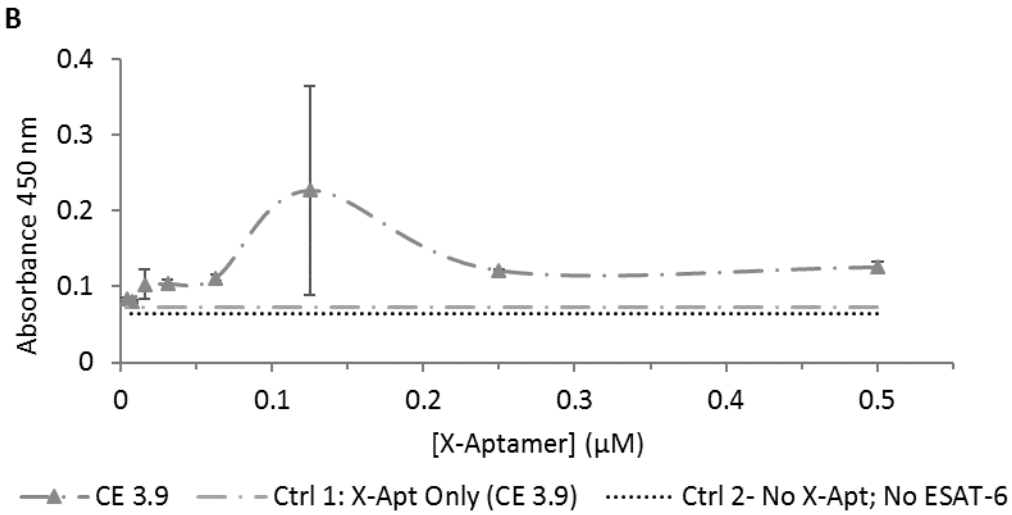

Figure A 16 Binding Curves with HIS tagged rESAT-6 (1 nM) and two-fold serial dilutions of X-Aptamers (0.5-0.004 µM). All wells were performed in duplicate. A) CE 3.6 B) CE 3.9. Points indicate the mean reading of duplicate or triplicate wells. Error bars indicate the minimum and maximum readings taken.

ELONA/ELISA: Streptavidin→ BSA→X-Aptamer→rESAT-6-HIS→Anti-HIS-HRP

Control 1: Streptavidin→BSA→ X-Aptamer (CE 3.9)→ PBS→ Anti-HIS-HRP (Ctrl 1: X-Apt Only)

Control 2: Streptavidin→BSA→ PBS→ PBS→ Anti-HIS-HRP (Ctrl 3: No X-Apt; No ESAT-6)

Biolayer Interferometry

OCTET Red

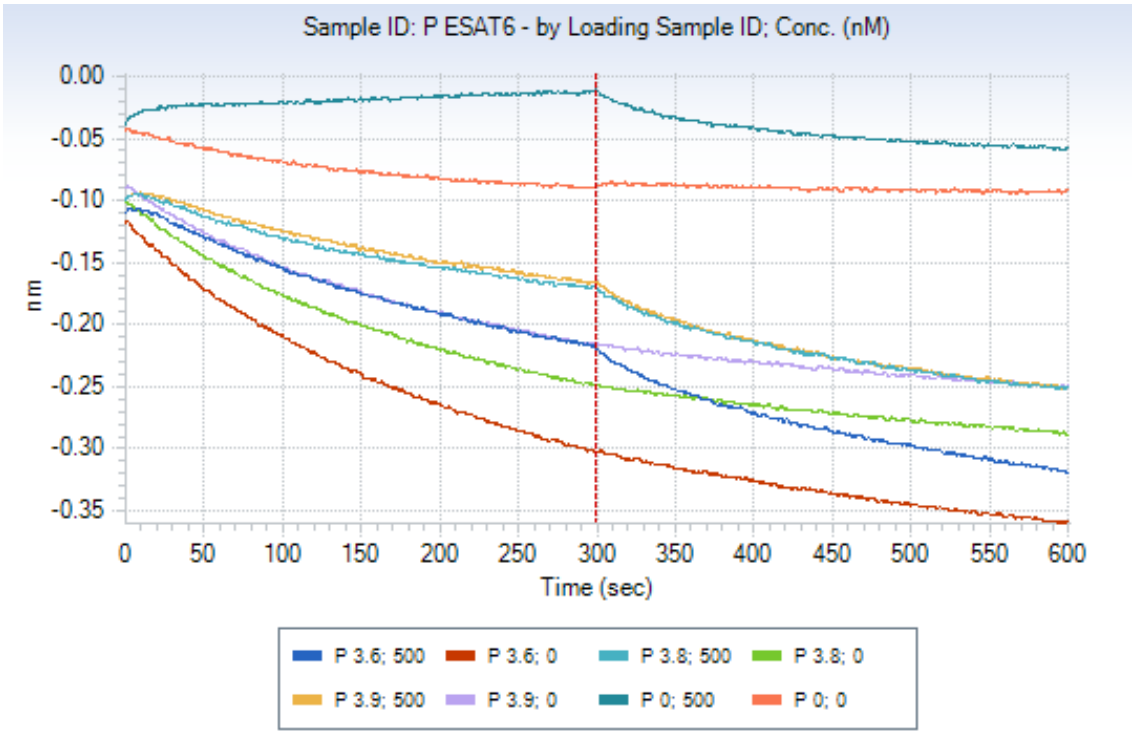

Figure A 17 ESAT6 is at 500nM or 0nM for comparison (in PBSTM). P0 is negative controls.

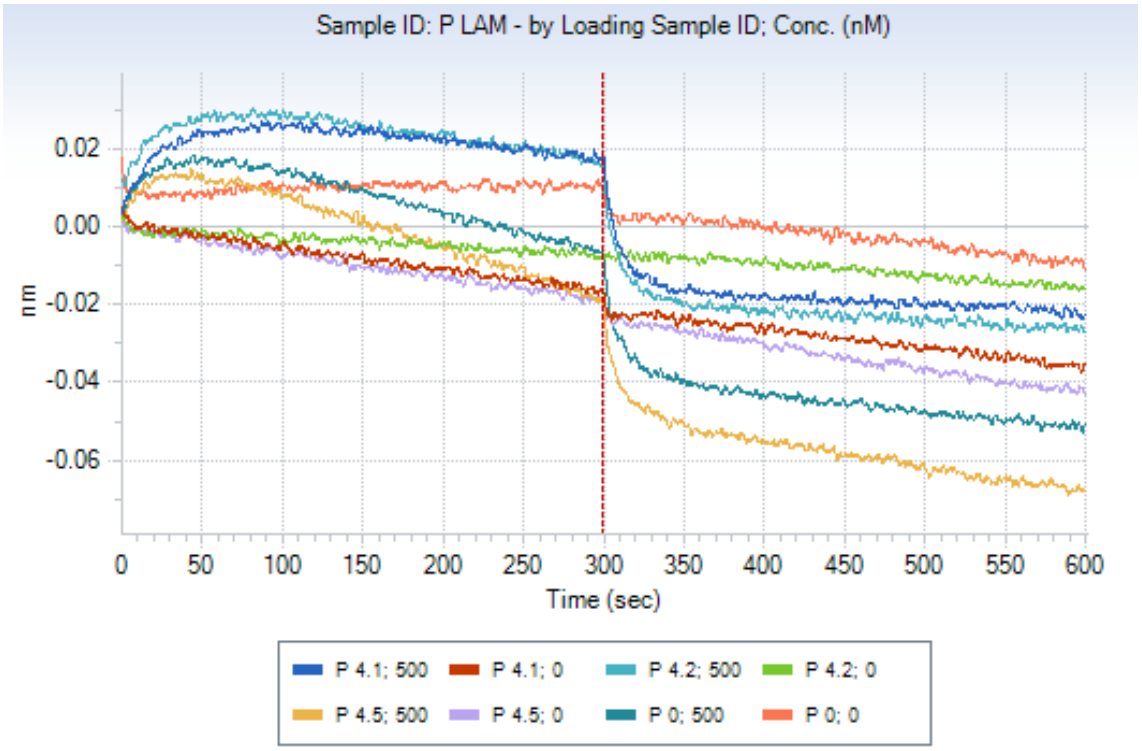

Figure A 18 LAM in PBS

LAM at 500nM or 0nM in different buffers.

OCTET K2

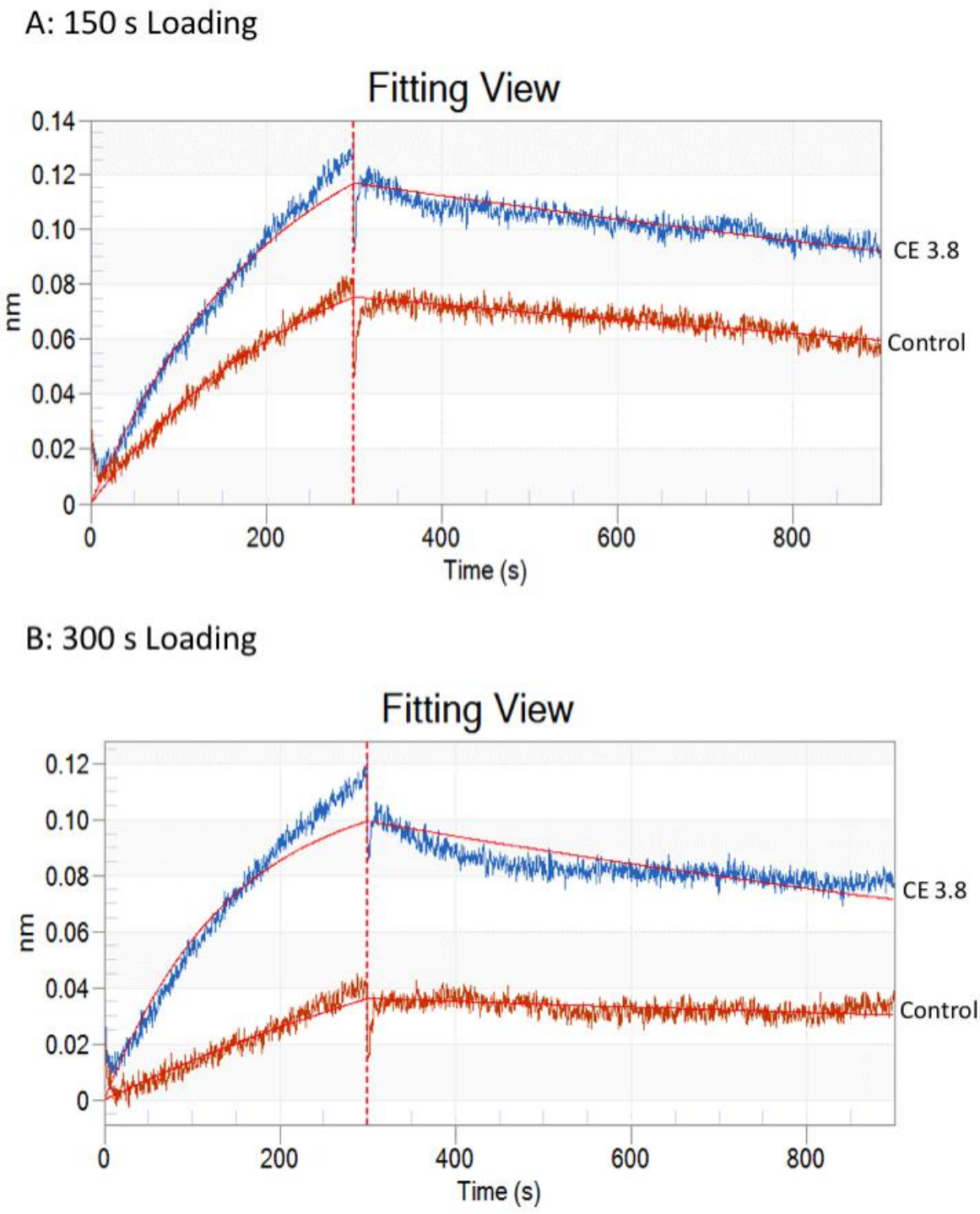

Figure A 19 Optimising Loading time